T cell phenotyping of a Mouse Model of Activated PI3Kδ Syndrome

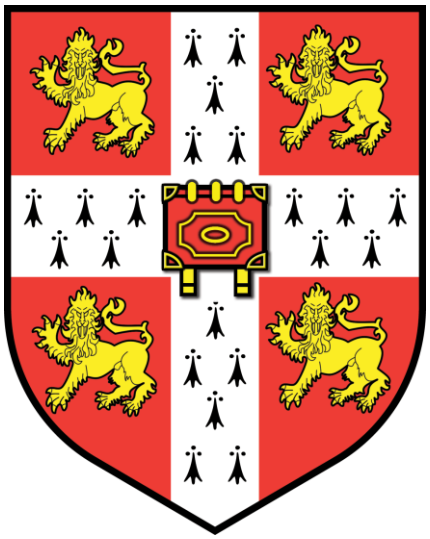

Rafeah Alam

Lucy Cavendish College

October 2018

This dissertation is submitted for the degree of

Doctor of Philosophy

Declaration

This dissertation is the result of my own work and includes nothing, which is the outcome of work done in collaboration except where specifically indicated in the text. It is not substantially the same as any that I have submitted or is being concurrently submitted for a degree or diploma or other qualification at the University of Cambridge or any other University or similar institution except as declared in the Preface and specified in the text. I further state that no substantial part of my thesis has already been submitted, or is being concurrently submitted for any such degree, diploma or other qualification at the University of Cambridge or any other University or similar institution except as declared in the Preface and specified in the text.

The dissertation does not exceed the word limit set by the Faculty of Biology of 60,000 words.

Acknowledgments

I would like to express my sincere gratitude to my supervisor Klaus, for his continuous support throughout my PhD research, for his patience, motivation and enthusiasm. Secondly, to my industrial co-supervisor Srividya for giving me the opportunity to carry out some experiments at GSK and for your overall support throughout the PhD. A special thanks to Anne my mentor, for all your input from beginning to end and for all the times I came into your office for advice (personally and professionally). Big up to Daisy, my fellow companion in this whole process, thanks for being there listening to all my struggles, for somehow always looking at the bright side and for getting me into Pokémon!

Thank you to Hicham, Krish and Ram for all your help and advice (work and life). Thank you for answering my countless questions and for all the random conversations that I thoroughly enjoyed. Thank you to Amy for welcoming me into the lab and for being patient with me when I always forgot where things were! Thanks to Lyn for answering my random questions. Thanks to Fiore for always making me laugh, for cheering me up when things did not go to plan and for always taking out the time to listen there. Thanks to Anita for all your help with all the experiments, for your advice, brainstorming potential experiments and for all the weirdest conversations possible. Thanks to Christina and Doreen for always helping me even when it was last minute and for all the mature conversations that took place in the TC or Cat 2 lab. Thanks to Tamara especially for all your help in the last few months. Thanks to Chiara and Valentina for the countless hugs given, makes me actually want to hug people now.

Thanks to my parents and grandparents for their prayers. Massive thanks to my mom, none of what I am today and where I am today would have been possible without your prayers. Thank you for feeding me and keeping me sane throughout this journey. Thank you for always being there. Special thanks to my sister Farah for all your help in the past few months. Massive thanks to my siblings (Sarah, Raniya, Bhaiya and Hamed) and my sister in law (Sana Bhabhi) for your prayers, help, advice and your encouragement (at times!). Thank you for keeping up with me during this time. Thank you to my friends (Zareen, Angela, Kafia, Ami, Reena and Fiona) who when things got tough somehow pulled me out of it.

1) Initial training in techniques and laboratory practice and subsequent mentoring:

- Anne Katrien Stark – cell culture, *in vitro* T cell-based assays, ELISA
- Hicham Bouabe – growth of attenuated Lm-OVA, counting bacterial load
- Krishendu Chakaraborty – Performing and training of Influenza infections, viral loads, growing BM-DC's
- Rachael Walker (Flow core facility) – flow cytometry
- Doreen Lau: Performing and training for injecting tumour cells

2) Data obtained from a technical service provider (e.g. DNA sequencing, illustrations, simple bioinformatics information etc)

- Arthur Davis, Rebecca Roberts, Lynzi Waugh, Atilla (Flow core facility) – cell sorting
- Babraham Biological Services Import Unit – animal husbandry, intravenous injections

3) Data produced jointly (e.g. where it was necessary or desirable to have two pairs of hands)

- Processing of tissues – Anne Katrien Stark, Christina Courreges, Anita Chandra, Tamara Veverek, Doreen Lau
- Data generated using NP-KLH experiments was a combined effort with Anita Chandra

4) Data/materials provided by someone else (e.g. one-off analysis, bioinformatics analysis, where parallel data or technical provision in a very different area is needed to provide a connected account in the thesis)

- PIP_3 and western blot data provided by Valentina Carbonaro
- Generation of volcano plots (and methods)– Christina Courreges
- Mass spectrometry sample processing and analysis (and methods) – Christina Rollings (College of Life sciences, University of Dundee)
- Gene microarray data analysis (and methods)- (Glyn Bradley GSK)

Summary

Activated PI3Kδ Syndrome (APDS) is immunodeficiency caused by a heterozygous gain-of-function mutation (E1021K) in the PIK3CD gene, encoding for the p110δ catalytic subunit of phosphoinositide 3-kinase (PI3K). APDS patients are lymphopenic, suffer from sinopulmonary infections and from increased susceptibility to bacterial and herpes group virus infections. Following T cell receptor (TCR) stimulation, T cells from these patients undergo increased activation induced cell death, which can be reversed by selective PI3Kδ inhibitors. I used a new conditional knock-in mouse (T-p110δ^{E1020K}) to investigate the effect of hyperactive p110δ on T cell function. Hyperactivation of p110δ led to increased PIP_3 and pAKT levels following TCR stimulation that was reduced using a selective p110δ inhibitor. Following *in vitro* TCR stimulation, T cells proliferated normally but showed increased apoptosis that was reversed by a p110δ specific inhibitor. Despite enhanced apoptosis, CD8$^+$ T cells displayed enhanced activation that was associated with increased levels of cytokines and granzyme B. CD4$^+$ T cells with hyperactive p110δ produced increased Th1, Th2, Th17 and Tfh cytokines but showed reduced Treg differentiation *in vitro*. Conditional T-p110δ^{E1020K} mice have reduced Tregs in the thymus but increased peripheral Tregs. These mice also have increased numbers of T follicular helper cells and germinal centre (GC) B cells upon immunisation with a T cell dependent antigen (NP-KLH). Reduced antigen specific IgG1$^+$ cells within GC B cells was detected in mice harbouring hyperactive p110δ mutation in B cells, implying that the antibody deficiencies observed in APDS patients is due to an intrinsic defect within B cells rather than limited help from T cells.

T-p110δ^{E1020K} mice mounted normal primary responses to acute infections. However adoptive transfer of ovalbumin-specific T cell receptor transgenic CD8 T cells (OT1) revealed an intrinsic defect in the primary expansion of CD8$^+$ T cells with hyperactive p110δ. This defect in primary expansion was found to be rescued in the presence of wild type OT1 cells. Following infection with acute pathogens, CD8$^+$ T cells with hyperactive p110δ displayed normal to increased effector function with phenotypically reduced memory cells as indicated by reduced memory precursor effectors cells (MPECs). In contrast, following chronic infection, T-p110δ^{E1020K} displayed increased signs of T cell exhaustion that is also characteristic of APDS patients as they suffer from chronic herpes virus infections. This set of work therefore shows that the mouse model recapitulates key aspects of APDS patients and give insights into the role of

p110δ signaling in different T cell subsets influenced by hyperactive p110δ activity. Further, in depth analysis of proteomics and gene array data of *in vitro* stimulated T cells generated during this study, can provide a better understanding of the mechanisms behind the T cell phenotype observed.

List of abbreviations

4E-BP1	Eukaryotic translation initiation factor 4E-binding protein 1
7-AAD	7-aminoactinomycin D
α-DG	α-dystroglycan
ActA	Actin assembly-inducing protein
α-GalCer	α-galactosylceramide
AHR	Aryl Hydrocarbon Receptor
AICD	Activation-induced cell death
AID	Activation-induced cytidine deaminase
ANA	Auto Nuclear Antigen
APDS	Activated PI3Kδ syndrome
ATP	Adenosine trisphosphate
BATF	Basic leucine zipper transcription factor, ATF-like
Bcl-6	B-Cell Lymphoma 6
BCR	B cell receptor
Blimp-1	B lymphocyte-induced maturation protein-1
BrdU	Bromodeoxyuridine / 5-bromo-2'-deoxyuridine
BTK	Bruton's tyrosine kinase
CD	Cluster of differentiation
CFU	Colony-forming units
CLL	Chronic lymphocytic leukaemia
CLR	C-Type Lectin Receptors
CSF	Colony-stimulating factor
CSR	Class switch recombination
CTL	Cytotoxic T lymphocyte
CTLA-4	Cytotoxic T lymphocyte antigen-4
DAG	Diacylglygerol
DC	Dendritic cell
DNA	Deoxyribonucleic acid

DTR	Diphtheria toxin receptor
EAE	Experimental autoimmune encephalitis
EDTA	Ethylenediaminetetraacetic acid
ELISA	Enzyme-linked immunosorbent assay
EOMES	Eomesodermin
FACS	Fluorescence-activated cell sorting
FBS	Foetal Bovine Serum
FOXO	Forkhead box O transcription factor
Foxp3	Forkhead box P3
FYC	Foxp3-YFP-cre
GAB	GRB2-associated-binding protein
GATA3	GATA binding protein 3
GC	Germinal Centre
GITR	Glucocorticoid-induced tumour necrosis factor-related receptor
GM-CSF	Granulocyte-macrophage colony-stimulating factor
GP	Glycoprotein
GPCRs	G-protein-coupled receptors
GSK	Glycogen synthase kinase
HA	Haemagglutinin
ICOS	Inducible T cell co-stimulator
IFN	Interferon
IKK	IκB kinase
IL	Interleukin
InA/B	Internalin A/B
Influenza	Influenza A virus
IP3	Inositol 1,4,5-trisphosphate
ITAM	Immunoreceptor tyrosine-based activation motif
ITIM	Immunoreceptor tyrosine-based inhibitory motif
ITK	Interleukin-2 tyrosine kinase
IRF	Interferon regulatory factor

ISG	Interferon-stimulated gene
JIA	Juvenile idiopathic arthritis
KLF2	Krüppel-like Factor 2
LAG3	Lymphocyte-activation gene 3
LCMV	Lymphocytic choriomeningitis virus
LLO	Listeriolysin O
Lm	Listeria monocytogenes
M2	Matrix 2
MACS	Magnetic-activated cell sorting
MAPK	Mitogen-activated protein kinase
MAVS	Mitochondrial antiviral signalling
MDSC	Myeloid-derived suppressor cell
MHC	Major histocompatibility complex
mTOR	Mammalian target of rapamycin
mTORc1/C2	mTOR Complex 1/2
MyD88	Myeloid differentiation primary response 88
NA	Neuraminidase
NFAT	Nuclear factor of activated T-cells
NK	Natural Killer
NK-κB	Nuclear factor-κB
NLRs	NOD-like receptors
NOD	Nucleotide-binding and oligomerization domain
NP	Nucleoprotein
NS	Nonstructural protein
OT-I	Ovalbumin-specific TCR transgenic
OVA	Ovalbumin
PAMP	Pathogen-associated molecular pattern
PBS	Phosphate-buffered saline
PC-PLC	Broad-range phospholipase C
PCR	Polymerase chain reaction

PD-1	Programmed death-1
PDL-1	Programmed death-1 ligand
pDC	plasmacytoid dendritic cell
PDK1	Phosphoinositide-dependent kinase 1
PD-L1	Programmed death-ligand 1
PFU	Plaque-forming units
PH	Peckstrin homology
PI	Phosphoinositide
PI3K	Phosphoinositide 3-kinase
PIB5PA	Phosphatidylinositol 4,5-bisphosphate 5-phosphatase A
PI-PLC	Phosphatidylinositol-specific phospholipase C
PKB/Akt	Protein kinase B
PKC	Protein kinase C
PLC-γ1	Phospholipase C-γ1
PplA	Peptide pheromone-encoding lipoprotein A
pPplA	Putative peptide pheromone-encoding lipoprotein A
PRR	Pathogen Recognition Receptors
PTEN	Phosphatase and tensin homolog
RA	Rheumatoid arthritis
RICD	Reactivation-induced cell death
RING	Really Interesting New Gene
RLK	Resting Lymphocyte Kinase
RLR	Retinoic acid-inducible gene-I-like receptors
RNA	Ribonucleic acid
RNP	Ribonucleoprotein
RORγ	Retinoid-related orphan receptor γ
RTK	Receptor tyrosine kinases
S1PR1	Sphingosine-1-phosphate receptor 1
S6K1	Ribosomal protein S6 kinase 1
SH2	Src homology 2

SHIP	SH2 domain-containing inositol 5'-phosphatase
SLE	Systemic lupus erythematosus
SLP76	SH2 domain-containing leukocyte protein of 76 kDa
SMAD	Contraction of Sma and Mad (Mothers against decapentaplegic)
STAT	Signal transducer and activator of transcription
STING	Stimulator of interferon genes
T-bet	T-box factor expressed in T cells
Tcon	Conventional T cell
TCR	T cell receptor
TEC	Tyrosine Kinase expressed in hepatocellular carcinoma
Tfh	T follicular helper cell
Tfr	T follicular regulatory cell
TGF-β	Transforming growth factor-β
Th	T helper cell
ThCTL	Cytolytic T helper cell
TIGIT	T-cell immunoreceptor with Ig and ITIM domains
TIM3	T cell immunoglobulin and mucin protein 3
TLR	Toll-like receptor
TNF-α	Tumour necrosis factor alpha
TNF-R1	Tumour necrosis factor-Receptor 1
TRAIL	TNF-related apoptosis-inducing ligand
TRAIL-R1/R2	TNF-related apoptosis-inducing ligand-Receptor 1/2
Treg	Regulatory T cell
VDJ	Variable (V), diversity (D) and joining (J) genes
WT	Wild-type
YFP	Yellow fluorescent protein
ZAP-70	Zeta-chain-associated protein kinase 70

Contents

Figure headings

Chapter 1

Chapter 2

Chapter 3

Chapter 4

Chapter 5

Chapter 6

Table legends

1 Introduction

1.1 The immune system

As part of the adaptive immune system, white blood cells called lymphocytes carry out the adaptive immune responses. There are two broad classes of responses, antibody responses and cell mediated immune responses carried out by B cells and T cell respectively. Collectively, B cells, $CD4^+$ T cells and $CD8^+$ T cells mount a coordinated immune response against an invading pathogen. Dysregulation of the coordinated responses by the adaptive and innate immune system can lead to an inappropriate reaction to self that is known as autoimmunity and involves loss of normal immune homeostasis. Additionally, ineffective immune responses can occur resulting in immunodeficiency that can be either primary due to a primary congenital defect or secondary due to acquiring it from another cause such as infections or therapeutic treatment leading to immunosuppression.

Due to the scope of this thesis, emphasis will be made on the T cell subset of the adaptive immune system

1.2 T cells

The development of functional T cells is essential for mounting a protective immune response against countless pathogens. While the majority of hematopoietic lineages mature in the bone marrow, T cell development takes place in a specialised organ: the thymus. In the thymus, progenitor T cells (thymocytes) undergo selection for the generation of T cells bearing a diverse T cell receptor (TCR) repertoire that is restricted to self-major histocompatibility complexes (MHC) and tolerant to self-antigens.

When entering the thymus, before negative and positive selections occur, the T cell precursors are double negative (DN) $CD4^-CD8^-$. The DN cells undergo a differentiation programme characterized by sequential variable-diversity-joining (V(D)J) recombination of the TCRβ and TCRα chains. DN T cell precursors undergo four sequential stages of differentiation depending on the expression of CD44 and CD25.The four stages are; DN1 ($CD44^+CD25^-$), DN2 ($CD44^+CD25^+$), DN3 ($CD44^-CD25^+$); and DN4 ($CD44^-CD25^-$). Proper rearrangement of the TCRβ is required at the DN3 stage by VDJ recombination, a process known as β-selection and thymocytes unable to do so die via apoptosis [1, 2]. The DN4 stage then undergoes a phase of

rapid proliferation before differentiation into a double positive (DP) CD4+CD8+ population, where these cells rearrange and express the TCRα chain. The double positive (DP) thymocytes undergo positive and negative selection to develop into $CD4^+$ αβ or $CD8^+$ αβ T-cells based on their binding to antigen presented on MHC and to eliminate autoreactive T cells by apoptosis [2]. The thymus also supports the differentiation into γδ T cells, natural killer (NK) T cells, regulatory T cells (Tregs) and intraepithelial lymphocytes [3]. Development of Tregs in the thymus occurs during a two-step process. TCR signalling in the DP cells poises them to express Foxp3, which then occurs in a second IL-2 dependent step that is TCR independent [4, 5]. Tregs bind to the MHC class molecules with a greater strength than conventional T cells, but remain below the threshold for induction of apoptosis by negative selection [6].

1.2.1 $CD4^+$ T cells

$CD4^+$ T cells are crucial in coordinating acquired immune responses and constitute one of the key arms of the adaptive immune system. Following activation, naïve $CD4^+$ T cells differentiate into functionally diverse T helper cell (Th) subsets, including Th1, Th2, Th9, Th17, Th22, Tfh and $Foxp3^+$ Tregs, depending on the cytokine milieu of the local environment. Collectively the different Th subsets are referred to as conventional $CD4^+$ T cells (Tcons). Each T cell subtype can be characterised by their cytokine profile and transcription factor expression. The specific master transcription factors and the signaling transducer and activator of transcription (STAT) proteins are essential for Th cell differentiation [7]. Effector functions of these cells are mediated by their cytokine profile that are critical to provide immunity against various pathogens. Specific $CD4^+$ Th subsets are able to help B cells make antibodies , enhance and maintain $CD8^+$ T cells responses , augment actions of innate immune components , regulate the magnitude and persistence of immune response to prevent autoimmunity and control immune responses against pathogens to avoid immune-mediated tissue damage [7].

For Th1 cells, the T-box transcription factor T-bet and STAT4 are important for Th1 differentiation and function. Th1 cell differentiation is primarily triggered by IL-12 and these cells produce interferon γ (IFNγ) and interleukin-2 (IL-2). Th1 cells are involved in promoting cell-mediated immune responses and are required for host defense against intracellular viral and bacterial pathogens [8]. For Th2 cells, GATA3 and

STAT6 are the major transcription factors involved, and these cells mainly produce IL-4, IL-13, IL-10 and IL-5. Th2 cells are generally important for producing immune responses against helminths and other extracellular parasites and also aid B cells in antibody production [9]. Th17 cells secrete IL-17, IL-22, IL-26, and granulocyte-macrophage colony-stimulating factor (GM-CSF) and express the orphan retinoid receptor RORγt, and require STAT3 for differentiation [10]. These cells are important in mounting an immune response against extracellular pathogens but are also implicated in the development of a number of autoimmune diseases that include rheumatoid arthritis (RA), psoriasis, juvenile idiopathic arthritis (JIA), Crohn's disease [11-13].

Th9 cells are a recently identified subset that predominantly secrete the pro-inflammatory cytokine IL-9. They play a role in providing antitumor immunity by secreting cytokines such as IL-3, IL-21 in addition to IL-9 [14]. Th9 cells are also able to induce inflammation and thereby exacerbate inflammatory diseases that include inflammatory bowel disease (IBD), allergic asthma, multiple sclerosis, RA and others [15]. The transcriptional profile is not fully described, and include STAT6 and GATA3 among others [14]. The Th22 subset primarily secretes IL-22 and tumour necrosis factor-α (TNFα), and do not express cytokines such as IL-17, IL-4 or IFNγ thus distinguishing them for the other Th subsets [16]. The expansion of Th22 cells seems to be regulated by the aryl hydrocarbon receptor (AHR) transcription factor. By producing proinflammatory cytokines, Th22 cells are implicated in the pathogenesis of inflammatory and autoimmune disorders [17].

Regulatory T cells (Tregs) are a subset of $CD4^+$ T cells identified by the constitutive expression of the IL-2 receptor α chain (CD25) and the transcription factor forkhead-box transcription factor Foxp3 (Foxp3) [18]. These cells exist as natural Tregs (nTreg or tTregs) that are thymus derived and as induced Tregs (iTreg) that develop in peripheral lymphoid organs after antigen priming [4]. Transforming growth factor beta (TGFβ) is the main cytokine responsible for development of iTregs. Tregs are important for maintaining and inducing peripheral tolerance to self and non-self antigens. This is achieved through different mechanisms that involve production of secreted immunosuppressive cytokines, direct contact with effector T cells or suppressive actions on dendritic cells [19].

1.2.2 $CD8^+$ T cells

$CD8^+$ T cells are specialised cells important for the immune defense against a range of intracellular pathogens that include bacteria and viruses as well as for tumor surveillance. $CD8^+$ T cells recognise specific antigenic peptides presented in the context of class I major histocompatibility complex (MHC) that is found in all nucleated cells through the TCR and CD8 co-receptor that consists of one CD8α and one CD8β chain [20].

Naïve $CD8^+$ T cells are normally found in the blood, spleen and lymph nodes, ready to interact with antigen presenting cells (APC) presenting cognate antigen leading to their activation. $CD8^+$ T cells circulate between the blood and lymph nodes via the high endothelial venule (HEV) [21]. Naïve $CD8^+$ T cells become activated, usually via 3 signals that include stimulation of TCR with peptide-MHC class I complexes presented by APC's , costimulatory signals via CD80/86:CD28 for example and inflammatory cytokines that include IL-12 and type I IFNs for example[20] .

Once activated, $CD8^+$ T cells undergo a dramatic shift in the expression of surface markers including the loss of CD62L (CD62L/L-selectin) and CC-chemokine receptor 7 (CCR7), preventing the cells from gaining access to the lymph nodes via the HEVs [21]. Additionally expression of other adhesion receptors such as CD44, CD11a and CD49d and chemokine receptors such as CXC-chemokine receptor 3 (CXCR3) is increased, contributing to the access of activated $CD8^+$ T cells to inflamed peripheral tissues [21].

Following activation, antigen-specific $CD8^+$ T cells undergo robust proliferation and acquire effector functions such as secretion of cytokines that include interferon gamma (IFNγ), tumor necrosis factor (TNFα) and production of cytotoxic granules containing perforin and granzymes, all of which contribute to pathogen clearance. Following the expansion phase, $CD8^+$ T cell undergo a contraction phase in which 90-95% of cells undergo apoptosis, while the remaining 5-10% of cells give rise to long-lived memory $CD8^+$ T cells [22]. Memory $CD8^+$ T cells exhibit augmented functional properties, and rapidly produce effector cytokines within a few hours of stimulation compared to naïve $CD8^+$ T cells that require days to fully differentiate into effector cells. The secondary response capacity of memory $CD8^+$ T cells is more rapid compared to the primary

clonal expansion requirements; therefore functional memory $CD8^+$ T cells are able to provide effective and long lasting immunity [20].

Progress has been made over the years to distinguish between activated $CD8^+$ T cells that are more likely to become memory $CD8^+$ T cells compared to those that will undergo apoptosis during the contraction phase. At the peak of the primary expansion phase, there are two populations of effector $CD8^+$ T cells termed short-lived effector cells (SLECs) and memory precursor effector cells (MPECs). These two subsets are differentiated based on the expression of cell surface molecules including the IL-7 receptor (CD127) and killer cell lectin-like receptor G1 (KLRG1) that is also a senescence marker. Characteristically. MPECs are $CD127^{high}KLRG1^{low}$ and SLECs are $KLRG1^{high}CD127^{low}$ [23]. Survival of MPECs is primarily dependent on cytokines such as IL-7 and IL-15. MPECs have the potential to remain long-lived whilst SLECs are regarded as being terminally differentiated cells [24]. The cytokines IL-7 and IL-15 play an important for the survival of MPECs, acting in part by upregulation of the anti-apoptotic molecule Bcl-2. IL-15 plays a role in SLEC's survival but does not lead to its long-term maintenance [23].

Differential expression of transcription factors that include increased levels of T-bet, Blimp-1, XBP-1, ID2 promote differentiation into SLECs, whereas increase expression of Eomesodermin (Eomes), Bcl-6, ID3 and Mbd2 favour MPEC differentiation [23, 25]. Differentiation into MPECs and SLECs is controlled by multiple mechanisms that include the strength or stimulation by antigen and the exposure to cytokines such as IL-2 and IL-12 [23]. Following pathogen clearance, MPECs that survive the contraction phase differentiate into long-lived memory T cells that consists of a heterogeneous pool memory cells. These include central memory (T_{CM}) cells and effector memory (T_{EM}) cells that are distinguished based on there their expression of cell surface markers that determine their migratory pattern [26]. Both of these subsets are capable for producing cytokines that include IFNγ and TNFα, both of them are capable of proliferating however, T_{CM} cells display increase proliferative capability and produce more IL-2. T_{CM} cells express lymph node homing receptors that include CD62L and CCR7 that allows them to circulate between bloodstream and secondary lymphoid organs [27]. On the other hand, T_{EM} cells lack surface markers and circulate through the bloodstream, permissive non-lymphoid tissues and secondary lymphoid organs.

The robust recall responses generated by memory $CD8^+$T cells are therefore important for enhanced protection against pathogen re-encounter.

The Phosphoinositide 3-kinase (PI3K) signaling pathway plays an important in the development, activation and homeostasis of T cells in response to stimuli, and it is this pathway, which will be the focus of this thesis.

1.3 Phosphoinositide 3-kinases (PI3Ks)

Phosphoinositide 3-kinases (PI3Ks) are a family of lipid kinase enzymes that are involved in a broad spectrum of cellular, physiological and pathological processes through the generation of secondary lipid messengers. They achieve their functions through phosphorylation of the 3' hydroxy group of phosphatidylinositol (PtdIns) and its phosphorylated derivatives (phosphoinositides), which then act as membrane docking sites for intracellular signalling effectors in downstream pathways [28]. In mammalian cells, the PI3K family consists of three classes, Class I, Class II and Class III, which are defined according to their structure, function and lipid specificity.

Class III PI3K is the oldest of the PI3Ks and is composed of a single member termed vacuolar protein sorting-associated protein 34 (Vps34) [28]. It is the only PI3K identified in yeast and has been evolutionally conserved through mammals [29]. Vps34 is active as part of at least two complexes, each with a different role and cellular localisation. Vps34 exists in a complex with Vps15 and Vps30, additionally either with Atg14, which is required for autophagy, or Vps38 required for vacuolar sorting [30]. Vps34 phosphorylates PtdIns to phosphatidlyinositol 3-phosphate (PI3P), the most abundant phosphoinositide species found in the cell [31]. Due to the importance in regulation of autophagy, Vps34 has been involved in a range of diseases such as, metabolic disorders and neurodegenerative diseases. T cell-specific Vps34 deletion led to defective T cell homeostasis, impaired autophagy and a wasting syndrome, another study reported that Vps34 is essential for naïve T cell homeostasis by modulating IL-7Rα trafficking and signalling [32, 33].

Class II PI3Ks consist of three Class II PI3K isoforms: PI3K-C2α, PI3K-C2β and PI3K-C2γ [34]. The activation of Class II PI3Ks is not well understood, however they seem

to be activated downstream of receptor tyrosine kinases (RTKs) or GPCRs [35]. PI3KC2α and PI3KC2β are widely expressed, while expression of PI3KC2γ is appears to be limited to exocrine glands [36]. These enzymes are least well understood, likely to use both PI and PI(4)P as substrates, producing PI(3)P or $PI(3,4)P_2$ at the plasma membrane or endosomes [31, 37]. These isoforms are reportedly activated downstream of several effectors that include hormones, growth factors, cytokines and chemokines. The three isoforms possess a C2 domain, a helical domain and a catalytic domain, all of which are present in the other classes of PI3Ks. Additionally these isoforms possess a Ras-binding domain and a class II specific C-terminal region consisting of second C2 domain and a PX (Phox homology) domain that preferentially binds to PIP_2, with the N-terminal region differing between each class II isoforms [37, 38]. Class II PI3K activity have been associated with certain cancers [36].

This project is primarily concerned with Class I PI3Ks, which will be discussed in further depth.

1.3.1 Class I PI3Ks

The Class I PI3Ks are heterodimeric enzymes composed of a catalytic p110 KDa subunit coupled to one of several regulatory subunits. Class 1 PI3Ks are further subdivided based on their mode of regulation into Class IA, which contains three isoforms, p110α, p110β and p110δ, and Class IB, which is comprised of only p110γ [39, 40]. The three Class IA catalytic subunits are encoded by PIK3CA, PIK3CB and PIK3CD, whereas p110γ is encoded by PIK3CG. Class IA catalytic isoforms couple to one of five p85 type regulatory subunits, which are encoded by three genes [41, 42]. p85α, p55α and p50α are splice variants of the PIK3RI gene, whereas PIK3R2 and PIK3R3 encodes p85β and p55γ respectively [43]. Each of the regulatory subunits contains a p110-binding region flanked by two Src Homology 2 (SH2) domains. These domains are able to bind phosphorylated tyrosines in YXXM motifs of membrane-associated proteins, therefore recruiting the catalytic subunits to the membrane and linking T cell receptor activation with downstream PI3K signaling [44]. Class IA catalytic isoforms consist of p85-binding domain, a RAS-binding domain, a helical domain and a catalytic domain (**Figure 1.1**)[28] . All of the p110 subunits are capable of binding to each of the p85 type regulatory subunits [28, 45]. The class IB p110γ subunit couples to either a p84/p87 or p101 regulatory subunit due to the absence of a p85 binding domain [46, 47].

Class IA PI3Ks signal downstream of Receptor Tyrosine Kinases (RTKs), which include T and B cell antigen, cytokine, costimulatory and Toll-like receptors [48]. Class IB PI3K signals downstream of G-protein coupled receptors (GPCRs) including chemokine receptors, which is mediated by binding of regulatory subunits to Gβγ subunits [49]. However there is also evidence that p110β and p110δ can signal downstream of GPCRs and p110γ of RTKs [50-52]. The expression of the catalytic p110δ and p110γ subunits is mainly restricted to leukocytes and are therefore important in immune responses. Whereas p110α and p110β are ubiquitously expressed, p110α being a common oncogene in ovarian and breast cancer amongst others and important for insulin like growth factor signaling and p110β playing a role in platelet biology [28, 53, 54]. This project is mainly concerned with the p110δ catalytic subunit of the Class IA PI3Ks.

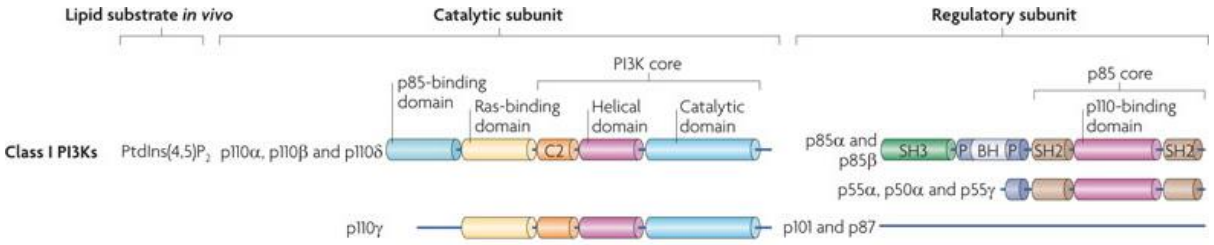

Figure 1.1: The Class I PI3K catalytic and regulatory subunits

Class IA PI3K catalytic isoforms p110α, p110β and p110δ bind to a p85 regulatory subunit (p85α, p85β, p55α, p50α or p55γ). Class IB p110γ isoform binds to the p101 or p84 regulatory subunits. Class IA catalytic subunits have the following domains; N-terminal p85 binding domain which binds the regulatory subunit, Ras binding domain (RBD), C2 domain, helical domain and catalytic domain. Class IA regulatory subunits contain a p110 binding domain flanked by two SH2 domains in their core, a BCR homology (BH) domain, which may possess intrinsic GTPase activating protein activity, and an SH3 domain. Class IB p110γ lack the N-terminal p85 binding domain. p101 and p84 regulatory subunits have no identifiable domains and lack homology to other proteins. Figure taken from [28].

1.3.2 Signaling via Class IA PI3Ks

Once activated, Class I PI3Ks are recruited to the membrane where they initiate a cascade of downstream signaling events through the phosphorylation of the 3'OH group of phosphatidylinositol-(4, 5)-diphosphate (PIP_2) to yield the lipid second messenger phosphatidylinositol (3,4,5) - triphosphate (PIP_3). Although the p110 catalytic subunits can phosphorylate both PI(4)P and PIP_2 *in vitro*, PIP_2 is the preferred substrate at the cell membrane [28]. PIP_3 in turn, interacts with pleckstrin homology (PH) domain-containing target proteins on the inner leaflet of the plasma membrane.

These include serine-threonine kinases, tyrosine kinases, GTPase-activating proteins, signaling adapter molecules and cytoskeletal molecules. Some of the effector proteins are able to bind to both PIP_2 and PIP_3. Activation of these proteins promotes a wide range of cellular responses such as cell cycle progression, growth, apoptosis, cell differentiation and migration (**Figure 1.2**).

The best studied of these proteins is Akt (also known as protein kinase B (PKB)), which can phosphorylate a large number of downstream substrates, thereby controlling many cellular functions [55]. The binding of PIP_3 to the PH domain is considered as the rate-limiting step for activation of Akt, and upon binding prompts the translocation of Akt to the membrane where is it fully activated by other kinases [28]. Akt activation requires phosphorylation by phosphoinositide-dependent kinase 1 (PDK1) at Thr^{308} and subsequent phosphorylation by mTOR Complex 2 (mTORc2) at Ser^{473} [56, 57]. Activation of Akt observed in peripheral T cells is dependent on p110δ and is often used as a measure for p110δ activity [58, 59]. A key effector substrate of Akt is mTOR, as Akt activation inhibits tuberous sclerosis complex TSC1/TSC2 (hamartin–tuberin) via phosphorylation, inhibiting the GTPase-activating function (GAP) of TSC1/TSC2 complex, which is unable to bind to RAS homolog enriched in brain (RHEB) that subsequently leads to the activation of mammalian Target of Rapamycin (mTORc1). In turn, mTORc1 activates ribosomal S6 kinase (S6K) and 4E binding protein 1 (4E-BP1) which results in increased protein translation, growth and proliferation. The PI3K/mTORc pathway plays an important role in promoting glucose metabolism required for $CD4^+$ T cell differentiation and presumably transition from effector to memory $CD8^+$ T cells [60]. However, while PDK1 has been shown to be necessary for mTORc1 signaling in activated $CD8^+$ T cells *in vitro*, this has shown to occur in an Akt independent manner. In activated $CD8^+$ T cells, mTORc1 activity is not blocked by the disruption of PI3K/Akt signaling by using various pharmacological and genetic strategies (Macintyre et al 2011). A PI3K/Akt independent pathway mediated by PDK1 and mTORC1 are crucial in controlling the expression of HIF1 (hypoxia-inducible factor 1) transcriptional complex. This mTORC1-HIF1 complex is important for sustaining glucose metabolism and glycolysis in $CD8^+$ effector T cells, that in turn control the expression of various molecules involved in $CD8^+$ T cell function and differentiation. These include glucose transporters, glycolytic enzymes, cytolytic effector molecules and T cell trafficking receptors (Finlay et al 2012).

These findings suggest that inactivation of TSC and subsequent mTORc1 activation requires another kinase other than Akt [61]. TSC2 can also be inhibited by ERK and other kinases, and therefore mTOR can be activated independently of PI3K [62]. mTORc1 exerts negative feedback inhibition on PI3K through its phosphorylation of S6K and, as a consequence, mTOR inhibition can lead to increased PI3K activity [63].

Phosphorylation of glycogen synthase kinase 3-β (GSK3β) by PI3K mediated signalling inhibits its activity. GSK3β has regulatory functions in different pathways that include cell cycle progression and glucose metabolism, along with regulating signalling pathways involved in T cell development such as Wnt, Hedgehog and Notch signalling (schoreder et al 2013, Jope et al 2007) . Forkhead box O (Foxo) transcription factors are the most evolutionary conserved downstream effectors of Akt, which include Foxo1, 3, 4 and 6 in mammals. Akt translocates to the nucleus and phosphorylates Forkhead box O (Foxo) transcription factors, resulting in the dissociation of Foxo from DNA, sequestration in the cytoplasm and subsequent degradation. Akt dependent phosphorylation of Foxo in the nucleus creates a 14-3-3 binding site, which upon binding to Foxo covers the nuclear localisation signal (NLS) that prevents nuclear translocation [64]. Foxo transcription factors control the transcription of many genes involved in cell cycle regulation, cell proliferation, apoptosis, migration and trafficking, such as: IL-7R, p27kip, Fas ligand, Bim, IkB and TRAIL (tumour necrosis factor-related apoptosis-inducing ligand). By inducing the expression of IL-7Rα , Foxo supports the survival of T cells and by promoting the expression of CCR7, CD62L and Sphingosine-1-phosphate receptor 1 (S1P1), can influence T cell trafficking [65].

Other PH domain-containing proteins also include the Tec (tyrosine kinase expressed in hepatocellular carcinoma) family protein tyrosine kinases that contains five members. Three Tec kinases that are expressed in T lymphocytes are IL-2 inducible T-cell kinase (Itk) highly expressed in naïve T cells and thymocytes, the other two are resting lymphocyte kinase (RLK) and Tec [66]. Itk , an important member of TCR mediated signaling is activated by the Src kinase Lck and the adaptor protein SLP-76, that once activated, phosphorylates PIP_2 to produce phospholipase C-γ1 (PLC-γ1), which induces inositol-1,4,5-trisphosphate (IP_3) and diacylglyerol (DAG) [67]. IP_3 leads to increased intracellular calcium (Ca^{2+}) levels that causes downstream activation of transcription factors including nuclear factor of activated T-cells (NFAT) [68]. DAG activates two signalling pathways, one of which is the Protein Kinase C (PKC) pathway

that leads to the activation of nuclear factor-kappaβ (NF- κB) and c-Jun amino-terminal kinase (JNK), The other one is the activation of mitogen activated protein kinase (MAPK) which activates extracellular signal regulated kinase (ERK) [69, 70]. In B cells, BTK fulfills a similar role [71]. Itk deficient mice have defects in T cell development, reduced numbers of mature thymocytes, reduced cell proliferation and compromised T cell activation. Additionally these mice have defective Th2 and Th17 generation, while maintaining the ability to develop Treg [68].

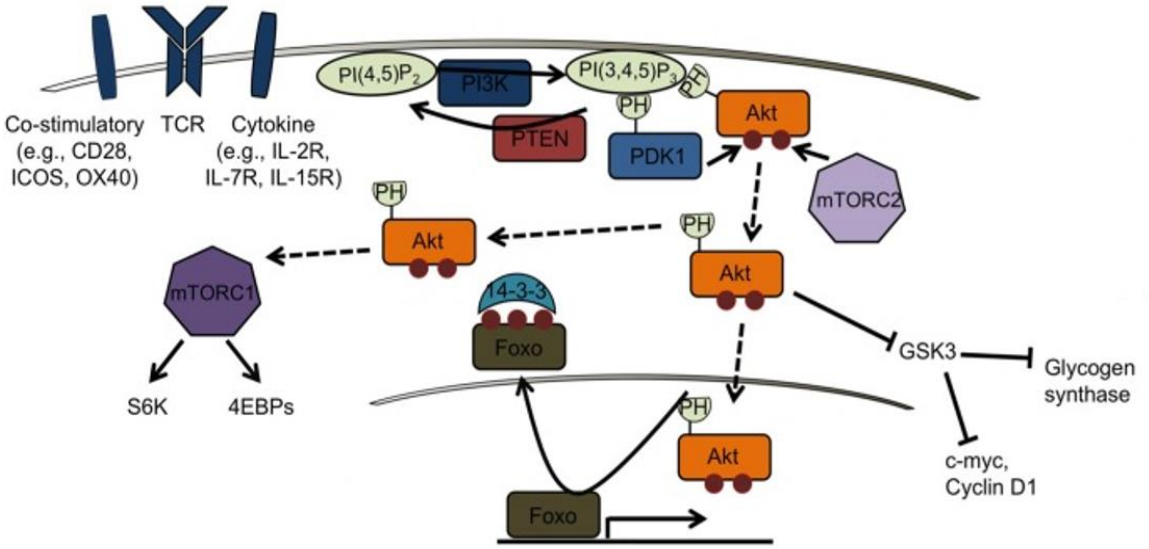

Figure 1.2: PI3K signalling in T cells

Signals from TCR, co-stimulatory molecules, cytokines or chemokines leads to activating PI3K pathway in T cells through the binding of the p85 regulatory subunit to a phosphorylated tyrosine residue. At the plasma membrane, the catalytic subunit p110 phosphorylates PIP_2 to form PIP_3, which acts as a secondary messenger for the activation of a range of protein kinases such as PDK1 and Akt. Full activation of Akt requires phosphorylation by PDK1 and mTORc2. In the cytosol, Akt phosphorylates and inhibits TSC1/2, a negative regulatory complex of mTORc1, which in turn promotes mTORc1 mediated protein synthesis and cell growth through modulating S6K and 4E-BP1. Cytosolic Akt by inhibiting GSK3β, regulates glucose metabolism. Nuclear Akt triggers the nuclear exclusion of FOXO transcription factors that are important for cell proliferation and survival. Regulation of PI3K activity by PTEN results in removal of a phosphate group from PIP_3 to form PIP_2. Figure adapted from

1.3.3 Regulation of PI3K signaling

Several different phosphatases regulate the PI3K pathway. The main one is phosphatase and tensin homologue (PTEN) that removes the 3' phosphate from PIP_3 to generate the original substrate PIP_2. Mutations in PTEN have been associated with

multiple cancers in humans that includes T cell malignancies [72]. Cells that lack PTEN display increased levels of PIP_3 as a result of increased PI3K activity [73]. TCR stimulation alone in the absence of PTEN results in hyperactivation of the PI3K pathway, thus implying that negative regulation by PTEN enforces the requirement of co-stimulation [74]. Conditional deletion of PTEN in T cells leads to the development of aggressive $CD4^+$T cell lymphoma and autoimmunity [75]. Recently it has been shown that PTEN phosphatase activity might be necessary for the prevention of T-cell lymphomagenesis [76]. T cells from PTEN heterozygous mice are hyperproliferative and resistant to activation induced cell death (AICD) [77]. Loss of PTEN in mature T cells results in hypersensitive T cells in response to stimulation, with enhanced inflammatory, antibacterial, and antitumor responses [78]. Other phosphatases SHIP1 and SHIP2 (SH2 domain-containing inositol 5′-phosphatase 1 and 2), function by removing the 5' phosphate from PIP_3 to generate the lipid phosphatidylinositol (3,4)-biphosphate PI(3,4)P [79]. Deletion of SHIP1 results in lethal autoimmunity caused by the aberrant activation of T cells, B cells and myeloid cells [79]. Deletion of SHIP within the T cell compartment identified a role for this phosphatase in regulating Th1/Th2 lineage decisions in addition to limiting $CD8^+$ T cell cytotoxicity [80].

1.3.4 Role of Class IA PI3K in T cells

Activation of T cells

In T cells, activation of PI3Ks can be mediated by the TCR, costimulatory receptors such as CD28 and Inducible T-cell costimulator (ICOS), and by receptors for chemokines and cytokines [48]. The exact process by which TCR activation leads to Class IA PI3K activation remains uncertain. However, it is known that lymphocyte specific tyrosine kinase (Lck) phosphorylates immunoreceptor tyrosine-based activation motifs (ITAMs) present on TCR associated CD3 (cluster of differentiation 3) and ζ (zeta) chains. Once phosphorylated, the ITAMS act as docking sites, recruiting and activating ζ -associated protein (ZAP-70). ZAP-70 in turn phosphorylates and activates the adaptor molecules SH2 domain containing leukocyte protein of 76kDa and linker for activation of T cells (SLP-76) [48, 81]. Activation of PI3K downstream of co-stimulatory molecules such as CD28 is dependent on the cytoplasmic tail containing a YxxM motif. Upon activation, tyrosine phosphorylation of CD28 by Lck leads to the recruitment of the p110 subunits via the SH2 domains of the p85

regulatory subunits [82] . The ICOS cytoplasmic tail contains an YMFM motif that binds the p85α subunit of class IA PI3K. The p85-SH2 binding domain of PI3K binds to ICOS with higher affinity than to CD28 and has been shown to recruit the smaller p50α subunit [83, 84]. Using a knock-in mouse model where a mutation is present within the YxxM motif of ICOS ($ICOS^{Y181F}$), resulting in disruption of PI3K binding, leads to loss of T follicular helper cells and impaired germinal centre reactions, therefore suggesting that the engagement of this motif is essential for ICOS function [85] .

T cell development

Most of the research carried out on T cell function is focused mainly on p110δ and p110γ, as these isoforms are abundantly expressed in leukocytes. Determining a role of p110α and p110β in T cells has been proven difficult due to the embryonic lethality of p110α and p110β deficient mice. However, p110α isoform is also abundantly present in lymphocytes and studies using isoform specific inhibitors has shown that p110α isoform might play a role in certain T cell functions [86, 87]. In models in which p110α is deleted in T cells using either $CD2^{Cre}$ or $CD4^{Cre}$ showed no significant differences in thymus development [88, 89]. Additionally, these mice have increased $CD8^+$ T cell effector function, reduced expansion of iTregs, increased T responses and reduced tumour progression [89]. p110δ deficient and p85α double knockout mice have normal numbers of thymocytes, but p110γ deficient mice have decreased thymocyte numbers due a survival defect in DP cells. However, combined deficiency of both isoforms profoundly affects thymocyte numbers, with a block at the DN stage of T cell development, associated with reduced pre-TCR signaling and increased apoptosis within the DP population. The apparent redundancy of p110δ and p110γ during T cell development has been shown to be due to pre-TCR signals being mediated by p110δ, and a requirement of p110γ-dependent CXCR4 signaling during β-selection.

$CD4^+$ T cell differentiation

Following activation of naïve T cells, production of PI3K mediated PIP_3 is the first measurable intracellular event to take place. p110δ has been shown to be

fundamental for PIP_3 production upon TCR and CD28 stimulation, and in addition is required for subsequent phosphorylation of downstream effector proteins. There is ample evidence to suggest that p110δ is the crucial PI3K isoform involved in Th cell differentiation and cytokine production. A significant body of T cell functional studies, investigating the role of p110δ, has been carried out using mice that have a genetic modification in the kinase domain of the p110δ subunit, substituting an aspartate residue with an alanine (D910A), which produces a kinase-inactivated version of the protein ($p110\delta^{D910A/D910A}$, in this thesis referred to as $p110\delta^{D910A}$) [90]. Additionally, conditional p110δ knockouts have been generated using the Cre-loxp systems in different immune cells subsets and selective p110δ inhibitors are also in widespread use [91].

T cells from $p110\delta^{D910A}$ mice have defective proliferative responses to anti-CD3 and peptide antigen stimulation [58, 90]. Using $p110\delta^{D910A}$ mice and p110δ specific inhibitors results in reduced production of cytokines generated by Th1, Treg, Th2 and Th17 subsets [58]. For example, $p110\delta^{D910A}$ mice exhibited significantly decreased Th2 cytokine responses and were protected against eosinophilic airway inflammation [92]. In experimental autoimmune encephalitis (EAE), a model of multiple sclerosis that is Th17 driven, inhibition of p110δ led to reduce clinical symptoms, histopathology and cellular infiltration of cells into the CNS, therefore suggesting p110δ inhibition as a potential therapeutic strategy [93, 94]. However inhibition of p110δ does not fully block $CD4^+$ T cell proliferation or differentiation suggesting potential input from other Class I PI3Ks might be required [58, 95] .

The effect of p110δ on T cell differentiation could be partly explained by the dependency on mTOR, which forms part of the mTORc1 and mTORc2 kinase complex, as mTOR inhibition blocks differentiation into Th1, Th2, and Th17 subsets. On the other hand, $CD4^+$ T cells activated in the absence of mTOR signaling via rapamycin or genetic deletion of mTOR adopt a default $Foxp3^+$ regulatory cell phenotype indicating that mTOR signaling blocks Treg development [96]. T cell-specific deletion mouse models have been key in dissecting the specific roles of mTORc1 or mTORc2 in T cell responses. Mice with T cells deficient in Rheb, an upstream activator of mTORc1 signaling, have impaired Th1 and Th17 differentiation [96, 97]. Deletion of *Raptor*, an essential component of mTORc1 also led to impaired

generation of Th17 differentiation [98]. Alternatively, deficiency of *Rictor* or mTORc2 signaling led to impaired Th2 differentiation, but not Th1 or Th17 [97]. However, a conflicting study suggested that mTORc2 signaling was also required for Th1 and Th2 differentiation [99]. Therefore, it seems that both mTORc1 and mTORc2 complexes play important roles in Th differentiation, with conflicting results with regards to the precise roles.

Regulatory T cells

As described in section 1.2.1, Tregs play an important role in peripheral tolerance induction. p110δ^{D910A} mice have increased numbers of Tregs in the thymus but reduced numbers in the peripheral organs, suggesting a role of p110δ in maintaining Tregs in the periphery [100]. Foxp3 expression is controlled by Foxo transcription factors Foxo1 and Foxo3a, and phosphorylation of Akt inactivates Foxo proteins by enforcing their exclusion from the nucleus. Foxo transcription factors directly activate Foxp3 expression by binding to the Foxo consensus binding sequence in the Foxp3 promoter [101]. Mice with T cell specific deletion of Foxo proteins developed a fatal inflammatory disease associated with compromised Treg cell differentiation, therefore suggesting a role for PI3K signaling in inhibiting Foxp3 induction [4]. Thymic development of natural Tregs (nTregs) could be attributed to regulation of Foxo by p110δ, as combined deletion of Foxo1 and Foxo3 results in severe defect of Foxp3^{+} nTregs [101, 102]. However, in these mice, the peripheral Tregs are only modestly reduced, suggesting that development of thymic Tregs require Foxo but are are not absolutely required for Foxp3 expression and maintenance [102]. Tregs from p110δ^{D910A} mice are impaired in their ability to suppress proliferation of CD4^{+} T cells and secrete the anti-inflammatory cytokine IL-10 [100]. In addition, these mice develop spontaneous colitis and are resistant to *Leishmania major* infections; however, p110δ^{D910A} mice are more susceptible to secondary *L. major* infections due to reduced Th1 cells [103]. Our group has shown that inhibition of p110δ in Treg cells enhanced killing of tumors by unleashing potent CD8^{+} T cell mediated cytotoxic responses [104].

Conditional deletion of PTEN in Tregs results in spontaneous autoimmune lymphoproliferative disease that is associated with excessive Th1, Tfh and germinal centre responses in mice [105, 106]. Uncontrolled PI3K signaling in these mice results in loss of CD25 expression and ultimately loss of Foxp3 expression as well. These

cells, termed exTregs, have a pathogenic phenotype associated with the expression of proinflammatory cytokines [105, 106].

T follicular helper cells

T follicular helper (Tfh) cells are a subset of T cells involved in facilitating the germinal centre reaction thereby supporting the B cells mediated immune response. Tfh cells rely on the expression of CXCR5 for migrating into the B cell follicles and require B cell lymphoma 6 (Bcl-6) for their development, expression of which could be further enhanced by IL-21[107-109]. The ability of the T-cell costimulatory receptor, ICOS to induce the generation of Tfh cells and GC reactions, antibody class switching and antibody affinity maturation is dependent on p110δ [85, 110]. Importantly, increased PIP_3 levels through PTEN deletion in activated T cells has the converse effect of increasing Tfh cells, GC B cells and antibody affinity [110]. ICOS via activating the PI3K pathway leads to inactivation of Foxo1 that leads to enhanced Bcl-6 expression resulting in increased Tfh differentiation [111]. ICOS can regulate the novel Tfh transcription factor Krüppel-like factor 2 (KLF2) that serves to restrain Tfh generation, via Foxo1 [112, 113]. KLF2 can hamper efficient Tfh cell production by promoting the expression of the trafficking receptor S1PR1. Furthermore, KLF2 induced expression of Blimp-1, which represses Bcl-6, leads to impaired Tfh generation [113]. T cell specific deletion of Foxo1 also leads to accumulation of Tfh cells, spontaneous formation of GCs and anti-DNA antibody production , therefore further backing up its role in negatively regulating Bcl-6 expression [102]. Additionally, inhibition of mTORc1 via rapamycin or RNA interference in an acute *Lymphocytic choriomeningitis virus* (LCMV) model resulted in inhibition of Tfh responses along with reduced GC B cell formation and long-term antibody responses [114]. These results therefore highlight that control of PI3K signaling is important in controlling the GC reactions, as either inhibition or hyperactivation via downstream effector proteins can be detrimental.

1.3.5 $CD8^+$ T cells

$CD8^+$ T cells deficient in p110δ have been associated with reduced expression of cytotoxic components related to $CD8^+$ T cell functions such as granzyme A , granzyme B, perforin, TRAIL, IFNγ and FasL [104, 115, 116]. Initial reports of p110δ playing a

role in T cell memory formation came from phenotyping of p110δ^{D910A} mice based on the expression of the adhesion molecule CD44 that can differentiate between naïve and memory T cells [117]. p110δ^{D910A} mice had fewer CD44^{high} CD8 and CD4 T cells suggesting p110δ^{D910A} have fewer memory cells [118]. In response to infection with *Listeria monocytogenes* (Lm), a Gram-positive intracellular bacterium, and Influenza A virus, CD8$^+$ T cells deficient of p110δ activity have impaired magnitude of the primary response as detected by reduced expansion of antigenic-specific CD8$^+$ T cells but were able to clear bacterial load more efficiently owing perhaps to greater innate immune responses [115, 119]. In contrast to *in vitro* data, CD8$^+$ T cells from p110δ deficient mice have a normal cytokine and cytotoxic prolife that is required for killing of pathogen infected cells or tumours and additionally are not defective in long term memory formation [104, 115, 119].

Increased T cell stimulation enhances the expression of transcription factors such as T-bet that play a role in promoting SLEC differentiation, that conversely leads to reduced expression of EOMES and T cell factor 1 (TCF-7/TCF1) that play a role in memory formation [23, 120]. In line with this, increased Akt activation in response to LCMV infection led to a phenotype of enhanced effector function and differentiation of CD8$^+$ T cells into terminal effectors [22, 121]. In addition, severely impaired memory CD8$^+$ T cell formation with reduced protective immunity was observed due to altering specific signalling pathways of Foxo, mTOR, and Wnt/b-catenin that are involved in differentiation and survival of cytotoxic T cells [121]. Notably, deletion of Pten, a crucial negative regulator of Akt–mTOR signaling, does not cause significant defects in memory formation in response to acute LCMV infection [122].

Foxo transcription factors, especially Foxo1, has been implicated in promoting memory CD8$^+$ T cell formation in response to different bacterial and viral pathogens. In response to acute LCMV infection , Foxo1 was not required for the primary phase and displayed an enhanced effector phenotype , however Foxo1 deficient CD8$^+$ T cells were unable to upregulate memory associated genes and were incapable to expand upon reactivation [123]. Additionally, *Rao et al* demonstrated that IL-12 mediated inactivation of Foxo1 led to increased T-bet and that inhibition by rapamycin of T-bet expression was Foxo1 dependent. They also established that Foxo1 played an important role in switching CD8$^+$ T cells from an effector to memory phenotype through enhanced Eomes expression [124]. Similarly, in response to Lm infection in mice with

Foxo1 deletion in activated $CD8^+$ T cells, resulted in enhanced SLEC differentiation with reduced MPEC generation. *C*onsequently these mice had poor recall responses associated with reduced expression of Foxo1 activated target genes that included Bcl2*,* Sell*,* Ccr7*, and* Tcf7 [125]. In contrast to Foxo1, studies that investigated the effect of Foxo3 in $CD8^+$ T cell responses to viral infections have shown that Foxo3 deficiency results in enhanced effector and memory $CD8^+$ T cells responses due to reduced expression of pro-apoptotic molecules such as BIM and PUMA during the various phases of response associated with increased numbers of MPECs and memory subsets compared to WT mice [126-130]. Foxo3 was shown to also enhance $CD8^+$ T cell responses by regulating inflammatory cytokine production such as IL-6 by Foxo deficient dendritic cells leading to increase T cell viability[130] . Together these studies highlight an important role for Foxo1 in establishing and maintaining the $CD8^+$ T cell memory programme that is essential for the formation of long-lived memory cells.

Substantial evidence is available implicating mTORc1 in limiting the differentiation of memory $CD8^+$ T cells. During the primary expansion phase following acute LCMV infection, treatment with low doses of rapamycin led to enhanced generation of MPECs and subsequently memory T cells at the expense of effector cell formation [131]. Additionally this effect appears to be $CD8^+$ T cell intrinsic since silencing *Raptor* expression in $CD8^+$ T cells largely recapitulated the effects of rapamycin treatment on memory formation [131]. Activation of mTORc1 activity is able to promote differentiation of $CD8^+$ T cells into terminal differentiation at the expense of forming memory $CD8^+$ T cells via the increased expression of T-bet whilst reducing expression of Eomes [132]. Mice with a T cell specific deletion of TSC2, a negative regulator of mTORc1 resulted in generation of highly glycolytic and potent effector $CD8^+$ T cells. These cells were unable to transition into a memory state and adopted a terminally differentiated phenotype due to constitutive mTORc1 activation [133]. Tuberous sclerosis complex 1 (TSC1) deficient T cells have been shown to mount normal primary responses but are impaired in their ability to transition into memory cells and are associated with defective recall responses to Lm expressing chicken ovalbumin (LM–OVA) [134]. Conversely, mTORc2 inhibition resulted in enhanced generation of memory $CD8^+$ T cells [133] . mTORc2 deficient mice favour memory formation with normal effector functions and mount more potent recall responses owing to enhanced

Eomes and Tcf-1 upregulation, repression of T-bet, enhanced mitochondrial spare respiratory capacity, and fatty acid oxidation. mTORc2 deficiency promotes $CD8^+$ T cell memory generation via nuclear accumulation of Foxo1 [135]. Overall, these studies illustrate that mTORc1 deficiency promotes effector $CD8^+$ T cell responses at the expense of memory $CD8^+$ T cell formation, whereas mTORc2 promotes memory formation without influencing the effector response.

mTORc activity has been shown to play a role in the response to chronic infection, a situation where antigen persists leading to dysfunctional T cells, characterised by the increased expression of different co-inhibitory receptors and reduced effector cytokine function [136]. In response to a chronic model of LCMV, Akt and mTOR signaling has shown to be impaired resulting in increased Foxo1 activity, subsequently causing upregulation of the inhibitory receptor, programed cell death protein 1 (PD-1) [136]. PD-1 blockade resulted in increased mTOR activity in virus specific $CD8^+$ T cells, additionally the therapeutic effects of PD-1 was abrogated due to inhibition of mTOR by rapamycin. This study shows a potential positive feedback pathway involving Akt/mTORc/Foxo1 in desensitizing antigen specific $CD8^+$ T cells to promote their survival during persistent infections.

Collectively all these studies highlight the PI3K pathway as an integral signaling pathway in the Akt/mTOR/Foxo axis in the involvement of memory and effector formation function following infection.

Due to the role of PI3Kδ in numerous immune cell functions, it is involved in a range of different diseases that include autoimmune inflammatory diseases such as RA, systemic lupus erythematosus (SLE), chronic lymphocytic leukemia (CLL). Recently has been associated with mutations leading primary immunodeficiency (PID).

PID is a group of heterogeneous disorders characterised by dysregulated functions of the immune system. The majority of PIDs are due to inherited loss of function mutations in genes involved in immune system development or function.

1.4 Activated PI3Kδ syndrome (APDS)

In 2013, two reports using whole exome sequencing described dominant heterozygous gain of function (GOF) mutations in the PIK3CD gene encoding the

p110δ isoform [137, 138]. At that time , it was termed activated phosphoinositide 3-kinase δ syndrome (APDS) or as p110δ-*a*ctivating mutation causing *s*enescent T cells, lymphadenopathy, and immunodeficiency (PASLI), now known as APDS1 due to subsequent mutations found in the p85α gene resulting in a similar clinical phenotype and called APDS2 [139]. In the first report APDS patients were identified by *Angulo et al* using whole exome sequencing in 17 patients by screening cohorts of PID patients with a high occurrence of recurrent chest infections and bronchiectasis [138]. The activating mutation identified results in a glutamic acid to lysine substitution at residue 1021 (E1021K) of the kinase domain in the p110δ protein [140]. The E1021K mutation leads to increased PI3K activity by enhancing association of the catalytic subunits with the membranes and by facilitating augmented phosphorylation of PIP_2. The catalytic subunits have been shown to have higher affinity for lipid vesicles compared to wild type p110δ.

Patient-derived T lymphocytes produced increased levels of PIP_3 associated with increased AKT phosphorylation and hyperactivation of mTOR post stimulation [138, 141]. Reports of an E1021K mutation in the PIK3CD gene was reported in 2006 in a patient diagnosed with primary B-cell immunodeficiency, however the nature of the mutation was not explained [142]. The E1021K mutation is analogous to the oncogenic mutation H1047R in the p110α subunit, leading to increased PI3K activity due to increased association with membranes and resulting increased phosphorylation of the substrate PIP_2 [143, 144]. Following on from this, Lucas *et al* also reported a series of PID patients demonstrating the same disease phenotype, but termed PASLI [137]. In addition to the E1021K mutation identified, two further mutations were reported,N334K and E525K within the C2 and helical domain of the p110δ protein respectively [141]. Since these initial reports, further novel mutations have been identified within the PIK3CD gene leading to APDS which are highlighted in Figure 2 [139, 145-150]. However, the E1021K mutation in the C terminal lobe of the p110δ protein remains the most prevalent mutation [139].

(A)

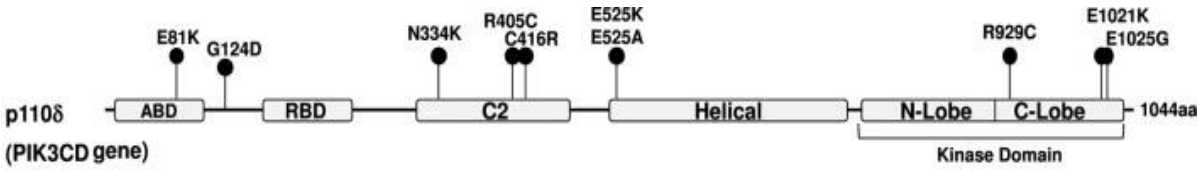

(B)

cDNA position	Mutation	Amino Acid

Figure 1: (A) Schematic of p110δ protein domains with positions of patient mutations highlighted. **(B)** APDS mutations within the PIK3CD gene. Figure adapted from [139]

Clinical symptoms

Overall, the clinical presentation of APDS patients is variable, but most patients (~98%) suffer from recurrent lower and upper respiratory infections. These respiratory tract infections include bacterial pathogens such as *influenzae* and *Streptococcus pneumoniae* along with variable response to polysaccharide vaccination [137, 138, 151]. Over time, these infections can be severe, leading to end-organ damage such as bronchiectasis. Some of the APDS patients (75%) also develop lymphoproliferative disease, which commonly presents as lymphoid hyperplasia, lymphadenopathy and splenomegaly and in about 20% of cases lymphoma [151]. Half of the cases reported (49%) also suffer from recurrent chronic viral infections caused by the Herpes group viruses, commonly Epstein-Barr virus (EBV) or Cytomegalovirus (CMV) infections, demonstrating that the patients have an inability to control these infections [137, 151]. Also, a subset of patients that were heterozygous for the PIK3CD mutation associated with hyper IgM syndrome, led to developments of non-EBV associated malignancies [145]. Autoinflammatory manifestations that include glomerulonephritis, arthritis, and colitis also occurred in approximately 34% of the cases in a cohort of 53 patients [151]. Surprisingly, neurodevelopmental delay also occurs in small proportion of patients suggesting a role for PI3Kδ in the central nervous system [151]. B cell immune phenotyping of APDS patients include progressive B cell lymphopenia, elevated IgM

and low IgG serum levels, increased circulating transitional B cells, probably due to abnormal B cell maturation in the bone marrow, immunoglobulin class switch recombination defect (CSR-D) and impaired vaccine responses [151]. A minority of these patients develop B cell lymphomas, suggesting that constitutively active p110δ predisposes to malignancies [141, 150, 152].

T cell phenotype in APDS patients

The main clinical indicator of abnormal T cell function in APDS patients is herpes viral infection. These patients have an inability to control viremia with EBV and CMV, which has been reported to occur in nearly half of the described cases. Additionally there was no association between herpes viruses infections and reduced Th or cytotoxic T cells, implying that a functional defect might be responsible for this susceptibility [151]. Typically, peripheral blood analysis in patients reveal a reduction in $CD4^+$ T cell counts and increased numbers of effector/effector memory $CD8^+$ T cells. These patients present with low numbers of naïve T cells, impaired proliferative responses, defective cytokine production and an accumulation of highly differentiated activated/effector T cells at the expense of memory formation [137, 138, 151, 153]. In addition, $CD4^+$ and $CD8^+$ T cells were shown to be highly susceptible to activation induced cell death (ACID) following activation with anti-CD3 and anti-CD28, which could potentially limit their effector functions [138, 141]. However, T cell blasts that escaped apoptosis and expanded after activation *in vitro* showed increased production of IFNγ, TNFα and granzyme B [141] . APDS patients have been shown to express markers associated with both senescent and exhausted T cells [137, 153] . Total and virus specific $CD8^+$ T cells from APDS patients were shown to have increased CD57 expression and shortening of telomere length, which indicates T cell senescence [137]. Additionally, APDS patient T cells have been reported to have increased expression of T cell exhaustion markers such as PD-1 , CD160 and 2B4, and *in vitro* PD-1 blockade was shown to reverse the T cell exhaustion phenotype [153, 154]. Recently Edwards et al showed increased expression of surface markers associated with senescence and exhaustion on $CD8^+$ T cell subsets in in a large cohort (n=39) of patients with APDS. Moreover, T cells displayed increased expression of cytotoxic markers such as granzyme B and perforin but impaired cytotoxicity, reduced expression of IL-2 and increased apoptosis [155]. This suggests that GOF mutations within the PIK3CD gene

might predispose T cells to undergo exhaustion in addition to immune senescence thereby contributing to their inability to clear virus. Whether one contributes to the other or more factors are involved remains to be determined. Additionally alterations in other immune cells subsets such as natural killer (NK) cells and B cells may also contribute to the inability to clear EBV [154, 155].

Other mutations related to APDS

Subsequent to the reports of gain of function mutation within the PIK3CD gene, dominant heterozygous gain of function splice site mutations were identified in the PIK3RI gene encoding for the regulatory subunit p85α. These also led to a similar disease phenotype consistent with the hyperactivating mutations in the PIK3CD gene [137, 156-160] . This immunodeficiency has been termed APDS2 or PASLI-R1. These patients have various mutations in p85α , with the most common one resulting in a splice variant that removes exon 11 resulting in deletion of amino acids 434-475 of p85α [137, 157]. The mutant p85α protein expressed in patients cells interrupts inhibitory interactions with p110δ, and due to loss of inhibitory contacts drives constitutive PI3K signaling [157]. Additionally the p85α splice variant leads to a selective activation of p110δ with insignificant effects on p110α activity, as all inhibitory interactions between p85α and p110δ were found to be disrupted with only partial disruptions of p85 mediated inhibitory interactions with p110α [161]. Growth retardation is a common symptom amongst APDS2 patients, and may be due to the association of dominant heterozygous mutations in PIK3R1 with SHORT syndrome (characterised by short stature, hyperextensibility of joints, hernia, ocular depression, Rieger anomaly and teething delay) [162-164]. However, the molecular mechanism of disease involves downregulation of the PI3K/Akt/mTOR pathway [162].

Reports of patients with a heterozygous loss of function mutation in PTEN gene have been reported to cause APDS like immunodeficiency due to aberrant PI3K dependent activation of lymphocytes and have been termed APDS like syndrome (APDS-L). Loss of PTEN function leads to suppression of the inhibitory function of PI3K which augments PIP_3 levels leading to increase phosphorylation of the Akt/mTOR/S6 pathway [146, 165]. Additionally a milder form of APDS has been associated with Cowdens syndrome caused by a heterozygous loss of PTEN, that is normally

associated with hamartomatous polyposis of the gastrointestinal tract, mucocutaneous lesions and increased risk of developing certain types of cancer [166]. In addition, there have been two groups that have reported patients with heterozygous mutations within the cytotoxic T lymphocyte antigen-4 (CTLA-4) gene displaying similar symptoms [167]. CTLA4 and CD28 play an important role in inhibiting and enhancing T cell activation respectively, and as both can lead to the activation of the PI3K pathway; collectively these mutations highlight the important role played by PI3Ks in immune homeostasis [168].

Current treatment strategies

Patients harboring these hyperactive mutations have been treated with intermittent or regular intravenous antibiotics, antiviral prophylaxis and immunoglobulin replacement therapies due to reduced IgG levels and poor vaccine responses [169]. Reports of one patient treated with rapamycin showed an improved circulating T cell profile, however the side effect profile of rapamycin might limit its use in the longer term [137]. Selective p110δ inhibitors such as IC87114 and CAL-101 (clinically known as Idelalisib) reduced the activity of the mutant p110δ enzyme *in vitro*, suggesting a therapeutic approach for APDS patients [138, 161]. The therapeutic potential of using selective p110δ inhibitors is an ideal option, given the recent approval of Idelalisib for treatment of chronic lymphocytic leukemia (CLL) and non-Hodgkin lymphoma [170, 171].

Currently, in APDS patients, two phase-II clinical trials are ongoing to study the pharmacokinetics and pharmacodynamics effects of different PI3Kδ inhibitors. The clinical trial that is sponsored by GSK uses an inhaled PI3Kδ inhibitor called nemiralisib (GSK2269557) [139]. The other clinical trial NCT02435173 sponsored by Novartis, is investigating the effect of an oral PI3Kδ inhibitor leniolisib. Initial data for the Novartis clinical trial in 6 APDS patients has reported that leniolisb was well tolerated, led to improvement in cellular immune dysfunction and reduction in lymphoproliferation [139, 172]. In terms of immune cell phenotyping, the study reported that the levels of circulating transitional and naïve B cells were normalised, along with reduced levels of elevated serum IgM levels. Reduction in exhausted ($PD\text{-}1^{+}$) and senescent ($CD57^{+}$) $CD4^{+}$ T cells as well as different inflammatory markers such as $IFN\gamma^{+}$, TNF^{+}, $CXCL13^{+}$ and $CXCL10^{+}$ [172]. Additionally, a 39% and 40% reduction in lymph nodes sizes and spleen volumes was seen [172]. Initially the

patients were part of a 12 week within subject dose escalation study where leniolisib was administered twice daily. This study has now continued to long term treatment with patients receiving leniolisib for over 9 months, and it has been well tolerated with no significant adverse events detected [172]. This study validates targeting PI3Kδ as a therapeutic approach and implies that an oral inhibitor might be more effective against systemic immune defects whereas inhaled inhibitor might be more effective in patients with severe respiratory infections.

In support of T cell exhaustion in APDS patients, a recent study published by Wentink et al demonstrated that inhibition of PD-1 signaling led to an increase in virus specific $CD8^+$ T cell proliferation and cytokine production in APDS patients [153]. Therefore, denoting that $CD8^+$ T cells in APDS undergo exhaustion and may contribute to the persistent herpes virus infections, and furthermore raising the possibility of using checkpoint inhibitors as a treatment strategy in combination with other therapies to help control the persistent viral infections.

In this thesis, I will be presenting data using three different infection models to look at the effect of hyperactive p110δ activity in $CD8^+$ T cells in response to acute and chronic infections. The models are discussed below in detail.

1.5 Mouse infection models

1.5.1 Listeria monocytogenes

Listeria monocytogenes (Lm) is a gram positive intracellular bacterium, that is able to infect a large range of species [173] . The ability to grow at low temperatures and being resistant to multiple environmental stresses such as low pH, allows Lm to alternate between surviving in the environment, and infecting mammalian hosts [173].

The natural infection route of Lm is targeting the intestinal epithelium followed by invasion of the lamina propria. Lm then disseminates to the rest of the body via the lymph and blood to target organs for example, the spleen and liver . Through this route of infection, Lm initially infects the intestinal epithelial cells through binding of Internalin A (InA) to the cell membrane receptor, E-cadherin. Thus, Lm can enter cells via receptor-mediated endocytosis [173, 174]. However, this utilisation of InA by Lm has been observed in humans but not in other species including mice [175]. This is due to

a single amino acid change within the EC1 domain of InA allowing species specificity of InA [175, 176]. The generation of transgenic mice with selective human InA expression, has allowed this barrier to be overcome [177]. However, the ability of InA deficient mice to still be able to invade the intestinal epithelium in mice, suggests InA is not imperative for invasion of the intestinal barrier by Lm [178, 179].

As mentioned above, after moving past the intestinal barrier, Lm proceeds to disseminate to the rest of the body, where it can enter macrophages via active phagocytosis [173]. Through this way, Lm is able to then travel to target organs such as the liver, where it can enter hepatocytes via InB, which binds to hepatocyte growth receptor, c-Met [180, 181].

Upon uptake of Lm by the host cell, the bacteria escapes the vacuole it is in, into the cytosol via listeriolysin O (LLO) and two different forms of phospholipase C, a phosphatidylinositol-specific phospholipase C (PI-PLC),and a broad-range phospholipase C (PC-PLC) [182]. Moreover, in mice it has been found that Lm further promotes it's vacuole escape utilising the peptide pheromone-encoding lipoprotein A (PplA), specifically, the encoded putative peptide pheromone pPplA [183]. The virulence factor LLO is imperative for Lm pathogenesis and triggering the immune response against the bacteria [184]. Once Lm has escaped into the host cytosol, it expresses other virulence factors and undergoes replication. Actin assembly-inducing protein (ActA) is another important virulence factor. ActA is an actin binding protein allowing Lm to move inside the host cell using the actin machinery of the cell by forming "actin comet tails" [175, 185]. ActA is also important for the spread of Lm into neighbouring cells, promoting dissemination [175]. For this reason, only cellular immune responses are effective at killing Lm since antibodies cannot gain access to it. Genetically modified strains of Lm lacking ActA are highly attenuated, indicating movement of Lm is essential for its virulence [175, 185] .

Many mouse models have been established for the studying immune responses to Lm [179]. The ability to perform epitope prediction and thus create recombinant Lm strains expressing epitopes of different pathogens allows detailed studying of antigen-specific $CD8^+$ T cell responses. One example of this is the Lm-OVA strain, a recombinant Lm strain engineered to express the ovalbumin antigen allowing to track antigenic-specific T cell populations [186].

Regarding the immune response to Lm, many Pathogen Recognition Receptors (PRRs) are engaged in recognition of the bacteria. Toll like receptor 2 (TLR2) is found to recognise peptidoglycans, lipoteichoic acid and lipoproteins [187]. The importance of TLR2 has been shown by TLR2- deficient macrophages producing lower levels of pro-inflammatory cytokines such as, TNFα and IFNγ in response to *in vitro* Lm infections [187, 188]. Moreover, TLR2 deficient mice are found to be more susceptible to Lm infections [189]. Other TLRs recognizing bacterial ligands are likely to be implicated in recognition of Lm such as, TLR5 which binds flagellin [187]. It is also important to note that Lm recognition via TLRs is largely dependent on signaling via the adaptor protein MyD88, with MyD88-deficient mice found to very susceptible to Lm infections [190, 191].

Aside from TLRs, the intracellular NOD-like receptors (NLRs) are involved in the recognition of Lm. The ligand for NOD2 is muramyl dipeptide (MDP), which is found in both the peptidoglycan of gram positive and negative bacteria [187]. NOD2 deficiency has been linked to mice being more susceptible to oral Lm infections. This is due to the NOD2 deficiency in mice resulting in the abnormal development of peyers patches allowing Lm to move unrestricted across the peyer's patches, and in turn the intestinal epithelial barrier to disseminate more easily [192, 193]. Amongst the family members of NLRs, NALP3 is one of many involved in inflammasome formation resulting in proinflammatory IL-1β and IL-18 production [187]. NALP3 has been found to be activated by Lm, but the mechanism of activation is unclear [192]. Detection of Lm may also occur intracellularly via (stimulator of interferon genes) STING due to the presence of cyclic di-AMP produced via bacterial lysis [173]. This in turn, results in the production of interferons via the transcription factor IRF3 [173].

The innate cells involved in Lm infections include, neutrophils and macrophages. The antibacterial activity of neutrophils makes them important innate cells in response to Lm [194, 195]. However, their role is more pronounced in the liver and especially during a high dose Lm infection [196, 197]. The cells possess the ability to phagocytose bacteria and kill them via generation of reactive oxygen and nitrogen species [195, 198]. These cells are found to be recruited quickly to infection sites via proinflammatory cytokines such as, IL-6 amongst others [187]. Neutrophils also promote macrophage recruitment to infection sites via chemokines and cytokines, for

instance colony stimulating factor 1 (CSF-1), and exist as a source of TNF-α for mediating Lm clearance [187, 195, 197].

Macrophages are essential for clearance of Lm infections. Resident macrophages such as, Kupffer cells in the liver are amongst the early macrophages involved in the killing of Lm bacteria in mice, acting in a similar manner as neutrophils [187, 199]. macrophages also produce important cytokines such as TNFα and IL-12, which promote NK cell recruitment [200]. These NK cells in turn produce IFNγ which also leads to macrophage activation, and further increase their bactericidal activity [201].

The activation of the adaptive response to Lm relies on DCs, with the spleen a major site for antigen-presentation during Lm infections [202, 203]. The importance of DCs in Lm infections is evident in DC-depleted mice, which are unable to produce a $CD8^+$ T cell response to infection [204]. Antigen-specific $CD8^+$ T cells become activated via antigen-presentation on MHC Class I. Either direct antigen presentation or cross-presentation can activate $CD8^+$ T cells, with cross-presentation found to be more efficient [205, 206]. Moreover, secreted antigen is found to be more effective in $CD8^+$ T cell activation compared to non-secreted antigen [207]. Upon activation of $CD8^+$ T cells, these cells gain effector functions such as producing cytokines that include TNFα and IFNγ for mediating effective killing of Lm infected cells [187]. The peak $CD8^+$ T cell response occurs around day 7-8 post infection in mice infected via the intravenous route, with the contraction phase typically starting from day 10 onwards [208].

Clearance of Lm infections relies on a robust $CD4^+$ T cell response as well. $CD4^+$ T cells are activated in a similar fashion to $CD8^+$ T cells with antigen presentation occurring via MHC Class II. However, it is important to note that the route of infection in mice influences the Th subsets that $CD4^+$ T cells differentiate into [179]. Intravenous Lm infections are found to promote Th1 effector cells formation whilst intranasal infections are found to promote Th17 subset [209].

Whilst T cells play a role in mediating the adaptive immune response to Lm, innate immune cells play a greater role in mediating early clearance of the bacteria. This is evident from lymphocyte deficient mice (SCID, $Rag^{-/-}$, and nude), which are resistant to Lm [210-212]. Studies with these mice have revealed lymphocytes being detrimental to the early innate immune response to the bacteria [212]. This occurrence

was observed with lymphocyte apoptosis occurring during the early days of the infection [212]. This in turn stimulated IL-10 release from macrophages and DCs allowing inhibition of the immune response which increased susceptibility to the infection [212]. Moreover, there is evidence to suggest type I IFNs and LLO may play a role in influencing this occurrence of lymphocyte apoptosis [213-215].,

It is also important to note that the route of infection influences the presence of the activated $CD4^+$ and $CD8^+$ T cells because this alters the main site of infection. Intravenous Lm infections result in the T cells migrating to the spleen and liver , whilst with intranasal Lm infections, T cells are found mostly in the lamina propria, the intestinal epithelium and liver [216].

Upon resolution of infection, the contraction phase occurs, resulting in only memory cells remaining. Reactivation of these cells upon secondary infection will result in a more robust and potent immune response. The adaptive immune response to LM is largely a T cell mediated response with B cells playing a minor role. For instance, B cells have been shown to be important in the maintenance of $CD8^+$ T cell memory generated in response to Lm infections [187, 217].

1.5.2 Influenza A virus

Influenza virus is a negative sense sRNA virus belonging to the *Orthomyxoviridae* family. There are four main types: A, B, C and recently discovered D [218-220]. Influenza A will be focused on here and denoted as “Influenza” in this thesis. Many subtypes of influenza A exist based on differences in haemagglutinin (HA) and neuraminidase (NA) [219]. These are the two major surface glycoproteins expressed by the virus, and are important for mediating viral entry via targeting sialic acid expressed on target host cells [219-221]. So far, 16 HA and 9 NA subtypes have been discovered circulating in animals and humans [220]. Concerning influenza’s structure, it has a lipid envelope on which the surface glycoproteins HA and NA are found, alongside the matrix (M2) ion channels which transverse the lipid envelope [219, 220]. This envelope overlaps a matrix of M1 proteins, which encase the virion core. Within the virion core, the nonstructural protein (NS2) and the ribonucleoprotein (RNP) complex is found [219]. This RNP complex consists of the viral RNA segments with the nucleoprotein and also the RNA-dependent RNA polymerase [219].

Animal models have played an important role in elucidating the immune response to influenza. influenza is not a common mouse pathogen, but serial passaging has allowed many strains to be utilised to establish useful influenza mouse models [222]. Amongst the multiple influenza strains used in mice, three will be discussed here: A/Puerto Rico/8/1934 (H1N1) (PR8) or A/WSN/1933 (H1N1) (WSN) and A/Hong Kong/1/1968 (H3N2) (X31) mice strains [222]. The H1N1 PR8 strain is derived from a human isolate in the 1930s [222, 223]. Serial passaging of this parent strain in mice has produced subsequent variants, which are similar in antigenicity to the parent strain, whilst still differing on expression of specific antigenic components [223]. It is a virulent strain as demonstrated by death in mice usually within in 8 days post infection, with higher viral load observed within 24 hours post infection compared to less virulent strains such as WSN [222, 224-226]. It is important to note that pathogenicity of different PR8 strains is also influenced by host and viral factors [227]. Similar to PR8, WSN strain is also a H1N1 strain originating from the 1930s but with reduced virulence compared to PR8 [222]. The WSN strain is a variant derived from the mouse brain passage of the A/WS/33 (H1N1) (WS) virus. A key difference between this strain from the parental strain is NA structure, which seems to have a preference for smaller substrates compared to that of the parental strain [228]. This in turn influences it's virulence via the role it plays for HA cleavage; thus to the ability of the virus to replicates in various tissues [229]. The X31 strain is of a different influenza subtype to the PR8 and WSN strains and is less virulent compared to the PR8 strain [222]. The strain is compiled of two subtypes with having the six internal genes of the PR8 strain, whilst the HA and NA genes are derived from the A/Aichi/2/1968 strain [222, 230, 231].

In mice, intranasal infection with influenza results in infection of the epithelial cells of the bronchi and the alveoli expressing the target, sialic acid [219, 222]. As influenza is cytopathic, the infection can result in severe lung damage, but pathogenesis of the infection is influenced by the virulence of the strain and dose administered [222, 224, 232]. The physical manifestation of the infection can be measured via features such as weight loss and survival, depending on the dose [222].

Upon infection of mice with influenza, the virus targets respiratory epithelial cells of the upper or lower respiratory tract leading to viral invasion and replication [233, 234]. This results in the initial interferon (IFN) mediated antiviral response, as these epithelial cells produce IFNs. However, they also produce pro-inflammatory cytokines and

chemokines including, TNF-α, IL-6 and CXCL8 (for neutrophil recruitment), which aids in the recruitment of an array of innate immune cells to the site of infection [234, 235]. The large array of innate immune cells recruited include but are not limited to, respiratory epithelial cells, macrophages, monocytes, NK cells and DCs [234]. The subsequent effect of this is the activation of the adaptive immune response via the activated DCs including, $CD103^{+}$ and $CD11b^{hi}$ DCs [234, 236, 237]. These DCs migrate to the mediastinal lymph nodes for antigen presentation to T cells; thus mediating viral clearance via the activation of the cell- and antibody-mediated immune responses [234, 236, 238].

Detection of influenza by these innate immune cells occurs via recognition of PAMPs (Pathogen-associated molecular patterns) via PRRs (Pathogen recognition receptors). PRRs important for influenza includes RLRs (retinoic acid-inducible gene-I-like receptors), TLRs (Toll-like receptors), NOD (Nucleotide-binding oligomerisation domain-like receptors) and C-Type Lectin Receptors (CLRs) [220, 234]. Regarding RLRs, one example is RIG-I that has been linked to detecting RNA of influenza [220, 239, 240]. Examples of TLRs linked to influenza includes, the intracellular TLRs -3, -7 and -8 [220, 241, 242]. Of the NLRs, NLRP3 has been linked to influenza with the formation of NLRP3 inflammasome and production of cytokines, mainly IL-1β and IL-18 [243, 244]. CLRs involved in influenza recognition includes, macrophage mannose receptor (MMR, CD206) , macrophage galactose-type lectin (MGL, CD301) and DC-specific ICAM3-grabbing non-integrin (DC-SIGN, CD209) [234].

The activation of these innate immune receptors results in the eventual production of a range of cytokines including, IFNs. This is through the activation of transcription factors including, interferon regulatory factor -3 (IRF3) and -7 (IRF7), and nuclear factor kappa-light-chain-enhancer of activated B cells (NF-κB) [220]. It is important to note that during the influenza antiviral innate immune response, the induction of IFNs specifically Type I IFNs, α and β allows the production of IFN-stimulated genes (ISGs) through interactions with their cognate receptors [220]. These ISGs proceed to target different stages of the influenza replication cycle [220, 245]. Examples of such ISGs include, the Mx family, and TRIM proteins [245, 246]. These are involved in restricting viral entry, with Mx family ISGs being the first recognised in restricting influenza infections in mice [246, 247]. These ISGs are produced by a range of cells including, both immune cells and non-immune cells [247].

The restriction and thus the resolution of the influenza infection relies on the cytotoxic $CD8^+$ T cell response. Upon activation of antigen-specific $CD4^+$ and $CD8^+$ T cells, the $CD8^+$ T cells differentiate and acquire effector functions for killing infected cells. The combination of activation via DCs on MHC-class I and cytokines such as Type I IFNs, IL-2 and IL-12 allow $CD8^+$ differentiation to occur [248]. These cells are recruited to the site of infection and mediate killing of virus-infected cells via the release of perforin/granzyme but can also induce apoptosis via Fas/FasL interactions, TNF and TRAIL [220, 222, 248]. In addition to $CD8^+$ T cells, $CD4^+$ T cells are also involved when activated via MHC-class II and provide T cell help via different Th subsets. However, some $CD4^+$ T cells may possess cytolytic activity [249]. Features of these Cytolytic Th (ThCTLs) may include, IFN-γ production, perforin/granzyme-B mediated killing, and expression of NK activating receptor isoforms NKG2C/E for mediating cytotoxicity of target cells [249-252].

Of the different Th subsets, Th1 and Th2 cells are considered to be involved in the influenza adaptive immune response [248]. Other T cell subsets involved include, Tregs, which regulate the T cell response, while Th17 cells can inhibit Treg function via IL-6 production, to enhance the T cell response [248]. The adaptive immune response to influenza also relies on effective antibody production by B cells. Tfh cells promote the germinal centre reaction as part of the antibody response [248]. B cell activation via antigen-specific T cells results in the production of neutralising antibodies targeting the influenza's HA and NA, but also other targets such as, M2 and NP [248, 253, 254]. During a primary infection with influenza, rapid production of IgA and of IgM involved in complement mediated cytotoxicity can be observed, with IgG production being associated with long-lived protection as part of the memory response [248].

It has been observed that due to conserved epitopes between different influenza strains, heterosubtypic immunity can occur [255]. This phenomenon is observed when a memory response formed to one influenza strain results in a more effective and robust immune response against a subsequent secondary infection with a different influenza strain due to the conserved influenza epitopes (for example, NP and M1),[220, 256-258]. As the NA and HA proteins, which are the main targets of neutralising antibodies, differ between the two strains, heterosubtypic immunity is mainly mediated by a $CD8^+$ T cell dependent memory response [255].

1.5.3 LCMV

Lymphocytic Choriomeningitis Virus (LCMV) is a noncytopathic negative sense RNA virus of the *Arenaviridae* family. It is a natural pathogen for mice and encodes for four proteins. These proteins include: the viral glycoprotein and nucleoprotein (encoded by the small RNA segment of the genome), and the L and Z proteins (encoded by the large RNA segment) [259]. The glycoproteins (GP) encoded, GP-1 and GP-2 serve to form spikes on the virion envelope, with GP-1 performing a further role in mediating cell entry to host cell surface receptor, α-dystroglycan (α-DG) [260-262].The L protein encodes for the viral RNA polymerase. The Z protein, which has a RING (Really Interesting New Gene) finger motif, serves many functions that include regulating viral replication and transcription [263-265].

Many mouse models have been established using multiple LCMV strains such as, the Armstrong strain, WE strain and Pasteur C1PV 76001 [266]. Further to elucidating the immune response to viral infections, these mouse models have enhanced understanding of the occurrence of acute versus persistent infections [267]. The mostly commonly used LCMV strains for understanding acute and chronic infections includes the Armstrong strain and Clone 13 strain, respectively [267].

The Armstrong strain was the first LCMV isolate derived from an infected patient in 1933 [268], whilst, Clone 13 was isolated from the spleen of a mouse with a persistent LCMV infection from birth [267]. The differences between the two strains is down to two important amino acid changes. The substitution of lysine to glutamine at position 1079 and phenylalanine to leucine at position 260 results in differences in the viral polymerase and (GP) genes, respectively [269, 270]. These mutations in Clone 13 are linked to greater infection of cells expressing the target receptor, α-DG, and higher viral loads [269, 271-274].

As with any antiviral immune response, both the innate and adaptive immune system is important for a robust immune response. Recognition of the virus is reliant upon PRRs expressed by innate cells including, macrophages and DCs. The innate receptors mainly involved in viral recognition includes RIG-I-like receptors (RLRs), which are expressed by most cells and Toll-like receptors (TLRs), for recognition of viral nucleic acid [275, 276]. There is evidence that LCMV activates plasmacytoid dendritic cells (pDCs) via TLRs through the MyD88-dependent pathway [277]. MyD88-

deficient mice were found to be defective in T-cell activation, cytotoxicity and IFNγ production in response to LCMV infections [277]. In addition, Jung et al also showed that induction of the $CD8^+$ T cell responses is influenced by TLR7 and TLR9, with mice deficient in these receptors showing diminished activation of these responses with LCMV infections [277].

Further to this, Clingan et al revealed the importance of RLRs in LCMV infection signalling via the adaptor protein mitochondrial antiviral signaling molecule (MAVS) [278]. MAVS deficiency was found to lead to defective induction of type I IFNs, restricting viral replication and induction of effective $CD8^+$ T cell responses in both acute and chronic LCMV infections, in MAVS knock out mice [278].

Upon engagement of the innate immune response, activated APCs will migrate to the lymphoid organs to activate the antigen-specific T cells to initiate the adaptive immune response. Activation of these T cells has been shown to involve antigen presenting cells, specifically, $CD8\alpha^+$ DCs [279]. In addition, type I IFNs act directly on T cells and induce expansion of antigen-specific T cells, with pDCs having been denoted as a major source of Type I IFNs in many murine infections [277, 280].

Upon activation of antigen specific $CD8^+$ and $CD4^+$ T cells by DCs, the adaptive response to LCMV manifests with it being predominately a $CD8^+$ T cell response for viral clearance. This entails the removal of virally infected cells via the perforin and granzyme B and Fas/FasL mechanisms [281].It is important to note that cytokines, (such as, IFNγ) play an important role in control of the infection [282]. $CD4^+$ T cells are involved in providing help for B cells in producing antiviral antibodies, whilst existing as a source of effector cytokines to provide help to $CD8^+$ T cells; thus, regulate the T cell response amongst other roles [283]. The exact $CD4^+$ T cell subsets involved differ in settings of acute and persistent LCMV infections as discussed later in this section.

The mechanism of acute and persistent LCMV infections differs mainly through viral clearance mediated by the T cell response [284]. Acute LCMV infections induce a robust $CD8^+$ T cell response, which allows the resolution of the infection through removal of virally infected cells [284]. This in turn, prompts the contraction phase during which majority of activated $CD8^+$ T cells are removed. Moreover, a memory cell pool is generated to remain, which will, upon reinfection promote a rapid immune response for more effective viral clearance [284]. In contrast, chronic LCMV infections

result in viral persistence [285]. This is in part mediated by the virus promoting sustained expansion of innate cells such as, Ly6C^{hi} monocytic and Gr-1^{hi} neutrophilic cells, that resemble Myeloid-derived suppressor cells (MDSCs) [286]. These cells work in inhibiting T cell proliferation as observed with chronic Clone 13 infections [286]. The persistence of high viral loads results in T cell exhaustion and therefore, ineffective CD8$^+$ T cell responses for viral clearance [287].

CD4$^+$ T cells also influence the manifestation of acute or persistent LCMV. In an acute setting, CD4$^+$ T cells are dispensable for viral clearance, but their absence can affect subsequent memory CD8$^+$ T cell responses upon re-exposure [288]. However, CD4$^+$ T cells are required for chronic LCMV infections, as CD4$^+$ T cell deficient mice show lifelong viremia with chronic Clone 13 infections [289].

Infections of mice with both Armstrong and Clone 13 follows a similar trend, with increased viral titres observed within the first three days post infection [271]. However, the course of the infection will differ based on the strain. With the acute Armstrong strain, viral titres decrease and become almost undetectable at about 7 days post infection [271]. This quick viral clearance is mediated by the robust CD8$^+$ T cell response induced, with the response peaking at days 7-8 post infection [271]. In contrast, infections with chronic strain, Clone 13, result in a CD8$^+$ T cell response that is reduced by day 7 post infection, allowing a persistent presence of the virus [271].

The subsets of CD4$^+$ T cells involved in acute and chronic LCMV infections differs. Both infections entail the involvement of CD4$^+$ T cells producing Th1 cytokines such as, IFNγ and TNFα, and aid in promoting the CD8$^+$ T cell response [288]. However, these cells decrease after the first week post infection with chronic LCMV, and develop defects in cytokine production as the infection persists [290]. This is likely to be linked with the occurrence of T cell exhaustion which implicate CD4$^+$ T cells as well but mechanisms of this are not completely understood [288]. This loss of Th1 cells is accompanied by the rise of Tfh cells with chronic LCMV infections [288, 291]. Furthermore, these cells are found to support B cells *in vitro* suggesting a role in providing B cell help, and so mediate antibody responses during chronic settings as a way to facilitate viral clearance [288, 291].

As mentioned above, a key hallmark observed with chronic LCMV infections is T cell exhaustion. T cell exhaustion is a phenomenon of dysfunctional T cells which can

progress to the deletion of these antigen-specific T cells during chronic infections [287, 292]. This occurrence was initially observed with LCMV but has been observed with other viral (for example, HIV), bacterial and parasitic infections that are chronic, as well as in many cancers, such as, melanoma [287, 292-294].

As observed with viral infections, T cell exhaustion of $CD8^+$ T cells is defined by a loss of function. This loss of function seems to occur in a hierarchal manner; initially, functions such as IL2 production, and capacity for high proliferation is lost [295]. As cells become more exhausted, further loss of functions happens such as, the inability to produce TNFα [287]. Severe exhaustion is defined by features including, the inability for large IFNγ production, amongst other features [287, 296]. The eventual result of exhaustion is the deletion of these antigen-specific T cells [287].

T cell exhaustion is largely mediated by cell surface inhibitory receptors. These inhibitory receptors are essential in the role they serve for adaptive immunity spanning their role in self-tolerance and preventing autoimmunity. Thus, transient expression of these receptors by immune cells occurs as part of immunoregulation [287]. However, it is the enhanced and consistent expression of these receptors that marks them as a feature of T cell exhaustion, an occurrence that has been witnessed with animal and human models [287]. Examples of co-inhibitory receptors includes: Programmed cell death-1 (PD-1), Cytotoxic T-lymphocyte-associated protein 4 (CTLA-4), T-cell immunoglobulin and mucin-domain containing-3 (Tim-3) and Lymphocyte-activation gene 3 (LAG-3), amongst others [297].

These co-inhibitory receptors have different mechanisms of actions. Firstly, CTLA-4 is considered to work by inhibiting co-stimulation of T cells via through competition with costimulatory CD28 with their shared ligands of CD80 and CD86 [297]. Similar to CTLA-4, PD-1 has shown to compete with CD28 for its ligand CD80 [298]. These inhibitory receptors may also exert their effects via their downstream signalling entailing the recruitment of inhibitory cytoplasmic motifs immunoreceptor-based inhibitory motif (ITIM), which in turn recruit phosphates such as SHIP-1 and -2 [297]. These phosphatases dephosphorylate downstream molecules involved in T cell ,B cell receptor and costimulatory signalling cascades, and thus, diminish downstream signalling as a result [297]. These inhibitory receptors have also shown to mediate inhibitory effects via upregulation of genes involved in T cell dysregulation [297]. For

instance, PD-1 signalling has found to induce overexpression of transcription factor basic leucine transcription factor, ATF-like (BATF), which has been found to reduce proliferation and IL-2 production in T cells [297, 299].

The occurrence of T cell exhaustion is also mediated by inhibitory cytokines, mainly IL-10. During T cell exhaustion, IL-10 levels are found to be enhanced [287]. IL-10 blockade has been found to boost viral control and T cell responses [300, 301]. During chronic infections, the source of IL-10 can differ. Regarding LCMV, mice studies identify DCs and $CD4^+$ T cells being IL-10 sources during this infection [287, 302]. On the other hand, monocytes are an IL-10 source during HIV infections [303]. Aside from IL-10, TGFβ has been linked to T cell exhaustion [287]. During chronic LCMV infections, expression of dominant negative receptors by $CD8^+$ T cells which prevented TGF-β signals being received, resulted in improved cell functionality [304]. However, further investigation is required to further elucidate the role of TGFβ in T cell exhaustion.

1.6 Aims of this thesis

Activating mutations in the PI3K pathway are frequently associated with hemopoietic cancers; therefore, discovery of an activating p110δ mutation that leads to an immunodeficiency has been surprising. Obtaining sufficient blood samples from patients in order to investigate in depth the impaired signaling downstream of hyperactive PI3Kδ mutation other relevant pathways affected is not practical due to limited numbers of patients. Therefore, the development of transgenic mouse models carrying the mutation will allow for further investigations and characterisation of the mechanisms underlying the immunodeficiency, and these findings can be translated into development of better treatment strategies. In line with this, the recent insurgence in the development of different transgenic mouse models has contributed to our knowledge of the involvement of specific immune cells subsets mainly focusing on B cells in driving some of the clinical phenotype in APDS patients [155, 305-307] . An understanding of the mechanisms behind T and B cell-mediated defects in these patients will provide a rationale of treatment with selective p110δ inhibitors.

Therefore, in this thesis, the focus will be on exploring the effects of hyperactive p110δ in the function of different T cell subsets. Primarily the aims of this thesis are:

- Establish whether a T cell conditional knock-in mouse harboring the hyperactive p110δ mutation recapitulates salient T cell features presented by APDS patients.

- Investigate the effect of hyperactive p110δ in different *in vitro* $CD8^+$ and $CD4^+$ T cell functional assays such measurement of effector cytokine production by $CD8^+$ T cells and $CD4^+$ T cell differentiation into different Th subsets. Additionally, the ability of T cells with hyperactive p110δ to undergo increase apoptosis following activation.

- Determine the effect of hyperactive p110δ on the primary response to acute infections with either a bacterial or viral strain

- Determine whether the formation of memory $CD8^+$ T cells is defective due to hyperactive p110δ mutation

- Establish whether the ability to mount effective recall responses is defective due to hyperactive p110δ

- Establish whether hyperactive p110δ leads to T cell exhaustion in a mouse model of chronic infection

Chapter 2
Material and methods

2.1 Mice

p110δ$^{E1020Kflox/WT}$ mice were generated by Ozgene, Australia, using homologous recombination in embryonic stem (ES) cells. A sequence corresponding to exon 22 but carrying the E1020K mutation was flanked by loxP sites and inserted 3' to the wild type sequence. The wildtype sequence was deleted and replaced by the mutated exon 22 through Cre mediated gene recombination as depicted in figure 2.1 [305]. To generate the T cell conditional heterozygous knock-in strain, p110δ$^{E1020Kflox/WT}$ mice were crossed with CD4 $^{Cre/WT}$ transgenic mice, to express the gain of function mutation in DP (CD4^{+}CD8^{+}) and consequently in CD4^{+} and CD8^{+} SP lymphocytes (T-p110δ^{E1020K}).

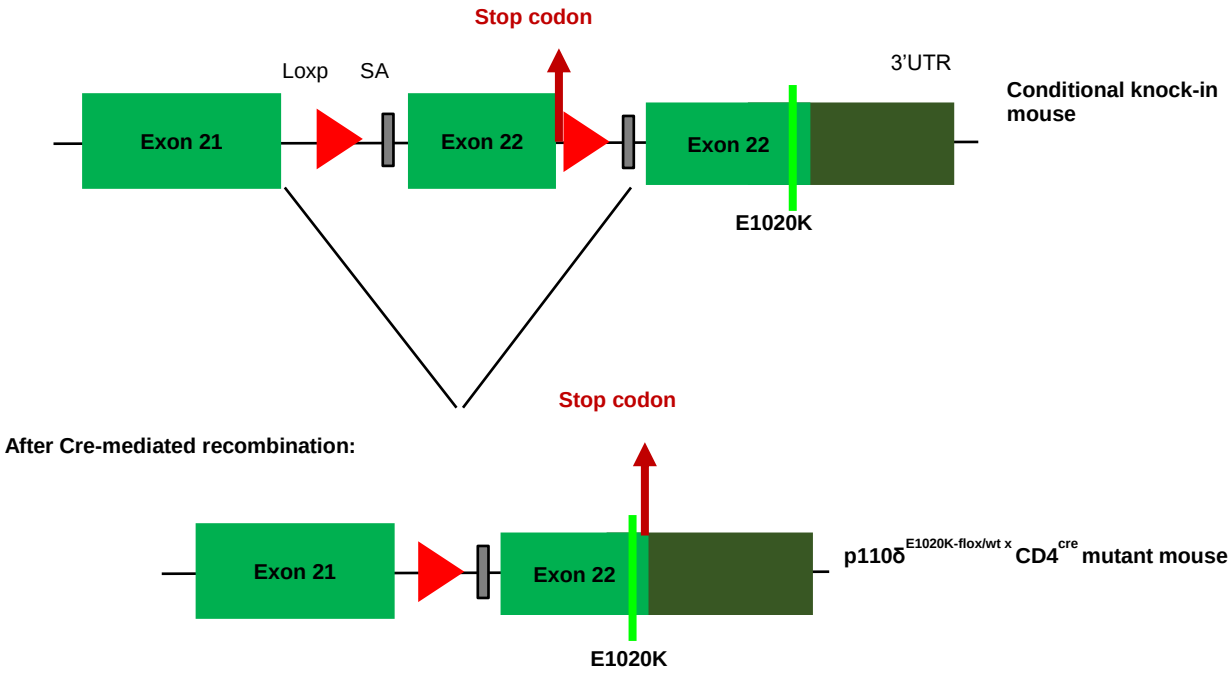

Figure 2.1: **Gene targeting strategy for generating conditional T-p110δ^{E1020K} mice.**
The p110δ^{E1020K} mice were generated by OzGene using homologous recombination in embryonic stem cells. A duplicate sequence corresponding to the last coding exon in PIK3CD was flanked by loxP sites and inserted 3' to the original sequence. The original sequence encoding E1020 was mutated to K1020. Upon Cre-mediated recombination with CD4$^{Cre/WT}$ mice, the wild-type sequence is replaced by the mutant E1020K sequence.

The p110δ$^{E1020Kflox/WT}$mice were also crossed with Mb1$^{Cre/WT}$ to generate B cell specific conditional knock-in mice (B-p110δ^{E1020K}). To generate mice in which the mutation is expressed in the germline, Tnfrsf4^{Cre} was crossed to p110δ$^{E1020Kflox/WT}$ mice (G-p110δ^{E1020K}). The CD4^{cre} and MB1^{cre} lines were a kind gift from Martin Turner (The Babraham institute, Cambridge) [308, 309]. Kinase dead p110δ$^{D910A/D910A}$ (p110δ^{D910A}) contain an aspartic acid (D) to alanine (A) point mutation in the catalytic domain of p110δ rendering the kinase inactive [90]. Wild type (WT) recipient mice used for adoptive transfer experiments were either C57BL/6.Babr (CD45.2) or B6SJL.Babr (CD45.1) and were obtained from the breeding colonies maintained at the Biological Services Unit, Babraham Institute. OT1 mice carry a Vα2-Vβ5 TCR transgene recognising chicken ovalbumin peptide OVA$^{257-264}$ (SIINFEKL) on MHC class IA (H2Kb)[310]. OT1 x p110δ^{E1020K} mice were derived from matings between OT1 and G-p110δ^{E1020K} mice (WT OT1 and E1020K OT1). Foxp3$^{YFP-cre}$ (FYC) mice express a YFP reporter in Foxp3-expressing cells, as well as the cre protein [311]. These mice were crossed with p110δ$^{E1020Kflox/WT}$ mice, such that the knock-in mutation was specifically expressed in Foxp3^{+} Tregs (F-p110δ^{E1020K}).

Wildtype (WT) littermate controls were used for each strain where appropriate. All mice used for *in vitro* and *in vivo* experiments were aged between 7-12 weeks unless stated otherwise, *in vitro* cohorts consisted of mixed genders and *in vivo* cohorts were gender matched. Throughout the study, the p110δ^{E1020K} allele was heterozygous in each colony whereas the p110δ^{D910A} allele was homozygous.

All mice were maintained in individually ventilated cages under specific pathogen-free conditions at the Babraham Institute's Biological Services Unit. The United Kingdom Office and institutional ethics review approved all protocols involving live animals.

2.1.1 Extraction of DNA from ear snips for genotyping

Ear biopsies were digested overnight in 300 µl Cell Lysis Solution (Qiagen #1045723) containing 50 µg/ml Proteinase K (Roche #03115879001). Following protein precipitation with 100 µl Protein Precipitation Solution (Qiagen #1045707), DNA was precipitated with 300 µl propan-2-ol (VWR #20842.330). Samples were then washed with 300 µl 70% ethanol (VWR #2804.330) and air dried. DNA was re-suspended in 50 µl of ddH20, for use in PCR reactions.

2.1.2 Genotyping PCR

The genotypes of transgenic mice were confirmed by polymerase chain reaction (PCR) set up as detailed below. Primers were supplied by Sigma-Aldrich as lyophilised stocks and used at a final concentration of 0.5 µM. PCR products were analysed on 2% agarose gels in Tris base, boric acid and EDTA (TBE) and run alongside a low range DNA ladder (Fermentas) at 150 V. Gels were then imaged using a GelDoc XR (BioRad). Below are the contents of the PCR reactions:

DNA	1 µl
5x GoTaq PCR buffer (Promega – Mg free)	2.5 µl
10x primer mix (0.5 µM of each)	5 µl
$MgCl_2$ (2.5 mM)	2.5 µl
dNTP (200 µM)(Bioline #BIO39049)	2.5 µl
ddH2O	12 µl

Table 2.1: Contents of polymerase chain reaction (PCR)

Allele	Mouse strains	Primer sequences	Expected band widths
$p110\delta^{D910A}$	$p110\delta^{D910A}$;	5'-GGGGTCTGAATACAGAGAGAAT-3' 5'-CCATTTATGGCTATTCTGTTC-3'	WT: 573bp $p110\delta^{D910A}$: 637bp
$p110\delta^{E1020K}$ flox/WT	T-$p110\delta^{E1020K}$ M-$p110\delta^{E1020K}$	5'-TTTCATCCCACGTCCTCCATCTG-3' 5'-GGCGCCTCCTACTGTCGGTTATC-3'	WT = 398 bp Recombined = 444 bp
OT-I	OT-I; G-$p110\delta^{E1020K}$ x OT-I	5'-CAAATGTTGCTTGTCTGGTG-3' 5'-GTCAGTCGAGTGCACAGTTT-3' 5'-AGGTGGAGAGAGACAAAGGATTC-3' 5'-TTGAGAGCTGTCTCC-3'	WT: 200bp OT-I: 300bp
Foxp3-$^{YFP\text{-}cre}$ (FYC)	FYC; FYC x $p110\delta^{E1020Kflox/WT}$	5'-AGGATGTGAGGGACTACCTCCTGTA-3' 5'-TCCTTCACTCTGATTCTGGCAATTT-3' 5'-TTCCAGTCAAAGAGCCCTCACAACC-3' 5'-GGTGAGTGCTTTGGGGTGTGAGTC-3'	WT: 211bp FYC: 346bp
$CD4^{Cre/WT}$	$CD4^{Cre/WT}$ T-$p110\delta^{E1020K}$	5'-GGTGTCATGGTAGGTATGGGT-'3 5'-CGCACAATCTCACGTTCAG-'3 5'-CAGATTCCCAACCAACAAGAGCTCAAGG-3' 5'-CCCAAATGTTGCTGGATAGTTTTTACTGCC-3'	WT = 753 bp KI = 333 bp

p110δ^{E1020Kgl}	G-p110δ^{E1020K} G-p110δ^{E1020K} x OT-1	5'-TCCTCATGGCATCCTTGTCC-3' 5'-ACCCGTTGACTCAATTAGATC-3'	Flox :1024bp Recombined: 439bp
MB1$^{Cre/WT}$	MB1$^{Cre/WT}$ B-p110δ^{E1020K}	5'-CCAAGTCTCCCATCATCTTTTTCTA-3' 5'-CTGCCATTGTTTTCACAGGTG-3' 5'AGCATCTTCCAGGTGTGTTCAG-3'	

Table 2.2: Details of primer sequences used to identify transgenic alleles by PCR.

2.1.1 PCR protocol used for genotyping

Cycle step	Temperature / Time
Step 1	94 ◦c / 2 min,
Step 2	94 ◦c / 30 sec
Step 3	65 – 55 ◦c (-0.5 ◦c /cycle) / 90 sec
Step 4	72 ◦c / 90 sec
Step 5	repeat steps 2-4, 20 times
Step 6	94 ◦c / 30 sec
Step 7	55 ◦c / 90 sec
Step 8	72 ◦c / 90 sec
Step 9	repeat steps 6-8, 20 times
Step 10	72 ◦c / 5 min
Step 11	15 ◦c / hold

Table 2.3: PCR protocol for genotyping

Genotyping of these mice was also outsourced to the Transnetyx automated genotyping service (Cordova, TN).

2.2 *In vivo* infections and immunisations

2.2.1 *Listeria monocytogenes* culture and stock

The *Listeria monocytogenes* expressing OVA strain was derived from the wild-type strain 10403s (WT-Lm) and modified to secrete ovalbumin protein (aa 134-387); and is erythromycin resistant [312]. Its attenuated derivative with the gene encoding ActA deleted (ActA- Lm-ova), was originally purchased from DMX Bio[313] .. All of these strains were obtained from Verity Pearce and were subsequently expanded by Hicham Bouabe. The attenuated Lm-OVA and Lm expressing an irrelevant antigen (attenuated Lm-YFP) was used in experiments to detect $CD8^+$ T cell responses. The Lm-YFP was used as a control to gate on antigen specific $CD8^+$ T cells. The virulent strain was used to measure colony-forming units (CFU) to assess bacterial load. The Lm-OVA strain

was grown in brain heart infusion liquid medium BBL™ Brain Heart Infusion (BHI) (BD) supplemented with 5ug/mL erythromycin (Sigma-Aldrich) at 37°C with shaking. Mid-log phase bacteria (OD_{500}=0.8-1.2) were washed in PBS, diluted, then intravenously injected into a mouse. After 48 hours, a single cell suspension of the spleen was prepared, diluted and grown on BHI agar plates. A single colony was picked and grown to mid-log phase, washed in PBS, and then stocks were stored in aliquots at -80°C in 20% glycerol (Sigma-Aldrich). For all *in vivo* infections with attenuated Lm-OVA, $5x10^6$ CFU was intravenously injected into the lateral tail vein. For bacterial load experiments 5×10^4 CFU virulent Lm-OVA was used. For each experiment, a new aliquot was used. Frozen stocks were thawed at room temperature, washed and diluted in PBS to the appropriate concentration and injected within 2hrs.

2.2.2 Assessing bacterial load in listeria infected tissues

To determine colony-forming units (CFU) in spleens and liver, mice were injected intravenously with the virulent strain of Lm-OVA and culled 48 hours post infection. Livers were perfused by cutting the hepatic vein and injecting 5 ml of phosphate-buffered saline (PBS) into the hepatic artery. Livers were weighed, following which spleens and livers were passed through 40µM nylon strainers (BD Falcon) to generate single cell suspensions. Tenfold serial dilutions of homogenates in PBS were plated out (100µL/plate) on BHI agar plates supplemented with 5µg/ml erythromycin (Sigma-Aldrich) for approximately 48 hours. Bacterial colonies were counted after incubation and enumeration of CFUs were calculated by using the formula CFU/mL= colony count on plate x dilution factor x10.

2.2.3 Influenza A virus infections

To assess primary immune responses, animals were anesthetized with Isoflurane by inhalation and infected via the intranasal route with 40 PFU of A/Puerto Rico/8/34 (PR8 H1N1) viral strain or with 10^3 PFU of the OVA $_{257\text{-}264}$- expressing influenza A/WSN/33 (WSN-OVA) virus strain in 30µl of sterile PBS. Body weight of mice were monitored in studies investigating the primary response to influenza. For recall responses, mice were first inoculated via the intraperitoneal route with 10^7 PFU of PR8 influenza virus in 100ul and then challenged with $10^{4.5}$ PFU of HKx31 (H3N2) influenza virus via the intranasal route in 30µl 64 days later. Martin Turner (Babraham institute, Cambridge)

and Alice Denton (Babraham institute, Cambridge) kindly provided stocks of PR8, WSN-OVA and HKx31 viruses. The choice of influenza virus infection dose was based on a dose that resulted in a clinical phenotype/weight loss but was not associated with lethality, based on previous experiments performed by Krishnendu Chakraborty.

2.2.4 LCMV infections

For chronic responses, mice were infected intravenously with 1 x 10^6 PFU of LCMV Clone 13 and culled at day 32-60 post infection. Body weight of mice were monitored for the first 30-35 days post LCMV clone 13 infections. For acute responses, mice were infected with 2 x 10^5 PFU of LCMV Armstrong and culled at day 8 post infection. Stocks of LCMV Armstrong was a kind gift from Dietmar Zehn (Technical University of Munich, Division of Animal Physiology and Immunology) and Sarah Caddy (MRC Laboratory of Molecular Biology, Cambridge) kindly provided stocks of LCMV Clone 13.

2.2.5 Viral load

At the time of dissection following influenza infection, the left lobe of the lung was snap frozen in liquid nitrogen to determine viral load. Infected lungs were weighed, and RNA was extracted by Ribopure kit (Ambion) and cDNA was synthesized using Superscript III (Life Technologies) with Matrix protein (MP) specific primer: 5'-TCTAACCGAGGTCGAAACGTA -3'. The Real time assay was performed with Platinum Quantitative PCR Super Mix UGD (Invitrogen) by using the following primers and probe specific for the MP encoding gene of influenza PR8 H1N1 virus strain. Sense primer sequence: 5'-AAGACCAATCCTGTCACCTCTGA-3', antisense primer sequence: 5'- CAAAGCGTCTACGCTGCAGTC-3', and probe sequence: FAM-5'-TTTGTGTTCACGCTCACCGT-3'- TAMRA. Viral loads of the experimental samples were calculated using a standard curve of a stock PR8 virus with known concentration of virus plaque forming unit per milliliter (PFU/ml). Fluorescence detection was conducted in a Real-Time PCR CFX96 system (Bio-Rad Laboratories Inc., USA) including CFX Manager™ software for data collection and analysis. The PCR program was comprised of 40 cycles, each cycle consisting of 95°C for 15 seconds and 60°C for one minute.

For LCMV infections, livers were perfused as described in section 2.2.2 and snap frozen in liquid nitrogen to determine viral load. Livers were weighed and RNA and

cDNA preparation was carried out as described above using random hexamers (Thermo Scientific #SO142) and GP-R (S pos. 970-991), 5'-GAACTGCTGTGTTCCCGAAAC-3' primer. For the real time PCR assay the primers used were GP-R (S pos. 970-991), 5'-GAACTGCTGTGTTCCCGAAAC-3', GP-F (S pos. 877-901), CATTCACCTGGACTTTGTCAGACTC and the probe used was FAM-AGAATCCAGGTGGTTATTGCCTGACC-TAMRA, designed by Sarah Caddy (MRC LMB, Cambridge). β-actin was used as a control for gene expression. The primers used for β-actin includes, the forward primer (5'-GAGGTATCCTGACCCTGAAGTA) ,and reverse primer (5'CACACGCAGCTCATTGTAGA). The β-actin probe used was, 5'-(6FAM)TGGCATTGTTACCAACTGGGACGA(TAM). The ΔΔCt method was used for data analysis. The C_t value for each sample within and between individual PCR runs was calculated using GraphPad Prism version 6.01 (GraphPad Software, San Diego, CA) and used to determine significant differences between samples.

2.2.6 *In vivo* NP-KLH immunisation

Mice were immunised intraperitoneally with 100µg NP-KLH (4-hydroxy-3-nitrophenyl) acetyl (NP)–keyhole limpet hemocyanin (KLH) (Biosearch) adhered to alum (Serva Electrophorese GmbH). First, 2 mg/ml NPKLH was mixed with sterile saline (Sigma) where after Alum was added to a 40% final concentration. The mixture was mixed by rotation for a minimum of 1 hour at room temperature before injecting into mice. Mice were culled 14 days post injection and spleens were dissected and processed as described in section 2.3.1.

2.3 Cell based assays

2.3.1 Preparations of single cell suspensions

Mice were euthanized by CO_2 inhalation followed by cervical dislocation. Single cell suspensions were prepared from peripheral (axillary and inguinal) lymph nodes, spleen and thymus by dissociating tissues through 40µm cell strainers (BD Falcon) with a syringe plunge. Bone marrow cells were collected by flushing cold PBS through femurs and tibias, filtered through 40µm cell strainers and washed by centrifugation in 5ml PBS. The cell suspension was then transferred to a 15ml tube (BD falcon) and washed once with PBS. After centrifugation at 1500rpm for 5 minutes, Red blood cell lysis was performed for homogenates from spleens, thymus and bone marrow, by resuspending cells in 2ml red blood cell lysis buffer (Sigma-Aldrich #R7757) and

incubated for 5 minutes at room temperature, before washing by centrifugation in PBS. Cells were then resuspended in PBS, and cell counts determined on the CASY cell counter. For blood staining, 20µl of blood was lysed twice with 200µl red blood cell lysis buffer and incubated for 5-8 minutes each time. Following lysing, cells were washed with PBS and centrifuged as before. Cells were then used in *in vitro* assays or for flow cytometry staining (protocols described below in sections **2.3.2** and **2.3.4**).

Lungs collected following influenza infections were perfused with 10ml cold PBS through the right ventricle and collected into cold PBS. Lungs were homogenized using a GentleMACS tissue dissociator and mouse lung dissociation enzyme kit from Miltenyi (#130-095-927) according to the manufacturer's instructions. The homogenate was transferred to 15ml tubes (BD Falcon), resuspended in 10ml PBS, and centrifuged at 500g for 5 minutes. The pellet was resuspended in 3ml 37.5% isotonic Percoll (Sigma) at room temperature and centrifuged at 650xg for 20min with low acceleration and no brake. The supernatant including tissue debris was removed, and the cell pellet was washed and resuspended in cold PBS.

2.3.2 Flow cytometry

Single cell suspensions prepared were resuspended in FACS Buffer (FB) (PBS/0.5% BSA, Sigma #A7906-100G) and centrifuged at 1500 rpm for 5 minutes at 4°C. 2-5 x10^6 cells were added to wells of a round-bottomed 96 well plate (Greiner)**.** Plates were centrifuged at 1500 rpm at 4°C for 3 minutes and cells then re-suspended in 30-50 µl FB containing conjugated antibodies against the required cell surface markers. Anti-CD16/CD32 (TruStain fcX clone 93, Biolegend; or, clone 2.4G2, Bio X Cell; approx. 2.5 µg/ml) was added to surface staining solutions to block non-specific binding of antibodies to Fc receptors. Plates were incubated for 45 minutes at 4°C; cells were then washed twice in FB and centrifuged as before. Cells were washed and fixed in 4% paraformaldehyde (Biolegend) for 10min at room temperature before washing 2x in PBS/0.5%BSA.

Subsequent staining for intracellular cytokines was done using the Cytofix/Cytoperm buffer (BD Biosciences, USA) following surface staining. For transcription factor staining, the eBioscence FoxP3/Transcription Factor staining Buffer Set was used according to the manufacturer's instructions, with 15-minute fixation at room

temperature, followed by intracellular staining in permeabilisation buffer for 45 minutes at 4°C.

For some experiments, non-fluorescent counting beads (AccuCount Blank Particles 5.3µm; Spherotech, USA) were added to quantify absolute cell numbers. Samples were kept at 4°C until analysis (BD Fortessa 5 or BD LSR II flow cytometer). Single stained controls were run in each experiment to calculate compensation. Analysis was carried out using FlowJo version 10 (Treestar, Inc.) analysis software. A complete list of fluorochrome-conjugated antibodies used in flow cytometric assays is given in Table 2.4.

The $CD8^+$ T cell response to influenza infections was quantified by staining with PE labelled H-$2D^b$ MHC class I tetramer loaded with influenza virus nuclear protein (NP) epitope $NP_{366-374}$ (ASNENMETM) at a dilution of 1 in 100 (NIH tetramer core facility, USA). For detecting the $CD4^+$ T cells response to influenza infection, brilliant violet 421 (BV421) MHC Class II I-A^b tetramer specific for the influenza $NP_{311-324}$ epitope was used at a dilution of 1 in 100. The $CD8^+$ T cells response to Lm-OVA infections was detected by using PE or BV421 labelled OVA $_{257-264}$ (SIINFEKL) peptide (MBL, USA or NIH tetramer core facility USA) at a dilution of 1 in 100. The $CD8^+$ T cell response to LCMV infections was detected by using PE labelled H-2D(b) LCMV GP_{33-41} (KAVYNFATC) peptide at a dilution of 1 in 100 (NIH tetramer core facility, USA). The $CD4^+$ T cell response to LCMV clone 13 was detected by using BV421 labelled I-A(b) LCMV epitope GP_{61-80} (GLKGPDIYKGVYQFKSVEFD) at a dilution of 1 in 100 (NIH tetramer core facility, USA). In experiments determining the T cell response to influenza and LCMV infections, cells were incubated first with the tetramers and Fc block for 30 minutes at 4°C before proceeding to stain with other surface markers.

Anti-mouse	Clone	Supplier	Flourochrome	Dilution
CD19	6D5	BD Biosciences	BV605,BV650, BV785, FITC,	1 in 500
CD25	PC61	Biolegend	APC, BV785, FITC	1 in 400
CD3	2C11	Biolegend	BV605, A700	1 in 300
CD4	GK1.5	Biolegend	BV510, PeCy7, PerCP-cy5.5	1 in 500
CD44	IM7	Biolegend	FITC,APC,PerCP-cy5.5	1 in 500
CD62L	MEL-14	Biolegend	PE,BV421,FITC, BV650	1 in 500
CD8a	53-6.7	Biolegend	APC,BV785, BV711	1 in 500
FoxP3	FJK-16s	eBioscence (ThermoFisher)	APC, EF450	1 in 200

IL-7R	A7R34	Biolegend	PE,APC	1 in 200
KLRG1	2F1	Biolegend	PEcy7, BV605	1 in 200
TCRβ	H57-597	Biolegend	A700, BV421,BV711	1 in 300
LAG3		Biolegend	PEcy7	1 in 200
Tim3		Biolegend	APC, PerCP-cy5.5	1 in 200
ICOS	7E.17G9	Biolegend	PE, PEcy5	1 in 400
GITR	DTA.1	Biolegend	PE, PEcy7	1 in 400
HELIOS	22F6	Biolegend	PE,APC	1 in 200
IFNγ	XMG1.2	Biolegend	APC, PEcy7	1 in 200
TNFα	MP6-XT22	Biolegend	EF450, A700, PerCP-ef710	1 in 200
IL-2	JES6-5H4	Biolegend	PE	1 in 200
CD38	90	Biolegend	PerCP-cy5.5, APC	1 in 400
CD39	24DMS1	Biolegend	PerCP710	1 in 400
Bcl-6	K1.12-91	Biolegend	PE	1 in 100
Ki67	16A8	Biolegend	A700	1 in 100
Granzyme B	GB11	Biolegend	FITC, APC	1 in 200
CD45.2	104	Biolegend	BUV395, PerCPcy5.5, FITC, APC	1 in 200
CD45.1	A20	Biolegend	BUV395, BV650,PerCPcy5.5, FITC	1 in 200
CD279 (PD-1)	J43	Biolegend	PEcy7, BV605	1 in 200
EOMES	Dan11mag	eBioscence (ThermoFisher)	PerCp710	1 in 200
T-BET	4B10	Biolegend	BV605	1 in 200
IL-7A	eBio17B7	eBioscence (ThermoFisher)	APC, PE	1 in 200
IL-10	JES5-16E3	Biolegend	PE	1 in 200
CXCR5	L138D7	eBioscence (ThermoFisher)	APC	1 in 50
TIGIT		1G9	PeDazzle	1 in 200
CTLA4	UC10-4B9	Biolegend	BV421	1 in 200 1 in 400
7-AAD		Biolegend		1 in 10
Fixable viability dye eFluor 780		eBioscience		1 in 4000/1 in 5000
Annexin 5		eBioscence (ThermoFisher)	FITC	1 in 100

Table 2.4: List of fluorochrome-conjugated antibodies used in flow cytometric analysis

2.3.3 Fluorescence-activated cell sorting (FACS)

Single cell suspensions of spleens and peripheral lymph nodes were combined in MACS buffer ((PBS/0.5% FCS (Labtech)/2 mM EDTA (Fisher Scientific #50-213-299)) (MB) after preparation as described in section 2.3.3. Populations of cells required for *in vitro* assays were acquired by immunomagnetic enrichment and FACS. T cell enrichment was performed by negative selection using the Miltenyi MACS magnetic bead-based separation system for either $CD4^+$, $CD8^+$ or total T cells, depending on the experiment concerned. Appropriate FITC labelled antibodies (or the corresponding Biotin labelled antibodies when purifying YFP^+ cells from F-p110δ^{E1020K}) were added; IA^b (MHCII) FITC (1:500), CD25 FITC (1:500), B220 FITC (1:200), CD19 FITC (1:200), CD49b FITC (1:500) , NK1.1 FITC (1:500), Ly6G/6C FITC (1:500) and either CD4 or CD8 FITC (1:200) in MB and incubated for 30 minutes on ice. Cells were washed in 10ml MB and centrifuged at 1500 rpm for 5 minutes before addition of 90µl MB, and 10µl anti-FITC beads (Miltenyi Biotec # 130-048-701) or anti-Biotin (Miltenyi Biotec #130-090-485) beads per 10^7 cells and incubation at 4°C for 15 minutes. Cells were further washed in 9ml MB (3ml at a time), centrifuged at 1500rpm for 5 minutes and resuspended in 1ml MB, before passing through a LS magnetic column (Miltenyi Biotec #130-042-401) on a MACS magnet (Miltenyi Biotec) and the flow-through was collected. Following this, cells were centrifuged at 1500rpm for 5 minutes and incubated with the appropriate surface antibodies for FACS sorting depending on the experiment. Cells were incubated for 45 minutes at 4°C, and then washed twice with MB. After washing, cells were passed through 30µm filters (Partec CellTrics) to remove clumps and resuspended in 400ul of RPMI containing 5% FCS. Cell sorting was carried out on a BD FACsAria/Influx/Fusion sorter. For *in vitro* experiments, viable $CD8^+$ and/or $CD4^+$ / $CD62L^{high}$ $CD44^{low}$ were FACS sorted. For *in vitro* Treg suppression experiments viable $CD4^+$ / $CD62L^{high}$ $CD44^{low}$ /$CD25^+$ YFP^+ cells were FACs sorted. Collection tubes contained 1ml RPMI with 5%FCS. Following sorting, cells were centrifuged at 1500rpm for 5 minutes, counted on CASY counter and resuspended to the appropriate cell concentration required for the experiment.

To measure antigen specific cytokine release from mice infected with either Lm-OVA, influenza or LCMV, $5x10^6$ splenocytes were stimulated in the presence of 10µM $NP_{366-374}$ (ASNENMETM) peptide (Think Peptide, UK) for influenza, 10nM $OVA_{257-264}$ peptide (SIINFEKL) (ProImmune, UK) for Lm, 1µg/ml GP_{33} (KAVYNFATC) peptide

(ProImmune) in the presence of 1µg/ml Brefeldin A (Biolegend or eBioscience) for 5.5 hours. Cells were then washed twice in PBS and centrifuged at 1500rpm for 3 minutes. Following this, cells were stained for surface antibodies, fixed and permeabilized with the cytofix/cytoperm reagent (BD Biosciences, USA) and co-stained for intracellular cytokines and granular substances as described in section 2.3.2. Samples were kept at 4°C until analysis (BD Fortessa 5 or BD LSR II flow cytometer) and data was analysed using FlowJo software (Tree Star).

2.3.4 *In vitro* stimulation with anti-CD3 and anti-CD28

For *in vitro* T cell stimulation assays, flat bottomed 96 well nunclon delta surface plates (#167008, Thermo Scientific) were coated overnight at 37°C with plate bound anti-CD3 (2µg/ml) (BioLegend, #100314) and anti-CD28 (2.5 µg/ml) (#102112). Following day preparation of cells (either total splenocytes, lymph nodes or sorted $CD4^+$ and $CD8^+$ T cells) was carried out as described earlier in section 2.3.1 and 2.3.3. In order to assess *in vitro* proliferation, equal numbers of cells from each sample was resuspended in 1ml PBS and mixed with an equal volume of 10µM Cell Proliferation Dye eFluor 450 (eBioscience, #65-0842-85) in PBS and incubated for 10 minutes at 37°C. Cells were then washed twice in PBS by centrifuging at 1500rpm for 5 minutes, before resuspending at 2 x 10^6 cells/ml in RPMI complete medium (RPMI 1640 (Life Technologies #21875-034) + 5% heat-inactivated FCS (Labtech) + 1% Pen/Strep (Invitrogen #15070-063) + 50 µM β-Mercapto-ethanol (Sigma-Aldrich #M3701)). 2x10^5 cells/100µl were plated out for each condition and then 100µl of RPMI complete medium containing 10nM GSK2269557 or DMSO were added (these were made up at 2x final concentration in order to take in account the dilution within the wells). Plates were incubated for 3 days at 37ºC (5%CO_2).

2.3.5 *In vitro* stimulation with Bone marrow-derived dendritic cells (BM-DCs)

For use as antigen-presenting cells, bone marrow cells from C57BL/6 mice were cultured for 8 days in complete RPMI medium (described in section 2.3.4) and 20 ng/ml recombinant murine GM-CSF (Peprotech) to yield BM-DCs. On day 8 LPS (Sigma-Aldrich) was added at a final concentration of 100ng/ml and the cells were cultured for 10-12 hours. During the last 2 hours, 10nM SIINFEKL peptide (ProImmune ThinkPeptides) was added. Following this, cells were collected and washed, then

frozen in FCS with 10% DMSO (Sigma-Aldrich) in aliquots of 2 x 10^6 cells/ml. Naïve $CD8^+$ T cells were sorted from WT OT1 and E1020K OT1 as described earlier in section 2.3.3. The $CD8^+$ T cells were then counted and resuspended in complete RPMI medium (described in section 2.3.4). BM-DCs were washed twice with PBS, counted and resuspended in complete RPMI medium before use. $CD8^+$ T cells and BM-DCs were co-cultured at a ratio of 5 $CD8^+$ T cells to 1 DC for 72 hours at 37ºC (5%CO_2). After culturing, the cells were stained to detect surface and intracellular markers by flow cytometry as described in section 2.3.2.

2.3.6 *In vitro* BrdU cell cycle analysis

In order to carry out in vitro cell cycle analysis, the BrdU phase flow kit (Biolegend# 3707040) was used. Total lymph node homogenates or naïve $CD4^+$ and $CD8^+$ T cells were prepared and cultured for 72 hours with anti-CD3 and anti-CD28 as described in section 2.3.1, 2.3.3-2.34. After 72 hours, cells were pulsed with 1mM BrdU made up in complete RPMI medium (described in section 2.3.4) and incubated at 37°C for 2 hours. Cells were then transferred into a 96 well round bottom plate and centrifuged at 540g for 3 minutes at 4C. Cells washed twice with PBS and centrifuged as before. Following this, cells were stained with appropriate surface antibodies in 50µl of FB and incubated for 45 minutes at 4°C. Cells were then washed twice with FB and centrifuged as before. Cells were fixed by adding 100µl of Buffer A (provided in the kit) and incubated at 4°C for 20 minutes. Cells were centrifuged as before, washed twice in PBS and left in FB overnight in the fridge. Following day cells was washed with Buffer B (Buffer B was diluted 1:10 with MilliQ water), centrifuged as before. Cells were incubated with 100µl Buffer C and incubated at room temperature for 10 minutes. Cells were centrifuged as before and washed once with Buffer B. The fixation step was repeating by incubating the cells with 100µl Buffer at room temperature for 5 minutes, following this cells were centrifuged as before and washed using Buffer B. Cells were centrifuged and treated with 30µl DNAse (Reconstituted DNAse by adding 1 ml of PBS (Ca/Mg2+) per vial, allowing for DNAse to dissolve for 2-3 minutes). Cells were incubated for 1 hour at 37°C. Following this, cells were centrifuged as before and washed in 200µl of Buffer B. Cells were then stained with anti-BrdU Antibody and incubated for 20 minutes at room temperature in the dark. Cells were centrifuged as before and washed first in Buffer B, then in FB. At the end cells were resuspended in

50µl FB containing 1:10 dilution of 7-AAD. Cells were incubated for 5-10 minutes before acquiring on BD Fortessa5.

2.3.7 *In vitro* Treg suppression assay

Naïve $CD4^+$ T cells (Tcons) and naïve FYC^+ cells (Tregs) were isolated as described in section 2.3.3. Tcons were counted and resuspended in 1ml PBS and labelled with 1ml of 10µM Cell Proliferation Dye eFluor 450 (eBioscience, #65-0842-85), incubated for 10 minutes at 37C. Cells were then washed twice with PBS, counted and resuspended at 1 $x10^6$ cells/ml in complete RPMI media (described in section 2.3.4). Tregs were washed twice with PBS, counted and resuspended at 1 x 10 6 cells/ml in complete RPMI media. Tcons were cultured with Tregs at ratios of 1:1, 1:2, 1:4, and 1:8. Cultures were stimulated with 2 x 10^4 anti-CD3/anti-CD28 coated dynabeads (ThermoFisher Scientific, # 11456D) for 72 hours at 37C/5%CO2. After 72 hours, cells were stained with cell surface markers as shown in section 2.3.2 and analysed on BD Fortessa 5 or BD LSR II flow cytometer.

2.3.8 Enzyme-linked immunosorbent assay (ELISA)

Cell culture supernatants were collected and stored immediately at -20^{o}C. IFNγ and IL-2 levels were assessed using the Mouse IL-2 ELISA Ready-SET-Go!® kits, (eBioscience) according to the manufacturer's instructions. Reactions were stopped with 2N H_2SO_4, and plates read at 450nm, minus 570nm, on a FLUOstar Omega plate reader. Standard curves were plotted using GraphPad Prism 7.0 and the interpolated sample values then exported and multiplied by the appropriate dilution factor.

2.3.9 Anti-Nuclear Antigens (ANA) ELISA

ANA levels were assessed in serum from naïve mice (T-$p110\delta^{E1020K}$, F-$p110\delta^{E1020K}$ and the appropriate littermate controls) by using the Mouse Anti-Nuclear Antigens (ANA/ENA) Igs (total (A+G+M)) ELISA Kit (Alpha Diagnostic International, # 5210) according to manufacturer's instructions**.** Blood samples were collected by cardiac puncture and serum collected and frozen at -20-80°C until further use. Briefly,100µl of provided calibrators, samples (diluted 1 in 100 in working sample diluent) and controls were added to pre-coated wells for 60 minutes. Wells were washed 4 times using working wash solution and pat dried. Wells were incubated with 100µl of anti-Mouse Ig HRP for 30 minutes, following the incubation wells were washed 5 times as before. 100µl of TMB substrate was added to each well and incubated for 10-15 minutes in

the dark. Reactions were stopped with 2N H_2SO_4, and plates read at 450 nm on FLUOstar Omega plate reader. Results were analysed as described above in section 2.3.7.

2.3.10 Detection of apoptotic T cells by Annexin 5 staining

An Annexin V/Dead Cell Apoptosis Kit with FITC annexin V (Thermofisher) was used alongside Fixable Viability Dye eFluor 780 (eBioscience) to detect apoptotic cells. Following 72 hours of *in vitro* stimulation of cells with anti-CD3 and anti-CD28, cells were washed twice with PBS and centrifuged at 1500rpm for 5 minutes. Cells were washed once with Annexin-binding buffer (ABD) and centrifuged as before. Cells were then stained with anti-CD4, anti-CD8, fixable viability dye and Annexin 5 in ABD for 20 minutes at room temperature in the dark. After the incubation period, cells were washed twice with ABD and resuspended in ABD for flow cytometry analysis. Samples were analysed within 1 hour of staining.

2.3.11 *In vitro* $CD4^+$ T cell differentiation

Naïve $CD4^+$ T cells were FACS sorted from WT and T-p110δ^{E1020K} mice as described before 2.3.3. Following FACS, cells were counted on CASY counter and resuspended at $2x10^6$ cell/ml in IMDM media (IMDM with GlutaMAX supplement (GIBCO) containing 5% FCS (LabTech), 100 U/ml penicillin/streptomycin (GIBCO)), and 50 µM β-mercaptoethanol (Sigma-Aldrich). For the different $CD4^+$ T cell helper subsets, the following conditions were used:

T helper subset	Cytokines	Antibodies
Th1	40ng/ml IL-12 (Peprotech)	5µg/ml anti-IL-4 (11B11, Biolegend)
Th2	10ng/ml IL-4 (Peprotech)	10µg/ml anti-IFNγ (XMG1.2, Biolegend)
Th17	1 ng/ml TGF-B (Peprotech) 20ng/ml IL-6 (Peprotech) 10ng/ml IL-23 (Peprotech) 10ng/ml IL-1β (Peprotech)	5µg/ml anti-IL-4 (11B11, Biolegend) 10µg/ml anti-IFNγ (XMG1.2, Biolegend)
Treg	10ng/ml TGF-B (Peprotech)	5µg/ml anti-IL-4 (11B11, Biolegend)

	20ng/ml recombinant human IL-2 (Glaxo-IMB)	10µg/ml anti-IFNγ (XMG1.2, Biolegend)
Tfh	20ng/ml IL-6 (Peprotech)	5µg/ml anti-IL-4 (11B11, Biolegend) 10µg/ml anti-IFNγ (XMG1.2, Biolegend)

Table 2.5: Conditions for $CD4^+$ T cell differentiation

In addition to these cytokines, 10nM GSK2269557 or DMSO (Sigma Aldrich) was also added to the wells. After 3 days of culture, the wells were supplemented with fresh media containing cytokines and either 10nM GSK2269557 or DMSO and cultured for a further 2 days. At day 5, 1µg/ml of Brefeldin A (Biolegend or eBioscience) was added to the wells and cultured for 2 hours, then the supernatant was collected, and the cells processed for flow cytometry analysis as described in section 2.3.2.

2.3.12 *In vitro* caspase assay

Total splenocytes ($2x10^6$ cells/100µl) were plated on anti-CD3 and anti-CD28 coated plates (as described before). On day 3, 0.75µM: Fluorescein-L-valyl-L-alanyl-L192 aspartic acid (methyl ester)-fluoromethyl ketone (FAM-VAD-FMK, Intracellular 193 Technologies) was added for 3h at 37°C. Cells were then stained and analysed by flow cytometry. Dead/necrotic cells (positive for viability dye) were gated out and the percent apoptotic (positive for FAM-VAD-FMK) $CD4^+$ and $CD8^+$ T cells was determined.

2.3.13 PIP_3 quantification (performed by Valentina Carbonaro)

PIP_3 quantification was performed by Valentina Carobonaro as previously described [305]. Briefly, total T cells were purified by negative selection from mouse spleen homogenates. The cells were then stimulated with anti-CD3 (1mg/ml), (145-2c11, Biolegend) and anti- CD28 (2µg/ml), (35.51, Biolegend) antibodies followed by crosslinking with anti- Armenian hamster IgG (10 µg/ml, Jackson ImmunoResearch labs) for 1min at 37°C. The reaction was terminated by addition of 750µl $CHCl_3$: MeOH:1M HCL (10:20:1) and the samples were immediately frozen on dry ice. PIP_3 levels were quantified by mass spectrometry as previously described [314].

2.3.14 Western blot (Performed by Valentina Carbonaro)

Western blot was performed by Valentina Carbonaro as previously described [305]. Briefly, total T cells were purified and stimulated for 5min as described for PIP_3 measurement. Lysates were prepared by the addition of ice-cold lysis buffer (50mM HEPES, 150mM NaCl, 10mM NaF, 10mM Indoacetamide, 1% IGEPAL and proteinase inhibitors (Complete Ultra tablets, Roche)) for 15-20 min. Following centrifugation at 15,000g for 10 min at 4°C, the supernatants were mixed with NuPage LDS sample buffer (life technologies) and heated at 70°C. Following resolution on 4-12% NuPage bis-tris gels (Invitrogen) and transfer to PVDF membranes, proteins were detected with the following antibodies: pAKT (T308, Cell Signaling, 1 in 1000 dilution); total AKT1 (2H10, Cell signaling, 1 in 2000 dilution); p110δ (Sc7176, Santa Cruz Biotechnology, 1 in 200 dilution); pS6 (S235/236, Cell Signaling, 1 in 500 dilution); pFoxo1/3a (T24/T32, Cell Signaling, 1 in 1000 dilution); pErk (p44/42, Cell Signaling, 1 in 200 dilution); βActin (Sc47778, Santa Cruz Biotechnology, 1 in 2000 dilution).

2.3.15 Inhibitors

Valentina Carbonaro performed an in-house titration of GSK2269557 (GlaxoSmithKline), and subsequently we used this compound at 10nM [315]. DMSO-treated control cells were included in all experiments requiring GSK2269557 treatment. For Fas dependent apoptosis, 10µg/ml LEAF purified anti-mouse CD178 (FasL) antibody, clone MFL3 (Biolegend, #106608) diluted in PBS was used. The wells not treated with anti-FasL received the same volume of PBS as a control.

2.4 *In vivo* assays

2.4.1 *In vivo* cytotoxicity assay

Equal numbers of splenocytes from naïve B6.SJL mice were pulsed for 1 hour with 10nM SINFEKL peptide and were subsequently labelled for 10 minutes at 37^0C with 10µM cell proliferation dye eFluor670 (ThermoFisher Scientific, # 65-0840-85) or not pulsed with peptide and were labelled with 10µM cell proliferation dye eFlour450 (ThermoFisher Scientific #65-0842-85). The two populations of cells were mixed together at a 1:1 ratio and $5x10^6$ mixed cells were transferred intravenously into mice that had been infected with Lm-OVA 8 days before or into uninfected control mice. Mice were culled 1 hour later, and the percentage of peptide loaded target cells and

peptide un-loaded control cells was quantified by flow cytometry (protocol described in section 2.3.2). The percentage of target cell killing was determined as 100-((percentage of peptide–pulsed targets in infected recipients/percentage of un-pulsed targets in infected recipients)/ (percentage of peptide-pulsed targets in naïve recipients/un-pulsed targets in naïve recipients) X 100).

2.4.2 *In vivo* adoptive transfer experiments

Single cell preparations were prepared as described in Section 2.3.1. Single cell preparations were incubated for 30 minutes at 4˚C with FITC-conjugated anti-CD4, anti-CD19, anti-B220, anti-NK1.1, anti-F4/80, anti-CD11b, anti-CD11c and anti-MHCII Abs in MB at a concentration of $1x10^8$ cells/ml. Next, the cells were washed in MB and incubated for 20 minutes at 4^0C with 100ul anti FITC MACS magnetic beads (Miltenyi Biotec) per 10^7 cells. Following this, cells were washed in MB and applied to a MACS LS column (Miltenyi Biotec) and the flow through was collected. The resulting cells were washed twice in MB and stained with fixable live dead dye, anti-CD8, anti-CD44, anti-CD62L and PE labelled H-$2D^b$ MHC class I tetramer loaded with SIINFEKL peptide made up in MB. Cells were incubated for 30-45 minutes, washed twice in MB and resuspended in RPMI media containing 10% FCS. Equal numbers of (10,000) naïve ($CD62L^{high}CD44^{low}$) WT OT1 and E1020K OT1 cells were transferred intravenously into WT recipient mice with a different congenic marker. One day later, the recipient mice were infected with 5 x 10^6 Lm-OVA. Mice were culled 8 days post infection to assess primary responses, or re-infected again on day 40 and culled 5 days later to access secondary responses. For co-transfer experiments, 10,000 naïve cells at a ratio of 1:1 of WT OT1 and E1020K OT1 cells were co-transferred into WT recipient mice.

2.5 Gene Array (Carried out by GlaxoSmithKline (GSK))

Naïve $CD4^+$ and $CD8^+$ T cells were FACS sorted from WT, T-$p110\delta^{E1020K}$ and $p110\delta^{D910A}$ mice as described earlier. Cells were stimulated with plate bound 2.5µg/ml anti-CD3 and 2.5µg/ml anti-CD28 for 72 hours. After which cells were collected, snap frozen in liquid nitrogen and transported to GSK. Samples were analysed (Affymetrix Genechip Mouse genome 430 2.0 Array) by Expression Analysis, Quintiles Global Laboratories. Glyn Bradley (Computational Biology and Statistics, Target Sciences, GSK, Stevenage) performed data analysis. Data was normalised using the robust

multiarray average method and quality checked in R/Bioconductor using the *affy* package [316-318]. A linear model was fitted to the RMA normalised data for each probset and differential expression analysis was conducted in the ArrayStudio software (Omicsoft Corporation). P-values were false discovery rate corrected by the method of Benjamini and Hochberg[50]. Probes with an absolute fold change >1.5 and an adjusted p-value <0.05 were called significant. Heat Maps were created using the Complex Heatmaps R/ Bioconductor package [319].

2.6 Mass spectrometry proteomics preparation and analysis (Carried out by Christina Rollings, Dundee)

Lymph node homogenates from WT, T-p110δ^{E1020K} and p110δ^{D910A} mice were prepared and resuspended at 5x10^6 cells/ml in complete RPMI medium. Cells were stimulated with 0.5µg/mL α-CD3, 0.5µg/mL α-CD28, 20ng/mL IL-2 and 2ng/mL IL-12 for 24hrs at 37°C/5%CO2. After 24 hours, cells were washed twice with PBS by centrifuging at 1500rpm for 5 minutes at 4°C. Following this cells were stained in 500µl of FB containing fixable live dead dye, anti-TCRβ, anti-CD4, and anti- CD8 antibodies for 45 minutes at 4°C. After which cells were washed twice in FB and resuspended in PBS containing 0.1% FCS. Cells were then FACS sorted, to obtain viable CD4$^+$ and CD8$^+$ T cells. After sorting, cells were then centrifuged, snap frozen in liquid nitrogen and couriered to Dundee for proteomics.

Sample processing

An SP3 approach was used to process samples for proteomic analysis (Hughes et al., 2014). Cell pellets were resuspended in 400 µL lysis buffer (4% SDS, 10 mM TCEP, 50 mM TEAB), boiled for 5 mins then allowed to cool for 5 mins while being shaken at 500 rpm on a thermomixer. Samples were then sonicated and incubated with 1 µL benzonase for 15 mins at 37°C. Protein concentration was determined using an EZQ assay. Cysteine residues were carbaminomethylated by incubation with 20 mM iodoacetemide for 1hr at room temperature in the dark. Magnetic beads (200 µg per sample of a 50:50 mix of hydrophobic and hydrophilic Sera-Mag Speedbead carboxylate-modified magnetic particles, GE Life Sciences) and 550 µL of a 10:1

acetonitrile: 10% formic acid solution was added to each sample. Samples were then incubated for 8 mins while mixing at 500 rpm, centrifuged briefly and the supernatant removed following 2 mins incubation on a magnetic rack. Beads were then washed twice with 1mL 70% ethanol and once with 1mL acetonitrile. Beads were air-dried briefly, resuspended in 65 µL digestion buffer (0.1% SDS, 50mM TEAB, 1mM $CaCl_2$) and LysC added at a ratio of 1 µg LysC per 100 µg protein. Samples were incubated overnight at 37°C with mixing at 500 rpm. Following digestion with LysC,1 µg trypsin/100 µg protein was added and samples were incubated overnight at 37°C with mixing at 500 rpm. Beads were washed with 1.425 mL acetonitrile, then 500 µL acetonitrile. Peptides were eluted following incubation with 189 µL 2% DMSO for 2 minutes and peptide concentration determined using a CBQCA assay. Samples were adjusted to 5% formic acid, then dried down in a SpeedVac.

Fractionation

Samples were resuspended with 210 µL 5% formic acid. For each sample, 200 µL was fractionated into 16 fractions using high pH reversed phase chromatography using an UltiMate 3000 HPLC with an XBridge Peptide BEH C18 column. The buffers used for separation were buffer A (10 mM ammonium formate/2% acetonitrile, pH 9.0) and buffer B (10 mM ammonium formate/80% acetonitrile, pH 9.0). A flow rate of 0.3 mL/min was used throughout fractionation. An elution gradient increasing the percentage of acetonitrile was used for fractionation, beginning with 90% buffer A and 10% buffer B, then moving to 50% buffer A and buffer B at 11 mins and to 0% buffer A and 100% buffer B at 12 mins. Following fractionation, fractions were combined to form 8 fractions per sample, dried down in a SpeedVac and resuspended in 5% formic acid for submission to the University of Dundee FingerPrints Proteomics and Mass Spectrometry facility.

Mass spectrometry

Mass spectrometry analysis was performed by the Proteomics Facility at the University of Dundee. A maximum of 1 µg per fraction was analysed. Before introduction to the mass spectrometer, samples were separated using an Ultimate 3000 HPLC (Thermo Scientific). Peptides were trapped and washed on an Acclaim PepMap 100 (C18, 100 µM x 2 cm) column with a 0.1% formic acid buffer, then separated on an Easy-Spray Pep-Map RSLC C18 column (75 µM x 50 cm). The buffers used for separation were

0.1% formic acid (buffer A) and 0.08% formic acid in 80% acetonitrile (buffer B), and a flow rate of 0.3µL/min was used throughout fractionation. Samples were separated using an elution gradient, beginning with 2% buffer B, switching to 5% buffer B at 6 mins, 35% buffer B at 130 mins and reaching 98% buffer B at 132 mins, which was held until 152 mins, at which point the buffers were reset to the starting concentration of 2% buffer B with a total run time of 170 mins. Samples were then introduced to an LTQ OrbiTrap Velos Pro (Thermo Scientific) using an Easy-Spray Source (Thermo Scientific) at 50°C and source voltage of 1.9 kV. The mass spectrometer was run in a data-dependent acquisition mode, using a top 15 method for selection of ions for fragmentation. MS spectra were collected over a range of 355 – 1800 m/z with a resolution of 60,000, using a full scan and in a positive ion mode. The top 15 most intense peptide ions were selected for fragmentation via CID (collision-induced dissociation) after the accumulation of 5000 ions, with normalised collision energy of 35%, activation Q of 0.25, and activation time of 10 ms.

Data analysis

The raw data files generated during mass spectrometry were analysed using MaxQuant version 1.6.1.0 and searched against the reviewed mouse Uniprot database, the contaminants database supplied with MaxQuant and a reversed database used for FDR (false discovery rate) determination. Cysteine carbamidolyation was set as a fixed modification and methionine oxidation, protein N-terminal acetylation, deamidation of asparagine and glutamine and pyroglutamic acid formationfrom glutamine were set as variable modifications. Minimum peptide length was set to 6, digestion was set to trypsin/P and LysC with a maximum of two missed cleavages. Match between runs was enabled. Quantification used unique and razor peptides. PSM (peptide to spectrum match) FDR and protein FDR were set to 1%.

Following protein identification and quantification, proteins identified in the reverse database, proteins listed as contaminants and proteins only identified by a modified peptide were filtered from the database. Copy numbers were then calculated using the proteome ruler plugin in the Perseus analysis software version 1.6.0.2 [320]. Copy numbers were $\log_2$ transformed and an unpaired T-test with unequal variance performed. Proteins with a 1.5-fold change in different conditions and a p value ≤ 0.05 were considered differentially abundant.

Generation of volcano plots (provided by Christina Courreges)

The generated protein list was filtered for potential contaminants, reverse hits, and ‘‘only identified by site’’. The label-free quantification (LFQ) values were transformed in log2 scale, the three technical replicates per experimental condition grouped and averaged based on the median. To identify the proteins with the most prominent differences in expression profiles within the different T cell subsets statistical significance ($p \leq 0.05$).

2.7 Statistical Analysis

Statistical analyses were carried out using Graphpad Prism. Data sets were checked for Gaussian distribution by using A’Agostino & Pearson. Where data were normally distributed, parametric tests were performed: unpaired students t-test with Welch’s correction was used when two groups were compared, or one-way ANOVA with Tukey post-test when three or more groups were compared. For data not following a normal distribution non-parametric tests were performed: the Mann-Whitney test was used when two groups were compared or the Kruskal-Wallis test with Dunns’ multiple comparison test was used when three or more groups were compared. Two-way ANOVA was used to compare mean differences in data sets influenced by the effect of two independent variables such as in cases where different genotypes and drug treatment were involved.

Chapter 3

Immunophenotyping of T cells with hyperactive p110δ

3.1 Introduction

The p110δ isoform is the major isoform signalling downstream of T and B cell antigen receptors, Toll like receptors, cytokine and co stimulatory receptors in immune cells [29]. PI3K signalling via p110δ plays a crucial role in the regulating key cellular processes within lymphocytes that include differentiation, proliferation, and survival and effector functions. The importance of p110δ in regulating immune cell functions is highlighted by mutations that activate p110δ in patients with immunodeficiency. Activated PI3K Delta Syndrome (APDS), is a primary immunodeficiency characterised by heterozygous, dominant gain-of-function mutations in PIK3CD gene encoding for p110δ. APDS is a combined immunodeficiency affecting both T and B cells [138, 141].

APDS is rare and therefore only few patients available to carry out any investigations. Additionally due to difficulties in using immune cells from APDS patients owing to not obtaining sufficient sample size or the increased cell death of immune cells, therefore to investigate the effect of hyperactive p110δ in immune cells, we generated a conditional knock-in mouse harbouring E1020K mutation in the PIK3CD gene ($p110\delta^{E1020KFlox/WT}$) [305]. The E1020K mutation corresponds to the most abundant mutation, E1021K, found amongst APDS patients [138, 141]. The $p110\delta^{E1020KFlox/WT}$ mice were crossed with a number of different Cre expressing lines to generate conditional and germline knock-in mice. In this chapter, I have used T-$p110\delta^{E1020K}$ mice that were generated by crossing $p110\delta^{E1020KFlox/WT}$ mice with $CD4^{Cre}$ mice. The use of $CD4^{Cre}$ mice leads to the knock-in mutation being expressed in the double positive thymocytes ($CD4^+CD8^+$) and ultimately in all $CD4^+$ and $CD8^+$ single positive T lymphocytes. For some experiments, germline mice were used where the mutation is expressed in all cells (G-$p110\delta^{E1020K}$), along with B-$p110\delta^{E1020K}$ mice that were generated using $Mb1^{Cre}$ mice, allowing the mutation to be specifically expressed in B cells (B-$p110\delta^{E1020K}$) [305]. I also made use of $p110\delta^{D910A}$ mice that have catalytically inactive p110δ and serve as a reliable control to the effect of hyperactive p110δ [90]. In addition, I investigated the effect of inhibiting hyperactive p110δ using a p110δ specific inhibitor GSK2269557, this inhibitor is currently in clinical trial and is clinically known as nemiralisib [315, 321]. Using $p110\delta^{D910A}$ mice gives an important advantage to gain a more complete understanding of the role of p110δ signalling as when compared with the $p110\delta^{E1020K}$ allele, it allowed us to compare the consequence of

too little or too much p110δ activity in immune responses. In addition, the use of a p110δ specific inhibitor allowed us to test the consequence of acutely inhibiting hyperactive and normal p110δ signalling, therefore providing information about potential treatment strategies. In the experiments described in this chapter, I used 7-12 weeks old mice that were mixed genders. Additionally, I used littermate mice that were Cre positive as wild type (WT) controls. The results in this chapter describe the effect of hyperactive p110δ on the differentiation, activation and functions of different T cells subsets.

3.2 Results

3.2.1 Generation of a T cell specific mouse model with hyperactive p110δ mutation

In order to understand how hyperactive p110δ mutation impacts T cell differentiation and function, a knock-in mouse model was generated in which p110δ^{E1020K} mice were crossed with CD4^{cre} mice to generate a T cell specific mutation. To verify that the hyperactive p110δ mutation was present in T cells, genomic DNA from FACs sorted T and B cells were screened via PCR for the presence of the recombined p110δ^{E1020K} allele in 5 T-p110δ^{E1020K} mice. **Figure 3.2.1** shows that the presence of the recombined band (444bp) was restricted to T cells and absent in B cells. There was no presence of p110δ^{E1020K} floxed alleles, suggesting recombination had taken place. These results demonstrate generation of a mouse model with a T cell specific mutation.

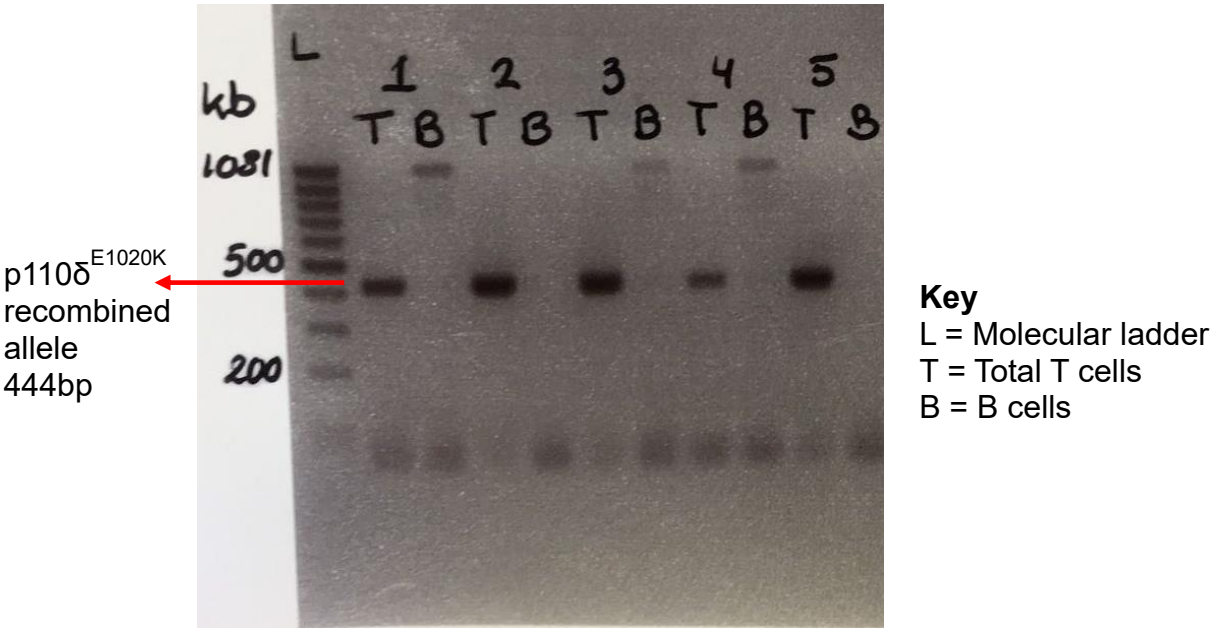

Figure 3.2.1: Generation of a T cell specific mouse model

T (TCRβ^{+}) and B (CD19^{+}B220^{+}) cells were FACs sorted from 5 T-p110δ^{E1020K} mice. Genomic DNA was isolated from the cells and analysed using a PCR (n=5 mice, randomly chosen).

3.2.2 Hyperactivation of p110δ leads to increased PIP_3 and pAKT levels

To confirm that T-p11δ^{E1020K} mice displayed increased p110δ activity similar to APDS patients, measurements of PIP_3 levels by mass spectrometry and quantification of downstream effector proteins of p110δ by western blots were carried out. The experiments presented in this section was performed by Valentina Carbonaro. PIP_3 levels in T cells from T-p110δ^{E1020K} mice were increased following stimulation with anti-CD3 and anti-CD28 compared to WT mice, with no differences at basal level. Treatment with the p110δ specific inhibitor 10nM GSK2269557 resulted in a reduction of PIP_3 in both WT and T-p110δ^{E1020K} mice (**Figure 3.2.2a**).

Having established that hyperactive p110δ resulted in increased PIP_3 levels in T cells, the next step was to determine the effect on downstream effector proteins of p110δ signaling. Akt is a pleckstrin homology (PH) domain containing protein that is recruited to the plasma membrane by PIP_3 [322]. Phosphorylation of Akt takes place at two sites; at serine 473 (Ser^{473}) by mTORc2 and at threonine 308 (Thr^{308}) by PDK-1 [323-325]. Following stimulation with anti-CD3 and anti-CD28, increased Akt Thr^{308} phosphorylation was observed in T-p110δ^{E1020K} mice compared to WT mice (**Figure 3.2.2a**). Phosphorylation of Erk and other Akt effector proteins such as Foxo were also enhanced due to hyperactive p110δ activity, the reversed was observed in T cells from p110δ^{D910A} mice. All phosphorylation events in WT and T-p110δ^{E1020K} T cells were reduced by inhibition with GSK2269557 (**Figure 3.2.2a**). Additionally T cells from G-p110δ^{E1020K} mice have increase phosphorylation of ribosomal S6, which is an important effector protein downstream of mTORc1 [305]. This set of data confirms an activated phenotype in T cells with hyperactive p110δ following T cell stimulation.

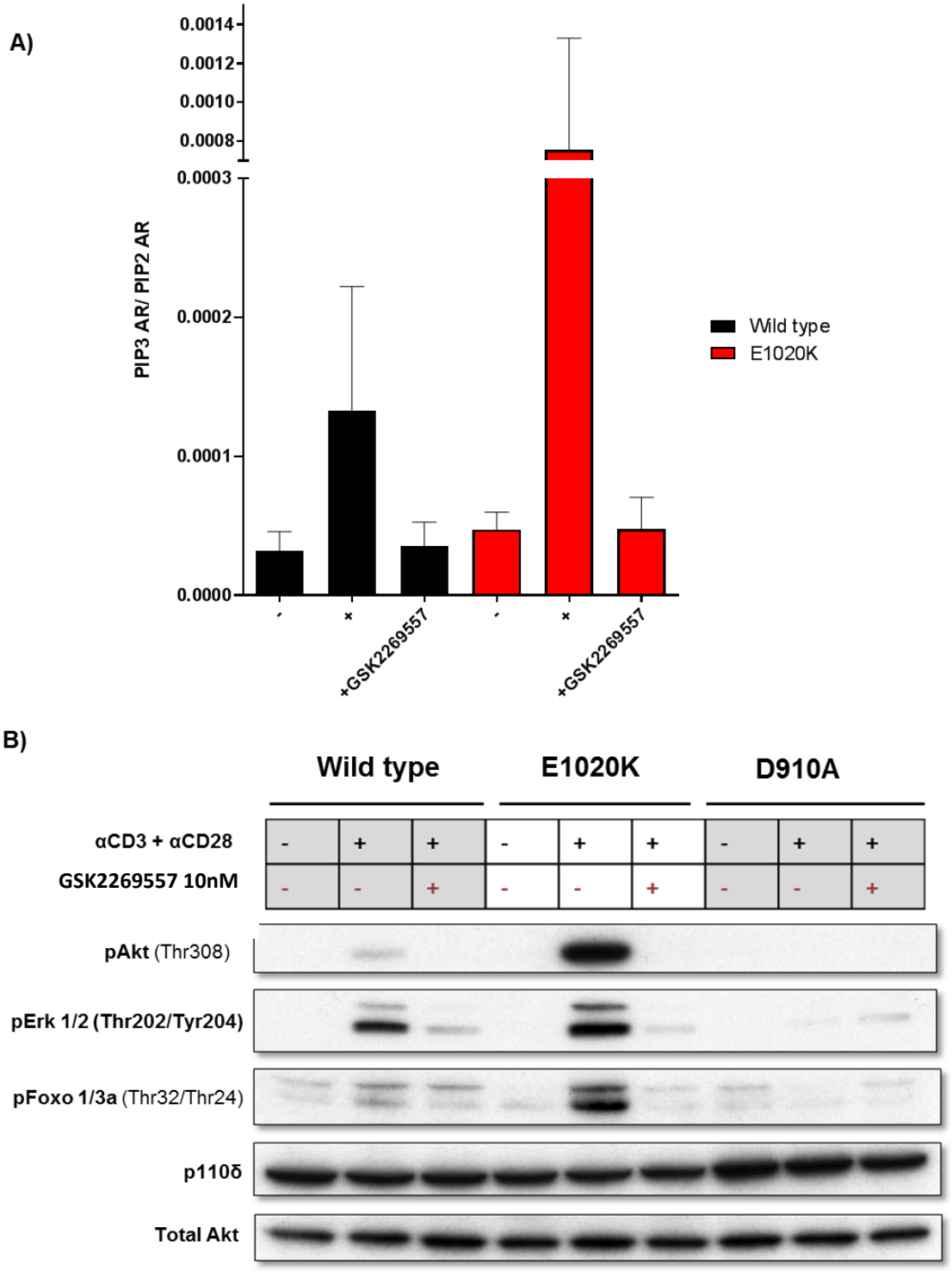

Figure 3.2.2: Elevated activity of p110δ in T cells leads to increased PIP_3 and pAKT levels that can be reduced using a selective p110δ inhibitor.

(A) PIP_3 levels in purified T cells from WT and T-p110δ^{E1020K} mice, unstimulated or stimulated with anti-CD3 and anti-CD28 in the presence or absence of 10 nM GSK2269557 , n=2 mice per genotype. **(B)** Western blots of purified T cells from WT, T-p110δ^{E1020K} and p110δ^{D910A} mice, unstimulated or stimulated with anti-CD3 and anti-CD28 in the presence or absence of GSK2269557. Experiments were performed by Valentina Carbonaro.

3.2.3 Normal T cell development in T-p110δ^{E1020K} mice

In order to investigate the consequences of hyperactive p110δ in T cell function, the first step was to carry out detailed immunophenotyping of naive T-p110δ^{E1020K} mice by examining the expression of T cell lineage and activation markers in the thymus, spleen and peripheral lymph nodes (pLN's) by flow cytometry. There were no visible differences observed in the organs upon sacrificing T-p110δ^{E1020K} mice compared to WT mice. There was no difference in the total number of splenocytes, pLN's cells and thymocytes in T-p110δ^{E1020K} mice compared with WT mice (**Figure 3.2.3a**). However, p110δ^{D910A} mice had visibly smaller spleens and hence fewer splenocytes compared to the other genotypes, which has been reported previously (**Figure 3.2.3a**) [90].

Next, T cell development in the T-p110δ^{E1020K} mice was examined by quantifying CD4 and CD8 single positive (SP), double positive (DP) and double negative (DN) T cell populations in the thymus. In addition, I also assessed the expression of CD25 and CD44 profile analysis on DN cells. According to the CD4 vs CD8 profile in the thymus, the T cell development progressed normally in T-p110δ^{E1020K} mice. Flow cytometry analysis revealed that T-p110δ^{E1020K} contained similar numbers of single positive (SP) $CD8^+$ and $CD4^+$ T cells (**Figure 3.2.3b and c)**. In addition, the proportions of DP and DN cells were similar between WT and T-p110δ^{E1020K} mice (**Figure 3.2.3b and c**). Further analysis of the DN subpopulations revealed no differences (**Figure 3.2.3d**). This shows that hyperactive p110δ mutation in the T cells does not have obvious effects on T cell development, however subtle effects on positive and negative selection and in other T cell subsets such γδ T cells can still exist.

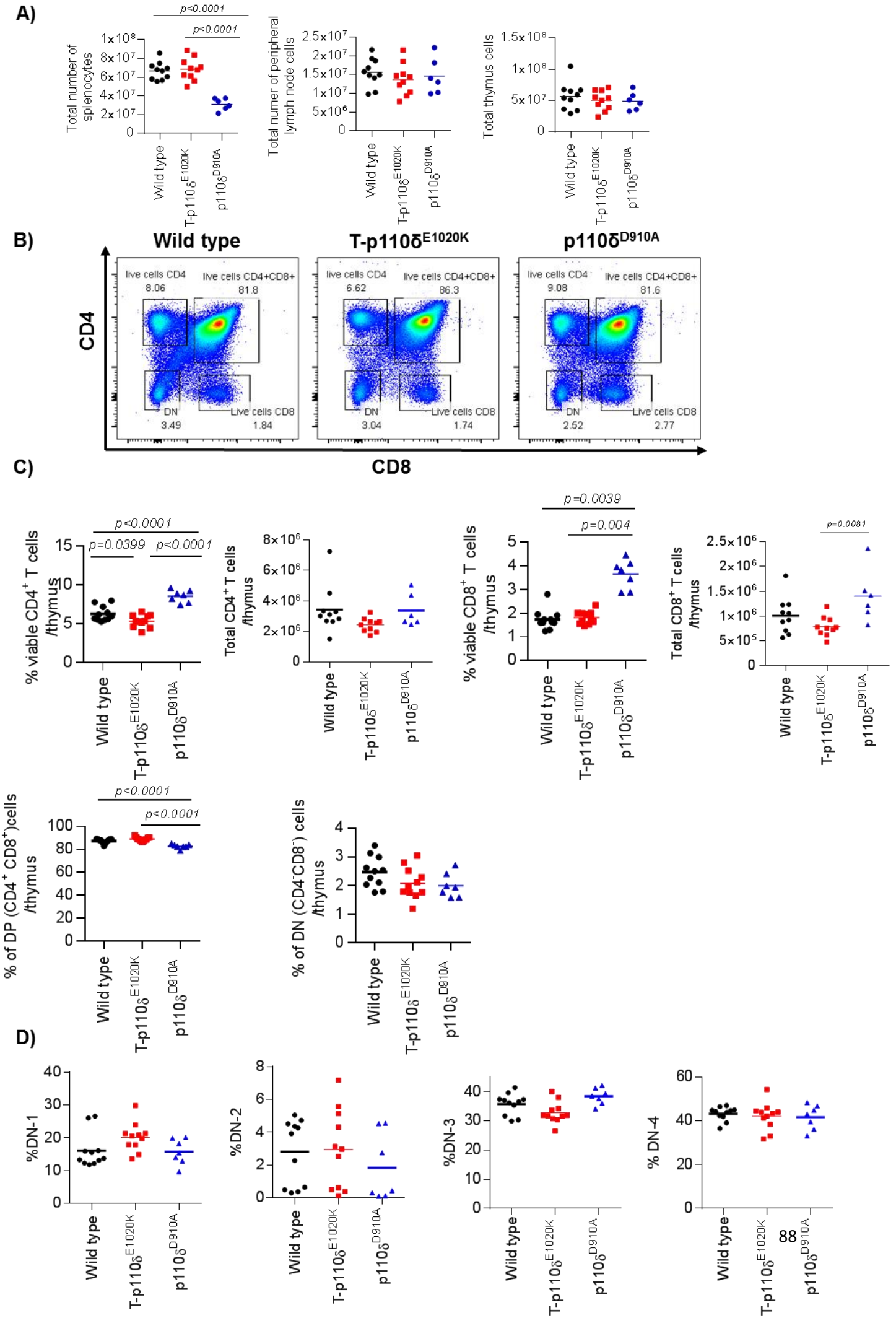
A)
Total number of splenocytes
p<0.0001
p<0.0001
Total numer of peripheral lymph node cells
Total thymus cells
Wild type
T-p110δE1020K
p110δD910A
B)
Wild type
T-p110δE1020K
p110δD910A
CD4
CD8
live cells CD4
live cells CD4+CD8+
8.06
81.8
DN
3.49
Live cells CD8
1.84
6.62
86.3
3.04
1.74
9.08
81.6
2.52
2.77
C)
% viable CD4+ T cells /thymus
p<0.0001
p=0.0399
p<0.0001
Total CD4+ T cells /thymus
% viable CD8+ T cells /thymus
p=0.0039
p=0.004
Total CD8+ T cells /thymus
p=0.0081
% of DP (CD4+ CD8+)cells /thymus
p<0.0001
p<0.0001
% of DN (CD4-CD8-) cells /thymus
D)
%DN-1
%DN-2
%DN-3
% DN-4
88

Figure 3.2.3: Normal T cell development in p110δ^{E1020K} mice

(A) Total number of cells in lymphoid organs was determined using CASY counter. **(B)** Flow cytometry analysis of T cells from the thymus stained with anti-CD4 and CD8 antibodies**. (C)** Graphs showing proportions and numbers of viable CD4^{+} and CD8^{+} single positive (SP), double positive (DP) and double negative (DN) cells in the thymus. **(D)** Graphs showing proportions of DN1, DN2, DN3 and DN4 populations in the thymus. Results are combined from four independent experiments comparing WT, T-p110δ^{E1020K} (n= 11, 7- 8 weeks old mice) and p110δ^{D910A} mice (n= 7, 7-11 weeks old). *P values* are shown.

3.2.4 Increase T cell activation in T-p110δ^{E1020K} mice

APDS patients show increased numbers of activated T cells [138, 141]. In order to determine if T-p110δ^{E1020K} mice also show an activated T cell phenotype by flow cytometry, I carried out immunophenotyping of T cells in the spleen and peripheral lymph nodes (pLNs). I used different cell surface markers (CD3^{+}, TCRβ^{+} CD4^{+} and CD8^{+}) to distinguish between naïve (CD62L^{high}) and activated (CD44^{high}) T cells. There were no differences in numbers of total viable CD4^{+} and CD8^{+} T cells in the spleen and pLNs of T-p110δ^{E1020K} mice compared to WT mice (**Figure 3.2.4a**). The number of viable CD4^{+} and CD8^{+} T cells were reduced in the spleens of p110δ^{D910A} mice, owing to the reduced size of the spleens in these mice, that has been reported previously (**Figure 3.2.4a**) [90, 115]. However, slight increases in CD4^{+} and CD8^{+} T cells were observed in the pLN's of p110δ^{D910A} mice compared to WT mice (**Figure 3.2.4a**).

Hyperactive p110δ signalling in CD4^{+} and CD8^{+} T cells resulted in enhanced activation as evidenced by the increased proportion of activated (CD44^{high}CD62L^{low}) and memory (CD44^{high}CD62L^{high}) T cells in the spleen and pLNs in T-p110δ^{E1020K} mice compared to WT mice. (**Figure 3.2.3b and c**). In addition, proportions of naïve T cells as characterised by CD62L^{high}CD44^{low} was slightly reduced compared to WT and p110δ^{D910A} mice (**Figure 3.2.4b and c**). In contrast, p110δ^{D910A} mice had reduced proportions of activated T cells (CD44^{high}CD62L^{low}) and memory (CD44^{high}CD62L^{high}) but enhanced proportions of naïve (CD62L^{high}CD44^{low}) T cells compared to WT mice in both spleens and pLNs, consistent with previous published data (**Figure 3.2.4b and c**) [90]. Additionally, the expression of IL-7Rα (CD127) that is associated with naïve T

cells, was significantly recued in T cells in T-p110δ^{E1020K} mice compared to WT mice, with the no difference observed in p110δ^{D910A} mice (**Figure 3.2.4d**).

Our group and others have shown a role of p110δ in the development, differentiation and function of Regulatory T cells (Tregs) [4]. Tregs can be identified by the expression of markers CD25 and Foxp3. Therefore, to examine the development of Tregs in the p110δ^{E1020K} mice, single cell suspensions were stained from thymus, spleen and pLNs with CD4, CD25 and intracellular Foxp3. In the peripheral lymphoid tissues of the T-p110δ^{E1020K} mice, there was an increase in the proportion of Tregs compared to WT mice, and a small reduction in the thymus (**Figure 3.2.4e**). In contrast in p110δ^{D910A} mice, an increase in Tregs in the thymus, and a reduction in peripheral lymphoid tissues was observed (**Figure 3.2.4e**) [100].

CTLA4 is a coinhibitory molecule that suppresses T cell responses, despite the costimulatory molecule CD28 and CTLA4 having opposing function they share the same ligands CD80 (B7.1) and CD86 (B7.2) [326]. CTLA4 is expressed in conventional T cells following activation and constitutively expressed in Foxp3^{+} Tregs [327] . CTLA4 is essential for Treg suppression function, as functional defects in Tregs have been reported in the absence of CTLA4 [328, 329]. I found that CTLA4 expression was significantly increased in splenic Tregs in T-p110δ^{E1020K} mice compared to WT mice (**Figure 3.2.34f**) [329]. Increased expression of CD38 has been previously associated with improved suppression ability, and CD38^{high} cells are reduced in p110δ deficient Tregs that is related to defective suppression ability [330]. Tregs with hyperactive p110δ activity had increased expression of CD38, therefore suggesting that Tregs in T-p110δ^{E1020K} mice have increased suppression capability (**Figure 3.2.4f**) [330]. Overall, these results indicate that hyperactive p110δ activity leads to an increased activated phenotype in T cells with some control due to the increase peripheral Tregs. A similar T cell phenotype has also been shown in germline E1020K mice (G-p110δ^{E1020K}), where the hyperactive p110δ (p110δ^{E1020K}) mutation is expressed in all the cells [305].

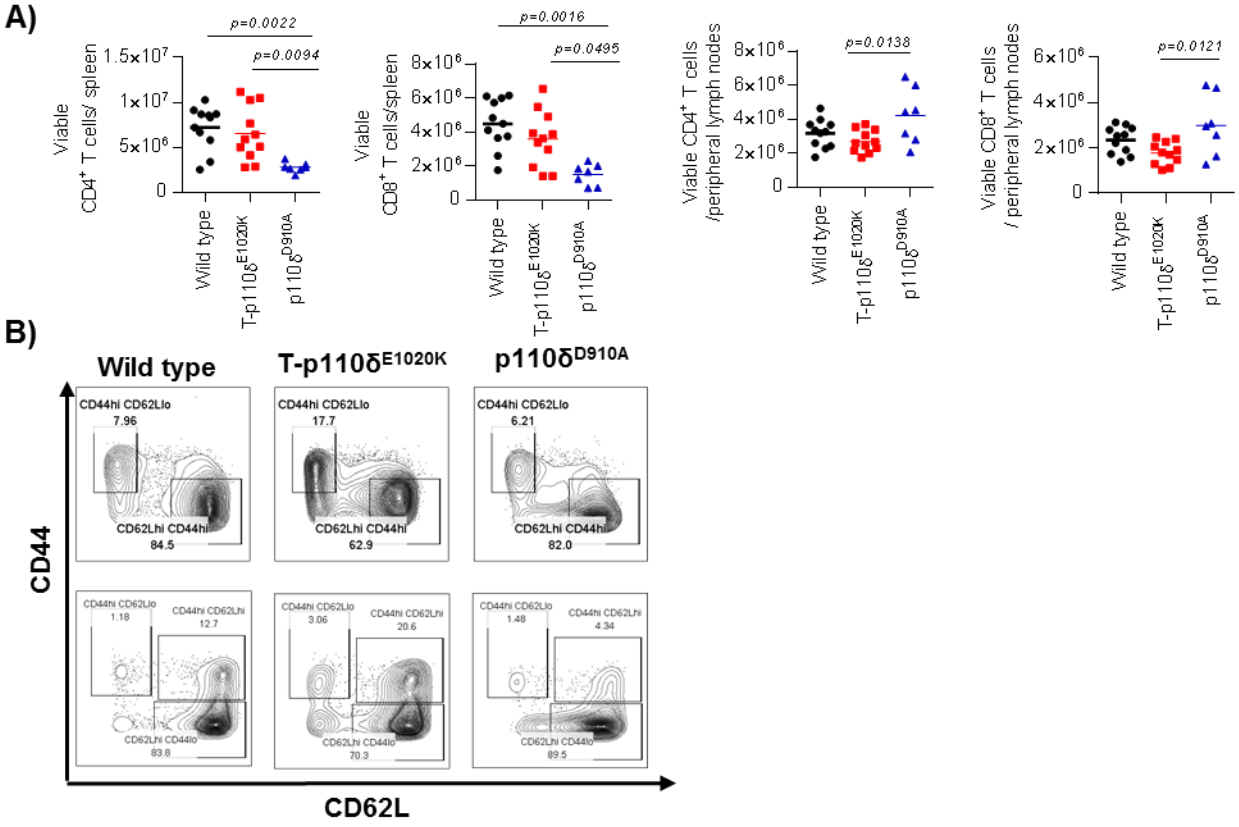
A)
Viable CD4+ T cells/ spleen
p=0.0022
p=0.0094
Viable CD8+ T cells/spleen
p=0.0016
p=0.0495
Viable CD4+ T cells /peripheral lymph nodes
p=0.0138
Viable CD8+ T cells / peripheral lymph nodes
p=0.0121
Wild type
T-p110δE1020K
p110δD910A

B)
Wild type
T-p110δE1020K
p110δD910A
CD44hi CD62Llo
CD62Lhi CD44hi
CD44hi CD62Llo
CD44hi CD62Lhi
CD62Lhi CD44lo
CD44
CD62L

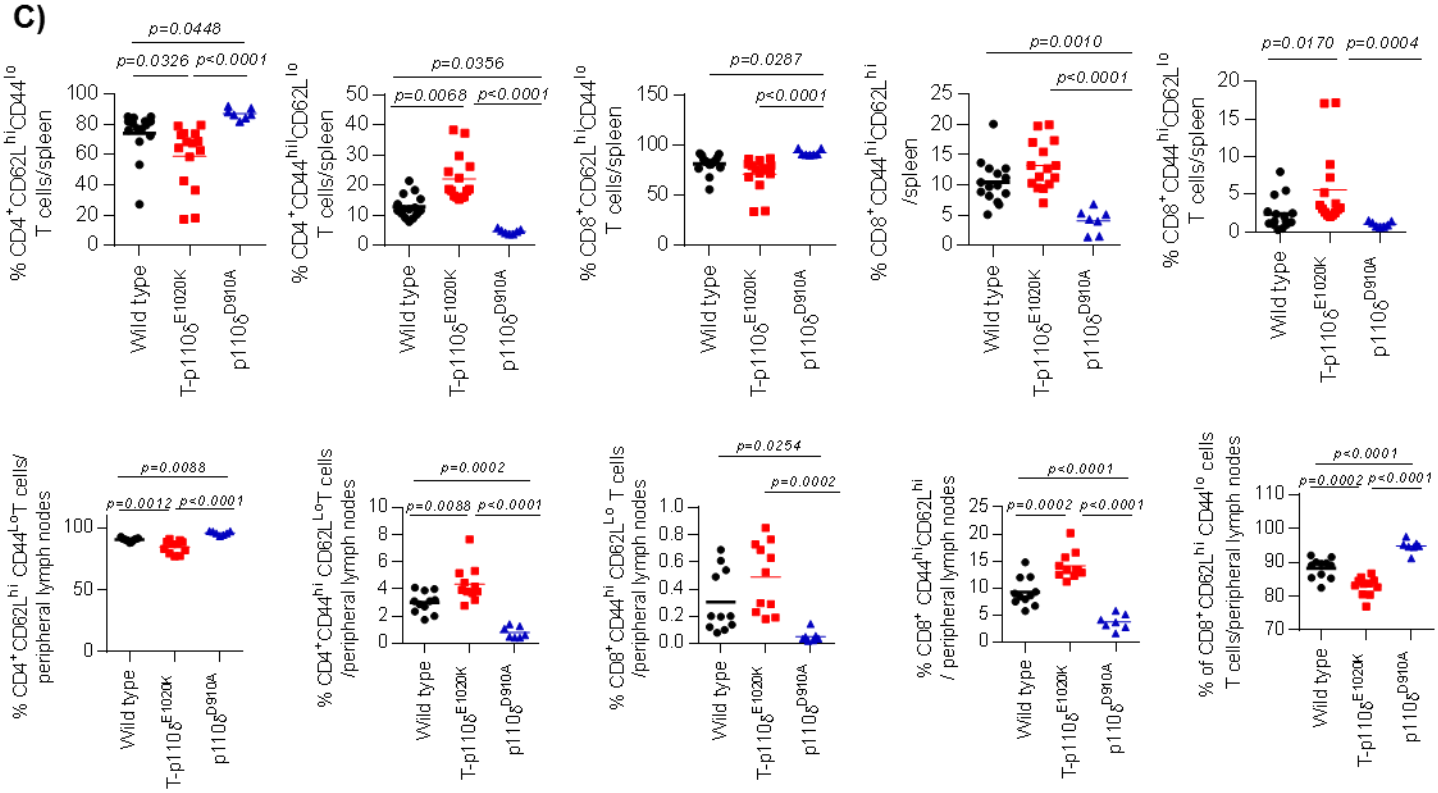
C)
% CD4+CD62LhiCD44lo T cells/spleen
p=0.0448
p=0.0326
p<0.0001
% CD4+CD44hiCD62Llo T cells/spleen
p=0.0356
p=0.0068
p<0.0001
% CD8+CD62LhiCD44lo T cells/spleen
p=0.0287
p<0.0001
% CD8+CD44hiCD62Lhi /spleen
p=0.0010
p<0.0001
% CD8+CD44hiCD62Llo T cells/spleen
p=0.0170
p=0.0004
% CD4+CD62LhiCD44LoT cells/ peripheral lymph nodes
p=0.0088
p=0.0012
p<0.0001
% CD4+CD44hiCD62LLoT cells /peripheral lymph nodes
p=0.0002
p=0.0088
p<0.0001
% CD8+CD44hiCD62LLo T cells /peripheral lymph nodes
p=0.0254
p=0.0002
% CD8+ CD44hiCD62Lhi / peripheral lymph nodes
p<0.0001
p=0.0002
p<0.0001
% of CD8+CD62LhiCD44lo cells T cells/peripheral lymph nodes
p<0.0001
p=0.0002
p<0.0001
Wild type
T-p110δE1020K
p110δD910A

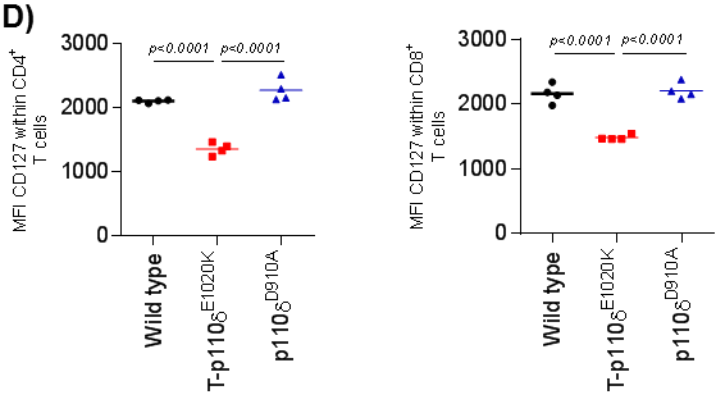
D)
MFI CD127 within CD4+ T cells
p<0.0001
p<0.0001
MFI CD127 within CD8+ T cells
p<0.0001
p<0.0001
Wild type
T-p110δE1020K
p110δD910A

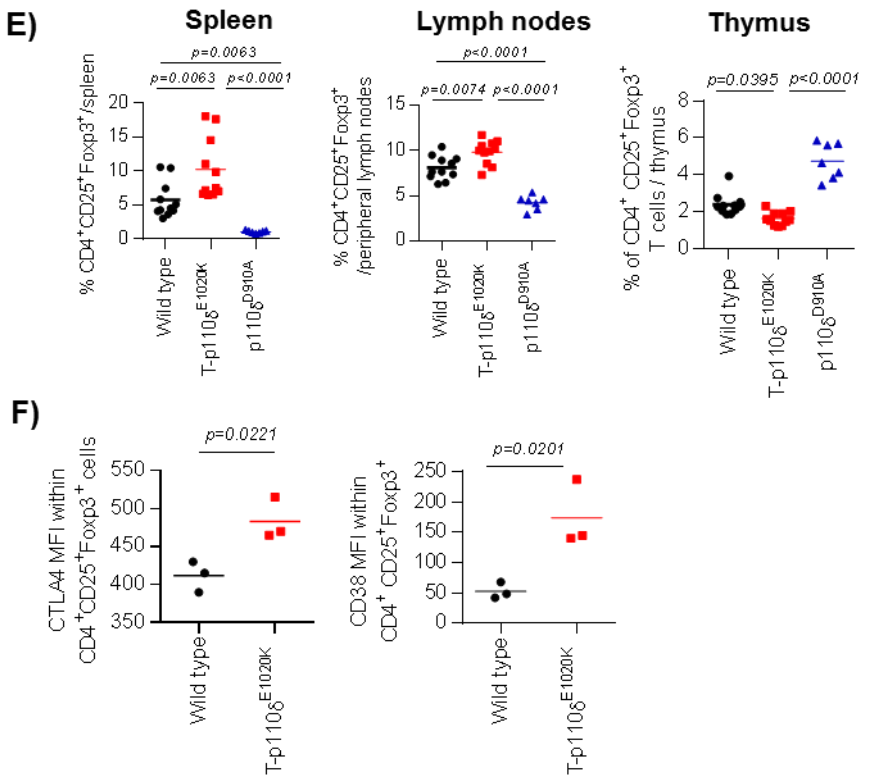

Figure 3.2.4: Increase activated phenotype in T-p110δ^{E1020K} mice.

T cell populations in the thymus, spleen and lymph nodes in WT, T-p110δ^{E1020K} and p110δ^{D910A} were analyzed by flow cytometry. **(A)** Graphs showing total numbers of viable CD4^{+} and CD8^{+} T cells in the spleen and lymph nodes **(B)** Representative flow cytometry plots of CD62L^{+} and CD44^{+} cells gated on CD4^{+} and CD8^{+} T cells in the spleen **(C)** Graphs showing the proportions of activated (CD44^{high}CD62L^{low}) ,memory (CD44^{high}CD62L^{high}) and naïve (CD62L^{high}CD44^{low}) T cells. **(D)** Graphs showing expression (MF) of CD127 in CD4^{+} and CD8^{+} T cells. **(E)** Graphs showing proportions of CD4^{+}CD25^{+}Foxp3^{+} regulatory T cells (Tregs) in the thymus, spleen and lymph nodes. **(F)** Graphs showing expression (MFI) of CTLA4 and CD38 in splenic Tregs in WT and T-p110δ^{E1020K} mice**.** Data in A-C are combined from 3-4 independent experiments (n=7-15), data in D from one independent experiment (n =4 per group), data in E combined from three independent experiments (n=7-11 per group) and data in F is from one independent experiment (n=3 per group). *P values* are shown.

3.2.5 Hyperactive p110δ enhances CD8$^+$ T cell function

To determine the effect of hyperactive p110δ mutation on the function of CD8$^+$ T cells, total lymph nodes dissected from WT, T-p110δ^{E1020K} and p110δ^{D910A} mice were stimulated with anti-CD3 and anti-CD28 for 72 hours. In these experiments, the effect of selective inhibition of p110δ using 10 nM of GSK552269557 was also assessed. Following stimulation, cells were treated with Brefeldin A for 2 hours followed by flow cytometry staining with different lineage, activation and intracellular markers. Post 72 hours stimulation, the proportions of activated (CD44^{high}CD62L^{low}) were enhanced in T-p110δ^{E1020K} compared to WT mice (**Figure 3.2.5a)**. The proportions of memory (CD44^{high}CD62L^{high}) and naïve (CD62L^{high}CD44^{low}) were reduced due to hyperactive p110δ activity. These proportions were reversed with the addition of GSK552269557 in CD8$^+$ T cells in T-p110δ^{E1020K} mice (**Figure 3.2.5a**). Treatment with GSK552269557 led to a reduction in the activated proportions with an increase in naïve CD8$^+$ T cells in WT mice (**Figure 3.2.5a)**. In p110δ^{D910A} mice, the proportions of activated CD8$^+$ T cells (CD44^{high}CD62L^{low}) were reduced with enhanced proportions of memory-like and naïve CD8$^+$ T cells. As predicted, treatment with GSK552269557 did not influence these populations in p110δ^{D910A} mice (**Figure 3.2.5a**).

CD8$^+$ T cells with hyperactive p110δ exhibited enhanced proportions of IFNγ$^+$ cells compared to WT mice at 72 hours post stimulation (**Figure 3.2.5b**). CD8$^+$ T cells from p110δ^{D910A} mice were deficient in their ability to produce IFNγ$^+$ compared to WT mice (**Figure 3.2.5b**). Moreover, the proportion of cells producing IFNγ$^+$ was significantly reduced using the p110δ inhibitor in T-p110δ^{E1020K} and WT mice, but not in p110δ^{D910A} mice after 72 hours of stimulation. (**Figure 3.2.5b)**. The expression of granzyme B and proportions of cells producing TNFα$^+$ was increased in CD8$^+$ T cells from T-p110δ^{E1020K} mice compared to WT mice that were reversed with GSK552269557 (**Figure 3.2.5b**). On the other hand, CD8$^+$ T cells from p110δ^{D910A} produced reduced levels of granzyme B and TNFα$^+$ compared to WT mice, with no influence with the addition of p110δ specific inhibitor (**Figure 3.2.5b**).

In order to determine whether the enhanced effector function observed in CD8$^+$ T cells from T-p110δ^{E1020K} mice was not due to the presence of previously activated CD8$^+$ T cells, naïve (CD62L^{high} CD44^{low}) CD8$^+$ T cells were FACS sorted from T-p110δ^{E1020K} mice and cultured for 72 hours in the presence of anti-CD3 and anti-CD28. Following

stimulation of naïve $CD8^+$ T cells, significantly enhanced proportions of cells producing $IFN\gamma^+$ and increased expression of granzyme B was detected in T-$p110\delta^{E1020K}$ mice compared to WT mice (**Figure 3.2.5c**). These increases in effector cytokines and granzyme B were significantly reduced in the presence of p110δ inhibitor in both WT and T-$p110\delta^{E1020K}$ mice (**Figure 3.2.5c**). This confirms that $CD8^+$ T cells from T-$p110\delta^{E1020K}$ mice have an enhanced effector function and is not due to the presence of previous activated $CD8^+$ T cells.

In order to determine the effector function of hyperactive $CD8^+$ T cells in a physiological setting, germline E1020K (G-$p110\delta^{E1020K}$) mice were crossed with OT1 mice that express a TCR specific for the SIINFEKL peptide. Naïve $CD8^+$ T cells were sorted from WT OT1 and G-$p110\delta^{E1020K}$ OT1 mice and stimulated with SIINFEKL peptide loaded bone marrow dendritic cells that were (BMDCs) derived from C57BL/6 mice, at a ratio of 5 $CD8^+$ T cells to 1 BMDC for 72 hours. Following stimulation, $CD8^+$ T cells with hyperactive p110δ activity produced increased proportions of $IFN\gamma^+$, $TNF\alpha^+$ cells and enhanced expression of granzyme B compared to WT OT1 mice (**Figure 3.2.5d**). This experiment was only performed once with two mice per group, therefore further repeats are required to confirm the results. However, this still gives an indication that following physiological stimulation, $CD8^+$ T cells with hyperactive p110δ activity are able to produce enhanced effector cytokines and granzyme B.

Additionally, proteomic analysis on $CD8^+$ T cells stimulated for 24 hours from WT, T-$p110\delta^{E1020K}$ and $p110\delta^{D910A}$ mice were performed in collaboration with Doreen Cantrell's group in Dundee. Christina Rollings in Dundee carried out the mass spectrometry analysis of this experiment. Total lymph node homogenates form WT, T-$p110\delta^{E1020K}$ and $p110\delta^{D910A}$ mice were stimulated in the presence of anti-CD3, anti-CD28, IL-2 and IL-12 for 24 hours. After 24 hours, $CD8^+$ and $CD4^+$ T cells were FACS sorted, snap frozen and were sent for proteomic analysis. Statistical analysis and generation of volcano plots was performed by Christina Courreges to classify proteins specifically up- or down-regulated in hyperactive $CD8^+$ T cells compared to WT $CD8^+$ T cells. A two-sided paired t-test was performed on the three biological replicates and the proteins presenting a p-value under or equal to 0.05 and a minimum 2-fold change between hyperactive p110δ $CD8^+$ T cells and WT $CD8^+$ T cells were considered significant. According to these criteria, 196 proteins were more abundant in

hyperactive $CD8^+$ T cells and 511 proteins were downregulated compared to WT $CD8^+$ T cells. Within the upregulated proteins, an increase in the abundance of effector proteins such as IFNγ and granyzme B in $CD8^+$ T cells from T-p110δ^{E1020K} mice compared to WT $CD8^+$ T cells was detected. In addition, treatment with p110δ inhibitor resulted in reduced abundance of these effector proteins (**Figure 3.2.5e**). The converse was true in p110δ^{D910A} mice, where a reduction was observed for IFNγ and granzyme B compared to WT mice, with no effect of the inhibitor (**Figure 3.2.5e**). Overall, these results confirm that hyperactive p110δ mutation in $CD8^+$ T cells leads to an enhanced activated phenotype with greater functional abilities that are reduced with treatment with a p110δ specific inhibitor.

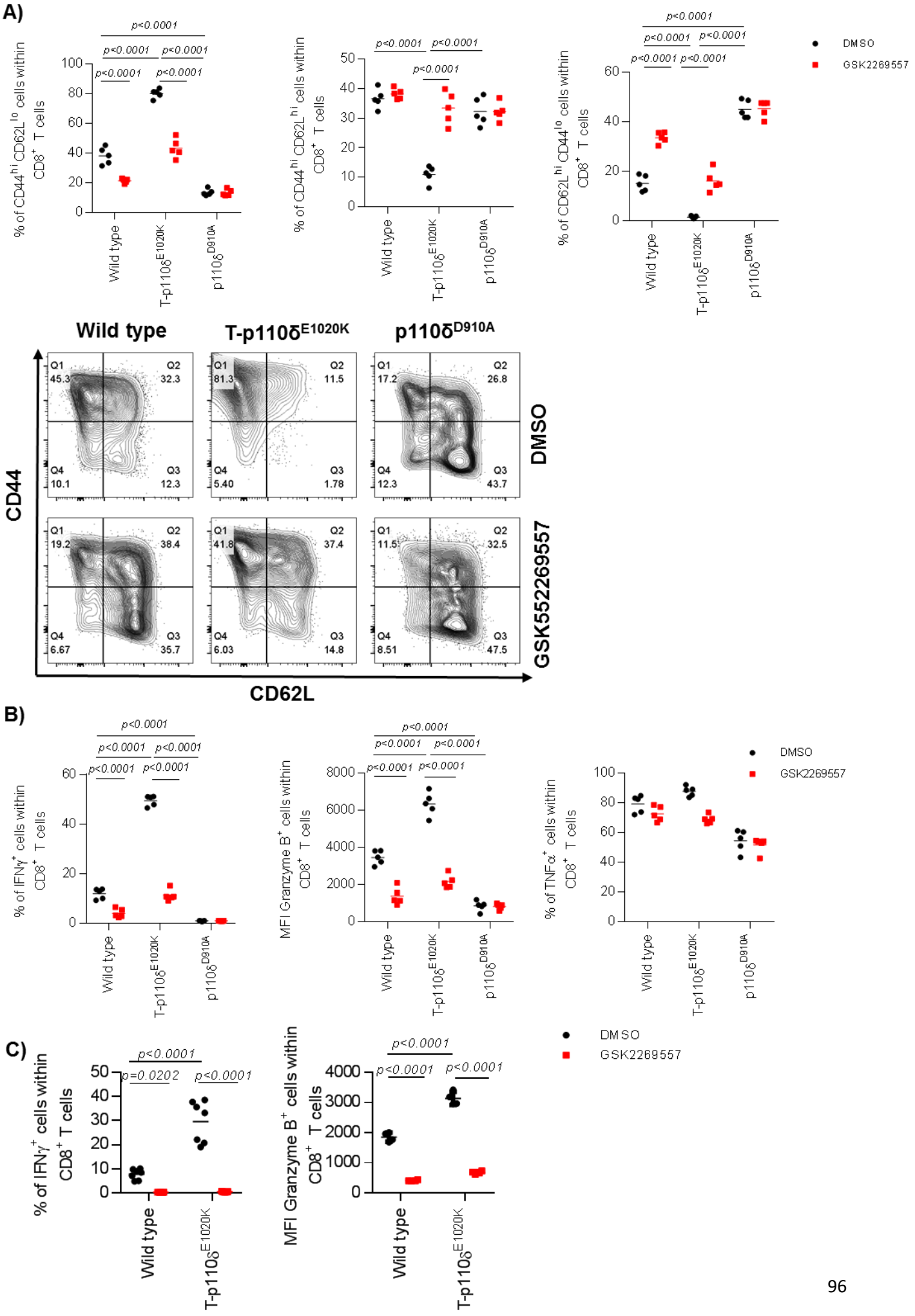
A)
% of CD44hi CD62Llo cells within CD8+ T cells
% of CD44hi CD62Lhi cells within CD8+ T cells
% of CD62Lhi CD44lo cells within CD8+ T cells
p<0.0001
p=0.0202
Wild type
T-p110δE1020K
p110δD910A
DMSO
GSK2269557
Wild type
T-p110δE1020K
p110δD910A
CD44
CD62L
DMSO
GSK552269557
Q1 45.3
Q2 32.3
Q4 10.1
Q3 12.3
Q1 81.3
Q2 11.5
Q4 5.40
Q3 1.78
Q1 17.2
Q2 26.8
Q4 12.3
Q3 43.7
Q1 19.2
Q2 38.4
Q4 6.67
Q3 35.7
Q1 41.8
Q2 37.4
Q4 6.03
Q3 14.8
Q1 11.5
Q2 32.5
Q4 8.51
Q3 47.5
B)
% of IFNγ+ cells within CD8+ T cells
MFI Granzyme B+ cells within CD8+ T cells
% of TNFα+ cells within CD8+ T cells
C)
% of IFNγ+ cells within CD8+ T cells
MFI Granzyme B+ cells within CD8+ T cells

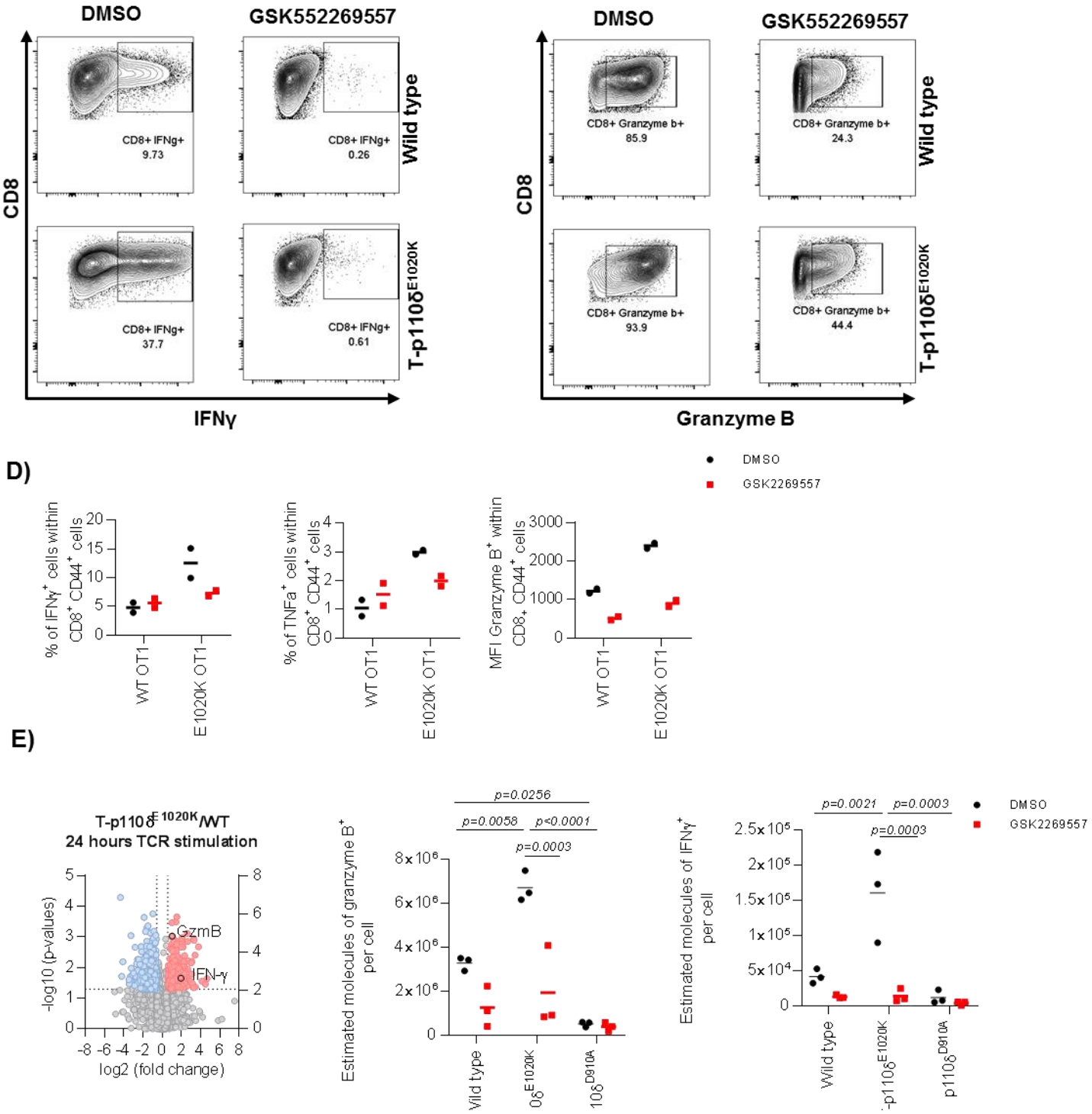

Figure 3.2.5: Hyperactive p110δ leads to enhanced CD8$^+$ T cell function following *in vitro* stimulation

Total lymph nodes from WT, T-p110δ^{E1020K} and p110δ^{D910A} mice were stimulated with anti-CD3 and anti-CD28 for 72 hours. Following stimulation cells were stained for different lineage, activation and effector cytokines markers and analysed by flow cytometry. **(A)** Graphs and flow cytometry plots representing proportions of CD44^{high}CD62L^{low} (activated), CD44^{high}CD62L^{high} (memory) and CD62L^{high}CD44^{low} (naïve) within CD8$^+$ T cells. **(B)** Graphs representing proportions of IFNγ$^+$, TNFα$^+$ and granzyme B$^+$ cells within CD8$^+$ T cells.

Naive ($CD8^+$ $CD62L^{high}$ $CD44^{low}$) $CD8^+$ T cells were FACS sorted from WT and T-$p110\delta^{E1020K}$ mice and stimulated with anti-CD3 and anti-CD28 for 72 hours, treated with either DMSO or 10nM GSK552269557. **(C)** Graphs and representative flow cytometry plots showing proportions of $IFN\gamma^+$ and granzyme B^+ cells. **(D)** Graphs showing proportions of $IFN\gamma^+$, $TNF\alpha^+$ cells and expression of granzyme B^+ cells within naïve $CD8^+$ T cells stimulated with BMDC's loaded SIINFEKL peptide for 72 hours. **(E)** Volcano plots showing fold changes in protein copy numbers vs. log-transformed P-values from mass spectrometry analysis of 24 hours stimulated FACS sorted $CD8^+$ T cells from T-$p110\delta^{E1020K}$ and WT $CD8^+$ T cells. Graphs showing abundance of $IFN\gamma^+$ and granzyme B^+ cells within 24 hours stimulated WT T-$p110\delta^{E1020K}$ and $p110\delta^{D910A}$ $CD8^+$ T cells. Data in A representative of two independent experiments (n=5 per group), data in B representative of two independent experiments (n=4 mice per group). Data in C representative of one independent experiment (n=2) per group. Data in E represents 3 technical replicates using 4-5 mice each time per group. *P values* are shown

3.2.6 Hyperactive p110δ affects CD4$^+$ T cell differentiation in response to cytokines

The adaptive immune response relies on different CD4$^+$ T helper (Th) subsets that are characterised by different transcription factors and cytokine profiles, and are dependent on the cytokine environment present at the time of activation [331]. Adaptive immune responses are tailored to different types of pathogens through differentiation of naïve CD4 T cells into functionally distinct subsets of helper T cells (Th1, Th2, Th9, Th17, Tregs and Tfh). Numerous studies have highlighted an important role played by p110δ in CD4$^+$ T cell differentiation [58, 90, 95, 100, 332]. Inhibition of p110δ via inhibitors or genetic manipulation using p110δ^{D910A} have shown reduced production of multiple cytokines such as IFNγ, IL-4, IL-5, IL-10 and IL-17. This indicates an important role played by p110δ signaling in different CD4$^+$ T cell subsets. Therefore, I assessed the ability of naïve CD4$^+$ T cells from T-p110δ^{E1020K} mice to differentiate into Th1, Th2, Th17, Tfh and Tregs cells using different cytokine conditions. The cytokine combinations used to differentiate CD4$^+$ T cells into different Th subsets has been described in chapter two.

Naïve (CD62L^{high}CD44^{low}) CD4$^+$ T cells were FACS sorted, cultured in the presence of anti-CD3, anti-CD28 and a specific cytokine combination to skew CD4$^+$ T cells into different Th subsets for 5 days. The cell culture media was replenished after 3 days with new media containing cytokines and either DMSO or 10 nM GSK2269557. In Th1 differentiated CD4$^+$ T cells, the production of IFNγ$^+$ cells and expression of T-bet was significantly enhanced in CD4$^+$ T cells with hyperactive p110δ activity compared to WT CD4$^+$ T cells, this was significantly reduced in the presence of GSK2269557 (**Figure 3.2.6a**). Inhibition of p110δ in WT CD4$^+$ T cells did not affect IFNγ$^+$ production but resulted in reduced T-bet expression (**Figure 3.2.6a**). IL-4 production and expression in CD4$^+$ T cells under Th2 skewed conditions were increased in T-p110δ^{E1020K} mice compared to WT mice, this was reduced with p110δ inhibition (**Figure 3.2.6b**). In differentiated Tfh cells, there was a trend towards increase expression of IL-21 by CD4$^+$ T cells in T-p110δ^{E1020K} mice compared to WT mice (**Figure 3.2.6c**). Differentiation into Th2 and Tfh cells were performed only once, therefore repeated experiments are required to confirm whether these findings are reproducible.

In differentiated Th17 cells, the proportions of IL-17A^{+} cells were also enhanced in T-p110δ^{E1020K} mice but was not inhibited with p110δ inhibitor (**Figure 3.2.6d**). Lastly, induced Tregs (iTregs) were significantly reduced in T-p110δ^{E1020K} mice but increased with p110δ inhibitor treatment (**Figure 3.2.6e**).

Preliminary analysis of gene microarray data (carried out by Glyn Bradley, GSK) of naïve CD4^{+} T cells from WT, T-p110δ^{E1020K} and p110δ^{D910A} mice stimulated with anti-CD3 and anti-CD38 for 72 hours, revealed increase in different transcription factors and cytokines associated with different Th lineage subsets in CD4^{+} T cells from T-p110δ^{E1020K} mice. Increased expression of Th1 associated genes (IFNG1, IL-2 and TBX21). In addition, increase in TNFα was also detected which can be produced by Th1 cells. Key transcription factors along with cytokines involved in Th2 differentiation (STAT6, GATA3, IL-4 and IL-13) were increased. The expression of these different markers was reduced with p110δ inhibition (**Figure 3.2.6f**). Overall, this set of data suggests that hyperactive p110δ promotes CD4^{+} T cell differentiation into different Th subsets but inhibits the differentiation of iTregs.

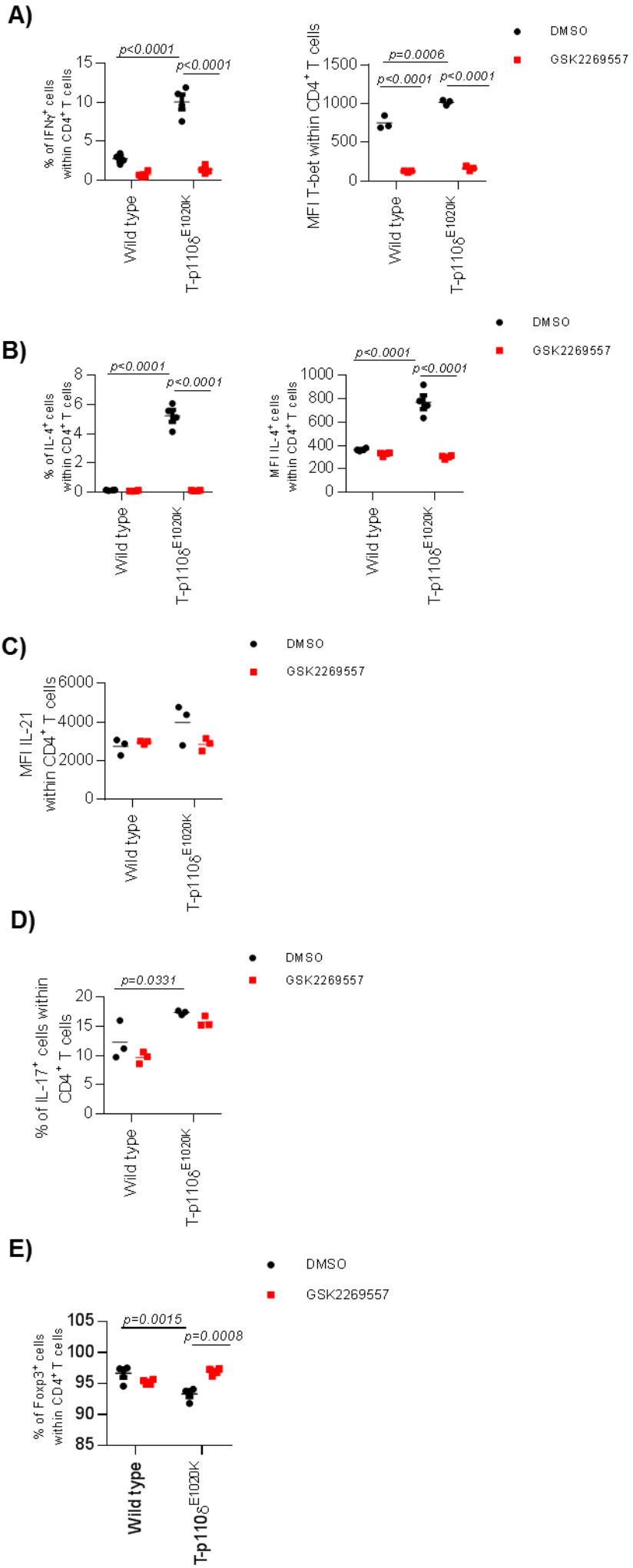
A)
% of IFNγ+ cells within CD4+ T cells
p<0.0001
p<0.0001
MFI T-bet within CD4+ T cells
p=0.0006
p<0.0001
p<0.0001
DMSO
GSK2269557
Wild type
T-p110δE1020K
B)
% of IL-4+ cells within CD4+ T cells
p<0.0001
p<0.0001
MFI IL-4+ cells within CD4+ T cells
p<0.0001
p<0.0001
C)
MFI IL-21 within CD4+ T cells
D)
% of IL-17+ cells within CD4+ T cells
p=0.0331
E)
% of Foxp3+ cells within CD4+ T cells
p=0.0015
p=0.0008

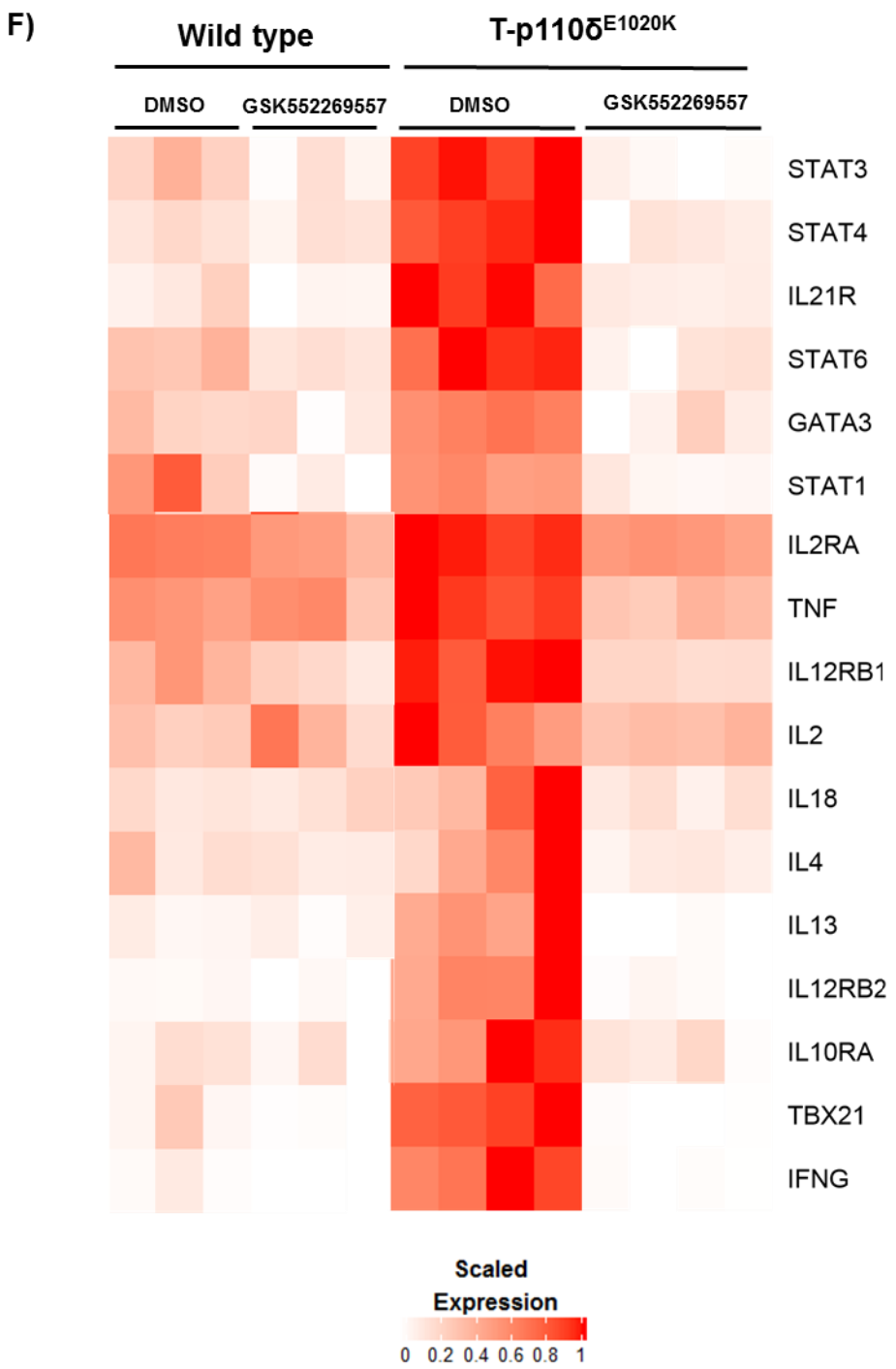

Figure 3.2.6 Increase CD4$^+$ T cell differentiation due to hyperactive p110δ activity in T cells

Naïve CD4$^+$ T cells (CD62L^{high}CD44^{low}) were FACS sorted from WT and T-p110δ^{E1020K} mice, stimulated in the presence of 2.5μg/ml anti-CD3 and 2μg/ml anti-CD28 and a combination of Th lineage specific cytokines for 5 days in the presence DMSO or 10 nM GSK552269557. Graphs showing **(A)** Proportions of IFNγ$^+$ cells and expression of T-bet cells in Th1 differentiated CD4$^+$ T cells. **(B)** Proportions and expression (MFI) of IL-4$^+$ producing cells in Th2 differentiated CD4$^+$ T cells. **(C)** Expression (MFI) of IL-21$^+$ cells in Tfh differentiated CD4$^+$ T cells. **(D)** Proportions of IL-17$^+$ cells within Th17 differentiated CD4$^+$ T cells. **(E)** Proportions of Foxp3$^+$ cells within iTreg differentiated CD4$^+$ T cells. **(F)** Heat map of gene microarray data illustrating key Th related cytokines and transcription factors in stimulated naïve CD4$^+$ T cells from WT and T-p110δ^{E1020K} mice. Data in A, D-E is representative of two independent experiments, data in B-C and F is representative of one independent experiment). *P values* are shown

3.2.7 Hyperactive p110δ leads to increased cell death following *in vitro* stimulation

Hyperactive p110δ signalling resulted in increased cell death in T cells from APDS patients upon anti-CD3 and anti-CD28 stimulation [138, 141]. In order to determine whether the same effect is observed in T-p110δ^{E1020K} mice, Annexin 5 was used as a marker to measure apoptosis. Naïve (CD62L^{high}CD44^{low}) CD4^{+} and CD8^{+} T cells were FACS sorted from WT and T-p110δ^{E1020K} mice, stimulated for 72 hours with anti-CD3 and anti-CD28, in the presence or absence of 10nM GSK2269557. Upon stimulation, the proportions of apoptotic cells as detected by Annexin 5 and live dead dye was significantly increased in CD4^{+} and CD8^{+} T cells from T-p110δ^{E1020K} mice compared to WT mice. This was significantly reversed by inhibition with 10nM GSK2269557 treatment in T-p110δ^{E1020K} and CD8^{+} T cells in WT mice but had a subtle reduction in CD4^{+} T cells in WT mice (**Figure 3.2.7a and b**). Additionally, the proportions of viable cells, identified as negative for Annexin5 ^{and} live dead dye staining, was reduced in T cells with hyperactive p110δ activity; this was rescued by the addition of GSK2269557. Similar results were observed. Additionally, naïve CD8^{+} T cells were sorted from WT OT1 and G-p110δ^{E1020K} OT1 mice and stimulated with SIINFEKL peptide loaded bone marrow dendritic cells that were (BMDCs) derived from C57BL/6 mice, at a ratio of 5 CD8^{+} T cells to 1 BMDC for 72 hours. Following stimulation, increased cell death was observed in CD8^{+} T cells with hyperactive p110δ activity compared to WT OT1 mice (shown in appendix).

In order to further confirm whether T cells from p110δ^{E1020K} mice were undergoing apoptosis, the fluorescently labelled peptide FAM-VAD-FMK (FAM) was used, which binds to activated caspases to detect apoptotic cells. An increase in FAM^{+} cells were detected amongst T cells in T-p110δ^{E1020K} mice in comparison to WT mice, which was decreased with p110δ specific inhibitor (**Figure 3.2.7c**). In p110δ^{D910A} mice, the proportions of FAM^{+} cells were significantly reduced in CD8^{+} T cells with a reduced trend in CD4^{+} T cells compared to WT mice, and no difference with the p110δ inhibitor (**Figure 3.2.7c**). Overall, this set of data provides evidence that T cells from p110δ^{E1020K} mice have an activated effector phenotype but undergo activation induced cell death following stimulation.

Fas/FasL (CD95/CD178) interaction plays a significant role in T cell mediated cell death and acts as a homeostatic mechanism of the immune system. *In vitro* activation of T cells results in increased expression of FasL, which, upon binding to and oligomerisation of Fas, results in the direct activation of caspase enzymes via their recruitment to a death-inducing signaling complex (DISC). Following activation of caspases, the apoptotic program is initiated, resulting in the demise of the cell by classical apoptosis [333, 334]. Interestingly, preliminary gene microarray data analysis (carried out by Glyn Bradley, GSK) on naïve $CD4^+$ T cells stimulated with anti-CD3 and anti-CD28 for 72 hours in the presence or absence of 10nM GSK2269557, revealed an increase in the expression of FAS and FASL in T-p110δ^{E1020K} mice compared to WT mice (**Figure 3.2.7d**). This increase in expression was reduced with the p110δ specific inhibitor (**Figure 3.2.7d**). Consistent with this, following stimulation of naïve $CD4^+$ and $CD8^+$ T cells for 72 hours with anti-CD3 and anti-CD28, a significant increase in Fas expression was detected by flow cytometry in T cells from T-p110δ^{E1020K} mice compared to WT mice, and this was significantly reduced with GSK2269557 treatment (**Figure 3.2.7e**). As engagement of the cell death surface receptor Fas by FasL results in apoptotic cell death, a preliminary experiment was carried out to determine whether inhibition of Fas using an anti-FasL antibody could rescue T cells from apoptosis in T-p110δ^{E1020K} mice. Naïve ($CD62L^{high}CD44^{low}$) $CD8^+$ T cells were FACS sorted and stimulated with anti-CD3 and anti-CD28 for 72 hours. Cells were treated with PBS or 10µg/ml purified anti-mouse FasL antibody. The clone used was MFL3 that has been reported to block Fas induced apoptosis. Following stimulation, increase in Annexin 5 expression was detected in $CD8^+$ T cells with hyperactive p110δ activity that was reduced with the addition of anti-FasL antibody (**Figure 3.2.7f**). The proportions of Annexin 5^+ cells were reduced to the levels of PBS treated $CD8^+$ T cells from WT mice (**Figure 3.2.7f**). The inhibition of Fas had no effect on $CD8^+$ T cells from the WT mice. These results further indicate increased activation induced cell death in T cells with hyperactive p110δ activity that can be rescued with p110δ inhibition and is dependent on increased Fas induced cell death.

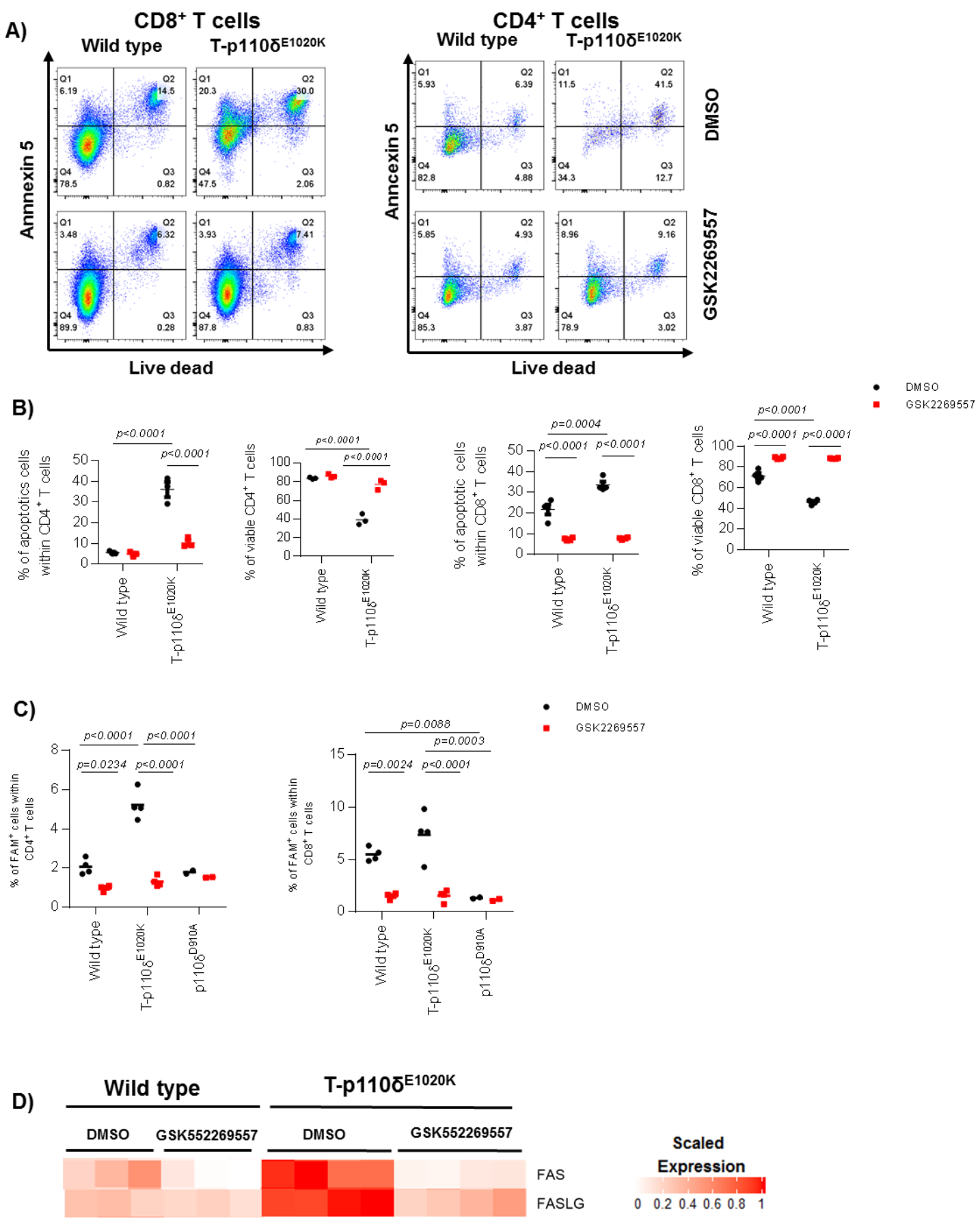
A)
CD8+ T cells
Wild type
T-p110δE1020K
CD4+ T cells
Wild type
T-p110δE1020K
Annnexin 5
Anncexin 5
Live dead
Live dead
DMSO
GSK2269557
Q1 6.19
Q2 14.5
Q4 78.5
Q3 0.82
Q1 20.3
Q2 30.0
Q4 47.5
Q3 2.06
Q1 3.48
Q2 6.32
Q4 89.9
Q3 0.28
Q1 3.93
Q2 7.41
Q4 87.8
Q3 0.83
Q1 5.93
Q2 6.39
Q4 82.8
Q3 4.88
Q1 11.5
Q2 41.5
Q4 34.3
Q3 12.7
Q1 5.85
Q2 4.93
Q4 85.3
Q3 3.87
Q1 8.96
Q2 9.16
Q4 78.9
Q3 3.02
B)
DMSO
GSK2269557
% of apoptotics cells within CD4+ T cells
% of viable CD4+ T cells
% of apoptotic cells within CD8+ T cells
% of viable CD8+ T cells
p<0.0001
p=0.0004
Wild type
T-p110δE1020K
C)
DMSO
GSK2269557
% of FAM+ cells within CD4+ T cells
% of FAM+ cells within CD8+ T cells
p=0.0234
p=0.0088
p=0.0003
p=0.0024
Wild type
T-p110δE1020K
p110δD910A
D)
Wild type
T-p110δE1020K
DMSO
GSK552269557
DMSO
GSK552269557
FAS
FASLG
Scaled Expression
0 0.2 0.4 0.6 0.8 1

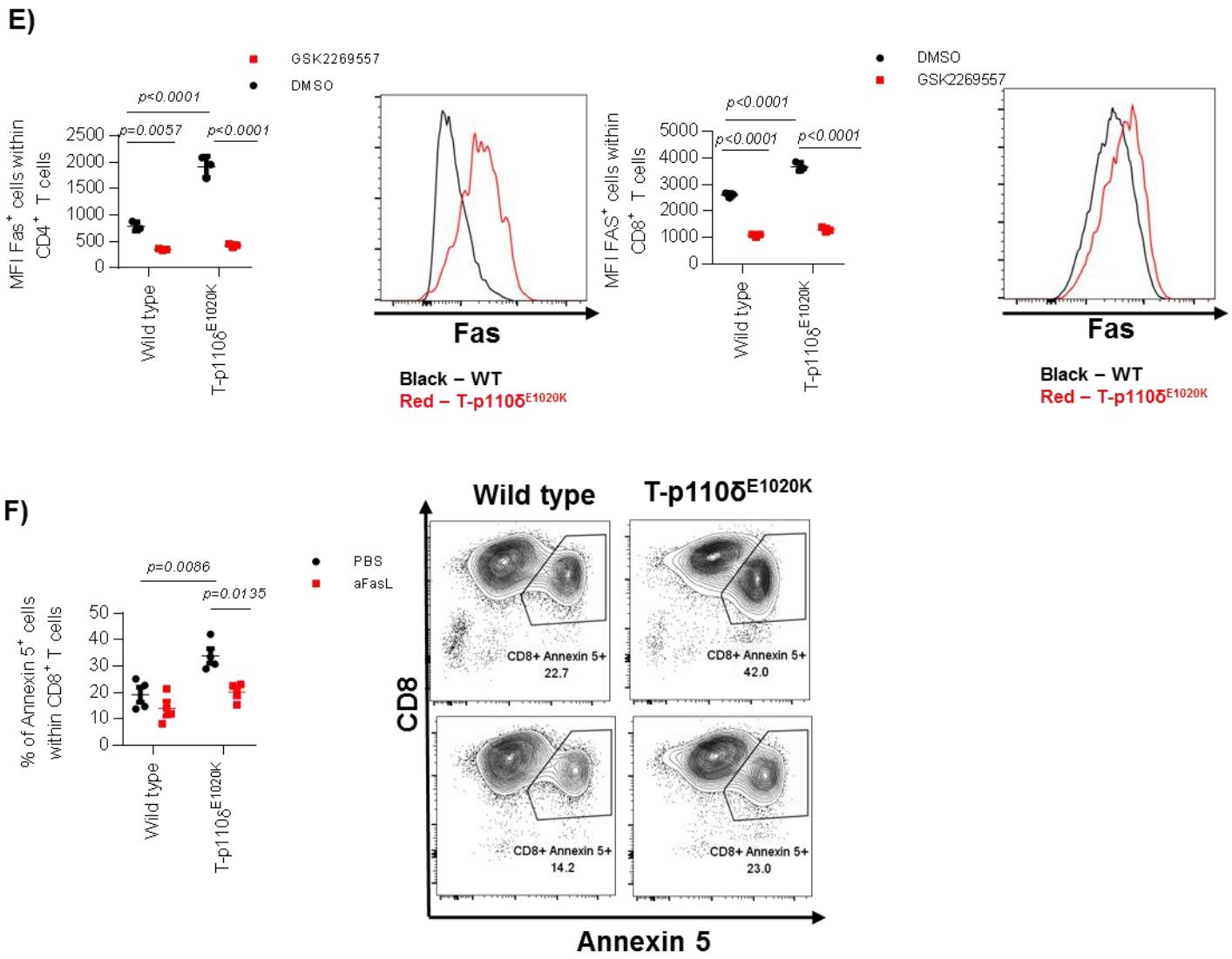

Figure 3.2.7: Increase cell death in T cells with hyperactive p110δ following stimulation

Naïve ($CD62L^{high}CD44^{low}$) $CD4^+$ and $CD8^+$ T cells were sorted from WT and T-$p110\delta^{E1020K}$ mice and stimulated with anti-CD3 and anti-CD28 in the presence or absence of 10 nM GSK2269557 for 72 hours. **(A)** Representative flow cytometry plots illustrating apoptotic cells as defined by Annexin 5^+ and viability dye^+ and viable cells as viability dye^- and Annexin 5^- in $CD8^+$ and $CD4^+$ T cells. **(B)** Graphs showing proportions of apoptotic and viable cells by using Annexin 5 and viability dye in $CD4^+$ and $CD8^+$ T cells. **(C)** Graphs showing percentage of apoptotic $CD4^+$ and $CD8^+$ T cells detected by using 0.75μM of a fluorescently labelled caspase peptide FAM-VAD-FMK following stimulation of total splenocytes with anti-CD3 and anti-CD28 for 72 hours. **(D)** Heat map illustrating the expression of FAS and FASL in stimulated $CD4^+$ T cells. **(E)** Graphs showing expression of CD95 (Fas) within $CD8^+$ and $CD4^+$ T cells following 72 hours of anti-CD3 and anti-CD28 stimulation. **(F)** Graphs showing proportions of Annexin 5^+ cells within $CD8^+$ T cells treated with either PBS or 10μg/ml αFasLigand. Data in A-B representative of two independent experiments, (n=4 for $CD8^+$ T cells and n=3 for $CD4^+$ T cells), data in C representative of two independent experiments (n=4 for WT and T-$p110\delta^{E1020K}$ and n=2 for $p110\delta^{D910A}$ mice) , data in D representative of one independent experiment (n=3-4), data in E representative of one experiment (n=3), data in F representative of one independent experiment (n=3). *P values* are shown.

3.2.8 No difference in T cell proliferation due to hyperactive p110δ

In order to investigate the effect of hyperactive p110δ on T cell proliferation, the proliferation dye Cell Trace Violet was used to detect cell division and was measured as successive halving of the fluorescence intensity of the dye with each cell division. Lymph node homogenates from WT, T-p110δ^{E1020K} and p110δ^{D910A} mice were stained with cell trace violet dye and the cells were stimulated with anti-CD3 and anti-CD28 for 72 hours in the presence or absence of 10 nM GSK2269557. There was no difference in proliferation detected after 48 and 72 hours of stimulation in CD4^{+} and CD8^{+} T cells in T-p110δ^{E1020K} mice compared to WT mice (**Figure 3.2.8a**). There were subtle defects in proliferation of CD4^{+} and CD8^{+} T cells in p110δ^{D910A} mice compared to WT mice and in mice treated with the p110δ inhibitor (**Figure 3.2.8a**). These results therefore indicate that hyperactive p110δ does not result in a proliferation defect in response to anit-CD3 and anti-CD28 stimulation. IL-2 levels were measured in the supernatants of anti-CD3/CD28 stimulated lymph nodes after 48 and 72 hours of stimulation. At 48 hours, I detected an increase in the levels of IL-2 in DMSO treated T-p110δ^{E1020K} T cells compared to WT mice, this was not inhibited by the p110δ specific inhibitor (**Figure 3.2.8b**). However, at 72 hours there was no difference between DMSO treated WT and T-p110δ^{E1020K} T cells, but treatment with p110δ specific inhibitor resulted in reduced levels of IL-2 in T-p110δ^{E1020K} mice with no differences in WT T cells (**Figure 3.2.8b**). Levels of IL-2 did not differ in p110δ^{D910A} mice compared to WT mice (**Figure 3.2.8b**).

To further understand whether specific cell cycle phases were affected by p110δ signalling, bromo-2′-deoxyuridine (BrdU) incorporation was assessed in CD4^{+} and CD8^{+} T cells in WT, T-p110δ^{E1020K} and p110δ^{D910A} mice. For these experiments, total lymph nodes homogenates were stimulated with anti-CD3 and anti-CD28 for 72 hours in the presence or absence of 10nM GSK2269557. No significant differences were observed between WT and T-p110δ^{E1020K} mice in the S, G0/G1 and G2/M phase of the cell cycle in both T cell subsets, with no differences with the p110δ inhibitor (**Figure 3.2.8c-d**). However, in the sub G1 phase which is a representation of apoptotic cells, increased proportions of CD4^{+} and CD8^{+} T cells were detected in the T-p110δ^{E1020K} mice compared to WT mice that was reduced with the p110δ inhibitor (**Figure 3.2.8c-d**). In p110δ^{D910A} mice, no differences for both T cell subsets was detected compared

to WT mice (**Figure 3.2.8c-d**). This set of data implies that in T-p110δ^{E1020K} mice, proliferation or cell cycle is not compromised compared to WT mice, but increased numbers of T cells undergo apoptosis.

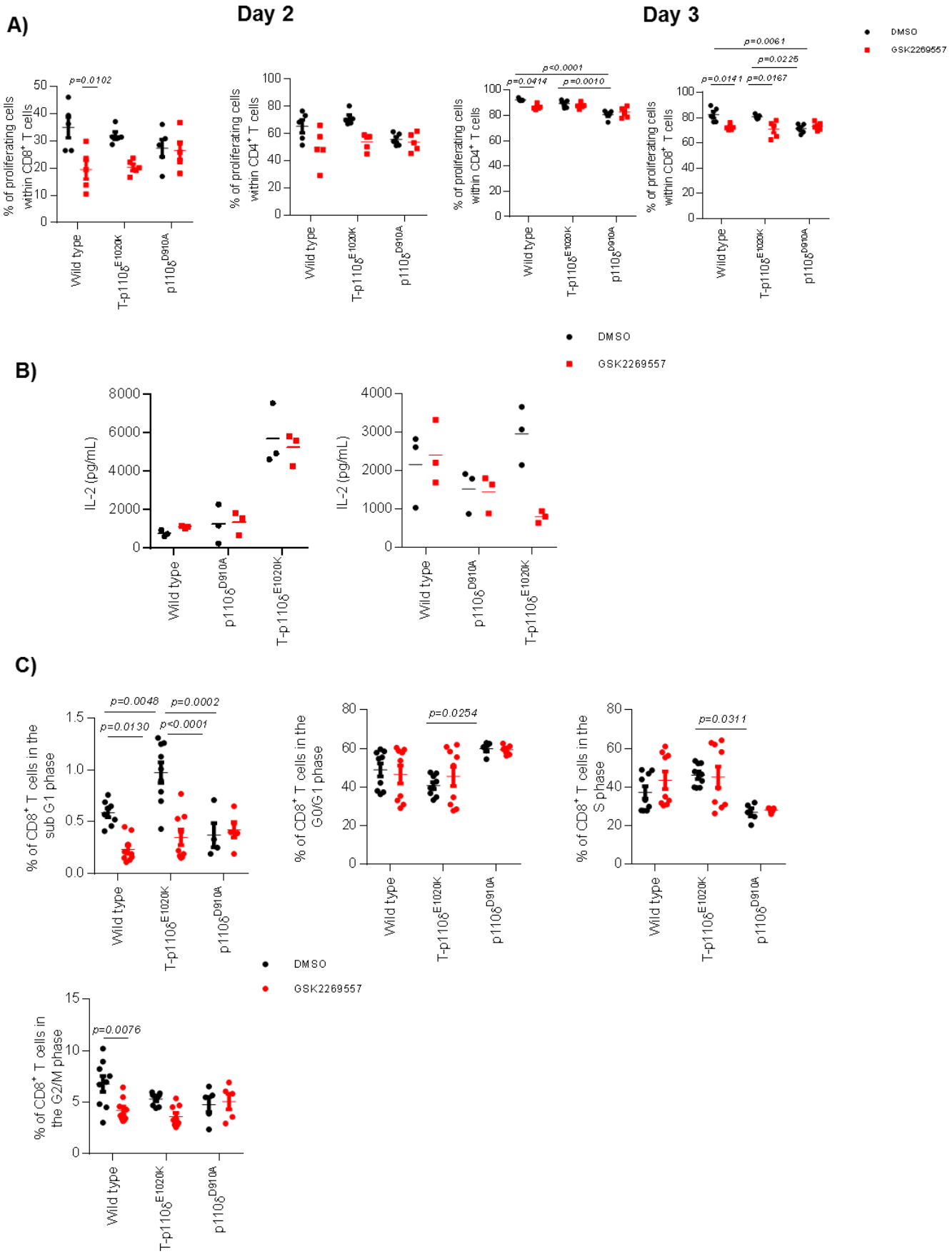
A)
Day 2
Day 3
DMSO
GSK2269557
% of proliferating cells within CD8+ T cells
% of proliferating cells within CD4+ T cells
p=0.0102
p<0.0001
p=0.0414
p=0.0010
p=0.0061
p=0.0225
p=0.0141
p=0.0167
Wild type
T-p110δE1020K
p110δD910A
B)
IL-2 (pg/mL)
C)
% of CD8+ T cells in the sub G1 phase
% of CD8+ T cells in the G0/G1 phase
% of CD8+ T cells in the S phase
% of CD8+ T cells in the G2/M phase
p=0.0048
p=0.0002
p=0.0130
p<0.0001
p=0.0254
p=0.0311
p=0.0076

D)

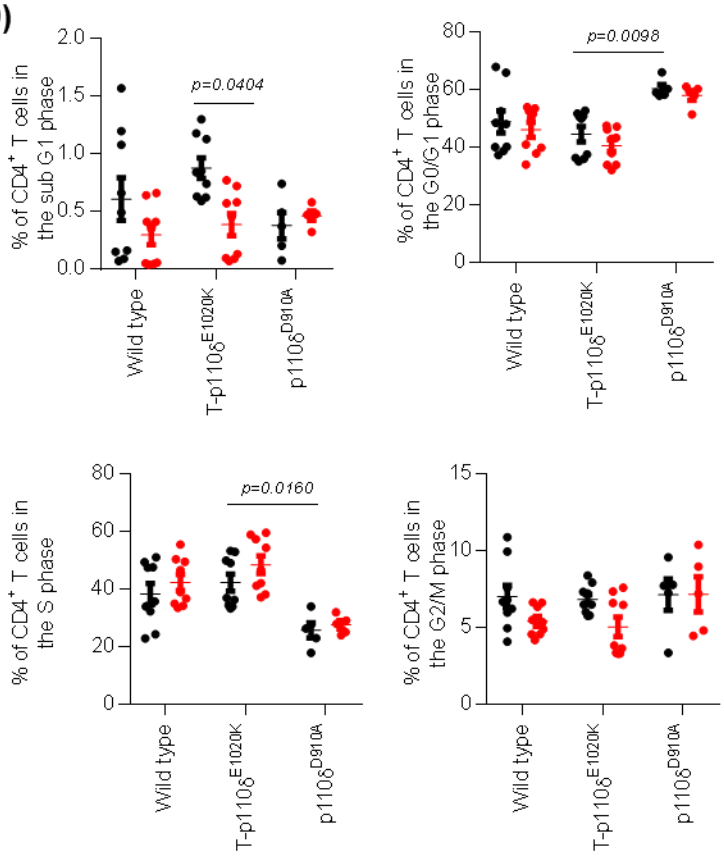
% of CD4+ T cells in the sub G1 phase
p=0.0404
% of CD4+ T cells in the G0/G1 phase
p=0.0098
% of CD4+ T cells in the S phase
p=0.0160
% of CD4+ T cells in the G2/M phase
Wild type
T-p110δE1020K
p110δD910A

E)

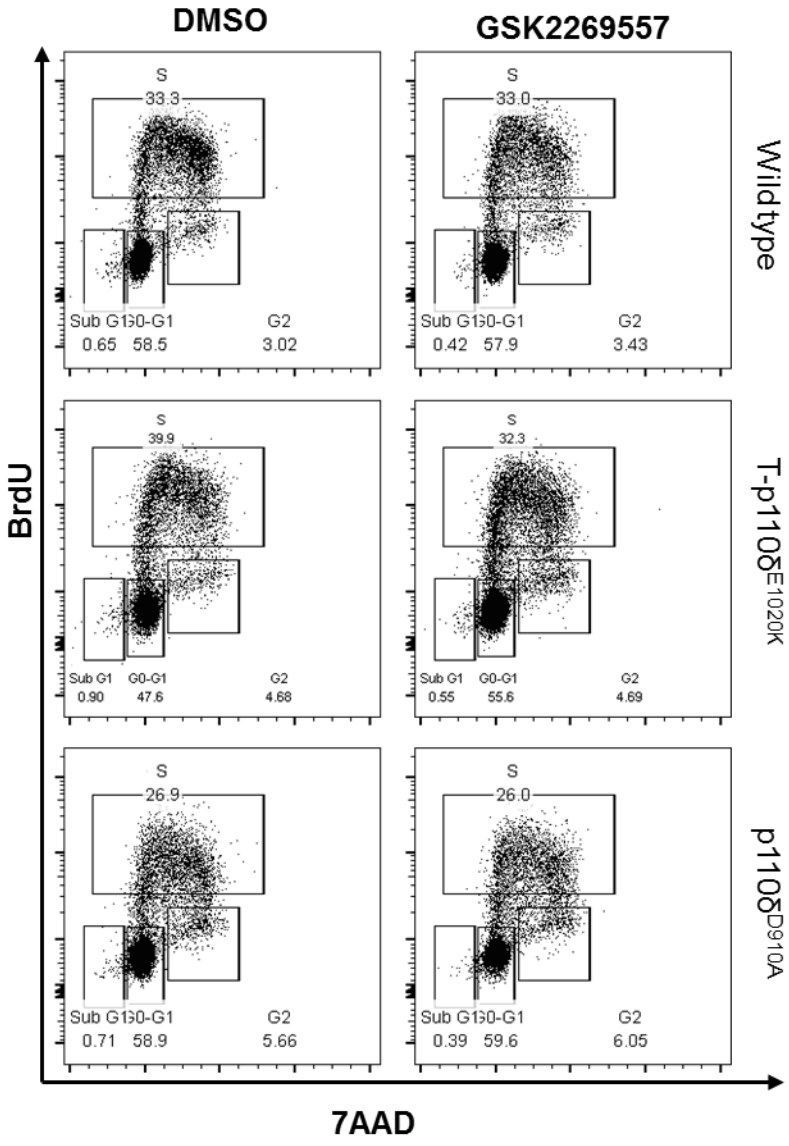
DMSO
GSK2269557
Wild type
T-p110δE1020K
p110δD910A
BrdU
7AAD
S
Sub G1
G0-G1
G2
33.3
0.65
58.5
3.02
33.0
0.42
57.9
3.43
39.9
0.90
47.6
4.68
32.3
0.55
55.6
4.69
26.9
0.71
58.9
5.66
26.0
0.39
59.6
6.05

Figure 3.2.8: No difference in proliferation in T cells due to hyperactive p110δ

Total lymph nodes from WT, T-p110δ^{E1020K} and p110δ^{D910A} mice were stimulated with anti-CD3 and anti-CD28 in the presence of DMSO or 10 nM GSK2269557 for 72 hours . **(A)** Graphs showing proportions of proliferating CD4^{+} and CD8^{+} T cells at 48 and 72 hours. **(B)** Graphs showing IL-2 levels measured by Elisa in supernatants harvested at 48 and 72 hours post stimulation. **(C)** Graphs showing cell cycle analysis of CD4^{+} and CD8^{+} T cells . **(D)** Flow cytometry plots illustrating the different cell cycle phases within CD8^{+} T cells .Data in A is from one independent experiment with n=5 per genotype , data in B is from one independent experiment with n=3 per genotype and data in C-D is combined from 2 independent experiments with n=5-9 per genotype. *P values* are shown

3.2.9 Increased T follicular helper cells due to hyperactive p110δ activity

T follicular helper (Tfh) cells provide essential help to B cells during germinal centre (GC) responses via CD40L and production of cytokines such as IL-4 and IL-21 [335]. They are important for activation of B cells, antibody class switching and for the formation of germinal centers (GC). Tfh cells are characterised by the expression of CXC chemokine receptor 5 (CXCR5), which is important for these cells to enter the B cell follicle. Tfh cells also express ICOS, programmed death 1 (PD-1) and transcription factor B cell lymphoma 6 (BCL-6) [108, 336]. T follicular regulatory (Tfr) cells, a subset of Foxp3^{+} Tregs that also express CXCR5 , ICOS , PD-1 and Bcl-6, localise in germinal centers to regulate humoral responses and ensure production of high-affinity antibodies that do not react to self-antigens [337, 338]. APDS patients have enlarged GC's, reduced class switched antibodies and impaired antibody responses to vaccination. Mice that lack p110δ activity have defective formation of Tfh cells and GC's, therefore demonstrating important roles played by p110δ in regulating GC reactions [110].

In order to determine whether B cell help from T cells harboring hyperactive p110δ affects efficient antibody responses, antigen dependent humoral responses were analysed. For these experiments different mouse models were utilised to determine which cell type is important for the defective antibody responses observed in APDS patients. Along with T-p110δ^{E1020K} and G-p110δ^{E1020K} mice, a B cell specific mouse model was used that was generated by crossing Mb1$^{Cre/WT}$ mice with p110δ$^{E1020Kflox/WT}$ mice (B-p110δ^{E1020K}).

WT, T-p110δ^{E1020K}, B-p110δ^{E1020K} and p110δ^{D910A} mice were immunised with the T cell dependent hapten NP (4-Hydroxy-3-nitrophenylacetyl) conjugated to carrier KLH (Keyhole Limpet Hemocyanin) in alum on day 0 and were culled on day 14 post immunisation. At day 14 post immunisation, T-p110δ^{E1020K} mice had significantly increased proportions of Tfh, Tfr and total GC B cells relative to the WT mice. In addition, these Tfh cells expressed increased Bcl-6, which is an important transcription factor for the differentiation of Tfh cells (**Figure 3.2.9a**). In contrast, p110δ^{D910A} mice had reduced proportions of Tfh cells consistent with previous published data (**Figure 3.2.9a**) [110]. In B-p110δ^{E1020K} mice, the proportions of Tfh, Tfr cells and Bcl-6 expression were comparable to WT mice (**Figure 3.2.9a**). The proportions of total GC B cells characterised as B220^{+}CD19^{+}CD95^{+}GL7^{+} were significantly increased in T-p110δ^{E1020K} mice compared to WT mice (**Figure 3.2.9b**) Interestingly in T-p110δ^{E1020K} mice, proportions of NP^{+} IgG1^{+} cells within GC B cells were similar to WT mice. On the other hand, in B-p110δ^{E1020K} mice, the proportions of total GC B cells were similar to WT mice, but the proportions of NP^{+}IgG1^{+} cells were significantly reduced, suggesting impaired antibody class switching. In G-p110δ^{E1020K} mice, increased proportions of Tfh and Tfr cells were detected owing to the hyperactive p110δ activity in T cells (**Figure 3.2.9c**). Additionally, the expression of ICOS, important for regulating Tfh differentiation downstream of PI3K signalling was increased in G-p110δ^{E1020K} mice compared to WT mice (**Figure 3.2.9c**). Total GC B cells were also increased in G-p110δ^{E1020K} mice; however, NP specific IgG1^{+} cells within GC B cells were reduced compared to WT mice (**Figure 3.2.9d**). Overall, these results suggest that help from Tfh cells with hyperactive p110δ is not a limiting factor but there is an intrinsic defect within hyperactive B cells that contribute to the defective antibody responses observed.

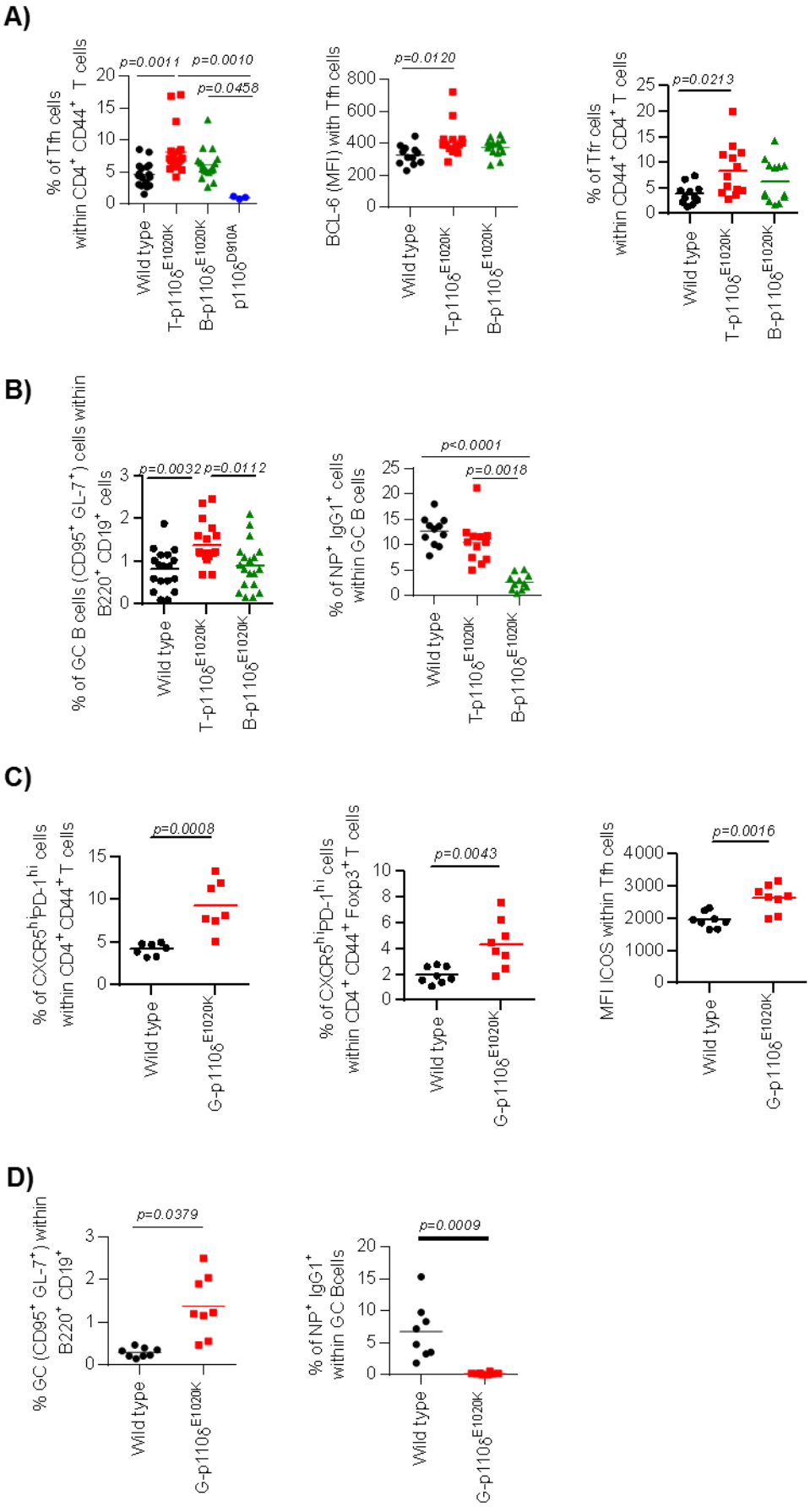
A)
% of Tfn cells within CD4+ CD44+ T cells
p=0.0011
p=0.0010
p=0.0458
Wild type
T-p110δE1020K
B-p110δE1020K
p110δD910A
BCL-6 (MFI) with Tfn cells
p=0.0120
% of Tfr cells within CD44+ CD4+ T cells
p=0.0213
B)
% of GC B cells (CD95+ GL-7+) cells within B220+ CD19+ cells
p=0.0032
p=0.0112
% of NP+ IgG1+ cells within GC B cells
p<0.0001
p=0.0018
C)
% of CXCR5hiPD-1hi cells within CD4+ CD44+ T cells
p=0.0008
G-p110δE1020K
% of CXCR5hiPD-1hi cells within CD4+ CD44+ Foxp3+ T cells
p=0.0043
MFI ICOS within Tfn cells
p=0.0016
D)
% GC (CD95+ GL-7+) within B220+ CD19+
p=0.0379
% of NP+ IgG1+ within GC Bcells
p=0.0009

Figure 3.2.9: Increase Tfh and Tfr cells due to hyperactive p110δ activity in T cells

WT, T-p110^{E1020K}, B-p110δ^{E1020K} and p110δ^{D910A} mice were immunized with NP-KLH on day 0 .Mice were culled on day 14 post immunisation. **(A)** Graphs showing proportions of Tfh (CD4^{+} CD44^{+} CXCR5^{+} PD-1^{+}), Tfr (CD4^{+}CD44^{+}CXCR5^{+}PD-1^{+}Foxp3^{+}) cells and expression (MFI) of Bcl-6 within Tfh cells. **(B)** Graphs showing proportions of total GC B cells (CD95^{+}GL7^{+}CD19^{+}B220^{+}) and IgG1^{+}NP^{+} cells within GC B cells. In another set of experiments WT and G-p110δ^{E1020K} mice were immunised with NP-KLH and culled on day 14 **(C)** Graphs showing proportions of Tfh, Tfr and expression of ICOS within immunised. **(D)** Graphs showing proportions of total GC B cells and IgG1^{+}NP^{+} GC B cells. Data in A-B representative of 2-3 combined experiments , data in C representative of one independent experiment (n=8 per genotype) .*P values* are shown

3.2.10 Hyperactive p110δ leads to increase in activated Tregs

For in depth analysis of the effect of hyperactive p110δ in Tregs, Foxp3$^{YFP\text{-}Cre}$ (FYC) mice were bred with p110δ$^{E1020Kflox/WT}$ mice to generate mice with mutation in Tregs (F-p110δ^{E1020K} mice). However, genotyping results did show that the Foxp3 Cre mediated recombination was not always specific to Tregs, resulting in the expression of activated p110δ in other cells as well. Nevertheless, splenomegaly and lymphadenopathy were observed in the 8-12 weeks old F-p110δ^{E1020K} mice but not in T-p110δ^{E1020K} or G- p110δ^{E1020K} mice, indicating that the mutation was having a specific effect on the Treg subset. To investigate how Tregs are influenced by hyperactive p110δ, detailed immunophenotyping by flow cytometry of 8-12-weeks old mice was undertaken.

F-p110δ^{E1020K} mice demonstrated signs of splenomegaly and lymphadenopathy when culled (**Figure 3.2.10a**). In addition, these mice had increased proportions of CD4$^+$ T cells and reduced proportions of CD8$^+$ T cells compared to WT mice (**Figure 3.2.10a**). The proportions of total FYC$^+$, CD25$^+$ FYC$^+$ and CD25$^-$FYC$^+$ Tregs were increased in F-p110δ^{E1020K} mice compared to WT mice in the spleen and lymph nodes (**Figure 3.2.10b**). The increase in CD4$^+$ T cells detected in F-p110δ^{E1020K} mice is most likely due to the increase CD4$^+$ FYC$^+$ T cell population detected.

Next, I measured the expression of different Treg-associated activation markers in WT and F-p110δ^{E1020K} mice. Glucocorticoid-induced tumour necrosis factor receptor-related protein (GITR), is a critical player in the differentiation of tTregs and expansion of Tregs, it has been associated with increase activation and suppressive activity of Tregs in both mice and humans [339]. CD39 is a member of ectonucleoside triphosphate diphosphohydrolase (ENTPD) family, which degrades extracellular ATP into adenosine monophosphate (AMP) which is in turn used by the ecto-5'-nucleotidase CD73 to synthesize adenosine [340]. Both CD39 and CD73 play an important role in the suppressive function and stability of Foxp3$^+$ Tregs [341, 342]. Helios is an Ikaros family transcription factor that previously appeared to be restricted to tTregs but has shown to be expressed within iTregs and natural CD4$^+$ Foxp3$^+$ cells in mice spleens and human peripheral blood [343]. ICOS is a CD28 superfamily costimulatory molecule that is expressed on activated T cells. ICOS expression has

been shown to enhance functional stability of Treg and and $ICOS^+$ Treg have more potent suppressive ability than $ICOS^-$ Treg [344, 345]. Hyperactive p110δ activity led to increase expression of ICOS, GITR, CD39 and CD38 amongst $CD4^+$ FYC^+ T cells (**Figure 3.2.10c**). In addition, the expression of Helios, which was measured by intracellular staining, was increased in $CD4^+$ $Foxp3^+$ cells in F-$p110\delta^{E1020K}$ mice (**Figure 3.2.10c**). However, the expression of CD25 did not differ between WT and F-$p110\delta^{E1020K}$ mice. This set of data implies that Tregs with hyperactive p110δ activity have an activated phenotype.

Additionally, following *in vitro* stimulation of splenocytes with PMA and ionomycin, increase $IFN\gamma^+$ producing cells were detected amongst the $Foxp3^+$ cells in F-$p110\delta^{E1020K}$ mice (**Figure 3.2.10d**). As a Th1 like Treg phenotype has been shown to be associated with autoimmune disease and loss of Treg suppressive function, I decided to carry out *in vitro* suppression assays to determine the suppressive ability of Tregs with hyperactive p110δ [346]. In these experiments, Tregs from WT and F-$p110\delta^{E1020K}$ mice were FACS sorted to obtain naïve ($CD62L^{high}CD44^{low}$) $CD4^+$ $CD25^+$ FYC^+ cells that were cultured with naïve conventional WT $CD4^+$ T cells (Tcons) at different ratios (1:1, 1:2, 1:4 and 1:8). At all the ratios tested, Tregs with hyperactive p110δ showed improved ability to suppress proliferation of Tcons compared to WT Tregs (**Figure 3.2.10e**). Therefore, despite the Th1 like phenotype, Tregs with hyperactive p110δ activity still have the ability suppress Tcons.

An increase in the proportions of Tfh cells were observed in F-$p110\delta^{E1020K}$ mice compared to WT mice (**Figure 3.2.10f**). Increase in proportions of Tfr cells were also detected, perhaps owing to the increase in Tregs detected (**Figure 3.2.10f**). Concentrations of anti-double stranded DNA (ANA) antibodies in serum from 8-12 weeks old and 32-44 weeks old F-$p110\delta^{E1020K}$ mice were measured by Elisa to determine whether signs of autoimmunity could be detected. As a comparison, serum from 8-12 weeks old T-$p110\delta^{E1020K}$ mice were also included to see whether there were differences between the two genotypes. With the younger mice (8-12 weeks old), there was no difference in the ANA levels in F-$p110\delta^{E1020K}$ and T-$p110\delta^{E1020K}$ mice when compared to the WT mice; however, aged F-$p110\delta^{E1020K}$ mice had enhanced levels of ANA suggesting that with age these mice are prone to developing autoimmunity (**Figure 3.2.10g**).

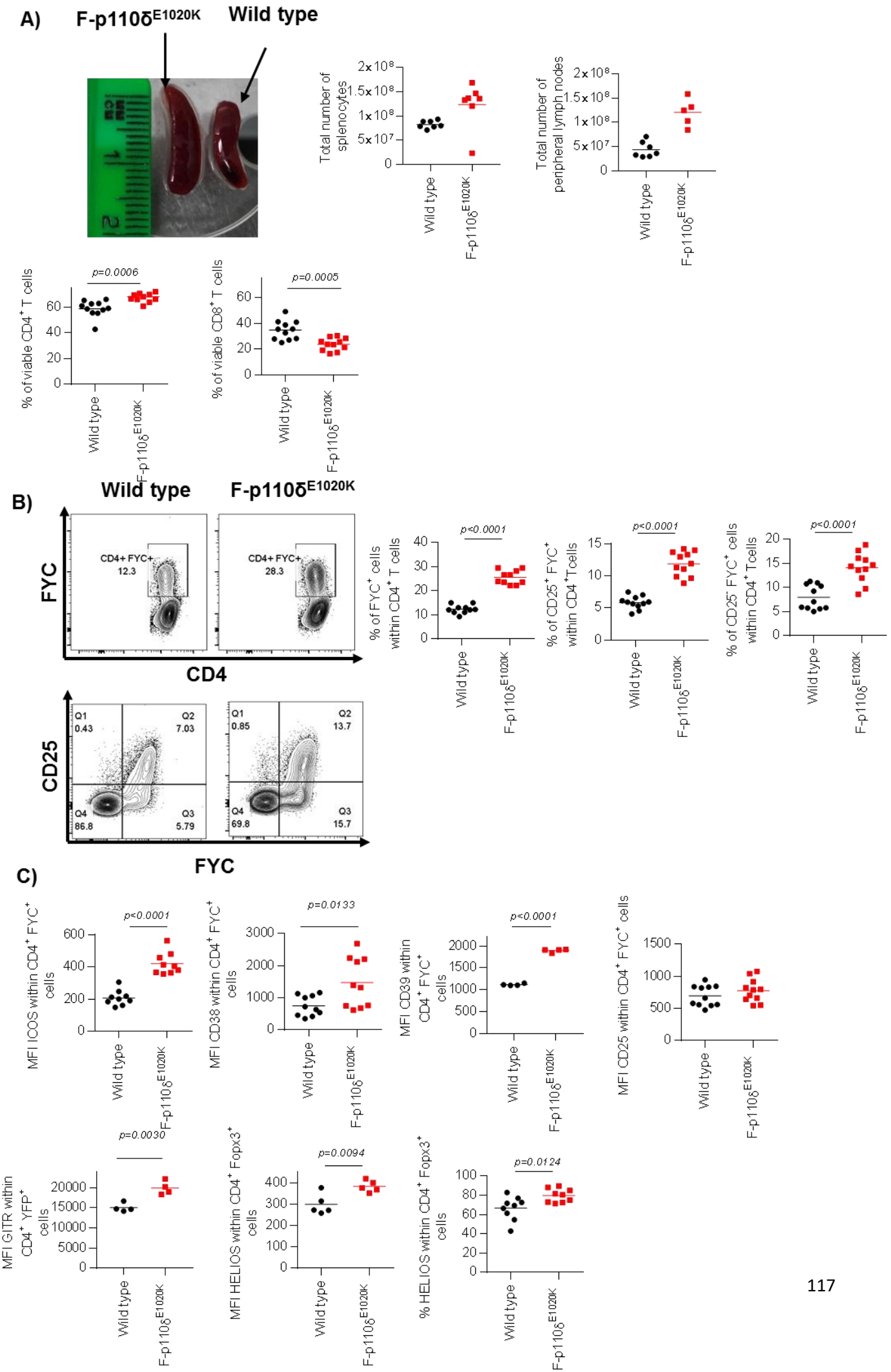
A)
F-p110δE1020K
Wild type
Total number of splenocytes
Total number of peripheral lymph nodes
% of viable CD4+ T cells
% of viable CD8+ T cells
p=0.0006
p=0.0005
Wild type
F-p110δE1020K
B)
Wild type
F-p110δE1020K
FYC
CD4
CD25
CD4+ FYC+ 12.3
CD4+ FYC+ 28.3
Q1 0.43
Q2 7.03
Q4 86.8
Q3 5.79
Q1 0.85
Q2 13.7
Q4 69.8
Q3 15.7
% of FYC+ cells within CD4+ T cells
% of CD25+ FYC+ within CD4+Tcells
% of CD25- FYC+ cells within CD4+ Tcells
p<0.0001
C)
MFI ICOS within CD4+ FYC+ cells
MFI CD38 within CD4+ FYC+ cells
MFI CD39 within CD4+ FYC+ cells
MFI CD25 within CD4+ FYC+ cells
MFI GITR within CD4+ YFP+ cells
MFI HELIOS within CD4+ Foxp3+ cells
% HELIOS within CD4+ Foxp3+ cells
p=0.0133
p=0.0030
p=0.0094
p=0.0124

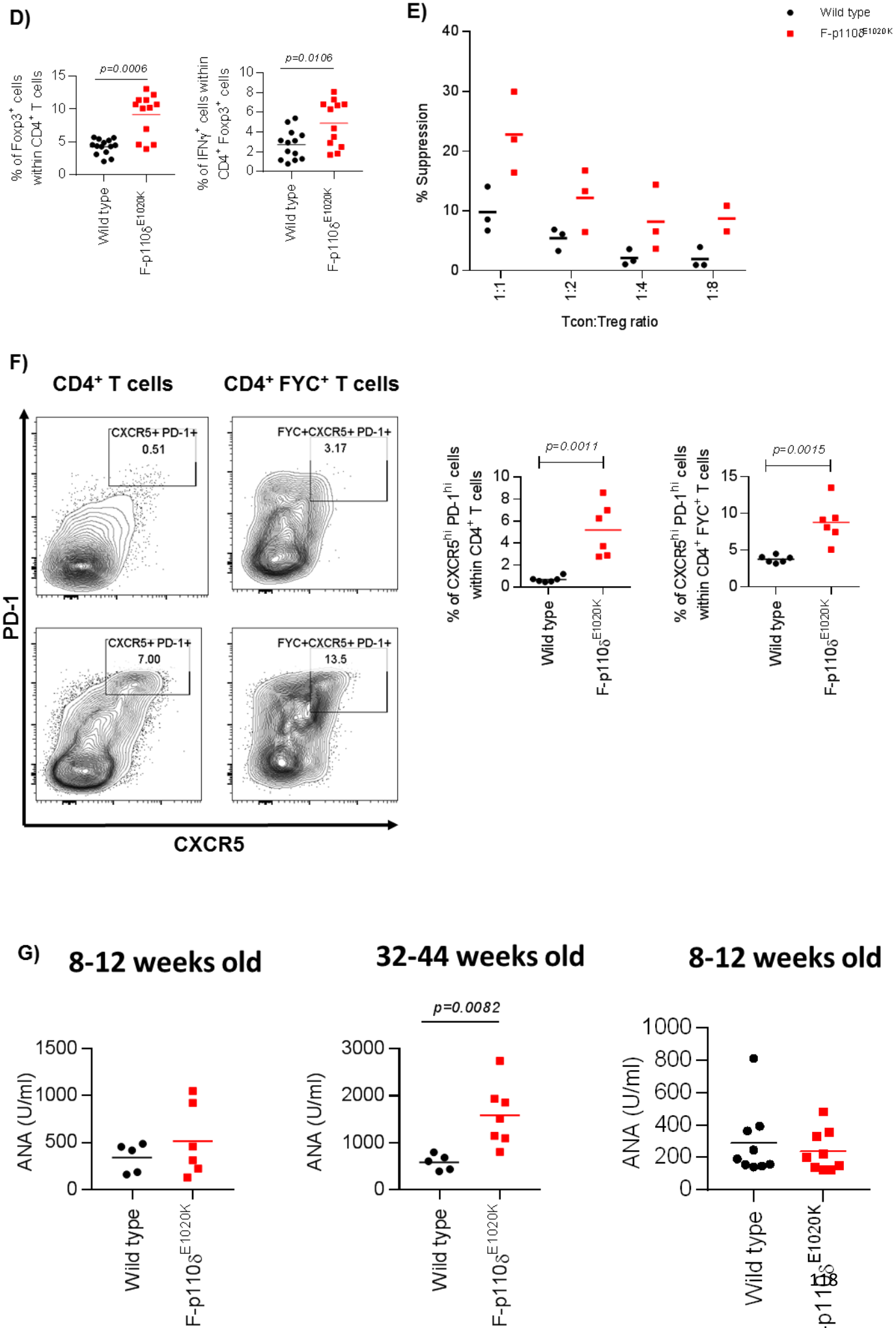
D)
% of Foxp3+ cells within CD4+ T cells
p=0.0006
Wild type
F-p110δE1020K
% of IFNγ+ cells within CD4+ Foxp3+ cells
p=0.0106
E)
Wild type
F-p110δE1020K
% Suppression
Tcon:Treg ratio
1:1
1:2
1:4
1:8
F)
CD4+ T cells
CD4+ FYC+ T cells
CXCR5+ PD-1+
0.51
FYC+CXCR5+ PD-1+
3.17
CXCR5+ PD-1+
7.00
FYC+CXCR5+ PD-1+
13.5
PD-1
CXCR5
% of CXCR5hi PD-1hi cells within CD4+ T cells
p=0.0011
% of CXCR5hi PD-1hi cells within CD4+ FYC+ T cells
p=0.0015
G)
8-12 weeks old
32-44 weeks old
8-12 weeks old
ANA (U/ml)
p=0.0082
T-p110δE1020K

Figure 3.2.10: Increased activated Tregs due to hyperactive p110δ in Tregs

(A) Image of spleens from WT and F-p110δE1020K mice , graphs showing number of cells within spleens and peripheral lymph nodes as determined on CASY counter **(B)** Graphs showing proportions of viable splenic $CD4^+$ and $CD8^+$ T cells **(C)** Graphs showing proportions of splenic $CD4^+$ FYC^+, $CD25^+FYC^+$, $CD25^-FYC^+$ within $CD4^+$ T cells . **(D)** Graphs showing expression (MFI) of ICOS, CD38, CD39,GITR and CD25 in $CD4^+$ FYC^+ T cells. **(E)** Graphs showing proportions and expression (MFI) of Helios determined by intracellular staining in $CD4^+$ $Foxp3^+$ cells . **(F)** Graphs showing proportions of $CD4^+Foxp3^+$ cells and proportions of $IFN\gamma^+$ cells within $CD4^+Foxp3^+$ cells in PMA/ionomycin stimulated splenocytes from WT and F-$p110\delta^{E1020K}$ mice. **(G)** Naïve ($CD62L^{high}CD44^{low}$) $CD4^+$ FYC^+ were sorted from WT and F-$p110\delta^{E1020K}$ mice and co-cultured at different ratios with cell trace violet labelled WT naïve Tcons. These were stimulated for 3 days with anti-CD3 and anti-CD28 coated beads . **(H)** Graphs and **r**epresentative flow cytometry plots of splenic Tfh cells ($CD4^+CXCR5^+PD\text{-}1^+$). **(G)** ANA levels detected in serum of 8-12 weeks old F-$p110\delta^{E1020K}$ and T-$p110\delta^{E1020K}$ mice and 32-44 weeks old F-$p110\delta^{E1020K}$. Data in A-F combined from 1-3 independent experiments (with each dot representing an individual mouse), data in G is combined from 3 independent experiments with each dot representing a technical repeat), data in G is from serum collected over 1-3 independent experiments (each individual dot represents a mouse). *P values* are shown

3.3 Discussion

The data presented in this chapter illustrates a mouse model that recapitulates many of the T cell features demonstrated by APDS patients.

Naïve T cell phenotyping

No significant defects in T cell development was detected in T-p110δ^{E1020K} mice, consistent with previous data suggesting that p110δ alone does not influence T cell development [90]. In addition, enlarged lymph nodes or spleens were not observed in T-p110δ^{E1020K}, possible due to efficient control by simultaneously increased peripheral Tregs. In the naïve mice, T cells in T-p110δ^{E1020K} mice display a tendency towards increase proportions of activated T cells (T_{CM} and T_{EM}) and reduced frequency of naïve (CD62L^{high}CD44^{low}) T cells in the spleen and lymph nodes compared to WT mice. Recently two other groups have published a similar activated phenotype in T cells due to hyperactive p110δ activity using difference mouse models [155, 307]. T cells with hyperactive p110δ also have reduced expression of CD127 that is important for T cell survival, possibly due to reduced phosphorylation of Foxo1 as hyperactive p110δ leads to increased phosphorylation of Akt causing Akt dependent inactivation of Foxo transcription factors. This is further supported by the increased phosphorylation of Akt and Foxo observed in T-p110δ^{E1020K} mice by western blot. Phenotypically T cells from Foxo deficient T cell mice also express higher proportions of activated (CD44^{high}) T cells along with compromised expression of CD62L and CD127 compared to WT mice [347, 348]. In contrast, p110δ^{D910A} mice displayed increased proportions of naïve T cells with a reduction in activated T cells , which is consistent with previously published data [90]. The differences in CD62L expression could be due to the role played by p110δ in causing impaired proteolysis of the CD62L ectodomain or suppression of gene transcription, additionally via inactivation of Foxo1 as well [125, 349] . Loss of PTEN, a major negative regulator of the PI3K pathway, results in increased PIP_3 production and Akt activity. Mouse models with T cell specific PTEN deletion develop thymic lymphoma early in life and following thymectomy these mice were unable to undergo malignant transformation but the mutation resulted in systemic autoimmunity [350, 351]. The differences between T-p110δ^{E1020K} and PTEN deficient T cell models could be due to other Akt independent roles of PTEN, or T cells in T-p110δ^{E1020K} might upregulate phosphatases as a compensation mechanism to help control some aspects

of hyperactive PI3K signalling. Overall, this analysis suggests that hyperactive p110δ activity might be causing subtle defects in T cells in the absence of stimulation.

T-p110δ^{E1020K} mice have reduced Tregs in the thymus with increased peripheral Tregs. Consistent with published data, p110δ^{D910A} mice had increased Tregs in the thymus with reduced Tregs in the periphery [100]. Mice with PTEN deletion in Tregs and activated CD4$^+$ T cells also have enhanced numbers of peripheral Tregs [78, 105, 106]. Additionally mice lacking Foxo1 and Foxo3 in T cells have decreased numbers of thymic Tregs; however, these were increased with age [102]. Increase Akt activation leads to inactivation of Foxo, consequently reducing Foxp3 expression in the thymus of T-p110δ^{E1020K} mice. Differences between numbers of Tregs in the periphery of p110δ^{D910A} and T-p110δ^{E1020K} mice could be due to differing levels of PI3K activity could be attributed to the amount of activation of TCR and IL-2 receptors that are important for homeostatic expansion of Tregs in the periphery.

Functional ability of CD8$^+$ T cells

Upon stimulation of CD8$^+$ T cells in T-p110δ^{E1020K} mice with either anti-CD3/anti-CD28 or peptide, revealed an increase in effector cytokines such as IFNγ and TNFα along with increase in granzyme B expression compared to WT CD8$^+$ T cells. GSK2269557, a p110δ specific inhibitor reversed the increased CD8$^+$ T cell effector phenotype observed in the T-p110δ^{E1020K} mice. Hyperactive p110δ result in reduced proportions of T_{CM} and naïve cells along with a parallel increase in T_{EM} cells following stimulation of CD8$^+$ T cells, these effects were reversed by the p110δ inhibitor. Therefore, implying important role played by p110δ in regulating the expression of CD62L via its downstream proteins. This set of data is consistent with that phenotype observed in APDS patients where an activated phenotype with enhanced effector function is observed under some conditions [138, 141]. Recently published data by Stuart Tangye and colleagues using a gain of function mouse model of p110δ generated by CRISPR/Cas9 system also replicated the salient features in CD8$^+$ T cell differentiation and function, similar to T-p110δ^{E1020K} mice [352]. p110δ^{D910A} mice exhibited reduced IFNγ$^+$, TNFα$^+$ producing cells and reduce expression of granzyme B$^+$ following stimulation, which is consistent with published data that p110δ function is required for *in vitro* IFNγ production [115, 116]. Future studies could focus on investigating the

antitumor response in T-p110δ^{E1020K} mice. The heightened cytotoxic function of CD8^{+} T cells with hyperactive p110δ could result in an improved anti-tumor CD8^{+} T cell response in T-p110δ^{E1020K} mice. However, the enhanced Tregs function in T-p110δ^{E1020K} might simultaneously suppress the anti-tumour response by restricting CD8^{+} T cell function.

CD4^{+} T cell differentiation

Numerous studies have shown that the PI3K pathway modulates the differentiation of Th cells into distinct subsets REF. Studies focusing on suppression of p110δ by either using p110δ^{D910A} mice or inhibitors have shown defective Th1 and Th2 differentiation along with reduced IL-17 producing cells [58]. Under appropriate skewing conditions, naïve CD4^{+} T cells with hyperactive p110δ activity were able to produce enhanced IFNγ, IL-4, IL-17 and IL-21. Consistent with the increases in cytokines, microarray data revealed increase expression of transcription factors associated with Th1 and Th2 lineage specific Th cell differentiation. This set of data highlights the important role played by p110δ in regulating CD4^{+} T cell differentiation. The effect of the p110δ inhibitor did not inhibit cytokine producing cells by WT CD4^{+} T cells possibly due to subtle increases observed in cytokines in the DMSO treated conditions upon stimulation or other class 1A PI3K isoforms might be playing a role.

PTEN deficient CD4^{+} T cells are also able to produce increased Th1 and Th2 cytokines upon anti-CD3 and anti-CD28 stimulation [75]. Deletion of PTEN in mature CD4^{+} T cells also results in increased Th cell function and cytokine production [78]. Foxo1 deficient CD4^{+} T cells also secrete increased quantities of IFNγ, IL-17 and IL-4, suggestive of increased T cell differentiation. T cells deficient of mTORc activity downstream of Akt, results in failure to differentiate into Th1, Th2 and Th17 effector T cells. This is due to a decrease in STAT activation and an inability to upregulate lineage specific transcription factors [96]. mTORc1 signaling promotes Th1 and Th17 differentiation whereas mTORc2 signaling promotes Th2 differentiation [97]. Additionally a recent report of an APDS patient showed an increase in Th2 , Treg and Tfh cells along with increases in plasma cytokine levels of IL-4, IL-17, IFNγ, IL-10, TNFα and IL-6 compared to age matched controls[353]. Induced Treg differentiation was partially reduced in CD4^{+} T cells with hyperactive p110δ activity. This is in

agreement with data indicating that constitutively active AKT, PTEN and Foxo knockout mice have shown to reduce TGFβ dependent iTreg differentiation, likely due to Akt dependent exclusion of Foxo from the nucleus that is important in controlling Foxp3 expression [101, 354, 355]. Inhibition of mTORc1 and mTORc2 also favours iTreg differentiation as demonstrated by treatment with rapamycin and mTORc1 knockout mice [96, 356]. Activation of downstream effector proteins of mTORc1 such as S6K and HIF-1α has been shown to play a role in blocking iTreg differentiation [357]. Therefore, the reduction in iTregs could be a combinatory effect of the exclusion of Foxo from the nucleus and mTOR mediated pathways. Overall, these results suggest that the Akt, mTORc1 and Foxo plays an important role in regulating differentiation of $CD4^+$ T cells.

T cell death and proliferation

In response to *in vitro* TCR stimulation, T cells from T-p110δ^{E1020K} mice proliferate normally but undergo increase apoptosis compared to WT T cells. Cell cycle analysis also revealed increased proportion of cells in the sub G1 phase that was reversed with p110δ specific inhibitor. Inhibition with a p110δ specific inhibitor rescues the T cells in T-p110δ^{E1020K} mice from apoptosis. Additionally, increased expression of Fas and FasL was detected in T cells with hyperactive p110δ activity and following treatment with anti-FasL resulted in reduced apoptosis in $CD8^+$ T cells with hyperactive p110δ. These results therefore suggest an unexpected role of PI3K/Akt in promoting a proapoptotic role in the Fas signaling process. In support of this, increased re-stimulation cell death (RCID) in $CD8^+$ T cells from APDS patients has also been associated with enhanced expression of FasL and the ability of $CD8^+$ T cells to undergo greater cell death [155].

Greater reduction in apoptosis was observed using the p110δ specific inhibitor compared to the anti-FasL antibody in stimulated $CD8^+$ T cells with hyperactive p110δ. There is a possibility that other death receptors are involved such as tumour necrosis factor receptor 1 (TNF-R1), tumour necrosis factor related apoptosis inducing ligand receptors 1 and 2 (TRAIL-R1 and TRAIL-R2) [358]. Inhibition with anti-FasL antibody did not influence apoptosis in WT $CD8^+$ T cells but treatment with p110δ specific inhibitor resulted in subtle reductions. There is a possibility that inhibition of p110δ is

influencing other markers involved in T cell survival such as IL-7Rα (CD127) for example, via Foxo1. The PI3K/Akt has been associated with the regulation of death receptor pathways by providing proapoptotic signals. Ligation of Fas receptor by FasL results in induction of tyrosine phosphorylation that leads to the activation of the PI3K pathway, involving transcriptional upregulation of Fas receptor resulting in sensitisation of cells to Fas induced cell death [359]. APDS patients also display increase hyperactivation of mTOR as measured by increase expression of phosphorylated S6, thereby promoting glycolysis [141]. Naïve T cells are normally in sate of quiescent metabolic state and rely on mitochondrial oxidative phosphorylation (OXPHOS) for ATP generation. On the other hand, effector T cells switch to glycolysis in order to proliferate and produce cytokines such as IFNγ. Recently a link has been established with glycolysis and increased AICD in human $CD8^+$ T cells involving the induction of FasL and Fas mediated apoptosis. Consequently reducing the glycolytic activity led to less sensitivity to AICD [360].

The increase apoptosis might be a mechanism adopted by T cells in T-p110δ^{E1020K} mice to constrain proliferation of effector T cells in order to maintain immune homeostasis by preventing nonspecific immunopathological damage to the host. Loss of PTEN in T cells leads to resistance to AICD and multiorgan autoimmunity. It is probable that as T cells in T-p110δ^{E1020K} mice undergo apoptosis following activation, this could contribute to the mice not developing autoimmunity, as sufficient effector T cells are not present. Defective FAS signalling has been associated with chronic benign lymphoproliferation resulting in splenomegaly and lymphadenopathy, autoimmune manifestations, and an increased risk for lymphoma. Therefore, the ability of the T cells to undergo Fas mediated apoptosis might be a mechanism to avoid hyperproliferation of T cells.

No significant differences in proliferation was detected in T cells from T-p110δ^{E1020K} mice compared to WT mice. Lucas et al reported defective proliferation and IL-2 of APDS $CD8^+$ T cells [141]. Subtle defects in proliferation of T cells from p110δ^{D910A} mice were observed consistent with previous data [58, 90]. However, following anti-CD3 and anti-CD28, p110δ does not play a considerable role in T cell proliferation and IL-2 production but has a great effect on cytokine production; perhaps using physiological stimuli might be ideal to investigate proliferation in T cells with

hyperactive p110δ activity. In response to peptide stimulation, IL-2 production is decreased in p110δ^{D910A} mice but following stimulation with anti-CD3 and anti-CD28 these mice are able to produce comparable levels of IL-2 to WT T cells [58, 90, 361] . Consistent with this, I did not detect differences between IL-2 secretion in T cells from p110δ^{D910A} mice compared to WT mice. Additionally, inhibition in WT T cells were not influenced by p110δ specific inhibition. In T-p110δ^{E1020K}, increased IL-2 secretion was detected at 48 hours post stimulation with no differences at 72 hours compared to WT mice. It could be that T cells with hyperactive p110δ produce normal amounts of IL-2 but as they are undergoing increased apoptosis, they are unable to consume IL-2 efficiently leading to an accumulation of IL-2. The increase IL-2 may contribute to aid existing T cells proliferate and that is why no differences in proliferation is detected. In contrast to previous publications, p110δ specific inhibitor reduced levels of IL-2 in T-p110δ^{E1020K} mice after 72 hours, reasons of which are uncertain. It could be that following treatment with p110δ specific inhibitor, T cells in T-p110δ^{E1020K} are rescued from apoptosis, therefore allowing increased number of T cells to use IL-2.

Regulatory T cells

Immunophenotyping data obtained in Tregs using F-p110δ^{E1020K} mice are consistent with studies where PTEN was conditionally knocked out in Tregs. PTEN deficient Treg mice demonstrated an increase in Th1 and Tfh cell responses, as well as increased GC formation [105, 106]. Additionally with age, these mice developed a systemic lymphoproliferative autoimmunity with enhanced antinuclear antibodies and immune complex glomerular nephritis [105, 106]. Functionally, Tregs with increased PTEN lost expression of characteristic Treg markers such as CD25^{+} and Foxp3^{+}, resulting in an accumulation of CD25^{-}Foxp3^{+} cells. Upon stimulation in F-p110δ^{E1020K} mice, Foxp3^{+} cells produced increased levels of the inflammatory cytokine IFNγ, implying that these cells adopt a Th1 like effector phenotype as observed in cancer, infection, and autoimmune diseases that is associated with loss of Treg suppressor function [346]. The PI3K/Akt/Foxo pathway has been implicated in generating Th1 like Treg cells that are characterised by increased T-bet, CXCR3 and IFNγ expression and defects in suppressive ability [346]. Blockade of this pathway can reverse this phenotype and restore suppressive capacity of Tregs, therefore providing a therapeutic strategy for autoimmune diseases. However, *in vitro* suppression assays carried out demonstrated

that Tregs with hyperactive p110δ are able to suppress conventional $CD4^+$ T cells more efficiently than WT Tregs. In addition, an *in vivo* tumor model using EG7-OVA was carried out to investigate the *in vivo* functional ability of hyperactive p110δ Tregs in F-$p110\delta^{E1020K}$ mice. Preliminary results suggested no differences in tumour weights on the day the mice were culled (data shown in appendix). Tregs with hyperactive p110δ demonstrate increased expression of Treg activation markers that included CD38, Helios, ICOS, GITR and CD39. In F-$p110\delta^{E1020K}$, the expression of CD25 a marker for suppression was similar to WT mice, perhaps the enhanced expression of the other Treg associated activation markers compensates for the comparable CD25 expression for increased suppressive ability. Given that, no differences in autoantibody levels were observed in 8-12-weeks-old T-$p110\delta^{E1020K}$ and F-$p110\delta^{E1020K}$ mice further support the intact suppressive ability of Treg with hyperactive p110δ. However, there is a possibility that aged mice harbouring hyperactive p110δ in Tregs are more prone to developing autoimmunity as indicated by the increase in ANA levels in older F-$p110\delta^{E1020K}$ mice. It is therefore possible that p110δ hyperactive Treg could lose their suppressive ability and result in a similar disorder as observed in the PTEN deficient Treg mice. Approximately 42% of a cohort of 53 APDS patients also develop autoimmune manifestations; in addition, enhanced p110δ activity has been associated with autoimmune diseases such as systemic lupus erythromatosus [151, 362]. These results stress the important role played by the PI3K pathway in controlling Treg plasticity, transient acquisition of Th1 like phenotype whilst still maintaining functional Treg capabilities.

T follicular helper cells

Following immunisation with NP-KLH, increased proportions of Tfh , Tfr and GC B cells were observed in T-$p110\delta^{E1020K}$ mice. Likewise, PTEN deletion in T cells led to increased Tfh and GC B cells [110]. In contrast, reduced proportions of Tfh cells were observed in $p110\delta^{D910A}$ mice, , therefore this supports previous data indicating that the formation of Tfh cells is critically dependent on p110δ activity in T cells [110]. Interestingly, despite having an increased proportions of Tfh cells in T-$p110\delta^{E1020K}$ mice, the proportions of $IgG1^+$ cells among NP specific GC B cells were not increased in comparison to WT mice, this could be due to simultaneous suppression from the increased Tfr cells observed. Future experiments could focus on measuring

suppressive ability of Tfr cells in a co-culture system in the presence of Tfh and B cells to measure IgG1 production.

ICOS driven PI3K activation is important for Tfh cell differentiation, as Tfh generation is impaired in mice selectively defective in activating PI3K through ICOS [85]. In support of increased generation of Tfh cells due to hyperactive p110δ, increased ICOS expression was detected in Tfh cells in G-p110δ^{E1020K} mice. Recently Preite et al showed that the increased generation of Tfh cells due to hyperactive p110δ activity overcomes the requirement of ICOS-ICOSL interactions for the differentiation and maintenance of Tfh cells [307]. Foxo1 plays an important role in differentiation of Tfh cells by regulating expression of genes such as ICOS, Bcl-6 and BATF (refs). In T-p110δ^{E1020K} mice, increase expression of Bcl-6 was detected. Therefore, it is possible that deletion of Foxo1 led to enhanced Bcl-6 expression and exaggerated differentiation of Tfh cells [111]. In line with this, Preite et al further went on to show that expression of Foxo1^{AAA}, an AKT-resistant Foxo1 mutant, decreased the frequency of hyperactive Tfh cells generated following *in vivo* immunisation [307]. Therefore, suggesting that activated p110δ signalling circumvents the need for ICOS to phosphorylate and inactivate Foxo1 that is an important inhibitor of Tfh cell differentiation.

Our data suggests that antibody defects observed in APDS patients maybe explained due to intrinsic defects in B cells. Mice in which hyperactive p110δ mutation was present in B cells alone, had similar total GC B cells but reduced IgG1^{+} cells within NP specific GC B cells as compared to the T-p110δ^{E1020K} mice. This was also confirmed in the G-p110δ^{E1020K} mice where increased Tfh cells were observed along with increased total GC B cells, but the proportions of switched NP specific GC B cells were reduced compared to WT mice. The function of Tfh cells is further supported by the increase in IL-21 and Th2 cytokines that were detected following CD4^{+} T cell differentiation in T-p110δ^{E1020K} mice. Therefore, despite the increase in Tfh and GC B cells, reduced antibody class switching as measured by IgG1^{+} cells is due to an intrinsic defect in B cells. The fact that the GC B cells in B-p110δ^{E1020K} were comparable to WT mice, suggests that the lack of NP specific IgG1^{+} cells is due to a general defect in class switch recombination (CSR) and not due to an impaired T-B cell collaboration. Foxo1 is important in regulating the expression of activation-induced

cytidine deaminase AID, which is a master regulator of somatic hypermutation and CSR. It has been shown that deletion of Foxo1 in B cells led to impaired CSR due to impaired AID upregulation [363]. Therefore, reduced $IgG1^+$ cells within antigen specific GC B cells observed could be explained by the inactivation of Foxo1 downstream of hyperactive p110δ signalling in B cells.

The results presented in this chapter give an overview of the effect of hyperactive p110δ signalling in different T cell subsets. In addition, it highlights the important role played by p110δ in regulating different T cell functions. It is apparent that hyperactive p110δ activity in T cells has the potential to both exacerbate and attenuate immune responses depending on the complex local environment. The next chapters will focus on the effect of hyperactive p110δ signalling in the $CD8^+$ T cell response to acute and chronic infections, with the aim to provide insight into the mechanisms underlying recurrent viral infections observed in APDS patients.

Chapter 4

The effect of hyperactive p110δ on $CD8^+$ T cell responses to primary acute infections

4.1 Introduction

In chapter 3, I have illustrated that the mice recapitulate the T cell phenotype observed in the APDS patients and therefore represents a good model for understanding the role of PI3Kδ in response to acute infections. The next question asked was whether hyperactive p110δ affects $CD8^+$T cell responses to acute infections.

In a typical immune response to an acute infection, $CD8^+$T cells respond to activation by antigen-presenting cells (APCs) in secondary lymphoid organs, in a characteristic way. Initially they undergo extensive clonal expansion where they differentiate into a heterogeneous pool of effector $CD8^+$T cells and acquire effector functions to help control the infection. The effector functions include the ability to produce effector cytokines in addition to secreting cytolytic molecules such as perforin and granzyme B. After clearance of the pathogen, the vast majority (90-95%) of antigen-specific $CD8^+$T cells die as part of the contraction phase and leave behind a population of long-lived, memory $CD8^+$T cells that provide protection upon re-challenge [20]. $CD8^+$T cells play an important role in providing immune protection against intracellular pathogens. Numerous factors contribute to the generation of effector and memory $CD8^+$T cells including the strength of TCR signalling, co-stimulation and the surrounding cytokine milieu.

The PI3K signalling pathway, especially p110δ, plays an important role in regulating $CD8^+$T cell function in response to activation. These functions include differentiation, cell division, and effector cytokine production, amongst others. Recently our group and others have demonstrated a critical role for the p110δ subunit in the generation of optimal primary and memory $CD8^+$ T cell responses for the resolution of acute infections [115, 119]. Previous work from our group has shown that upon infection with *listeria monocytogenes* (Lm) in $p110\delta^{D910A}$ mice, the differentiation of memory $CD8^+$ T cells is favoured over effector cells [115]. Conversely, in APDS patients, the $CD8^+$ T cell pool exhibit an activated phenotype and lack memory $CD8^+$ T cells [138, 141]. This suggests that heightened p110δ signalling favours differentiation of $CD8^+$T cells to an effector-like phenotype at the expense of memory. Thus, in order to determine the effect of hyperactive p110δ on $CD8^+$ T memory formation, it was important first to establish the effect on the primary immune response to infection.

Two infection models were utilised in order to analyse $CD8^+$T cell responses with hyperactive p110δ: Listeria monocytogenes (Lm) and Influenza A virus. Lm is a gram-positive bacterium, which is highly effective at raising a potent $CD8^+$T cell response. An attenuated strain of this bacteria was used, which lacked actin assembly-inducing (ActA) protein expression, removing the ability of the bacteria to move between mammalian cells; thus, reducing its virulence. In addition, the strain was engineered to express ovalbumin (Lm-OVA) which allows $CD8^+$ T cells specific for a peptide spanning ovalbumin residues 257-264 to be tracked via MHC class I tetramers.

The second infection model utilised was PR8 H1N1 influenza virus. I used this virus to assess whether the effect of hyperactive p110δ on $CD8^+$ T cells is independent of the type of pathogen used. A primary infection with influenza virus results in a localised pulmonary infection, eliciting an influenza specific $CD8^+$ T cell immune response that is necessary for viral clearance. Both $CD8^+$ and $CD4^+$ T cells are important in mediating influenza specific immune responses. For this model, MHC class I tetramers loaded with the $NP_{366-374}$ immunodominant peptide were used to identify antigenic specific $CD8^+$T cells. To assess $CD4^+$ T cell responses, MHC Class II I-A^b tetramer specific for the influenza $NP_{311-324}$ epitope was used. Both Lm and influenza virus are widely used to study T cell biology due to their ability to induce a robust $CD8^+$ T cell response.

In this chapter, the effect of hyperactive and inactive p110δ in $CD8^+$T cell responses to infection was explored by using different mouse models, including T-p110δ^{E1020K} and p110δ^{D910A} mice, which have been discussed in chapter 3. In addition, T cell receptor (TCR) transgenic mice that recognise ovalbumin peptides were used to study effect of hyperactive p110δ on intrinsic $CD8^+$T cell responses.

4.2 Results

4.2.1 No difference in numbers of antigenic specific CD8$^+$T cells in T-p110δ^{E1020K} in response to primary infection with Lm-OVA

On day 0, WT, T-p110δ^{E1020K} and p110δ^{D910A} mice were infected with an attenuated strain of Lm-OVA and were culled on day 8 post infection. Lm-OVA specific CD8$^+$ T cells were detected by flow cytometry, using fluorochrome labelled MHC class I H2Kb tetramer loaded with $OVA_{257-264}$ (SIINFEKL). Upon infection, the frequency and absolute numbers of Lm-OVA specific CD8$^+$ T cells were comparable between WT and T-p110δ^{E1020K} mice in spleen and lymph nodes (**Fig 4.2.1a and b**). However, in the spleen, a trend was observed of increased Lm-OA specific CD8$^+$ T cells in T-p110δ^{E1020K} mice but this was not significant. Similarly, at day 7, was no difference in Lm-OVA specific CD8$^+$ T cells in T-p110δ^{E1020K} mice was observed compared to WT mice (data shown in appendix). The number and proportions of Lm-OVA specific CD8$^+$ T cells were significantly less in p110δ^{D910A} mice compared to WT mice, therefore confirming previously published data that p110δ activity is required for normal primary CD8$^+$ T cell responses to Lm-OVA (**Figure 4.2.1a and b**) [115, 119].

In addition, bacterial load in WT and T-p110δ^{E1020K} mice was measured at 48 hours post infection with a virulent strain of Lm. The bacterial load was enumerated in the spleen and liver and there was no difference between WT and T-p110δ^{E1020K} mice (**Figure 4.2.1 c**). Similarly, our group has observed in CD4^{cre} x p110δ$^{flox/flox}$ mice, a model in which p110δ is deleted in all T cells that bacterial load was similar to WT mice following infection (data not shown). This indicates that p110δ activity in T cells does not affect the bacterial load following Lm infection. In p110δ^{D910A} mice, the bacterial load was found to be significantly lower compared to WT mice, due to enhance bacterial clearance by the innate immune system Lm is cleared before Lm-OVA specific CD8$^+$ T cells were detected [115]. Overall, these findings demonstrate that hyperactive p110δ does not affect CD8$^+$ T cell expansion in response to Lm-OVA infection in T-p110δ^{E1020K} mice.

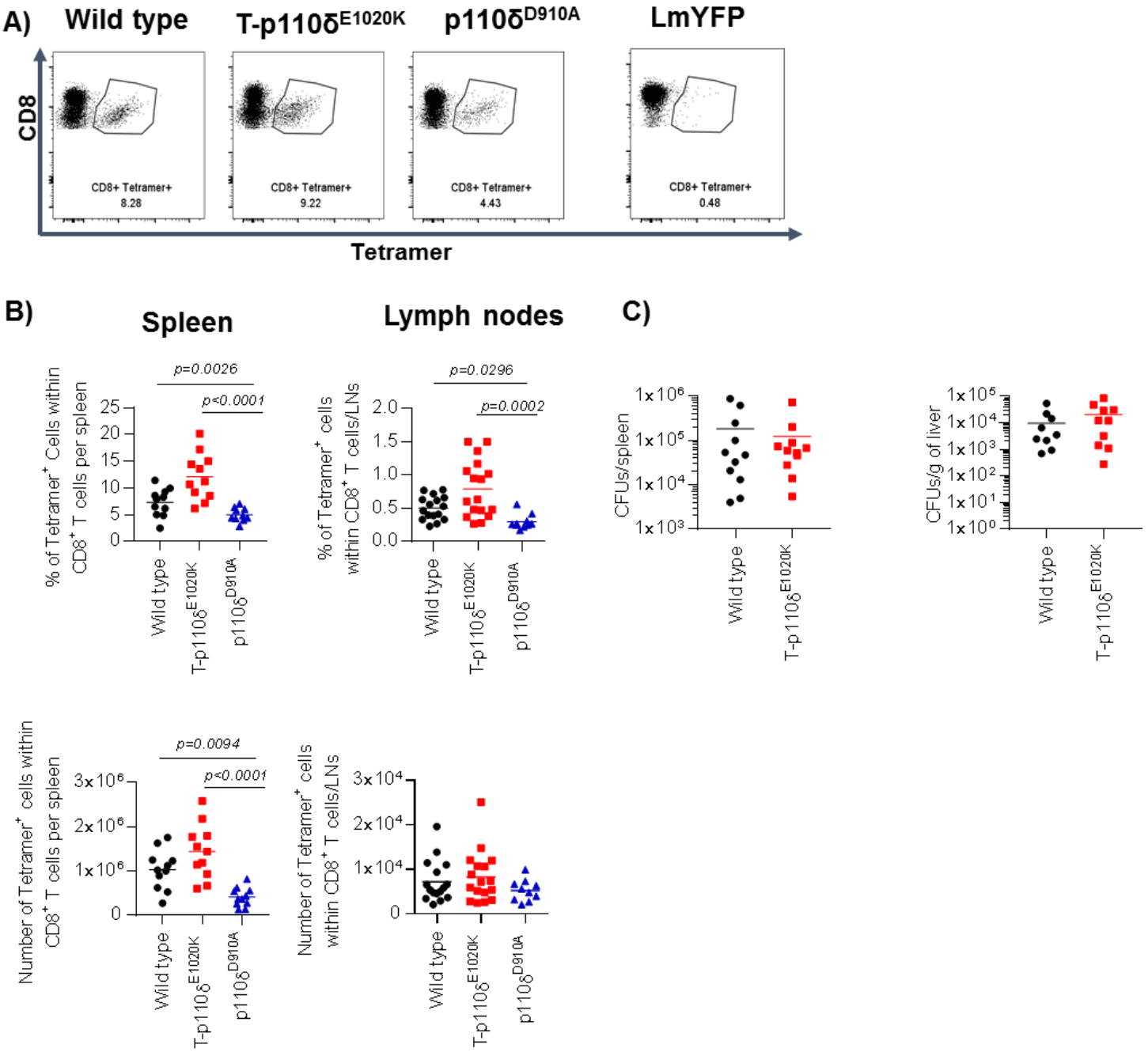

Figure 4.2.1: No difference in antigenic specific CD8$^+$ T cells in T-p110δ^{E1020K} in response to primary infection with Lm-OVA

WT, T-p110δ^{E1020K} and p110δ^{D910A} mice were infected with 5 x 10^6 CFU of Lm-OVA and were culled at day 8 post infection. **(A)** Representative flow cytometry plots of Lm-OVA specific CD8$^+$ T cells in spleen. **(B)** Numbers and proportion of Lm-OVA specific CD8$^+$ T cells in spleen and lymph nodes. **(C)** WT and T-p110δ^{E1020K} were infected with 5 x 10^4 CFU of virulent Lm-OVA at day 0 and culled 48 hours post infection. Bacterial load was quantified from spleen and liver. Results in A and B are combined from three independent experiments (n = 9- 16 per group) and results in C are combined from two independent experiments (n=11 per group). *P values* are shown.

4.2.2 Hyperactive p110δ leads to an intrinsic CD8$^+$ T cell defect in response to primary Lm-OVA infection

The function of CD4$^+$ expressing cells is also affected due to hyperactive p110δ in T-p110δ^{E1020K} mice as shown in Chapter 3. Therefore, the CD8$^+$ T cell response to Lm could be the result of an indirect effect of other subtypes of T cells that could potentially influence the CD8$^+$ T cell immune response in T-p110δ^{E1020K} mice. In order to determine the intrinsic CD8$^+$ T cells response , we crossed germline E1020K mice (G-p110δ^{E1020K}) onto the OT1 TCR transgenic background in which CD8$^+$ T cells express a SIINFEKL peptide specific TCR (OVA$_{257-264}$). As hyperactive p110δ mutation causes a slight increase in the frequencies of activated (CD44^{high}) CD4$^+$ and CD8$^+$ T cells, naïve CD8$^+$ T cells (CD62L^{high}CD44^{low}) were FACs sorted for all the OT1 adoptive transfer experiments. To examine how hyperactive p110δ may control CD8$^+$ T cell mediated immune responses *in vivo,* 10,000 naive FACs sorted WT and E1020K OT1 donor cells (CD45.2$^+$ or CD45.1$^+$ CD45.2$^+$) were adoptively transferred into congenically marked WT recipient mice (CD45.1 or CD45.2) on day -1. These mice were subsequently infected with Lm-OVA the next day and were culled at day 8 post infection.

Upon infection, the frequencies and numbers of E1020K donor OT1 cells were significantly reduced compared to WT donor OT1 cells in the spleen, lymph nodes and bone marrow **(Figure 4.2.2 a-d**). One possibility for this reduction may have been that p110δ hyperactivity resulted in apoptosis of the OT1 donor cells. To test this hypothesis, Annexin V a marker of early cell death was measured. However, no difference in expression of Annexin V was detected at day 8 post infection amongst E1020K OT1 donor cells compared to WT OT1 donor cells (**Figure 4.2.2e**). It is plausible that differences in cell death may have been apparent at earlier time points or the hyperactive p110δ OT1 cells may have had a proliferation defect. Another possibility is that flow cytometry sorting could add stress to FACs sorted donor cells , therefore a pilot experiment was carried out in which CD8$^+$ OT1 donor cells were isolated using an immunomagnetic CD8$^+$ T cell isolation kit (MACS). Similar observations were observed using FACs sorted or MACs isolated cells (**Figure .2.2f**).

Overall, these observations reveal a cell intrinsic defect in CD8⁺ T cells due to hyperactive p110δ in response to primary Lm-OVA infection.

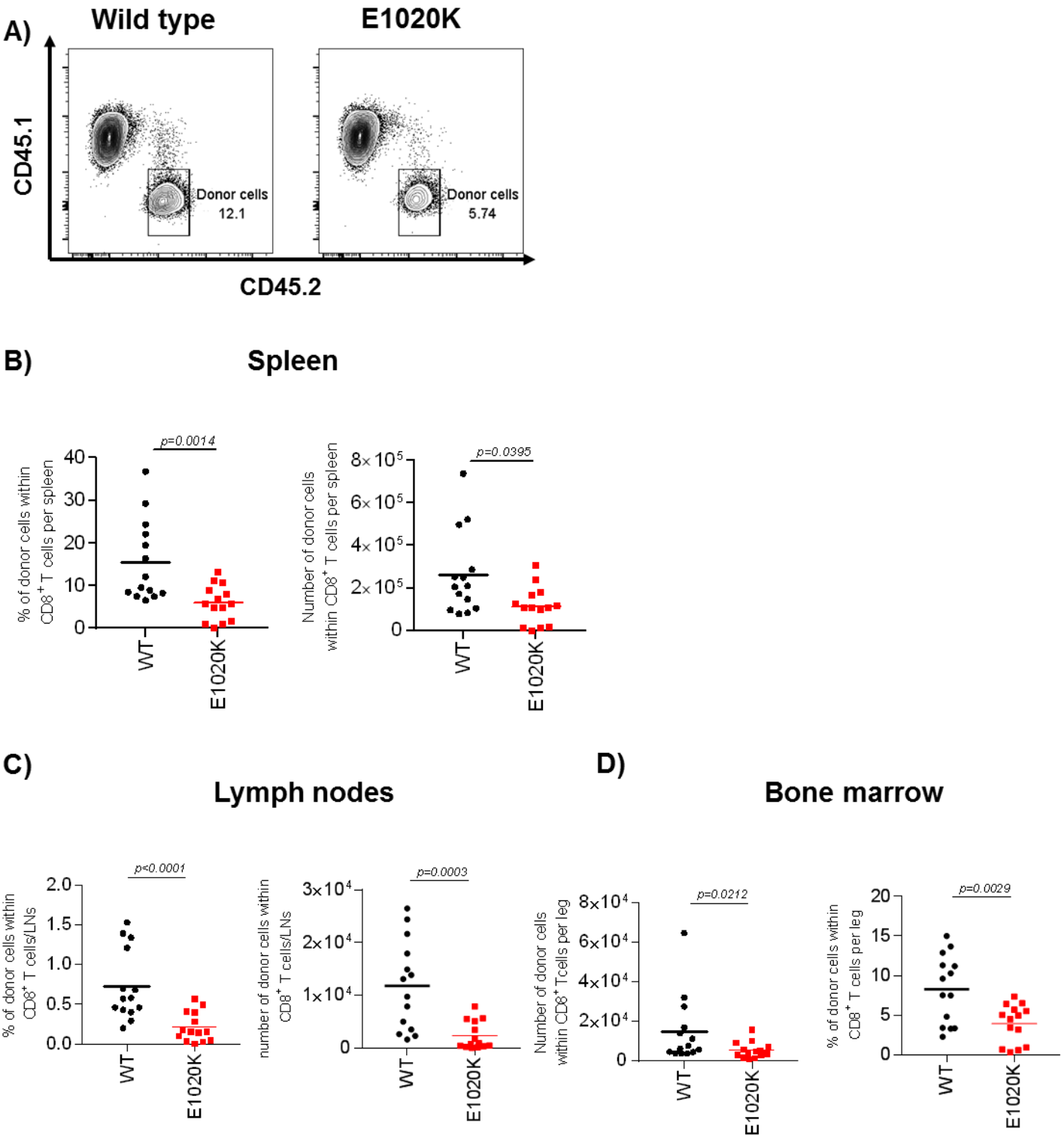

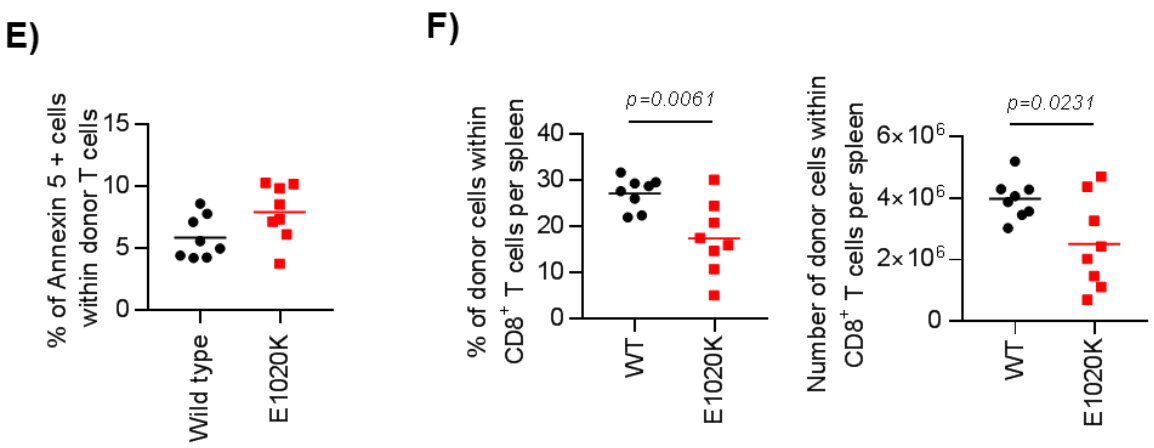

Figure 4.2.2: Hyperactive p110δ causes intrinsic CD8⁺ T cell expansion defect following primary infection with Lm-OVA

10,000 naïve ($CD62L^{high}CD44^{low}$) FACs sorted WT or E1020K OT1 donor cells ($CD45.2^+$ or $CD45.1^+$ $CD45.2^+$) were transferred into WT hosts (CD45.1 or CD45.2) on day -1. Mice were then infected with 5 x 10^6 CFU of Lm-OVA on day 0 and culled at day 8 post infection. **(A)** Representative flow cytometry plots of donor OT1 cells in spleens of Lm-OVA infected mice at day 8. Graphs showing numbers and proportions of donor OT1 cells in the **(B)** Spleen, **(C)** Lymph nodes and **(D)** Bone marrow. **(E)** Proportions of Annexin 5^+ cells amongst WT and E1020K OT1 donor cells in spleens of infected recipient mice. Data in A-D are combined from two independent experiments with 4 donors per group. Data in E is from one independent experiment with 2 donors per group.

10,000 MACs sorted WT or E1020K OT1 donor cells ($CD45.2^+$) were transferred into WT hosts (CD45.1) on day -1. Mice were then infected with 5 x 10^6 CFU of Lm-OVA on day 0 and culled on day 8. **(F)** Graphs showing numbers and proportions of OT1 donor cells in spleen. Data representative of one independent experiment with 2 donors per group. *P values* are shown.

4.2.3 Hyperactive p110δ mutation reduces differentiation into MPECs in response to Lm-OVA infection

Following infection, activated $CD8^+$ T cells differentiate into a heterogeneous pool of effector cells that are divided as being short lived effector cells (SLECs) or memory precursor effector cells (MPECs) amongst other subsets. SLECs that are defined by the high expression of killer cell lectin-like receptor G1 (KLRG1) and low expression of IL-17Ra (CD127) have a short lifespan and deplete during the contraction phase of infection. In contrast MPECs are defined by high expression of CD127 and low expression of KLRG1, have increased potential to differentiate into functional and long lived memory $CD8^+$ T cells [126, 364, 365].

In order to investigate the effect of hyperactive p110δ in the differentiation of Lm-OVA specific $CD8^+$ T cells into SLECs and MPECs, antigen-specific $CD8^+$ T cells in WT, T-$p110\delta^{E1020K}$ and $p110\delta^{D910A}$ mice were immunophenotyped following Lm-OVA infection by staining for CD127 and KLRG1. Following infection there was a significant increase in the frequencies and numbers of SLECs and a reduction in MPECs within Lm-OVA specific $CD8^+$ T cells in T-$p110\delta^{E1020K}$ mice compared to WT mice in the spleen and lymph nodes (**Figure 4.2.3a and b**). In $p110\delta^{D910A}$ mice, although the proportions of MPECs were significantly higher, the numbers were unchanged compared to WT mice. In contrast, both the proportions and numbers of SLECs were significantly reduced compared to WT mice in the spleen and lymph nodes. (**Figure 4.2.3a and b**).

I also determined the differentiation of naïve $CD8^+$T cells into MPECs and SLECs following transfer of WT and E1020K OT1 donor cells into recipient mice. Following infection, the proportions of MPECs were significantly reduced amongst the E1020K OT1 donor cells compared to the WT OT1 donor cells in the spleen and lymph nodes (**Figure 4.2.3c**). In addition, the proportion of SLECs were higher amongst the E1020K OT1 donor cells compared to the WT OT1 donors cells (**Figure 4.2.3c**). Overall, these results suggest that hyperactive p110δ activity can favour differentiation of SLECs over MPECs following primary Lm-OVA infection in a $CD8^+$ T cell intrinsic manner.

Differentiation of antigen-specific $CD8^+$ T cells into MPECs and SLECs is controlled by the differential expression of certain transcription factors. Eomes is important for promoting the differentiation of MPECs whereas T-bet is shown to be crucial for the development of SLECs [23, 366]. In T-$p110\delta^{E1020K}$ mice, there was no difference in

the expression of T-bet amongst the Lm-OVA specific $CD8^+$ T cells whereas the expression of Eomes was significantly reduced compared to WT mice (**Figure 4.2.3d**). However, in the single OT1 adoptive transfer experiments, there was no difference in the expression of Eomes, but the expression of T-bet was significantly increased amongst the E1020K OT1 donor cells (**Figure 4.2.3e**). These results suggest that the presence of other cells can influence the expression of transcription factors in T-$p110\delta^{E1020K}$ mice following Lm-OVA infection.

Reduced central memory CD8 T cells in T-$p110\delta^{E1020K}$ mice following primary infection with Lm-OVA

Due to the heterogeneity of effector $CD8^+$T cells following infection, other sub populations of effector cells also exist that can be distinguished by the expression of different surface proteins. Amongst the pool of effector cells there are two main memory subsets- $CD62L^{high}$ $CCR7^{high}$ $CD44^{high}$ central (T_{CM}) and $CD44^{high}$ $CD62L^{low}$ $CCR7^{low}$ effector (T_{EM}) memory cells, that are characterised based on the expression of different homing receptors [367, 368]. These subsets have different features and tissue distribution, ensuring instant and long-term protection against secondary infection. T_{CM} cells resides in lymphoid tissue, mainly produce IL-2, are better equipped to persist in the host and have a higher proliferative potential. Conversely, T_{EM} cells are found in peripheral tissues where they seem to provide a first line of defense by displaying potent *ex vivo* cytotoxicity and producing a greater effector cytokine response, have a reduced ability to proliferate and produce IL-2 [369]. T_{EM} cells can also express KLRG1, a marker associated with reduced proliferation and senescence [365, 370].

At day 8 Following Lm-OVA infection, there was no difference in T_{EM} ($CD44^{high}CD62L^{Low}$) cells among the Lm-OVA specific $CD8^+$ T cells in T-$p110\delta^{E1020K}$ mice compared to WT mice in the spleen and lymph nodes. However, there was a significant reduction in the frequencies of Lm-OVA specific $CD8^+$ T cells with a $CD44^{high}$ $CD62L^{high}$ central memory phenotype in T-$p110\delta^{E1020K}$ mice but no differences in numbers (**Figure 4.2.3f-h**). In $p110\delta^{D910A}$ mice, the numbers and proportions of T_{EM} ($CD44^{high}$ $CD62L^{low}$) cells were significantly reduced in the spleen and lymph nodes compared to WT mice. The proportions of T_{CM} cells were significantly increased in $p110\delta^{D910A}$ mice; however, there was no difference in numbers (**Figure**

4.2.3 f-h). Overall, the results indicate that following Lm-OVA infection, $CD8^+$ T cells in T-p110δ^{E1020K} mice acquire a more effector-like phenotype at the expense of a memory phenotype.

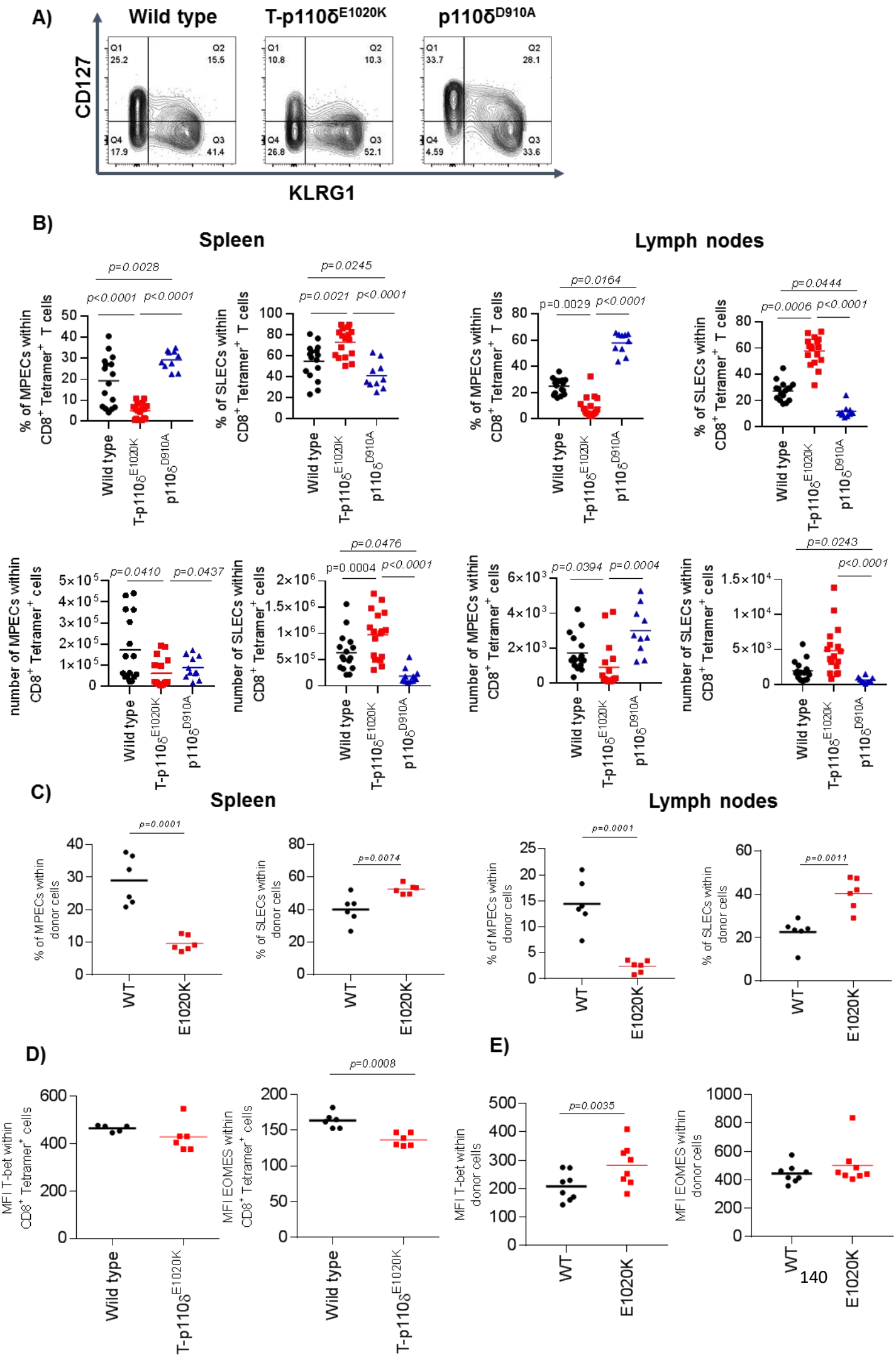
A)
Wild type
T-p110δE1020K
p110δD910A
CD127
KLRG1
Q1 25.2
Q2 15.5
Q4 17.9
Q3 41.4
Q1 10.8
Q2 10.3
Q4 26.8
Q3 52.1
Q1 33.7
Q2 28.1
Q4 4.59
Q3 33.6
B)
Spleen
Lymph nodes
% of MPECs within CD8+ Tetramer+ T cells
% of SLECs within CD8+ Tetramer+ T cells
number of MPECs within CD8+ Tetramer+ cells
number of SLECs within CD8+ Tetramer+ cells
p=0.0028
p<0.0001
p<0.0001
p=0.0245
p=0.0021
p<0.0001
p=0.0164
p=0.0029
p<0.0001
p=0.0444
p=0.0006
p<0.0001
p=0.0410
p=0.0437
p=0.0476
p=0.0004
p<0.0001
p=0.0394
p=0.0004
p=0.0243
p<0.0001
Wild type
T-p110δE1020K
p110δD910A
C)
Spleen
Lymph nodes
% of MPECs within donor cells
% of SLECs within donor cells
p=0.0001
p=0.0074
p=0.0001
p=0.0011
WT
E1020K
D)
MFI T-bet within CD8+ Tetramer+ cells
MFI EOMES within CD8+ Tetramer+ cells
p=0.0008
Wild type
T-p110δE1020K
E)
MFI T-bet within donor cells
MFI EOMES within donor cells
p=0.0035
WT
E1020K

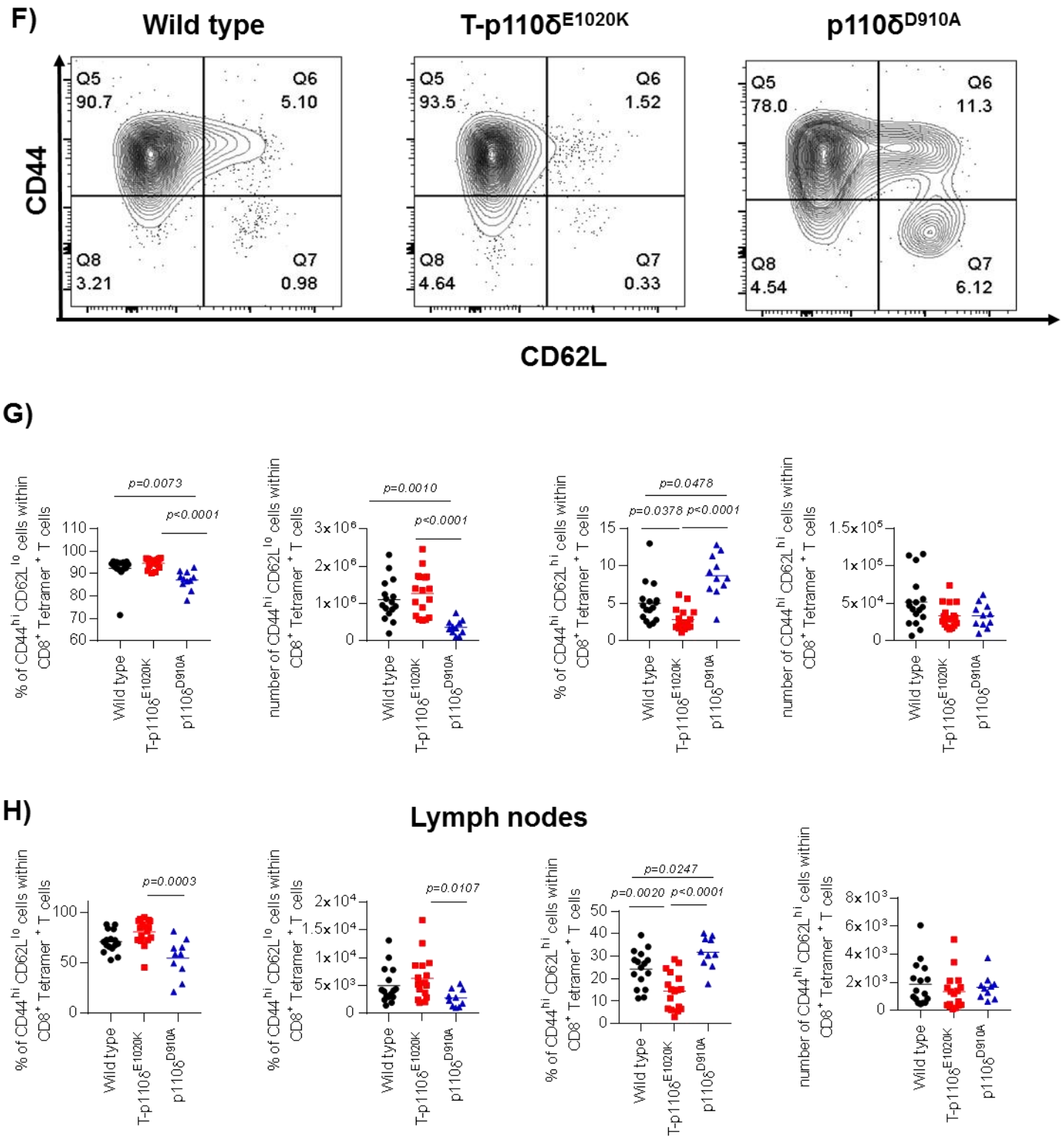

Figure 4.2.3: Reduced generation of memory precursor effector cells (MPEC) due to hyperactive p110δ mutation in CD8$^+$ T cells

WT, T-p110δ^{E1020K} and p110δ^{D910A} mice were infected with 5 x 10^6 CFU of Lm-OVA on day 0 and were culled at day 8 post infection. **(A)** Flow cytometry plots of CD127 and KLRG1 expression in Lm-OVA specific CD8$^+$ T cells. **(B)** Proportions and numbers of MPECs and SLECs within Lm-OVA specific CD8$^+$ T cells in the spleen and lymph nodes of infected mice.**(C)** Proportions of MPECs and SLECs in E1020K and WT OT1 donor cells in spleen and lymph nodes of recipient mice following Lm-OVA infection. **(D)** Expression of Eomes and T-bet in Lm-OVA specific CD8$^+$ T cells in WT and T-p110δ^{E1020K} mice. **(E)** Expression of Eomes and T-bet in WT and E1020K OT1 donor cells.

(F) Flow cytometry plots of CD62L and CD44 expression in Lm-OVA specific $CD8^+$ T cells. Graphs showing Proportions and numbers of central memory ($CD44^{high}CD62L^{low}$) and effector memory ($CD44^{high}CD62L^{low}$) within Lm-OVA specific $CD8^+$ T cells in the **(G)** spleen and **(H)** lymph nodes of infected mice. Data in A-B combined from three independent experiments (n=9-16 per group), data in C is representative of two independent experiments (n=6 recipient mice and 2 donors per group), data in D representative of one independent experiment (n = 6 per group), data in E representative of one independent experiment (n= 6 recipient mice and 2 donors per group) and data in F-H combined from three independent experiments (n=9-16). *P values* are shown.

4.2.4 No difference in expansion of E1020K $CD8^+$ T cells when co-transferred with WT OT1 cells

To exclude any effects of the inflammatory microenvironments in the different recipient hosts and taking advantage of the fact that different congenic markers can distinguish WT and E1020K OT1 donor cells, competitive adoptive transfer experiments were carried out. In these experiments 10,000 naïve ($CD62L^{high}CD44^{low}$) FACs sorted WT ($CD45.2^+$) and E1020K ($CD45.1^+$ $CD45.2^+$) OT1 T cells were adoptively co-transferred at a 1:1 ratio into the same WT host mice ($CD45.1^+$). The host mice were infected the following day with Lm-OVA and were bled at different time points to track the OT1 donor cell populations. Surprisingly, at day 8 post infection in the blood, E1020K OT1 donor cells responded normally when transferred alongside WT OT1 donor cells (**Figure 4.2.4a and b**). In another experiment, mice were bled at day 5 and a similar result was observed (data not shown). However, higher proportions of $KLRG1^+$ SLECs and reduced $CD127^+$ MPEC proportions were observed amongst the E1020K OT1 donor cells at day 8 with no differences in CD44 and CD62L populations (**Figure 4.2.4c**). These results suggest that WT OT1 T cells are able to help co-transferred E1020K OT1 T cells allowing them to respond normally. In addition, this result also support a $CD8^+$ T cell intrinsic role of hyperactive p110δ in promoting SLECs while inhibiting MPEC differentiation.

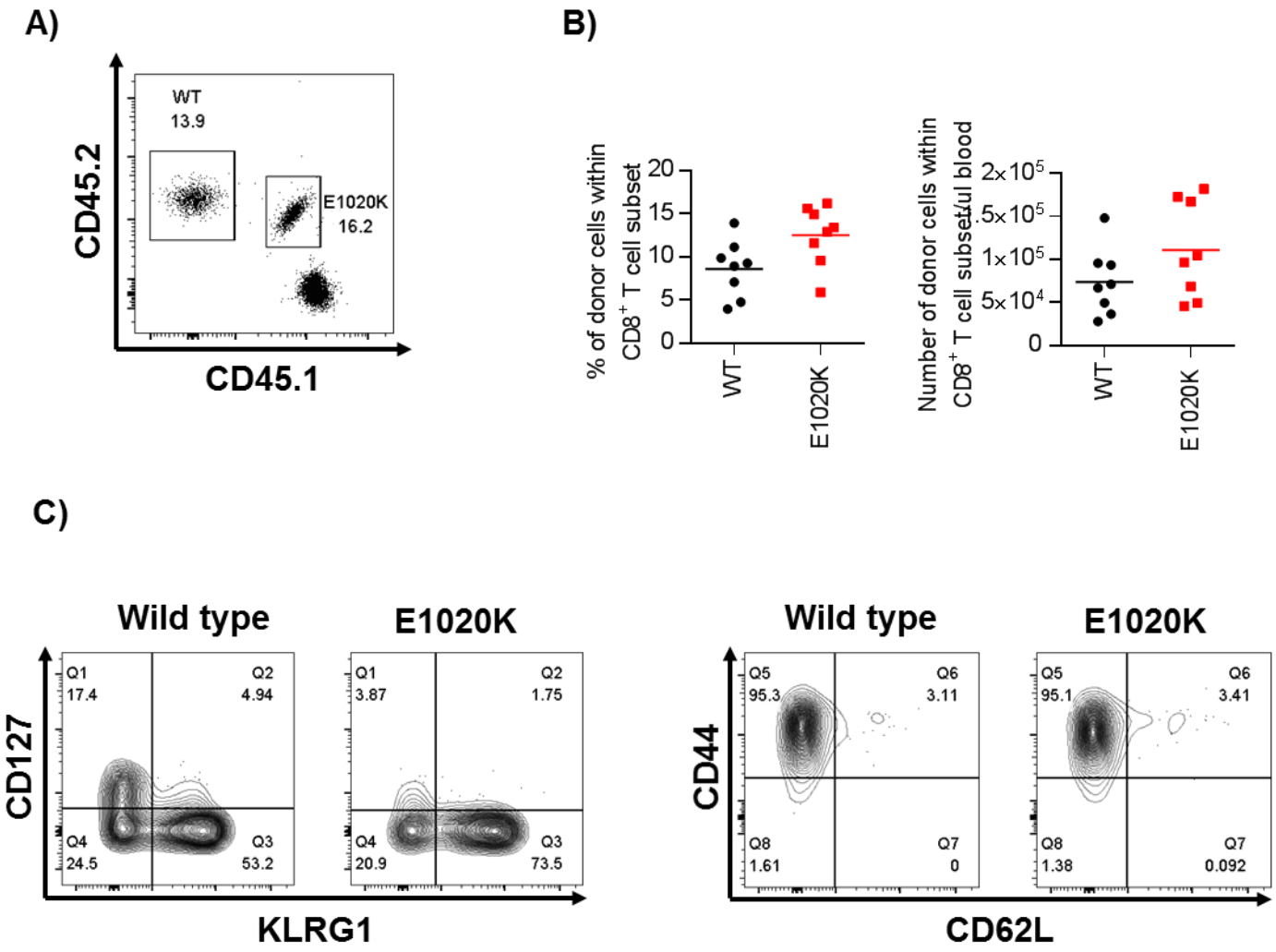

Figure 4.2.4: E1020K OT1 CD8$^+$ T cells are rescued when transferred alongside WT OT1 CD8$^+$ T cells into a WT host

1:1 mix of 10,000 naïve (CD62L^{high}CD44^{low}) WT OT1 (CD45.2$^+$) and E1020K (CD45.1$^+$CD45.2$^+$) were co-transferred into WT host mice (CD45.1$^+$) on day -1 and infected with Lm-OVA on day 0. Transferred cells were enumerated in the blood at different times points. **(A)** Representative flow cytometry plots of WT and E1020K OT1 donor cells at day 8 in the blood. **(B)** Graphs showing proportions and numbers of donor OT1 cells in the blood at day 8. **(C**) Flow cytometry plots illustrating proportions of MPECs, SLECs, CD44 and CD62L populations**.** Data representative of one independent experiment (n=8, 1 WT OT1 and E1020K OT1 donor), with a repeat done where mice were bled at day 5 instead of day 8.

4.2.5 Increased effector function due to intrinsic hyperactive p110δ activity in CD8$^+$T cells following Lm-OVA infection

Hyperactive p110δ mutation causes an increase in IFNγ$^+$, TNFα$^+$ and granzyme B$^+$ production following *in vitro* stimulation of CD8$^+$ T cells with anti-CD3/anti-CD28 as well as peptide stimulation (shown in chapter 3). Therefore, I wanted to know whether this was also true in response to infection with Lm-OVA. To assess cytokine production WT, T-p110δ^{E1020K} and p110δ^{D910A} mice were infected with Lm-OVA on day 0 and culled at day 8 post infection. Splenocytes from infected mice were stimulated *ex vivo* with SIINFEKL peptide in the presence of brefeldin A for 5.5 hours. Using intracellular straining I found that there was a trend in proportions towards increase proportions of IFNγ$^+$ and TNFα$^+$ single positive T cells, as well IFNγ$^+$TNFα$^+$ double positive T cells following SIINFEKL peptide stimulation although these differences were not statistically significant with no differences in numbers. There was no difference in the IFNγ$^+$ and TNFα$^+$ populations amongst CD44^{high} CD8$^+$ T cells in p110δ^{D910A} compared to WT mice (**Figure 4.2.5a-d**).

I also assessed cytokine production in the single OT1 adoptive transfer experiments following *ex vivo* SIINFEKL peptide stimulation. I found significantly increased proportions of IFNγ$^+$, TNFα$^+$ single positive and IFNγ$^+$ TNFα$^+$ double positive cells among E1020K OT1 donor cells compared to WT OT1 donor cells (**Figure 4.2.5e**). Additionally, I was able to measure IL-2$^+$ production within IFNγ$^+$ TNFα$^+$ cells in one experiment and found that it was significantly reduced amongst the E1020K OT1 donor cells compared to WT OT1 donor cells. Overall, these results suggest that hyperactive p110δ within CD8$^+$ T cells specifically results in increase effector cytokine production.

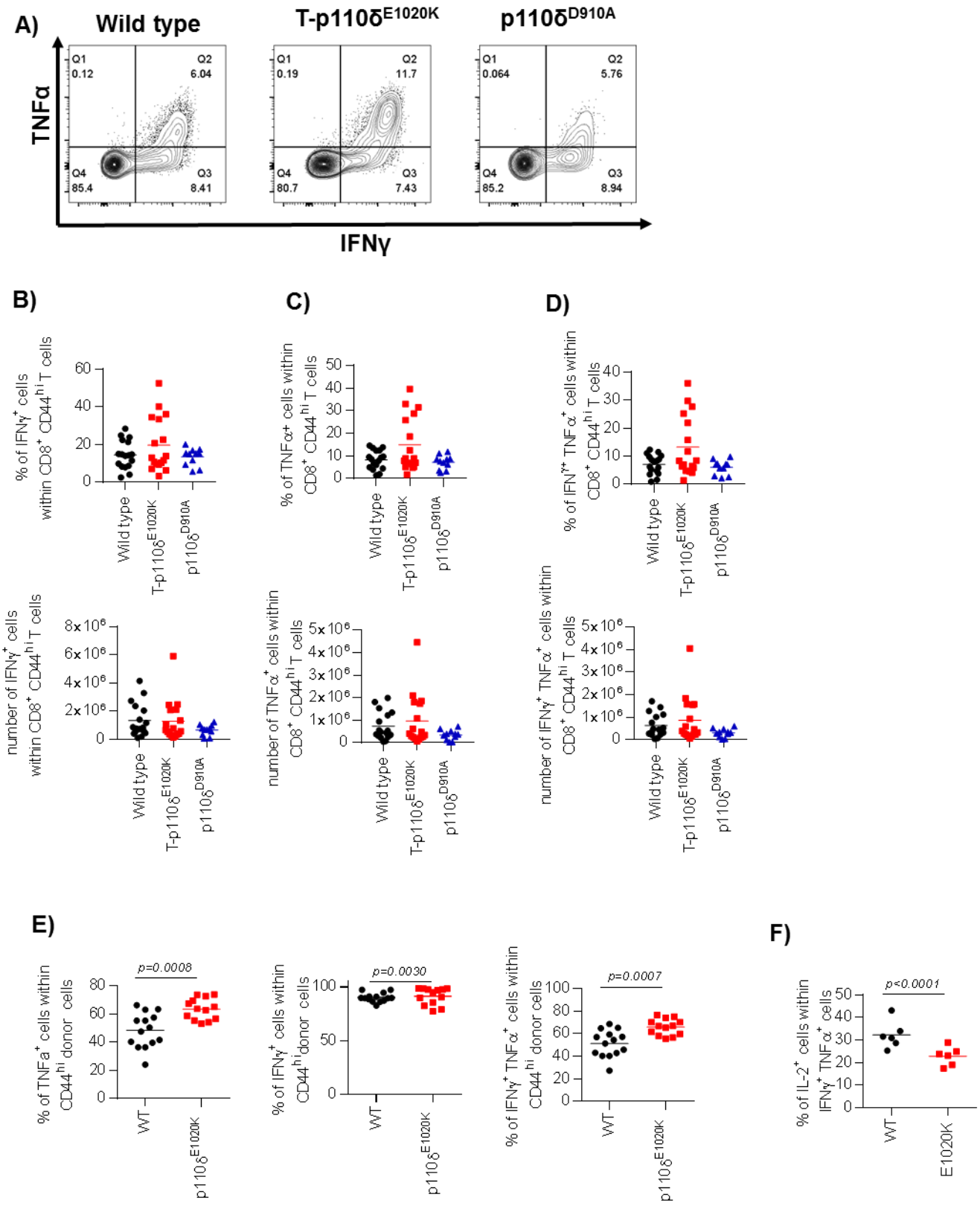
A)
Wild type
T-p110δE1020K
p110δD910A
TNFα
IFNγ
Q1 0.12
Q2 6.04
Q4 85.4
Q3 8.41
Q1 0.19
Q2 11.7
Q4 80.7
Q3 7.43
Q1 0.064
Q2 5.76
Q4 85.2
Q3 8.94
B)
% of IFNγ+ cells within CD8+ CD44hi T cells
number of IFNγ+ cells within CD8+ CD44hi T cells
C)
% of TNFα+ cells within CD8+ CD44hi T cells
number of TNFα+ cells within CD8+ CD44hi T cells
D)
% of IFNγ+ TNFα+ cells within CD8+ CD44hi T cells
number of IFNγ+ TNFα+ cells within CD8+ CD44hi T cells
Wild type
T-p110δE1020K
p110δD910A
E)
% of TNFa+ cells within CD44hi donor cells
% of IFNγ+ cells within CD44hi donor cells
% of IFNγ+ TNFα+ cells within CD44hi donor cells
p=0.0008
p=0.0030
p=0.0007
WT
p110δE1020K
F)
% of IL-2+ cells within IFNγ+ TNFα+ cells
p<0.0001
WT
E1020K

Figure 4.2.5: Intrinsic hyperactive p110δ activity in CD8$^+$ T cells leads to increase in effector cytokines following Lm-OVA infection.

Splenocytes from Lm-OVA infected WT, T-p110δ^{E1020K} and p110δ^{D910A} were stimulated *ex vivo* with 10nM SIINFEKL peptide for 5.5 hours. Following stimulation, cells were stained for surface markers and intracellular cytokines. **(A)** Representative flow cytometry plots of IFNγ$^+$ and TNFα$^+$ gated on CD44^{high} CD8$^+$ T cells. Graphs showing numbers and proportions of **(B)** IFNγ$^+$ **(C)** TNFα$^+$ **(D)** IFNγ$^+$ TNFα$^+$ cells within CD44^{high} CD8$^+$ T cells. **(E)** Graphs showing proportions of IFNγ$^+$, TNFα$^+$ single and co-producers within WT and E1020K OT1 donor cells in recipient mice. **(F)** Graphs showing proportions of IL-2$^+$ cells within IFNγ$^+$ TNFα$^+$ cells within WT and E1020K OT1 donor cells in recipient mice. Data in A-D combined from three independent experiments (n=9-16). Data in E combined from two independent experiments (n=4 donors per group) and data in F is from one independent experiment (n=2 donors per group). *P values* are shown

4.2.6 Increase *in vivo* killing ability of target cells in T-p110δ^{E1020K} mice following primary Lm-OVA infection

Next, I wanted to examine the ability of CD8$^+$ T cells in T-p110δ^{E1020K} mice to kill antigenic specific target cells following Listeria infection. Granzyme B and perforin are important effector molecules responsible for cytotoxicity in CD8$^+$ T cells [371]. Therefore, WT, T-p110δ^{E1020K} and p110δ^{D910A} mice were infected with Lm-OVA on day 0 and culled the mice at day 8 post infection. Using intracellular staining, I found a significant increase in the expression and proportions of granzyme B in Lm-OVA specific CD8$^+$ T cells from T-p110δ^{E1020K} mice compared to WT mice (**Figure 4.2.6a and b**). I also found similar results in another experiment when gating on CD44^{high} CD8$^+$T cells post infection. In addition, the expression and proportion of granzyme B in Lm-OVA specific CD8$^+$ T cells were significantly reduced in p110δ^{D910A} mice compared to WT and T-p110δ^{E1020K} mice. However, when I looked at the expression of perforin on Lm-OVA specific CD8$^+$T cells, I did not detect any differences between WT and T-p110δ^{E1020K} mice, whereas the expression was reduced in p110δ^{D910A} mice (**Figure 4.2.6b**).

In order to examine the *in vivo* killing ability of antigen-specific CD8$^+$ T cells following Lm-OVA infection, SIINFEKL peptide pulsed and non-peptide pulsed splenocytes were labelled with different fluorescent dyes in order to identify the cells by flow cytometry. The cells were mixed at a 1:1 ratio and then injected on day 8 into mice previously infected with Lm-OVA infected WT and T-p110δ^{E1020K} mice. The mice were culled one hour after injection of the cells, and the LmYFP control showed almost 1:1

ratio of the mixed injected population. I found that the SIINFEKL loaded cells were eliminated to a greater extent in T-p110δ^{E1020K} mice compared to WT mice (**Figure 4.2.6 d and e**). Together this set of data suggest that hyperactive p110δ activity in CD8^{+}T cells enhances their cytotoxic effector function post primary Lm-OVA infection.

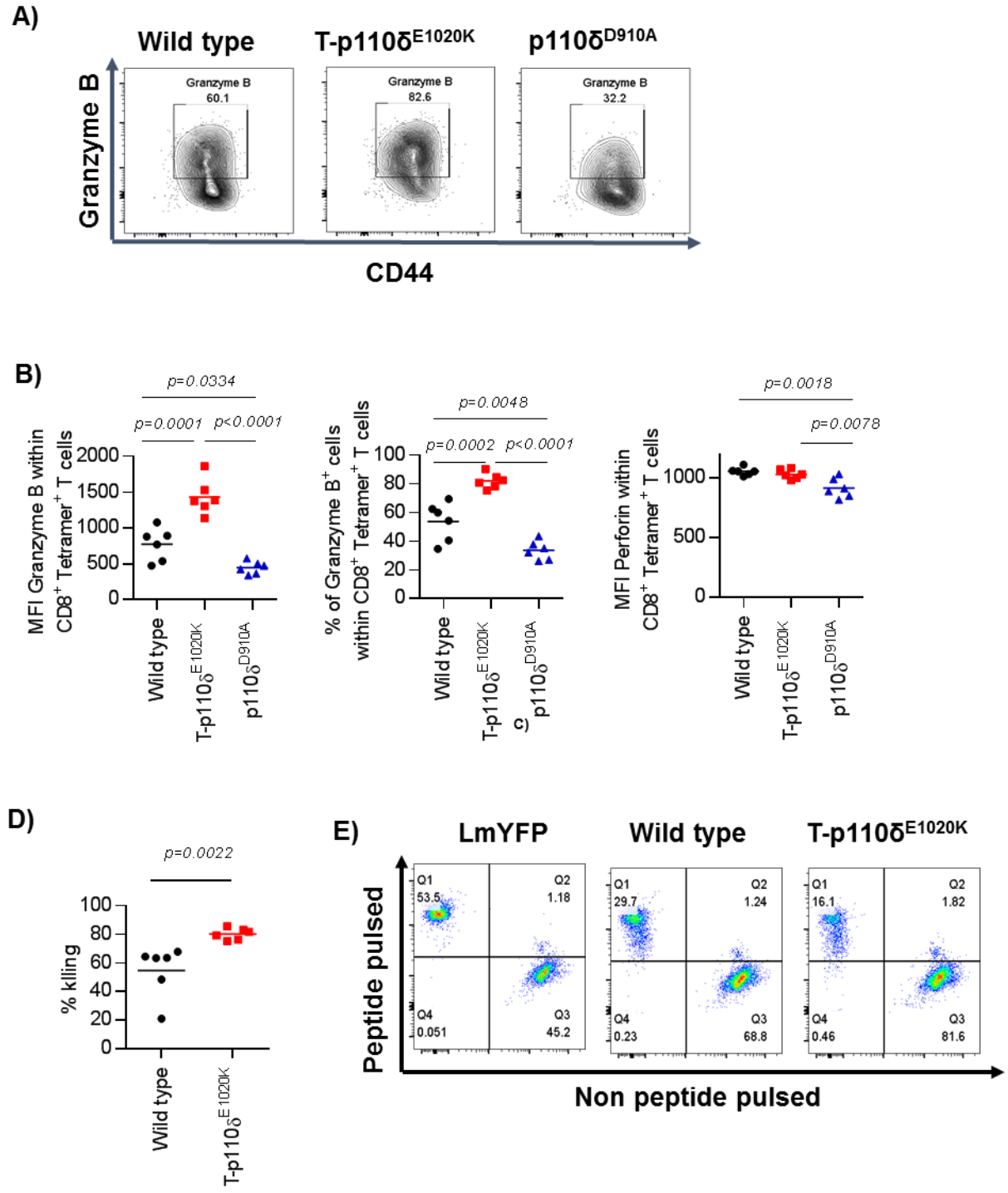

Figure 4.2.6: Increase *in vivo* killing ability of target cells in T-p110δ^{E1020K} mice following Lm-OVA infection.

(A) Representative flow cytometry plots of granzyme B within Lm-OVA specific CD8$^+$ T cells in WT, T-p110δ^{E1020K} and p110δ^{D910A} at day 8 post Lm-OVA infection. **(B)** Expression and proportions of granzyme B cells within Lm-OVA specific CD8$^+$ T cells. **(C)** Expression of perforin with Lm-OVA specific CD8$^+$ T cells **(D)** SIINFEKL peptide pulsed target cells and non-peptide target cells were labelled with different flourochrome dyes , mixed at a 1:1 ratio and intravenously transferred into Lm-OVA infected WT and T-p110δ^{E1020K} mice on day 8 .One hour post transfer, mice were culled and the percentages of antigen-specific killing activity was calculated in the spleen. **(E)** Representative flow cytometry plots of peptide pulsed and non-peptide pulsed populations. Data in A and B representative of one independent experiment (n=6 mice per group). Data in **(D)** and **(E)** representative of two independent experiments (n=6 mice per group). *P values* are shown.

4.2.7 Loss of p110δ activity, not hyperactivation in T cells affects clinical progression of influenza infection

Next, to address whether the effect of hyperactivation of p110δ in CD8$^+$ T cell response following primary infection with Listeria in T-p110δ^{E1020K} mice was also true against other pathogens, the response to an acute localised infection with influenza A virus was assessed. In order to do this, WT, T-p110δ^{E1020K} and p110δ^{D910A} mice were infected via the intranasal route with a sub-lethal dose of Influenza A Virus strain A/Puerto Rico/8/1934 H1N1 (PR8) and body weights were monitored to study disease progression. No differences in body weights between WT and T-p110δ^{E1020K} mice were observed (**Figure 4.2.7a**). Viral load was also measured in the lungs at day 10 post infection and no differences were seen between WT and T-p110δ^{E1020K} mice (**Figure 4.2.7b**). In contrast, p110δ^{D910A} mice showed significant weight loss at day 9 and day 10 compared to WT mice following infection (**Figure 4.2.7a**). p110δ^{D910A} mice showed significant increase in the viral load when compared to WT mice (**Figure 4.2.7b**). This suggests that hyperactive p110δ in CD8$^+$ T cells does not affect disease progression in response to influenza virus, whereas reduced p110δ activity can be detrimental.

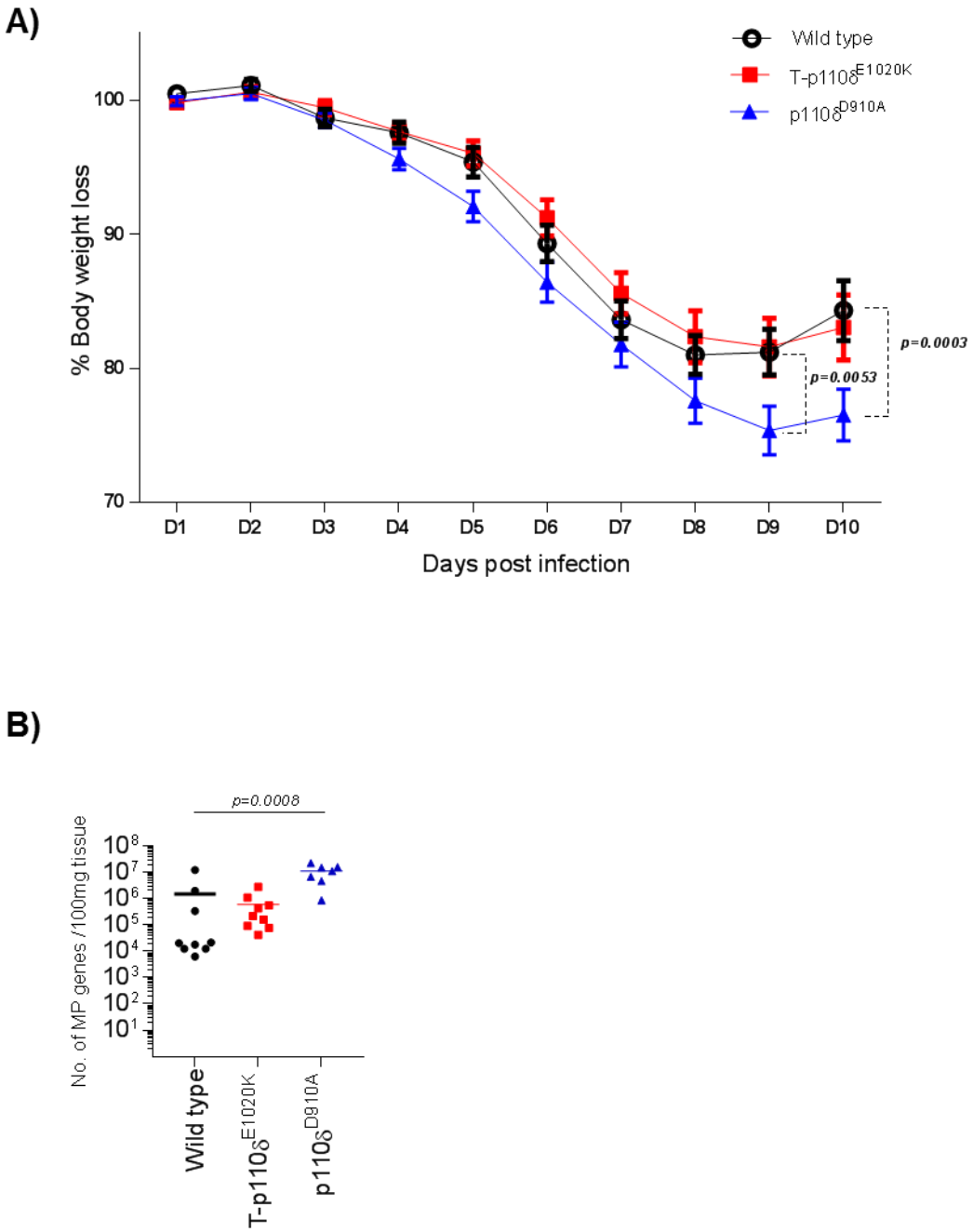

Figure 4.2.7: T-p110δ^{E1020K} mice are resistant to sub-lethal PR8 viral infection.

WT, T-p110δ^{E1020K} and p110δ^{D910A} mice were infected with 40 PFU of PR8 by intranasal infection at day 0 and mice were culled at day 10 post infection. **(A)** Graph representing body weight of WT , T-p110δ^{E1020K} and p110δ^{D910A} mice at different time points post sub-lethal PR8 influenza infection, relative to weight at day 0, set as 100%, data represents combination of four experiments with n=18-20 per genotype **(B)** Viral load in the lungs of WT, T-p110δ^{E1020K} and p110δ^{D910A} mice after day 10 post sub-lethal PR8 influenza infection, represents combination of 2 experiments with n=10 per genotype. For A, *P values* were determined by 2 way ANOVA .

4.2.8 Expansion of antigen-specific CD8⁺T cells is unaffected in T-p110δ^{E1020K} in response to primary influenza infection

Antigen-specific CD8⁺ T cells play an important role in the clearance of influenza virus from infected tissues, therefore antigen-specific CD8⁺ T cell response was assessed to the immunodominant epitope $NP_{366-374}$ in the lungs and spleens of WT, T-p110δ^{E1020K} and p110δ^{D910A} mice at day 10 post PR8 infection by using MHC class I tetramers. Interestingly, the numbers and proportions of total T cells and CD8⁺ T cells were increased in T-p110δ^{E1020K} mice and decreased in p110δ^{D910A} mice compared to WT mice in the lungs, possibly due to a migratory defect (**Figure 4.2.8 a and b**). Assessment of the proportions and numbers of $NP_{366-374}$ specific CD8⁺T cells in the spleen and lungs showed comparable primary expansion in T-p110δ^{E1020K} and WT mice (**Figure 4.2.8c and d**). There was a significant reduction in the numbers of $NP_{366-374}$ specific CD8⁺T cells in the spleens and lungs of p110δ^{D910A} compared to WT, while the proportions were significantly fewer in the spleen with a trend observed in the lungs of p110δ^{D910A} mice (**Figure 4.2.8 c and d).** From these results, it seems that primary expansion to either viral or bacterial infection is not influenced by hyperactive p110δ activity in CD8⁺ T cells in T-p110δ^{E1020K} mice.

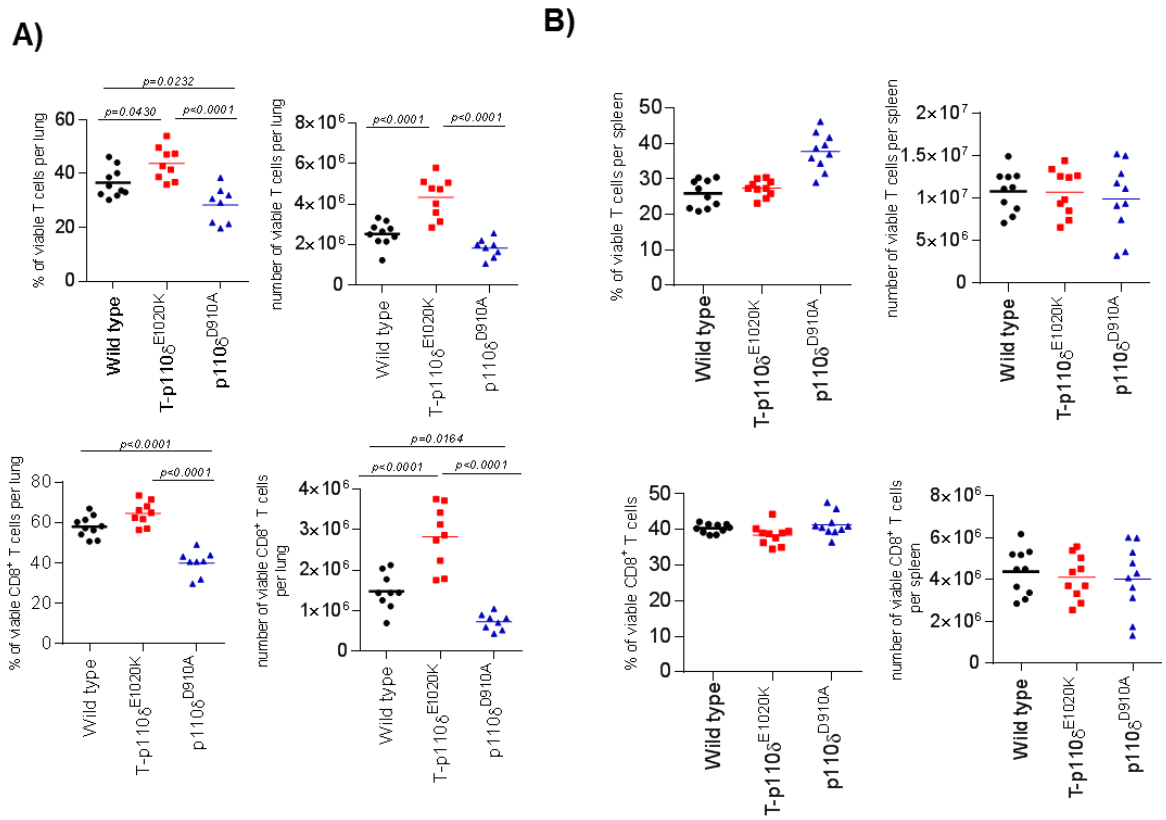

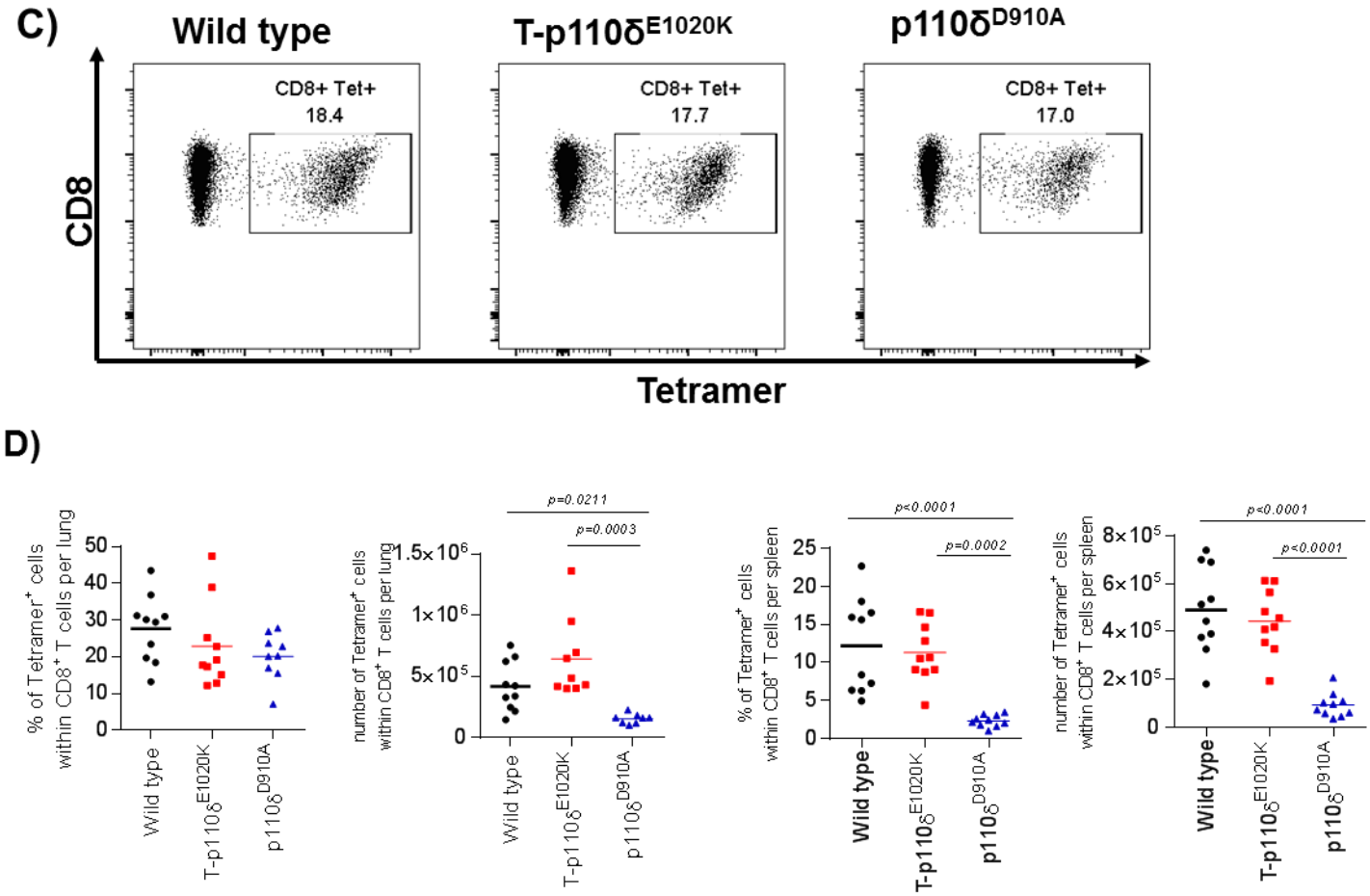

Figure 4.2.8: No difference in expansion of antigenic specific CD8$^+$ T cells in T-p110δ^{E1020K} mice compared to WT mice.

Wild type, T-p110δ^{E1020K} and p110δ^{D910A} mice were infected via intranasal route with 40 PFU PR8 on day 0 and were culled at day 10 post infection. **(A)** Graphs showing proportions and numbers of viable T cells in the lungs and spleens **(B)** Graphs showing the proportions and numbers of viable CD8$^+$ T cells in the lungs and spleens **(B)** Representative flow cytometry plots showing the frequency of $NP_{366-374}$ specific CD8$^+$ T cells among viable CD8$^+$ T cells in the lungs at day 10 post PR8 infection **(C)** Graphs showing proportions and numbers of $NP_{366-374}$-specific CD8$^+$ T cells in the lungs and spleens at day 10 post PR8 infection. Data combined from two independent experiments (n=8-10 mice per group). *P values* are shown.

4.2.9 Reduced generation of memory precursor cells in T-p110δ^{E1020K} mice in response to influenza infection

Next, antigen-specific CD8$^+$ T cells following influenza infection were immunophenotyped for different effector and memory markers as discussed previously in section 4.2.3. Upon infection at day 10, increased proportions of SLECs were found in the spleens and lungs of T-p110δ^{E1020K} mice compared to WT mice (**Figure 4.2.9a**). Conversely, the proportions of MPECs were reduced in T-p110δ^{E1020K} mice compared to WT mice (**Figure 4.2.9a**). The contrasting result was true for p110δ^{D910A} mice, where the MPECs were increased and SLECs were significantly reduced compared to WT mice (**Figure 4.2.9a**). The proportions of T_{EM} (CD44^{high}CD62L^{low}) within antigen-specific CD8$^+$T cells in spleens and lungs were comparable between T-p110δ^{E1020K} and WT mice but reduced in p110δ^{D910A} mice (**Figure 4.2.9b**). There was a trend towards reduced proportions of T_{CM} (CD44^{high}CD62L^{high}) antigen-specific CD8$^+$ T cells in T-p110δ^{E1020K}, but this was not significant when compared to WT mice (**Figure 4.2.9b**). The proportions of T_{CM} amongst antigenic-specific CD8$^+$T cells were increased in p110δ^{D910A} mice compared to WT mice (**Figure 4.2.9b**). Overall, these results are similar to that observed following Lm-OVA infection; in that memory-associated markers are reduced due to hyperactive p110δ activity.

Next, cytokine production following *ex vivo* $NP_{366-374}$ peptide re-stimulation of splenocytes from infected WT, T-p110δ^{E1020K} and p110δ^{D910A} mice following PR8 infection was measured. Using intracellular flow cytometry there were no differences in the production of IFNγ$^+$ or TNFα$^+$ by CD44^{high} specific CD8$^+$ T cells in T-p110δ^{E1020K} mice compared to WT mice (**Figure 4.2.9c**). There was a trend towards increased granzyme B production by CD44^{high} CD8$^+$ T cells in T-p110δ^{E1020K} mice. There was no difference in IFNγ$^+$ and granzyme B production in p110δ^{D910A} mice compared to WT mice (**Figure 4.2.9c**); however, there was a trend towards reduced TNFα$^+$ production by CD44^{high} CD8$^+$ T cells in p110δ^{D910A} mice, suggesting that insufficient p110δ activity may contribute to TNFα$^+$ production following primary influenza infection. This is consistent with previously published work by Gracias et al using T cell conditional p110δ knockout mice (CD4^{cre}) in to the context of influenza infection [119].

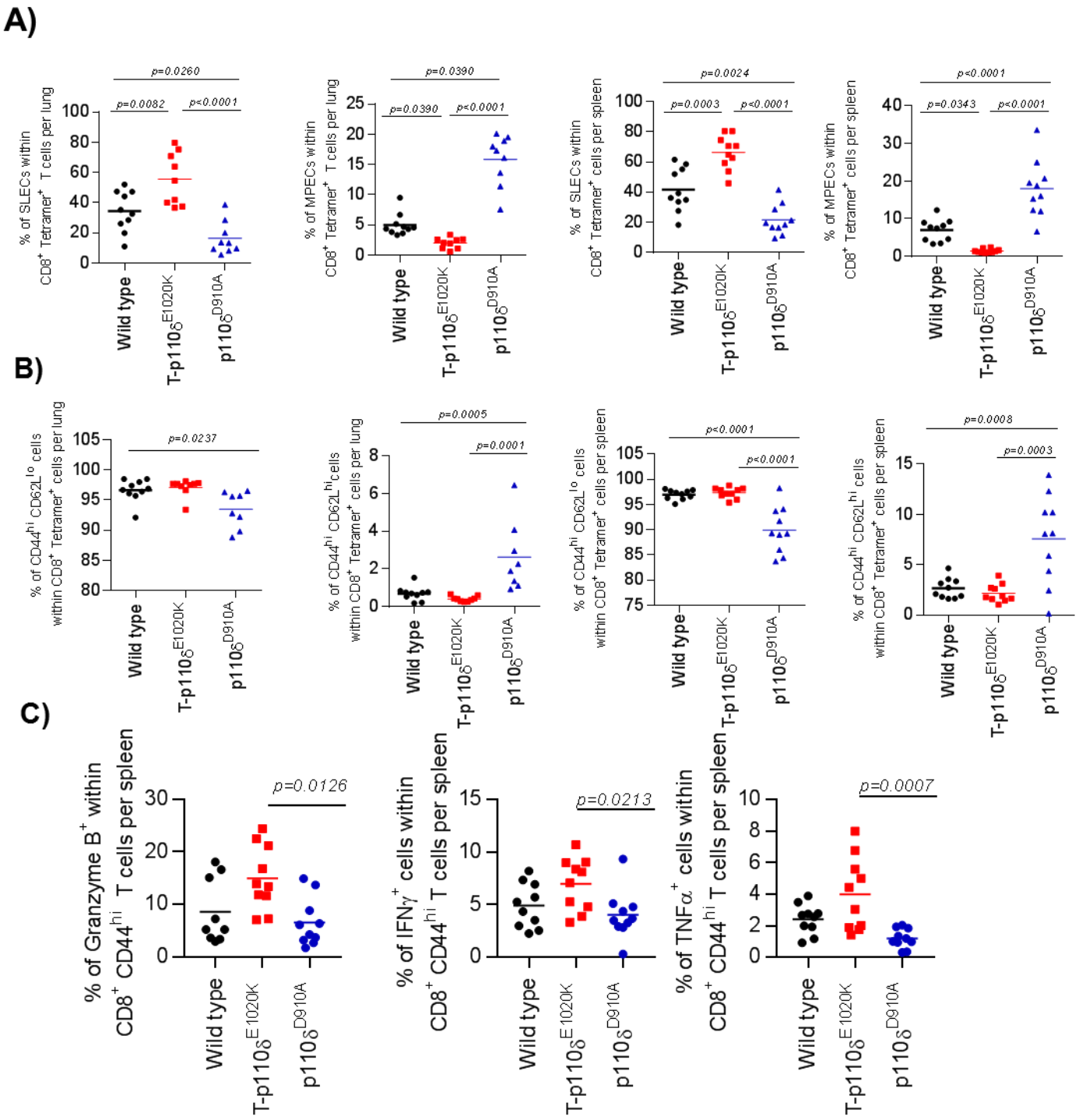

Figure 4.2.9: Reduced generation of memory precursor effectors cells in T-p110δ^{E1020K} mice following influenza infection.

WT, T-p110δ^{E1020K} and p110δ^{D910A} mice were infected with 40 PFU PR8 via intranasal route on day 0 and were culled at day 10 post infection. **(A)** Graphs showing proportions of KLRG1^{hi}CD127^{lo} (SLECs) and CD127^{hi}KLRG1^{lo} (MPECs) among antigenic-specific CD8^{+} T cells in lungs and spleens. **(B)** Graphs showing proportions of CD44^{high}CD62L^{low} (T_{EM}) and CD44^{high}CD62L^{low} (T_{CM}) among antigenic-specific CD8^{+} T cells in lungs and spleen **(C)** Graphs showing percentage and numbers of IFNγ^{+} , TNFα^{+} and Granzyme B^{+} within splenic CD44^{hi} CD8^{+} T cells following *ex vivo re*-stimulation with with $NP_{366-374}$ peptide stimulation for 5.5 hours. Data combined from two independent experiments, for A-B n =8-10 mice per group and for C n = 9-10 mice per group. *P values* are shown.

4.2.10 Elevated T follicular helper cells and Regulatory T cells in T-p110δ^{E1020K} mice following influenza infection

$CD4^+$ T cells are critical immune response mediators in providing help to $CD8^+$ T cells and B cells during viral infections. Depleting $CD4^+$ T cells was shown to result in significantly reduced recruitment of $CD8^+$T cells to the lung, delayed ability to clear the virus and increased disease outcome [372].

In order to assess the antigen-specificity of the $CD4^+$ T cell response, $CD4^+$ T cells were stained with MHC Class II I-A^b tetramer specific for the influenza $NP_{311-325}$ epitope. Upon infection, in the spleen there was no difference in the numbers of total $CD4^+$ T cells across all three groups; however, the numbers of $CD44^{high}$ $CD4^+$ T cells were significantly reduced in p110δ^{D910A} mice with no difference in T-p110δ^{E1020K} mice compared to WT mice (**Figure 4.2.10a**). There was no difference in the proportions and numbers of $NP_{311-325}$ specific $CD4^+$ T cells in T-p110δ^{E1020K} compared to WT mice. In p110δ^{D910A} mice, the numbers of $NP_{311-325}$ specific $CD4^+$ T cells were significantly reduced compared to WT mice but there was no difference in proportions (**Figure 4.2.10b**). In comparison to WT mice, there was a trend toward increased numbers and proportions of total Tfh cells in T-p110δ^{E1020K} mice; this was significantly reduced in p110δ^{D910A} mice (**Figure 4.2.10c**). The same trend in numbers was observed for antigenic specific Tfh cells for all three groups (**Figure 4.2.10d**).

Tregs induced by influenza virus have been shown to be highly suppressive, indicating that they represent a limiting factor to $CD4^+$ and $CD8^+$T cell effector responses during infection [373]. Following PR8 influenza infection at day 10, increased numbers of $Foxp3^+$ cells were seen among total $CD4^+$ T cells in the spleens of T-p110δ^{E1020K} mice compared to WT mice. Conversely, this population was significantly reduced in p110δ^{D910A} mice compared to WT mice (**Figure 4.2.10e**). These data indicate that $CD8^+$ T cells in T-p110δ^{E1020K} mice could be influenced by the subtle increases in Tregs and Tfh cells observed following influenza infection. It is unclear to what degree these $CD4^+$ T cell subtypes could contribute to the $CD8^+$ T cell response; this is something to investigate in future experiments.

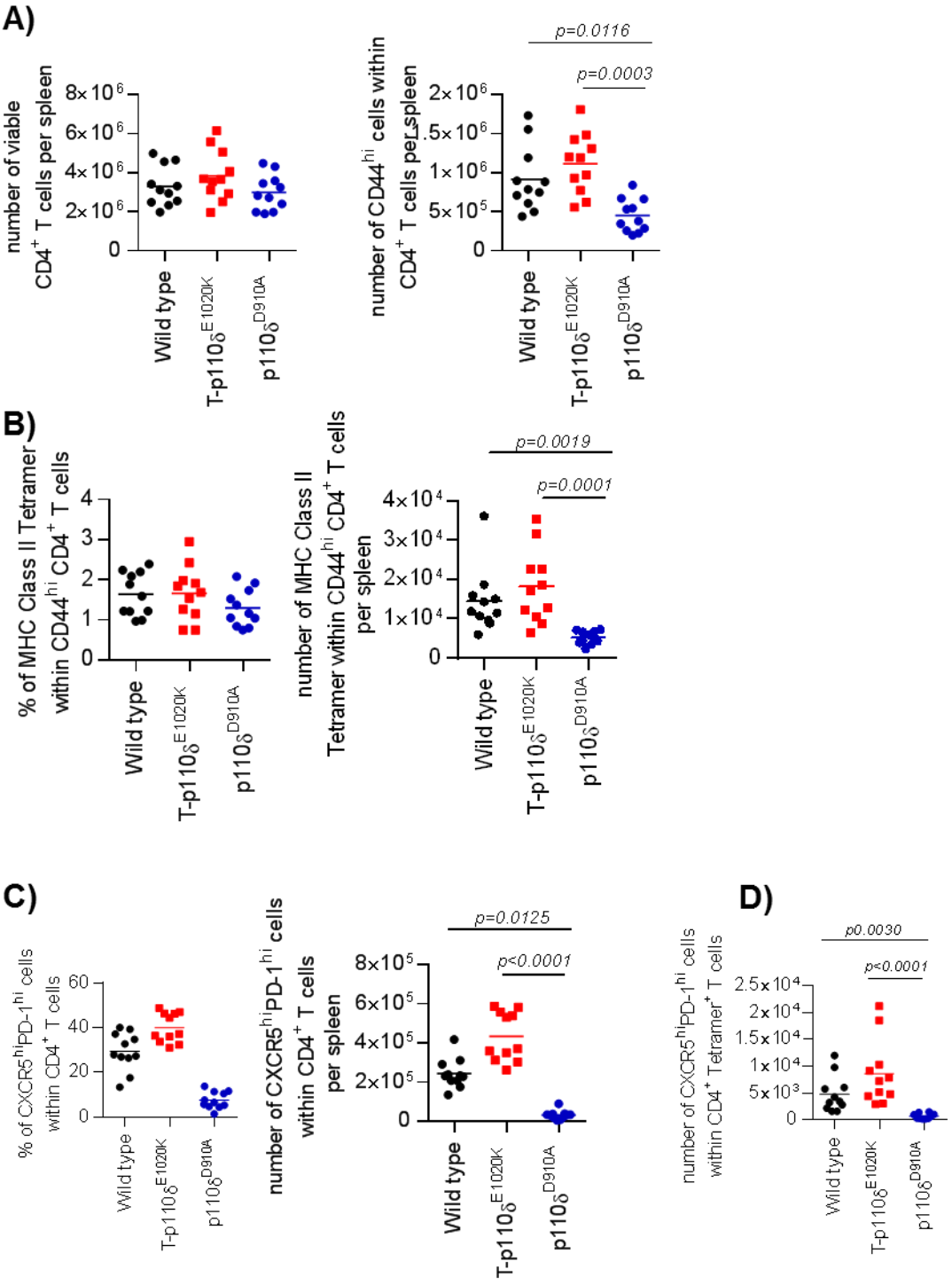
A)
number of viable CD4+ T cells per spleen
8×10^6
6×10^6
4×10^6
2×10^6
0
Wild type
T-p110δE1020K
p110δD910A
number of CD44hi cells within CD4+ T cells per spleen
p=0.0116
p=0.0003
2×10^6
1.5×10^6
1×10^6
5×10^5
0
B)
% of MHC Class II Tetramer within CD44hi CD4+ T cells
4
3
2
1
0
number of MHC Class II Tetramer within CD44hi CD4+ T cells per spleen
p=0.0019
p=0.0001
4×10^4
3×10^4
2×10^4
1×10^4
0
C)
% of CXCR5hiPD-1hi cells within CD4+ T cells
60
40
20
0
number of CXCR5hiPD-1hi cells within CD4+ T cells per spleen
p=0.0125
p<0.0001
8×10^5
6×10^5
4×10^5
2×10^5
0
D)
number of CXCR5hiPD-1hi cells within CD4+ Tetramer+ T cells
p0.0030
p<0.0001
2.5×10^4
2×10^4
1.5×10^4
1×10^4
5×10^3
0
E)
Number of Foxp3+ cells within CD4+T cells
p<0.0001
p=0.0335
p=0.0033
8×10^5
6×10^5
4×10^5
2×10^5
0

Figure 4.2.10: Increase in Tfh and Treg cells in T-p110δ^{E1020K} mice at day 10 post influenza infection

Wild type, T-p110δ^{E1020K} and p110δ^{D910A} mice were infected via intranasal route with 40 PFU PR8 on day 0 and were culled at day 10 post infection. **(A)** Graphs showing proportions and numbers of viable CD4$^+$ T cells and CD44^{high} CD4$^+$ T cells in the spleens **(B)** Graphs showing the proportions and numbers of $NP_{311-325}$ specific CD4$^+$ T cells in the spleens (**C)** Graphs showing proportions and numbers of total Tfh cells in the spleen. **(D)** Graph showing numbers of Tfh cells within $NP_{311-325}$ specific CD4$^+$ T cells in the spleens. **(E)** Graphs showing total numbers of Foxp3$^+$ cells within CD4$^+$ T cells in the spleen. Data combined from two independent experiments with n=8-10 mice per group. *P values* are shown.

4.2.11 Hyperactive p110δ results in an intrinsic defect in CD8$^+$T cells in response to influenza virus

As it is recognised that influenza specific CD4$^+$ T cells also contribute to primary immune responses by either generating T-dependent B cell responses or becoming IFNγ producing Th1 cells that can migrate to the lung and aid in resolving the infection. Therefore, to rule out the possibility of any extrinsic factors contributing to the intrinsic CD8$^+$ T cell response, I again made use of the OT1 adoptive transfer. Naïve sorted 10,000 WT and E1020K OT1 donor cells were injected into recipient mice on day -1, and mice were infected the following day with a modified H1N1 influenza virus (WSN-OVA) that is engineered to express $OVA_{257-264}$ peptide. At day 10 post infection, a significant reduction was observed I the numbers and proportions of E1020K OT1 donor cells in both lungs and spleens compared to WT donor cells (**Figure 4.2.11 a and b**). These data suggest that hyperactive p110δ causes an intrinsic defect in CD8$^+$T cells in response to different pathogens.

I further characterised the donor OT1 cells by looking at functional properties following *ex vivo* SIINFEKL peptide re-stimulation. I found a significant increase in IFNγ$^+$, TNFα$^+$ and granzyme B within E1020K OT1 donor cells compared to WT donor cells (**Figure 4.2.11 c**. It is important to note that this experiment was performed once and one with one donor per group, therefore these results are preliminary and need repeating to confirm the results observed. Nonetheless, these results are consistent with those observed in response to Lm-OVA infections, in that hyperactive p110δ causes an

intrinsic defect in CD8$^+$ T cells, which favour effector cell differentiation at the cost of memory.

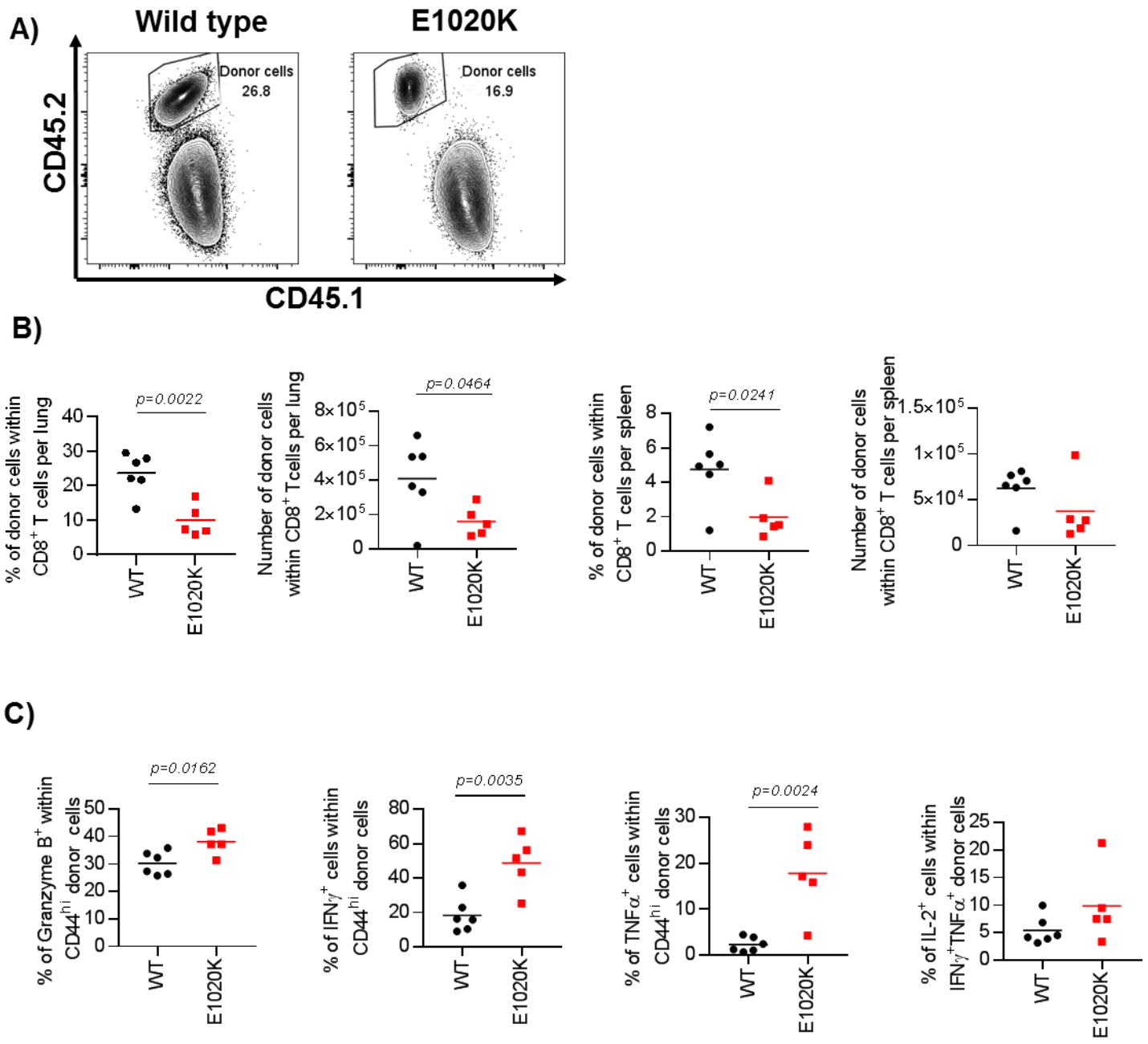

Figure 4.2.11: Hyperactive p110δ regulates the intrinsic CD8$^+$ T cell response to influenza virus

10,000 naïve (CD62L^{high}CD44^{low}) FACs sorted WT (CD45.1$^+$ CD45.2$^+$) and E1020K (CD45.2$^+$) OT1 donor cells were transferred into WT host (CD45.1+) on day -1 , infected on day 0 with WSN-OVA and culled on day 10. **(A)** Representative flow cytometry plots of WT and E1020K donor OT1 cells within lung CD8$^+$ T cells of recipient mice (CD45.1). **(B)** Numbers and proportions of WT and E1020K OT1 donor cells within CD8$^+$ T cells of lungs and spleens of recipient mice. **(C)** Proportions of Granzyme B , IFNγ$^+$, TNFα$^+$ and IL-2$^+$ cells amongst WT and E1020K donor OT-I cells in lung following *ex vivo* SIINFEKL peptide re-stimulation. Data representative of one independent experiment (1 donor and 5-6 recipient mice). *P* values are shown.

3.4 Discussion

The aim of this chapter was to investigate the effect of hyperactive p110δ in regulating $CD8^+$ T cell responses to primary infections with an acute bacterial and viral pathogen.

Primary expansion of $CD8^+$ T cells

Upon infection with either Lm-OVA or influenza, the expansion of $CD8^+$ T cells in T-$p110\delta^{E1020K}$ mice did not differ from WT mice. Additionally, body weight loss and viral loads were comparable in T-$p110\delta^{E1020K}$ and WT mice following influenza infection. On the other hand, in response to both pathogens, loss off p110δ activity using $p110\delta^{D910A}$ mice resulted in defective expansion of antigen-specific $CD8^+$ T cells compared to WT mice. The reduction in numbers of antigen-specific $CD8^+$T cells also correlated with the increase viral load and body weight loss observed in $p110\delta^{D910A}$ mice at day 10 following influenza infection. This is likely to be due to the reduced numbers of antigenic- specific $CD8^+$ and $CD4^+$ T cells detected in $p110\delta^{D910A}$ mice, that are required to ultimately eliminate the virus. These results indicate that a degree of p110δ activity is required for mounting normal $CD8^+$T cell immune responses to Lm-OVA and influenza but elevated p110δ activity is neither beneficial nor detrimental. These results also confirm published data showing that p110δ activity is required to control the magnitude of primary $CD8^+$T cells responses to acute infections [115, 119]. Gracias et al further went on to show that the defect due to p110δ deficiency was caused by impaired proliferation, activation of Akt and reduced TCR-activated oxidative phosphorylation and aerobic glycolysis within $CD8^+$ T cells [119]. Interestingly, the number of total T cells and $CD8^+$ T cells in the lungs were increased in T-$p110\delta^{E1020K}$ mice and reduced in $p110\delta^{D910A}$ mice compared to WT mice. This could potentially be differences in the expression of different chemokine or integrin receptors such as CCR4 and CD11a involved in migration into the infected lung, which could be p110δ dependent. Gracias et al also noted reduced numbers of $CD8^+$ T cells in the lungs of infected p110δ deficient T cell mice [119].

In T-$p110\delta^{E1020K}$ mice, hyperactive p110δ leads to increase phosphorylation of Akt and Foxo1/3 as shown in chapter 3. Activated Akt phosphorylates the Foxo family of transcription factors, leading to exclusion from the nucleus and degradation by proteolysis in the cytosol, consequently diminishing transcription of Foxo target genes involved in different cellular processes. [64]. Numerous studies investigating the role

of Foxo1 and Foxo3 on $CD8^+$ T cell responses to primary acute infections have been published with contrasting results. Deletion of Foxo3 in T cells leads to increase in T cell survival during the primary phase of infection due to a Foxo3-dependent down regulation of the proapoptotic Bcl2 family proteins Bim and PUMA [126, 128, 129] . On the other hand, Foxo1 has little effect on the primary expansion of $CD8^+$ T cells but plays a greater role in memory formation [123, 125].Therefore with regards to T cell survival, Foxo1 and Foxo3 have opposing roles, Foxo3 promotes apoptosis of T cells whereas Foxo1 supports survival of T cells by inducing the expression of CD127 (IL-7α receptor), which plays a role in promoting IL-7-induced Bcl-2 expression [22]. These results also illustrate the fact that there is no compensation between Foxo1 and Foxo3 and that they play differential roles in $CD8^+$ T cells response to infections. Therefore, the expansion of $CD8^+$ T cells observed in T-$p110\delta^{E1020K}$ mice could be due to the combined effects of inhibition/activation of different downstream effector proteins of Akt.

The use of $CD4^{cre}$ mice complicates the study of intrinsic $CD8^+$ T cell function because extrinsic factors such as the effect of $CD4^+$ T cell subsets harbouring hyperactive p110δ activity could influence the $CD8^+$ T cell response. Therefore, in order to exclude the contribution of possible extrinsic factors to the $CD8^+$ T cell response in T-$p110\delta^{E1020K}$ mice, I made use of the OT1 adoptive transfer system. Upon infection with either Lm-OVA or WSN-OVA, the numbers and proportions of E1020K OT1 donor cells were significantly reduced compared to WT OT1 donor cells in the recipient mice. These results imply that hyperactive p110δ causes an intrinsic defect in the expansion of $CD8^+$ T cells following primary infection. This could be due to a survival defect, as I have shown *in vitro* that upon stimulation $CD8^+$ T cells undergo increased cell death compared to WT $CD8^+$ T cells; however, there was no differences in apoptosis as assessed by Annexin 5 detection at day 8 post Lm-OVA infection. It is possible that differences might become apparent at an earlier time point or it could be due to a proliferation defect, this is something to investigate in the future. $CD8^+$ T cells in APDS patients are prone to AICD and display low $CD4^+$ T cell counts; it is likely that this scenario might be existing in the single genotype OT1 adoptive transfer experiments. In APDS patients, the hyperactive mutation is present in all cell types and due to persistent infections with different pathogens; the inflammatory environment is more

severe than that in T-p110δ^{E1020K} mice. This might serve as potential caveat for using mice to study defects occurring in human patients.

Based on the results from the OT1 adoptive transfer experiments, it is therefore plausible that CD4$^+$ T cells could be contributing to the CD8$^+$ T cell responses in T-p110δ^{E1020K} mice. CD4$^+$ T cells plays an important role in promoting CD8$^+$ T cell immunity to different pathogens. CD4$^+$ T cell help has been shown to be critical for survival of antigen-specific CD8$^+$T cells to Lm infection [374]. Through the interaction of CD40L on CD4$^+$ T cells with antigen bearing CD40 expressing dendritic cells can help CD8$^+$ T cells during infection, whether CD4$^+$ T cells in T-p110δ^{E1020K} express increased CD40L expression will have to be confirmed. As shown in chapter 3, T-p110δ^{E1020K} mice have increased Treg, Tfh and Th1 cells, and each of these could contribute to the CD8$^+$T cell response in T-p110δ^{E1020K} mice. CD4$^+$ T cells in T-p110δ^{E1020K} mice could be promoting survival of activated antigen-specific CD8$^+$ T cells during the primary response via production of different cytokines. Th1 cells play a crucial role in aiding CD8$^+$ T cell responses during infection due to their signature cytokine IFNγ. Following influenza infection, the numbers of Tregs were increased that could be suppressing the expansion of antigenic-specific CD8$^+$ T cells in the T-p110δ^{E1020K} mice. Additionally Tregs can indirectly promote Tfh responses by regulating the availability of IL-2, as IL-2 can prevent Bcl-6 expression required for Tfh differentiation [375]. Therefore, depriving IL-2 as a suppressive mechanism used by Tregs can actually enhance Tfh responses. Following influenza infection, I detected increased Tfh cells in T-p110δ^{E1020K} mice, these cells are important producers of IL-21 cytokine. IL-21 has been shown to support CD8$^+$ T cell survival and functionality during certain infections by inducing pro-survival molecules, such as Bcl-2 and Bcl-xL, in a STAT1 and STAT3-dependent fashion [57]. In addition, IL-21 can activate the PI3K pathway, which is involved in IL-21-induced CD8$^+$ T cell proliferation [376].It is important to note that the effect of IL-21 can be complex and vary depending on the experimental design [377]. The mechanism by which CD4$^+$ T cells provide survival signals requires further investigation; they could be providing direct survival signals or act indirectly via a different cell type. There is a possibility that either the cellular expansion or functional abilities or both of antigenic-specific CD8$^+$ T cells in T-p110δ^{E1020K} mice is influenced by a combination of multiple CD4$^+$ T cell subsets. One

way of excluding the effect of $CD4^+$ T cells in T-$p110\delta^{E1020K}$ mice would be to deplete $CD4^+$ T cells using a monoclonal depleting antibody. This would provide insight into the role of $CD4^+$ T cells in the regulation of $CD8^+$ T cell responses in T-$p110\delta^{E1020K}$ mice. In addition, it would be interesting to compare the effects of total $CD4^+$ T cell depletion with Treg-specific depletion in T-$p110\delta^{E1020K}$ mice by using $Foxp3^{DTR}$ mice. These mice serve as a model of acute and transient depletion of Tregs, these mice express a diphtheria toxin receptor (DTR) under the control of the Foxp3 locus, which following administration of diphtheria toxin results in the ablation of Tregs [378].

The competitive co-transfer experiments surprisingly revealed that WT OT1 cells could help E1020K OT1 cells during the primary expansion at day 5 and 8 in the blood. It is possible that WT cells are providing IL-2, which enhances the proliferation of E1020K OT1 cells in the same host. Indeed, lower levels of IL-2 in the Lm-OVA single genotype adoptive transfer experiment were detected among the E1020K OT1 donor cells compared to WT OT1 donor cells. Furthermore, it is known that IL-2R signals can promote $CD8^+$ T cell expansion [379]. Additionally help could be provided via CD40L expression on WT OT1 cells, as expression of CD40L on $CD8^+$ T cells can promote the proliferation of other CD40L expressing $CD8^+$ T cells or bystander effector $CD8^+$ T cells present [380]. However, it will be important to determine the expression of CD40L on both WT and E1020K OT1 $CD8^+$ T cells to determine if this is the case. Previously our group has shown that in a competitive setting, WT OT1 cells were also able to provide help to $p110\delta^{D910A}$ OT1 cells such that their primary expansion was same in the co-transfer experiments compared to single adoptive transfer experiments in response to Lm-OVA [115]. Therefore, these findings suggest that normal p110δ activity is required for $CD8^+$ T cells to either support the survival or proliferation of other responding cells.

$CD8^+$T cell effector populations

A common result observed in response to both pathogens, using either T-$p110\delta^{E1020K}$ mice or OT1 donor cells was an increase in the numbers and proportions of SLECs ($KLRG1^{high}$ $CD127^{low}$). This was associated with a decrease in MPECs ($CD127^{high}$ $KLRG1^{low}$), the cells that are important in forming long-lived memory cells. Additionally, the proportions of central memory T cells characterised by $CD44^{high}CD62L^{high}$ were lower in $CD8^+$ T cells with hyperactive p110δ following infection. The converse was

true for p110δ^{D910A} mice in response to both Lm and influenza. The expression of Eomes was reduced on Lm-OVA specific CD8$^+$ T cells in T-p110δ^{E1020K} mice, which further points to a defective memory cell phenotype, as Eomes expression promotes the generation and persistence of memory CD8$^+$T cells. Additionally, analysis of Epstein Barr virus (EBV) positive cells from APDS patients also show reduced expression of both CD62L$^+$ and CCR7$^+$ naïve and central memory T cells and a greater abundance of effector memory T cells relative to control patients [138, 141]. Magnitude of Akt activation is important in determining the differentiation of MPECs and SLECs. Persistent Akt activation leads to defects in MPEC generation, in contrast Akt inhibition increased memory CD8$^+$ T cells whilst rescuing SLECs from deletion [121, 122]. These results are consistent with the known functions of Akt in regulating T cell survival, trafficking and memory genes via controlling Foxo activity. Hyperactive Akt causes Foxo1 to lose its positive regulation over genes involved in T cell memory and trafficking such as IL-7Ra (CD127), Sell (CD62L), Tcf7, CCR7, Eomes and others. A possible complication associated with this analysis lies in the fact that Foxo1 transcriptionally induces both CD62L and CD127; therefore, the decrease may not truly reflect CD8$^+$ T cell differentiation. However, these results are consistent with studies focusing on the role of Foxo1 in regulating CD8$^+$ T cell responses to infections that have shown defective memory responses due to downregulation of memory genes controlled by Foxo1[123-125, 381] .

Effector functions

In terms of CD8$^+$ T cells effector functions such as production of cytokines IFNγ and TNFα, inhibition or hyperactivation of p110δ signalling using p110^{D910A} and T-p110δ^{E1020K} did not reveal any significant differences compared to WT mice in either of the infection models used. However, CD8$^+$ T cells in T-p110δ^{E1020K} mice produced increased levels of the cytotoxic molecule: granzyme B, compared to WT and p110δ^{D910A} mice. In response to Lm-OVA infection, the killing ability of Lm-OVA specific CD8$^+$ T cells was increased in T-p110δ^{E1020K} mice compared to WT mice. HIF1α is activated downstream of the PI3K-mTOR pathway, and plays an important role in promoting the expression of cytolytic effectors such as granzyme B [61]. The reduced granzyme B levels observed in p110δ^{D910A} mice differs from previously published data where the expression of granzyme B was comparable to WT mice [115, 119]. In contrast, *in vitro* activated CD8$^+$T cells from tumor-bearing p110δ^{D910A} mice

showed lower expression of cytolytic effectors. The differences observed between these studies could be due to differences in the strength of the inflammatory stimuli. Overall, $CD8^+$T cells in T-p110δ^{E1020K} mice were inefficient effector cells as they were unable to produce a strong cytokine response. I also looked at the expression of T-bet in one experiment and found no significant differences between WT and T-p110δ^{E1020K} mice. This could potentially explain why there were no differences in IFNγ production between WT and T-p110δ^{E1020K} since T-bet plays a role in promoting IFNγ expression [25, 382].

In contrast to the results in T-p110δ^{E1020K} mice, there was a significant increase in the proportions of $IFN\gamma^+$ $TNF\alpha^+$ single and co-producers amongst the E1020K OT1 donor cells compared to the WT OT1 donor cells. This was true for both Lm-OVA and WSN-OVA infection models. In addition, expression of T-bet was increased amongst E1020K OT1 donor cells in response to Lm-OVA infection. This implies that perhaps in T-p110δ^{E1020K} mice, other T cell populations such as Tregs could be suppressing cytokine production and perhaps T-bet expression. Tregs are able to decrease the effectiveness of the adaptive immune response to different pathogens and could be the reason why an increase in effector cytokines was not observed in T-p110δ^{E1020K} mice [383, 384]. Additionally in APDS patients, the T cells that do survive AICD display characteristics of enhanced effector function [141].

Numerous studies have shown that PI3K signaling increases $CD8^+$ T cell effector populations whilst causing reduced generation of memory cells [131, 132]. This occurs mainly via inhibitory Foxo transcription factor activity due to increased Akt signaling, leading to negative regulation of genes involved in memory $CD8^+$ T cell survival and trafficking. In addition, Foxo1 dependent repression of T-bet, IFNγ and granzyme B is able to reduce effector $CD8^+$T cell differentiation [123]. In this chapter, I have shown that following primary infections with either Lm-OVA or influenza, $CD8^+$ T cells in T-p110δ^{E1020K} mice are able to expand normally. However, during single genotype OT1 adoptive transfer experiments, hyperactive p110δ causes a defect in the expansion of $CD8^+$ T cells. The surviving $CD8^+$ T cells display a short lived effector phenotype with elevated cytokines and granzyme B. Additionally in both intact T-PI3Kδ^{E1020K} mice and OT1 adoptive transfer experiments, hyperactive p110δ leads to reduced expression of markers involved in maintenance of long-lived memory cells.

Chapter 5

Effect of hyperactive p110δ in $CD8^+$ T cell responses to secondary infections

5.1 Introduction

The primary expansion phase to an acute infection is typically followed by a period of contraction, during which time the majority of effector $CD8^+$ T cells undergo apoptosis, and the remaining virus-specific $CD8^+$ T cells persist as a stable memory population that differs both phenotypically and functionally from the naive $CD8^+$ T cell population. Memory $CD8^+$ T cells are able to persist for a longer time due to interactions with IL-7 and IL-15 that mediate their survival and renewal by undergoing homeostatic proliferation [385]. These memory $CD8^+$ T cells can rapidly differentiate into secondary effectors on subsequent reinfection and confer long-lasting, protective immunity.

In chapter 4, I demonstrated that $CD8^+$ T cells in T-p110δ^{E1020K} mice have a normal primary expansion phase in response to two different pathogens. Moreover, having hyperactive p110δ in $CD8^+$ T cells only leads to reduced expansion of $CD8^+$ T cells with greater functional abilities. A consistent phenotype observed following primary infection was of reduced memory precursor effector cells (MEPCs) in $CD8^+$ T cells with hyperactive p110δ. These cells are destined to survive and become long-lived memory $CD8^+$ T cells; my results therefore predicted that memory T cell responses may be impaired.

Generating a protective memory CD8 T cell response is considered a hallmark of adaptive immunity. At the peak of the primary response, $CD8^+$ T cells with hyperactive p110δ fail to acquire characteristics of memory cells whilst retaining some aspects of effector T cells. Additionally, APDS patients also display reduce memory $CD8^+$ T cells, therefore, I wanted to know the impact of reduced MPECs detected in T-p110δ^{E1020K} at the peak of the primary response on the maintenance, contraction and recall response of $CD8^+$ T cells to secondary infection. In this chapter, most of the results presented utilised the Lm-OVA infection model along with the use of OT1 TCR transgenic mice to investigate the effect of hyperactive p110δ in development of memory $CD8^+$ T cells and in mounting effective recall responses following re-challenge. Additionally, I also used the influenza virus to detect whether the response observed is independent of the type of pathogen used. For influenza virus reinfections, mice were first immunised with the PR8 (H1N1) strain and then subsequently challenged with the heterosubtypic Hkx31 (H3N2) virus, which expresses distinct

haemagglutinin (HA) and the neuraminidase (NA) but shares the same six internal genes as PR8. In this way, the assessment of the secondary $CD8^+$ T cell response can be carried out in the absence of cross- reactive protective antibodies against influenza virus [255].

5.2 Results

5.2.1 Similar numbers of resting memory CD8$^+$ T cells at day 40 post Lm-OVA infection in T-p110δ^{E1020K} mice

Following primary expansion of CD8$^+$ T cells, majority of the antigenic specific CD8$^+$ T cells are depleted during the contraction phase of the immune response and a small fraction of CD8$^+$ T cells persist and differentiate into long-lived memory T cells (REF). Following infection with Listeria, fewer memory precursor effector cells (MPECs) were detected in T-p110δ^{E1020K} mice at day 8 post infection (Chapter 4); therefore, the consequence of reduced MPECs on the establishment of memory CD8$^+$ T cells was investigated. In order to do this, Lm-OVA specific CD8$^+$ T cells in WT, T-p110δ^{E1020K} and p110δ^{D910A} mice were quantified at day 40 post (establishment of memory) infection in different organs. The proportions and numbers of Lm-OVA specific CD8$^+$ T cells were comparable between WT and T-p110δ^{E1020K} mice in the spleen and bone marrow (**Figure 5.2.1 a and c**). There was a trend towards reduced proportions and numbers of Lm-OVA specific CD8$^+$ T cells in the lymph nodes but this was not significant (**Figure 5.2.1b**). In the blood, there was no difference in the numbers but a trend towards increase proportions of Lm-OVA specific CD8$^+$ T cells. In regards to p110δ^{D910A} mice, there was a significant reduction in the numbers of Lm-OVA specific CD8 T cells in the spleen and lymph nodes compared to WT mice (**Figure 5.2.1a and b**). Therefore, I can conclude that hyperactive p110δ in T-p110δ^{E1020K} mice does not affect the number of resting memory CD8$^+$ T cells generated in response to Lm-OVA infection despite reduced MPECs detected at day 8 post primary infection.

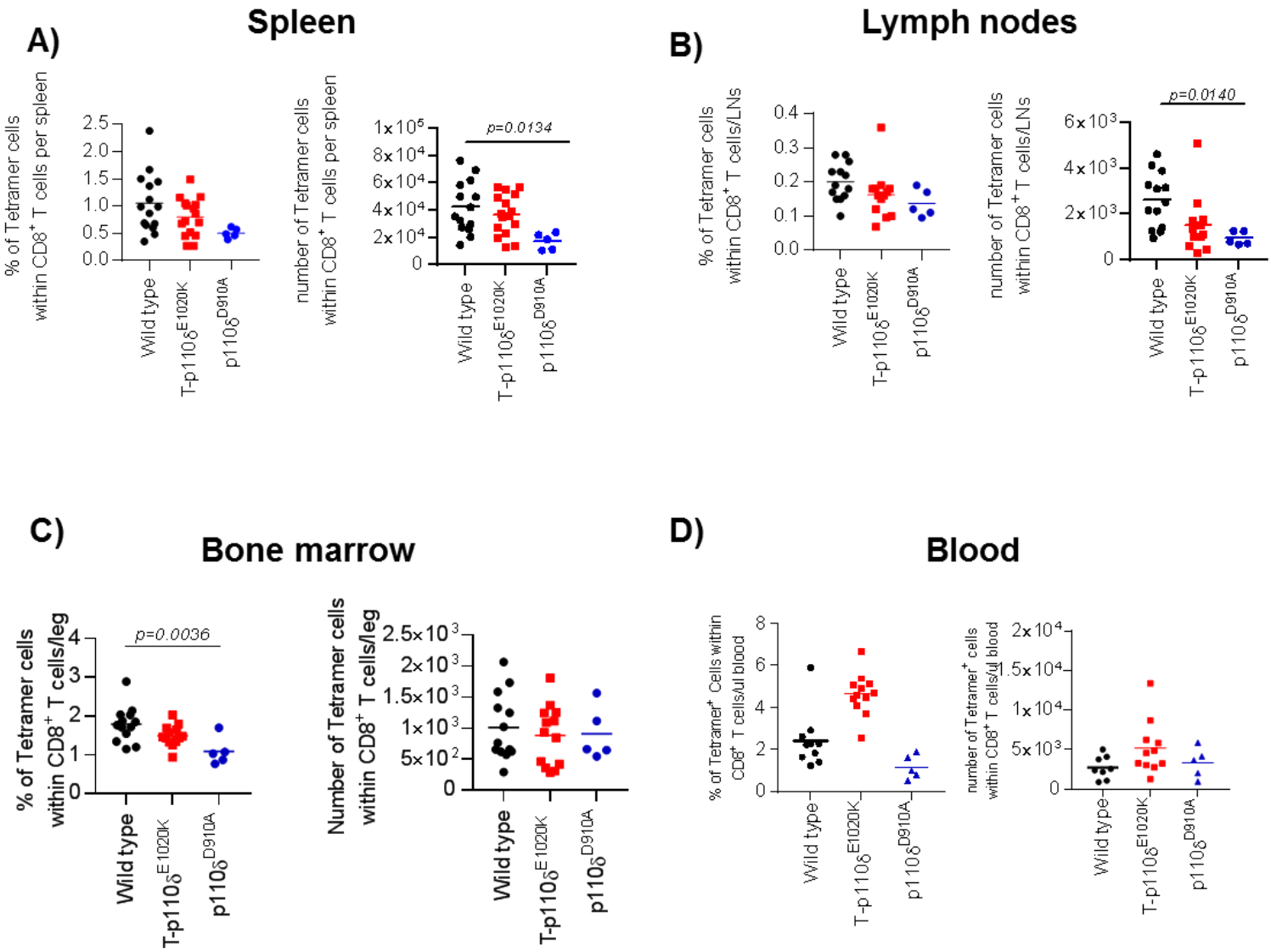

Figure 5.2.1: No difference in Lm-OVA specific resting memory CD8$^+$ T cells in T-p110δ^{E1020K} mice at day 40 post primary Lm-OVA infection

WT, T-p110δ^{E1020K} and p110δ^{D910A} mice were infected with 5 x 10^6 CFU of Lm-OVA on day 0 and culled at day 40. Graphs showing numbers and proportions of Lm-OVA specific resting memory CD8$^+$ T cells in **(A)** Spleen **(B)** Lymph nodes **(C)** Bone marrow and **(D)** Blood. Data in A is combined from three independent experiments (n = 5-16 per group), data in B-D is combined from two independent experiments (n = 5-13 per group). *P values* are shown.

Phenotypically reduced memory CD8$^+$ T cells in T-p110δ^{E1020K} mice at day 40 post Lm-OVA infection

Memory CD8$^+$ T cells can be divided into central memory (T_{CM}) and effector memory CD8$^+$ T cells (T_{EM}) based on the expression of several cell surface molecules such as CD62L, CCR7 and CD44. CD62L expression is useful in distinguishing between these two subsets because T_{CM} cells are mostly CD62L^{high}, whereas T_{EM} cells are CD62L^{low}. These have been discussed in more detail in chapter 4. I proceeded to look at the expression of characteristic memory and effector markers on Lm-OVA specific CD8$^+$ T cells at day 40 post infection. Upon infection, the proportions and numbers of T_{CM} cells characterised as CD62L^{high}CD44^{high} were significantly reduced in the spleen and lymph nodes of Lm-OVA specific CD8$^+$ T cells in T-p110δ^{E1020K} mice compared to WT mice (**Figure 5.2.2a**). There was no difference in the T_{EM} populations between these two groups as characterised by CD44^{high}CD62L^{low} (**Figure 5.2.2a**). On the other hand, in p110δ^{D910A} mice, the proportion of T_{CM} cells in the spleen was significantly increased with no differences in numbers. In lymph nodes, no differences in proportions but a significant reduction in numbers of T_{CM} cells amongst Lm-OVA specific CD8$^+$ T cells in p110δ^{D910A} mice compared to WT mice (**Figure 5.2.2a**). The reduction in numbers could be attributed due to the reduced numbers of Lm-OVA specific CD8$^+$ T cells detected in the lymph nodes at day 40 post infection. The numbers of T_{EM} population was significantly reduced in p110δ^{D910A} mice across the different organs compared to WT mice (**Figure 5.2.2a**).

Furthermore, I also observed the expression of KLRG1 and CD127 on Lm-OVA specific CD8$^+$ T cells to differentiate into MPECs and SLECs. At day 40 post infection, significantly reduced numbers and proportions of MPECs characterised as CD127^{high}KLGR1^{low} in the spleen were detected in Lm-OVA specific CD8$^+$ T cells in T-p110δ^{E1020K} mice compared to WT mice (**Figure 5.2.2b)**. The proportions of SLECs were significantly increased in T-p110δ^{E1020K} mice and a trend towards increase in numbers were observed (**Figure 5.2.2b**). Interestingly no differences proportions of MPECs and SLECs were detected in p110δ^{D910A} mice but a trend towards reduced numbers compared to WT mice (**Figure 5.2.2b**).

As described previously in chapter 4, T-bet and Eomes that belong to the T-box transcription factor family are required for the formation of CD8$^+$ T cell effector and memory subsets [23, 386, 387] .Therefore I looked at the expression of Eomes and T-

bet on Lm-OVA specific $CD8^+$ T cells across the three different genotypes. The expression of memory related transcription factor Eomes was reduced amongst Lm-OVA specific $CD8^+$ T cells from T-p110δ^{E1020K} mice, whereas there was no difference in the expression of T-bet compared to WT mice (**Figure 5.2.2c**). In contrast to hyperactive p110δ, in p110δ^{D910A} mice, the expression of Eomes was significantly increased and the expression of T-bet was significantly reduced compared to WT mice (**Figure 5.2.2c**). These findings suggest that the phenotypic changes in T-p110δ^{E1020K} mice are consistent with a defective memory phenotype.

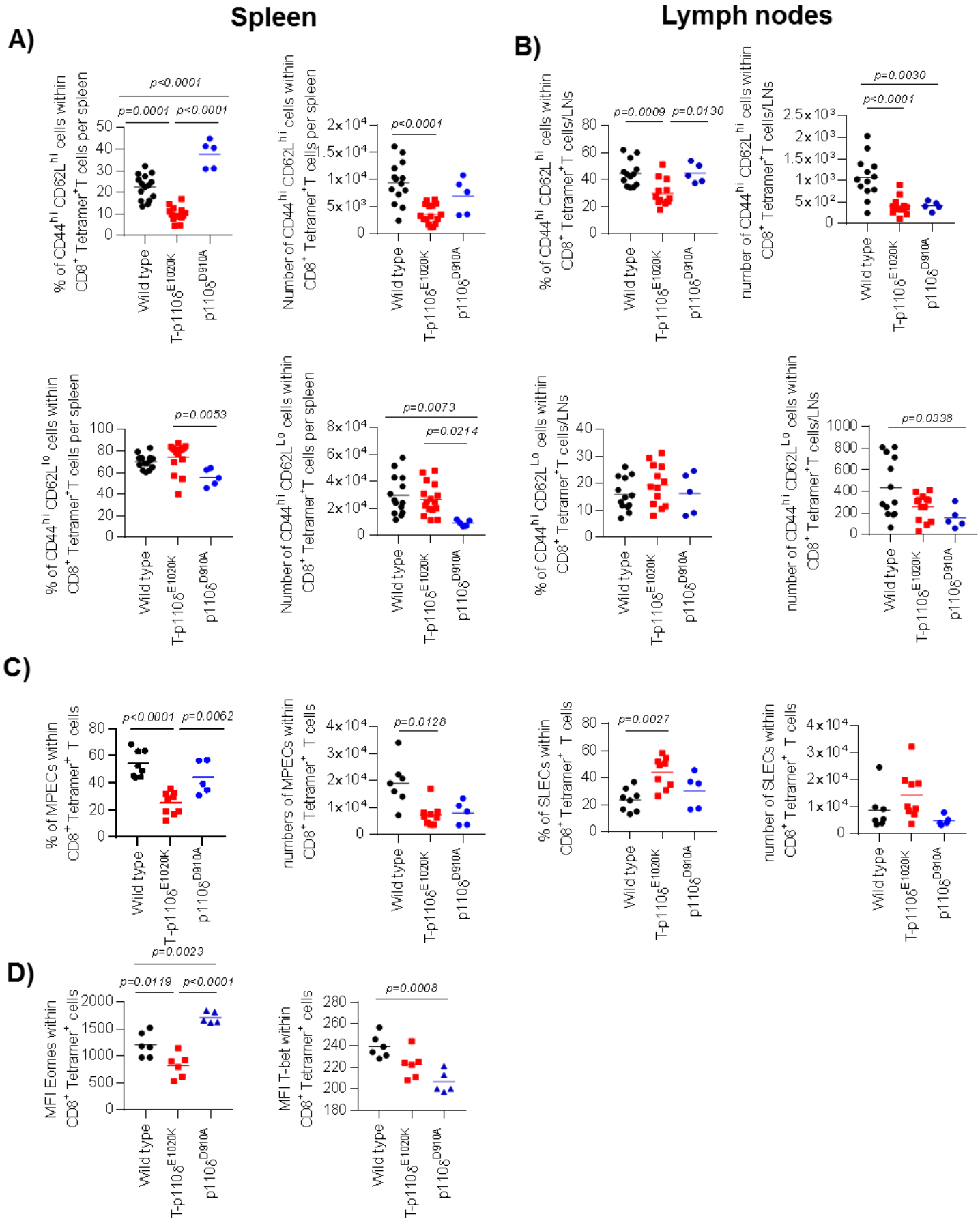
Spleen
Lymph nodes
A)
B)
C)
D)
% of CD44hi CD62Lhi cells within CD8+ Tetramer+T cells per spleen
Number of CD44hi CD62Lhi cells within CD8+ Tetramer+T cells per spleen
% of CD44hi CD62Lhi cells within CD8+ Tetramer+T cells/LNs
number of CD44hi CD62Lhi cells within CD8+ Tetramer+T cells/LNs
% of CD44hi CD62Llo cells within CD8+ Tetramer+T cells per spleen
Number of CD44hi CD62Llo cells within CD8+ Tetramer+T cells per spleen
% of CD44hi CD62Llo cells within CD8+ Tetramer+T cells/LNs
number of CD44hi CD62Llo cells within CD8+ Tetramer+T cells/LNs
% of MPECs within CD8+ Tetramer+ T cells
numbers of MPECs within CD8+ Tetramer+ T cells
% of SLECs within CD8+ Tetramer+ T cells
number of SLECs within CD8+ Tetramer+ T cells
MFI Eomes within CD8+ Tetramer+ cells
MFI T-bet within CD8+ Tetramer+ cells
Wild type
T-p110δE1020K
p110δD910A
p<0.0001
p=0.0001
p<0.0001
p<0.0001
p=0.0009
p=0.0130
p=0.0030
p<0.0001
p=0.0053
p=0.0073
p=0.0214
p=0.0338
p<0.0001
p=0.0062
p=0.0128
p=0.0027
p=0.0023
p=0.0119
p<0.0001
p=0.0008

Figure 5.2.2: Phenotypically reduced memory CD8$^+$ T cells in T-p110δ^{E1020K} mice at day 40 post Lm-OVA infection.

WT, T-p110δ^{E1020K} and p110δ^{D910A} mice were infected with 5 x 10^6 CFU of Lm-OVA on day 0 and were culled at day 40 post infection. **(A)** Graphs showing proportions and number of T_{CM} and T_{EM} in Lm-OVA specific CD8$^+$ T cells in the spleen and lymph nodes. **(B)** Proportions and numbers of MPECs and SLECs within Lm-OVA specific CD8$^+$T cells in the spleen and lymph nodes. **(C)** Expression of Eomes and T-bet amongst Lm-OVA specific CD8$^+$ T cells**.** Data in A combined from three independent experiments (n=5-15 per group), data in B combined from two independent experiments (n=5-9 per group) and data in C is representative of one independent experiment (n = 6 per group). *P values* are shown

5.2.3 Reduced cytokine production in T-p110δ^{E1020K} mice post 40 days of Lm-OVA infection

I next sought to investigate the ability of the memory CD8$^+$ T cells to produce cytokines as functional maturation into memory T cells involves acquiring ability to produce effector cytokines. In order to do this splenocytes from infected WT, T-p110δ^{E1020K} and p110δ^{D910A} mice were re-stimulated *ex vivo* with SIINFEKL peptide, at day 40 post infection. Following re-stimulation, the numbers and proportions of CD44^{high} CD8$^+$ T cells were comparable between WT and T-p110δ^{E1020K} mice (**Figure 5.2.3a**). However, the numbers of CD44^{high} CD8$^+$ T cells were lower in p110δ^{D910A} mice with no difference in proportions compared to WT mice (**Figure 5.2.3a**). The difference in numbers in the spleen could be attributed to fewer Lm-OVA specific CD8$^+$ T cells detected in p110δ^{D910A} mice at day 40. There was a trend towards reduced proportions of IFNγ$^+$ and TNFα$^+$ single and co-producing cells amongst CD44^{high} CD8$^+$ T cells in T-p110δ^{E1020K} compared to WT mice, however the numbers of IFNγ$^+$ and TNFα$^+$ single producers were significantly lower (**Figure 5.2.3 b**). There was no difference in numbers and proportions of IFNγ$^+$ and TNFα$^+$ in p110δ^{D910A} mice compared to WT mice (**Figure 5.2.3b**). This set of data suggests that hyperactive p110δ causes a functional defect in the maturation of memory CD8$^+$ T cells following infection with Lm-OVA.

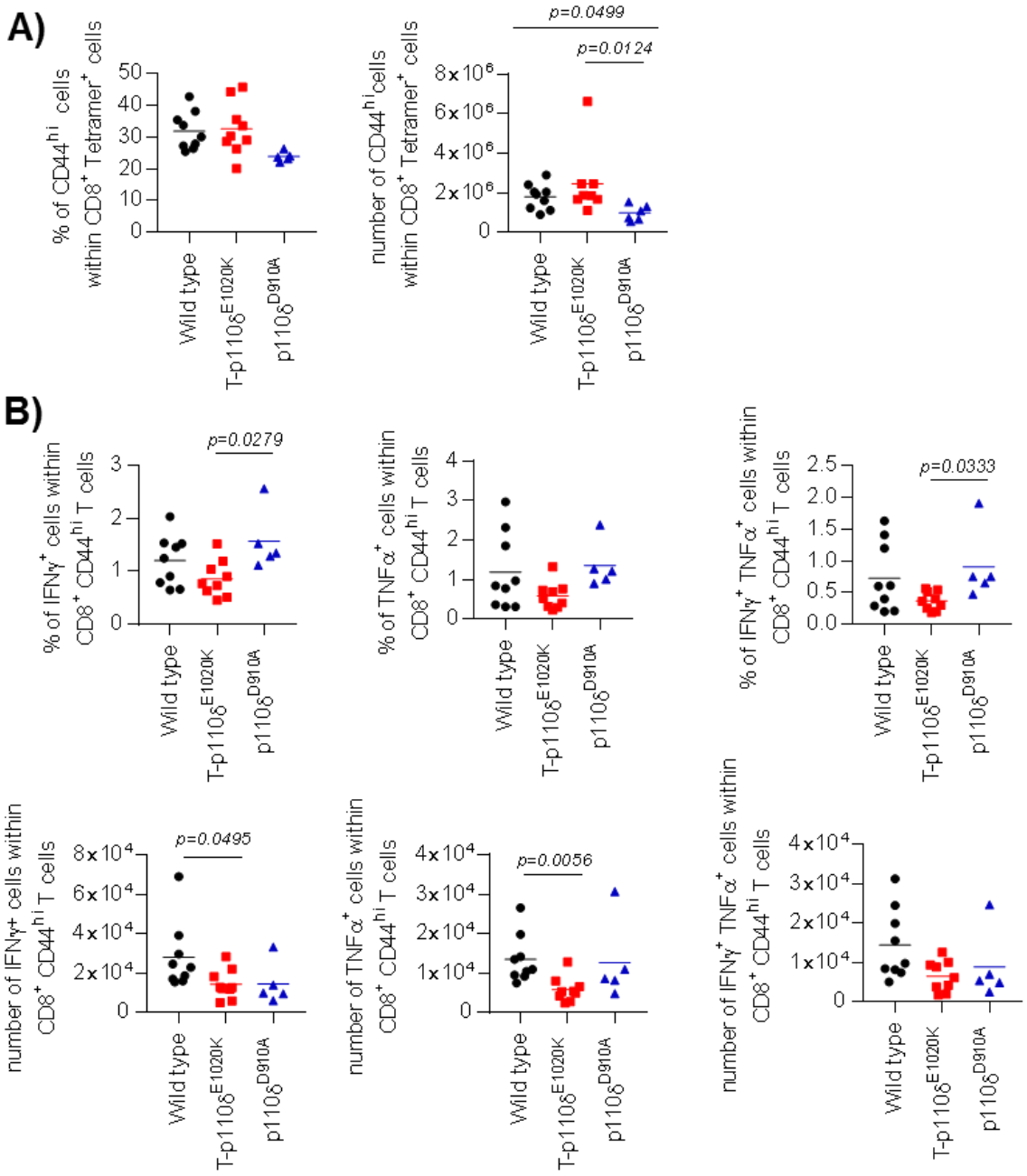

Figure 5.2.3: Trend towards reduced cytokine production in T-p110δ^{E1020K} mice at day 40 post Lm-OVA infection.

WT, T-p110δ^{E1020K} and p110δ^{D910A} mice were infected with 5 x 10^6 CFU of Lm-OVA on day 0 and culled at day 40. Splencoytes were re-stimulated *ex vivo* with SIINFEKL peptide for 5.5 hours in the presence of brefeldin A. **(A)** Proportions and numbers of CD44^{high} CD8$^+$ T cells in infected spleens **(B)** Proportion and numbers of CD44^{high} CD8$^+$ T cells producing IFNγ$^+$, TNFα$^+$ single and co-producers. Data combined from two independent experiments (n =5-9 per group). *P values* are shown.

5.2.4 Early defect in recall response to Lm-OVA in T-p110δ^{E1020K} mice

A hallmark property of memory CD8$^+$ T cells is the ability to mount robust secondary responses upon re-infection. Therefore, in order to test the ability of memory CD8$^+$ T cells to mount secondary responses, WT and T-p110δ^{E1020K} mice were infected with Lm-OVA on day 0 and subsequently re-challenged with Lm-OVA at day 40. Mice were culled at day 5 post-secondary infection, as the peak of the secondary infection is regarded to be earlier than the peak for primary infection. Following re-infection with Lm-OVA, there were comparable proportions and numbers of Lm-OVA specific CD8$^+$ T cells in WT and T-p110δ^{E1020K} mice in the spleen, lymph nodes and blood (**Figure 5.2.4a).** Therefore, hyperactive p110δ in CD8$^+$ T cells in T-p110δ^{E1020K} mice does not compromise protective immunity against Lm-OVA re-challenge despite producing fewer memory CD8$^+$ T cells. To assess cytokine production in WT and T-p110δ^{E1020K} mice following re-infection with Lm-OVA, splenocytes from infected mice were stimulated *ex vivo* with SIINFEKL peptide in the presence of brefeldin A for 5.5 hours. Using intracellular straining I found that in T-p110δ^{E1020K} mice the proportions of IFNγ$^+$ TNFα$^+$ double positive cells among CD44^{high} CD8$^+$ T cells were increased. Additionally, the proportions of granzyme B$^+$ cells were significantly increased compared to WT mice (**Figure 5.2.4b**).

A subsequent experiment was carried out in which WT, T-p110δ^{E1020K} and p110δ^{D910A} mice were infected with Lm-OVA on day 0 and then on day 50. Mice were culled on day 3 instead of day 5, in order to see whether a defect is observed earlier on following secondary infection. The numbers and proportions of splenic viable CD8$^+$ T cells were similar in WT and T-p110δ^{E1020K} mice; however, the numbers of viable CD8$^+$ T cells were reduced in p110δ^{D910A} mice with no differences in proportions (**Figure 5.2.4c**). Interestingly at day 3 post secondary infection, the proportions and numbers of Lm-OVA specific CD8$^+$ T cells were reduced in T-p110δ^{E1020K} mice compared to WT mice in the spleen. A reduction was also observed in the numbers of splenic Lm-OVA specific CD8$^+$ T cells in p110δ^{D910A} mice compared to WT mice, however no differences was detected in proportions (**Figure 5.2.4d**). These results suggest that an earlier defect in recall response to Lm-OVA is detected in T-p110δ^{E1020K} mice that can be overcome at a later time point.

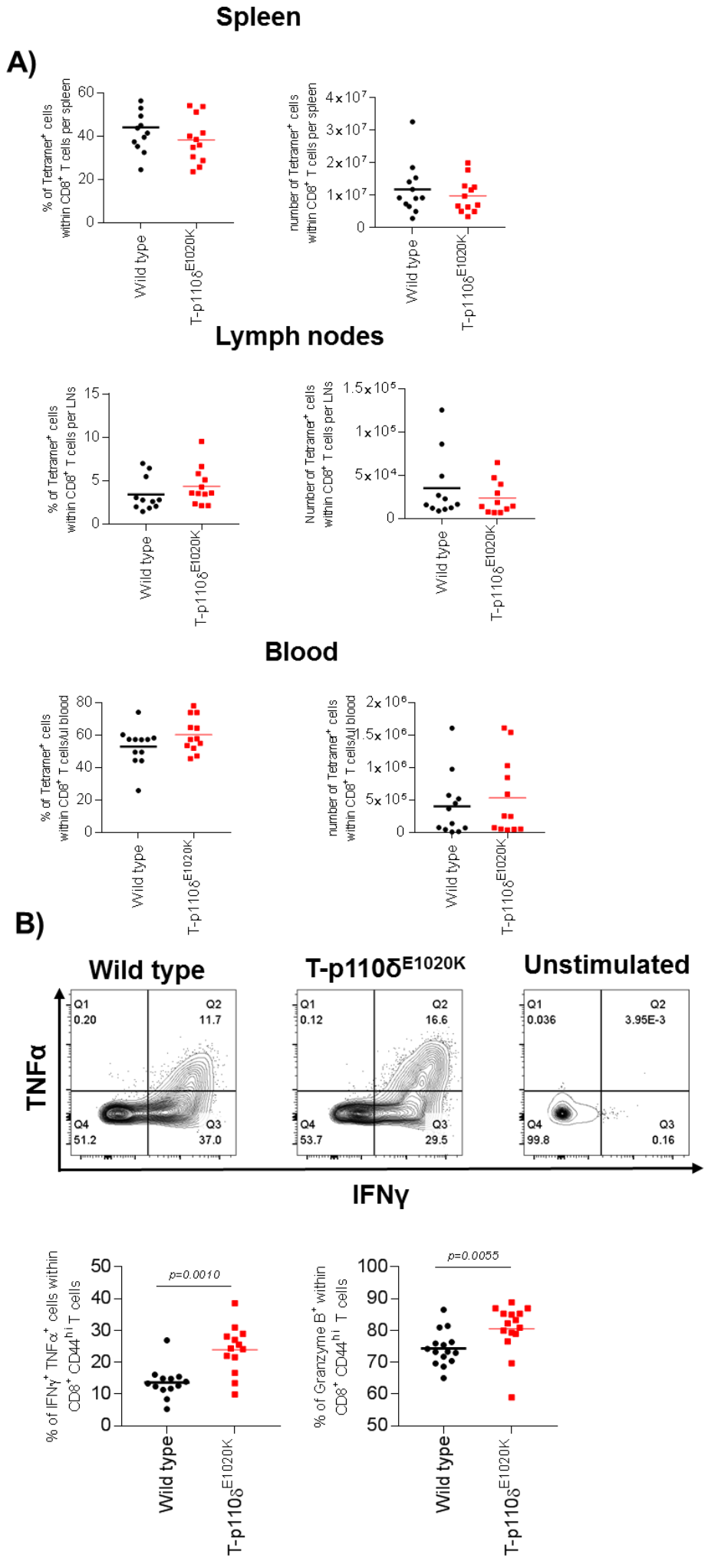
Spleen
A)
% of Tetramer+ cells within CD8+ T cells per spleen
number of Tetramer+ cells within CD8+ T cells per spleen
Wild type
T-p110δE1020K
Lymph nodes
% of Tetramer+ cells within CD8+ T cells per LNs
Number of Tetramer+ cells within CD8+ T cells per LNs
Blood
% of Tetramer+ cells within CD8+ T cells/µl blood
number of Tetramer+ cells within CD8+ T cells/µl blood
B)
Wild type
T-p110δE1020K
Unstimulated
TNFα
IFNγ
Q1 0.20
Q2 11.7
Q4 51.2
Q3 37.0
Q1 0.12
Q2 16.6
Q4 53.7
Q3 29.5
Q1 0.036
Q2 3.95E-3
Q4 99.8
Q3 0.16
% of IFNγ+ TNFα+ cells within CD8+ CD44hi T cells
p=0.0010
% of Granzyme B+ within CD8+ CD44hi T cells
p=0.0055

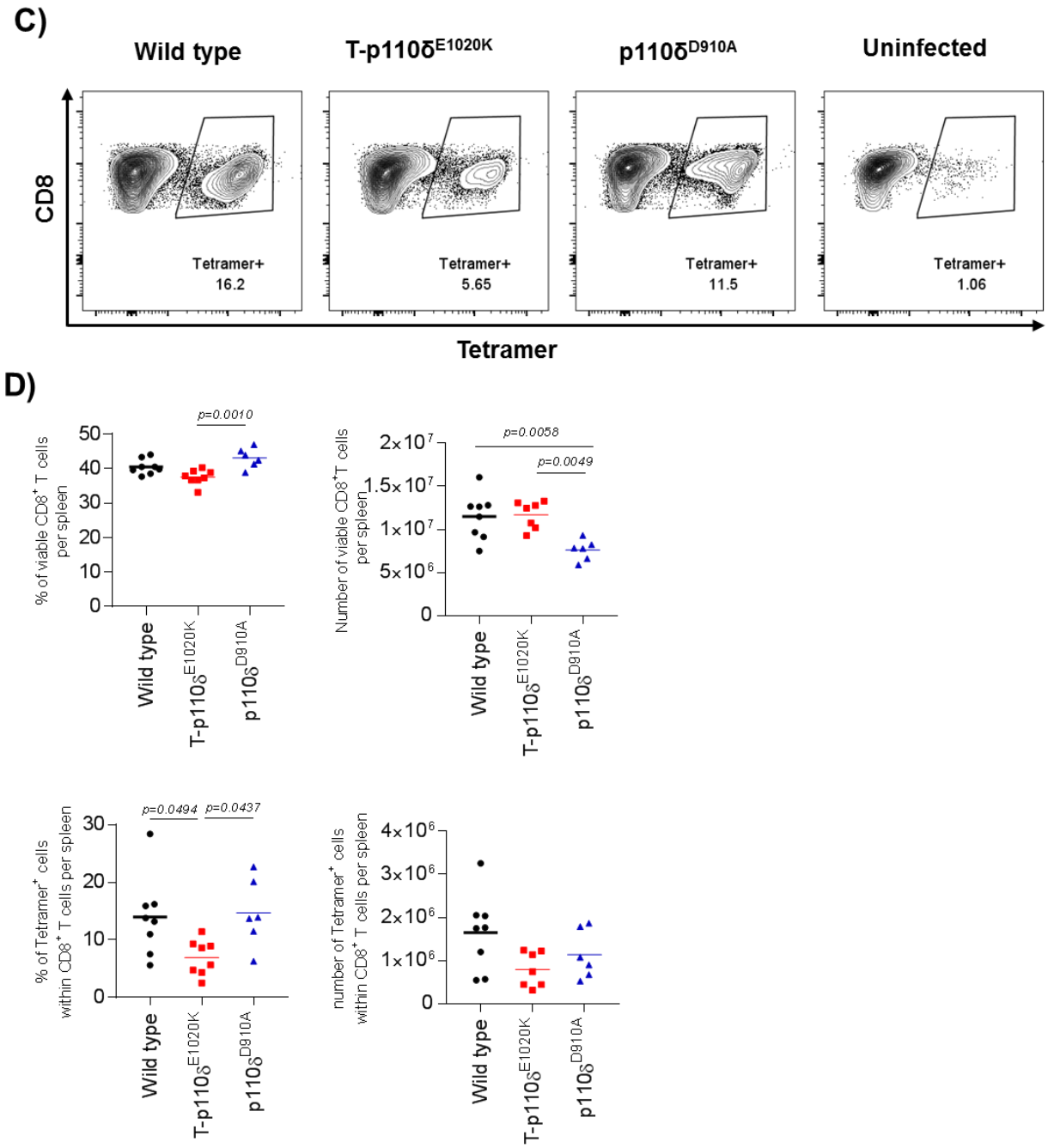

Figure 5.2.4: CD8$^+$ T cells in T-p110δ^{E1020K} mice mount a defective recall response to Lm-OVA that is overcome at a later time point

WT and T-p110δ^{E1020K} mice were infected with Lm-OVA on day 0 and 40. Mice were culled 5 days post-secondary infection. **(A)**Graphs showing numbers and proportions of antigenic specific CD8$^+$ T cells in spleen, lymph nodes and blood. **(B)** Proportions of IFNγ$^+$ TNFα$^+$ co-producers and granzyme b$^+$ cells within CD44^{high} CD8$^+$ T cells following *ex vivo* re-stimulation with SIINFEKL.
WT, T-p110δ^{E1020K} and p110δ^{D910A} mice were infected Lm-OVA on day 0 and 50. Mice were culled 3 days post-secondary infection. **(C)** Flow cytometry plots of Lm-OVA specific CD8$^+$ T cells. **(D)** Graphs showing numbers and proportions of Lm-OVA specific CD8$^+$ T cells. Data in A-B combined from two independent experiments (n= 11-12 per group), data in C-D representative of one independent experiment (n = 6-8 mice per group). *P values* are shown

5.2.5 Hyperactive p110δ leads to defective recall response to Lm-OVA due to intrinsic defect in CD8$^+$ T cells

Following the results observed in T-p110δ^{E1020K} mice, next I wanted to examine whether hyperactive p110δ activity in CD8$^+$ T cells specifically, affects recall response to Listeria infection. In order to examine this, 10,000 naïve FACs sorted (CD62L^{high} CD44^{low}) WT and E1020K OT1 donor cells were injected into separate recipient mice on day -1 and the subsequent day infected with Lm-OVA. The mice were re-infected on Day 42 and were culled 5 days post-secondary infection. As in response to primary infection, I observed reduced E1020K OT1 donor cells in the blood at day 8 and subsequent time points (**Figure 5.2.5a**). Following secondary infection, the proportions and numbers of E1020K OT1 donor cells were significantly reduced in the spleen and lymph nodes (**Figure 5.2.5b and c**). This indicates that the E1020K OT1 donor cells are not able to expand as well as the WT OT1 donor cells following secondary infection with Lm-OVA.

Next, the ability of hyperactive p110δ in CD8$^+$ T cells on cytokine production was assessed following secondary infection to Lm-OVA. Upon *ex vivo* re-stimulation with SIINFEKL peptide, there was no significant differences in the proportions of IFNγ$^+$ and TNFα$^+$ co-producers but an increased trend amongst E1020K OT1 donor cells compared to WT OT1 donor cells (**Figure 5.2.5 d**). However, there was a significant increase in the proportion of granzyme B$^+$ cells among the E1020K OT1 donor cells (**Figure 5.2.5d**). These results suggest that hyperactive p110δ activity in CD8$^+$ T cells specifically can still mount an enhanced effector response despite an impaired expansion to recall response.

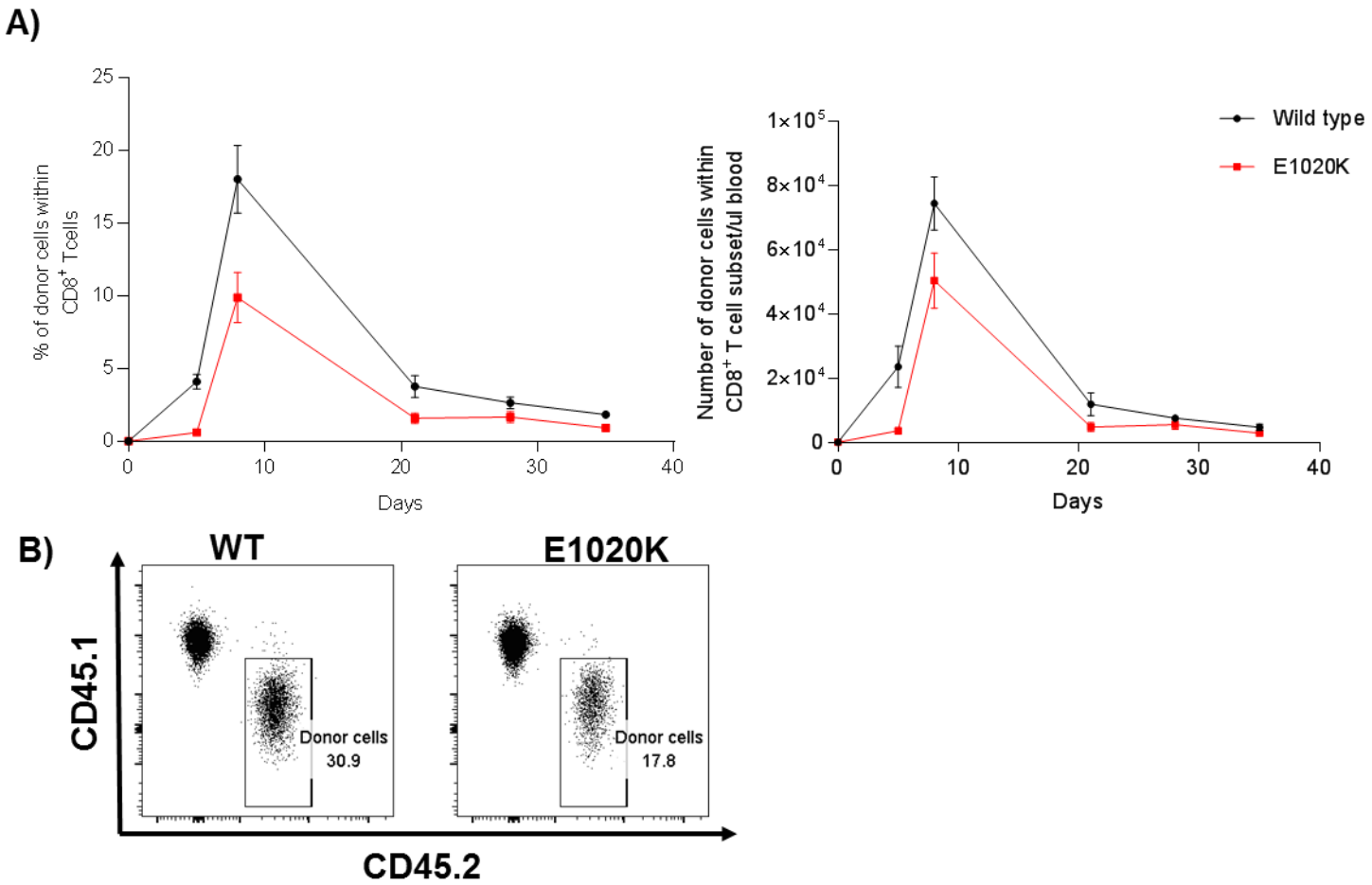
A)
% of donor cells within CD8+ Tcells
Days
Number of donor cells within CD8+ T cell subset/ul blood
Wild type
E1020K
B)
WT
E1020K
CD45.1
CD45.2
Donor cells 30.9
Donor cells 17.8
C)
% of donor cells within CD8+ T cells per spleen
p=0.0001
Number of donor cells within CD8+ T cell per spleen
p=0.0045
% of donor cells within CD8+ T cells/LNs
p=0.0006
Number of donor cells within CD8+ T cells/LNs
p=0.0052
WT
E1020K
D)
% IFNγ+ TNFα+ cells within donor OT1 cells
% of Granzyme B+ within donor OT1 cells
p=0.0001

Figure 5.2.5: Hyperactive p110δ activity causes an intrinsic expansion defect in CD8$^+$ T cells upon secondary Lm-OVA infection.

10,000 naïve (CD62L^{high} CD44^{low}) sorted WT or E1020K OT1 donor cells were transferred into WT recipient mice on day -1, then infected with 5 x10^6 CFU of Lm-OVA i.v. on day 0 and subsequently on day 42 . Mice were culled 5 days post-secondary infection. **(A)** Numbers and proportions of donor cells in the blood at day 8 , 14, 21, 28 and day 35 . **(B)** Representative flow cytometry plots of transferred donor OT1 cells in the spleen of WT hosts. **(C)** Number and proportions of donor OT1 cells in spleens and lymph nodes. **(D)** Proportions of IFNγ$^+$TNFα$^+$ and granzyme B$^+$ cells within CD44^{high} WT and E1020K OT1 donor cells following *ex vivo* SIINFEKL re-stimulation. *P values* are shown.

5.2.6 Hyperactive p110δ in CD8$^+$ T cells only causes impaired recall response to Lm-OVA in a competitive adoptive transfer system

In order to assess the quality of hyperactive p110δ memory cells in terms of their ability to respond to antigen re-exposure in a competitive environment, I decided to carry out competitive adoptive transfer experiments. Naïve (CD62L^{high} CD44^{low}) CD8$^+$ T cells were FACs sorted from congenically different WT (CD45.2$^+$) and E1020K (CD45.1$^+$ CD45.2$^+$) OT1 mice, mixed at a 1:1 ratio and co-transferred into CD45.1$^+$ WT recipient mice , followed by Lm-OVA infection one day later. This experimental setting allows CD8$^+$ T cells from different mice to proliferate in exactly the same environment along the infection time course. Two repeats of this experimental setting were carried out, in the first experiment recipient mice were re-infected on day 42 and in the second experiment at day 57. Mice were culled 5 days post-secondary infection. The recipient mice were subsequently bled at different times points to track the donor cells, of which I talked about the results in chapter 4. The ratio of adoptively transferred WT and E1020K OT1 cells were close to 1:1 in both experiments albeit slight differences in the second (**Figure 5.2.6a**) . In both experiments, I found that the contraction phase did not differ in terms of the proportions of transferred cells at different time points following primary infection (**Figure 5.2.6b**). However, following re-infection, the proportions of splenic E1020K OT1 donor cells were significantly reduced compared to WT OT1 donor cells (**Figure 5.2.6c-d**). Taken together these results reveal a cell intrinsic role for hyperactive p110δ in CD8 T cells in causing memory impairment in a competitive environment.

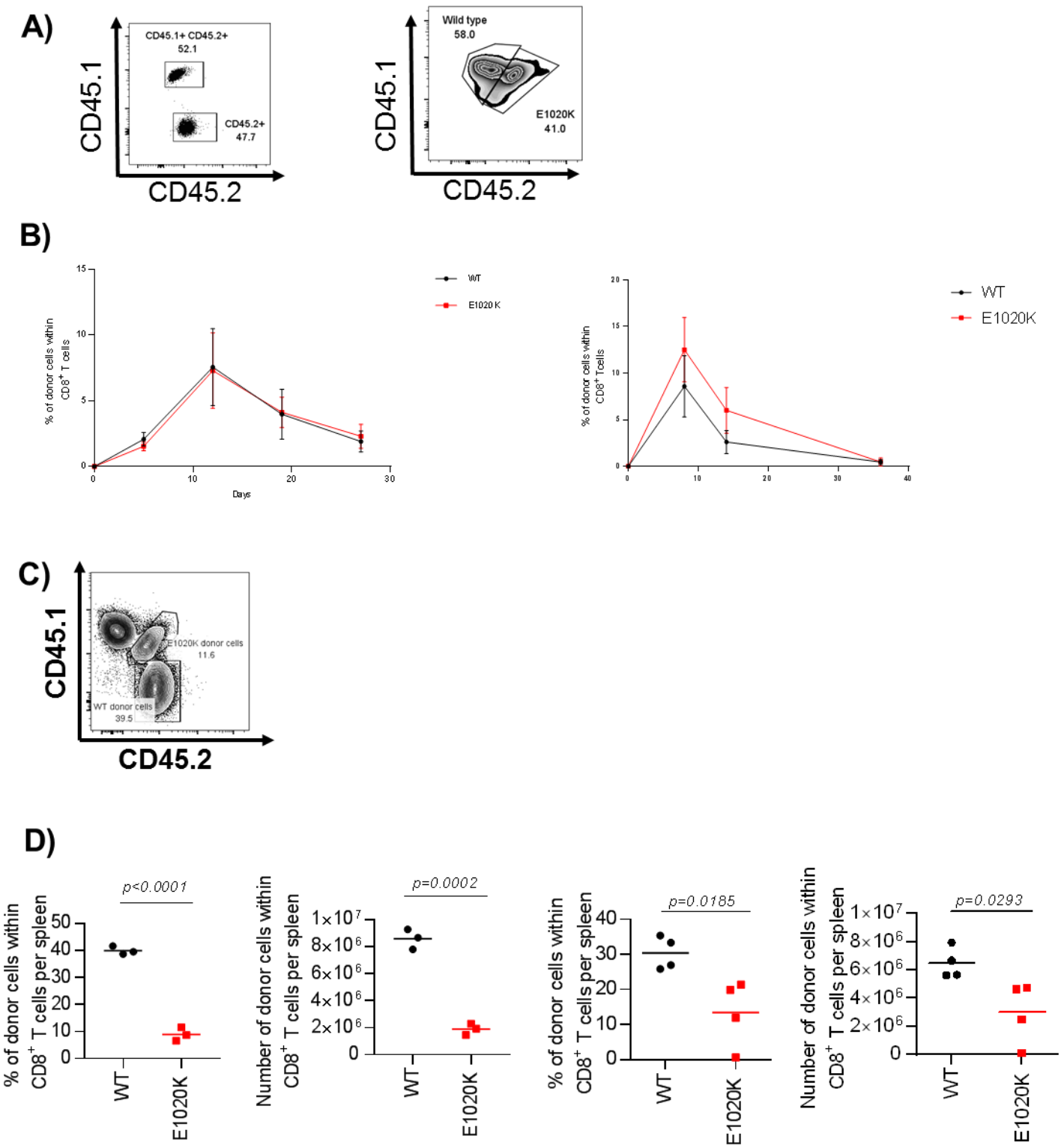

Figure 5.2.6: E1020K OT1 donor cells have a defect during the secondary response to Lm-OVA when co-transferred with WT OT1 cells.

1:1 mix of 10,000 naïve ($CD62L^{High}CD44^{Low}$) FACs sorted WT and E1020K OT1 donor cells were transferred into WT recipient mice on day-1, then infected with Lm-OVA on day 0 and subsequently on day 40 in one experiment and day 56 in another experiment. **(A)** Representative flow cytometry plot of the 1:1 mixture transferred in the two individual experiments. **(B)** Graphs showing the proportion of donor OT1 cells at different time points. **(C)** Representative flow cytometry plots of donor OT1 cells in spleen following re-infection. **(D)** Graphs showing number and proportions of donor OT1 cells in the spleen following re-infection. *P values are shown*

5.2.7 No difference in recall capacity of CD8$^+$ T cells in T-p110δ^{E1020K} in response to influenza infection

To examine the role of hyperactive p110δ on the ability of memory CD8$^+$ T cells to mount a secondary response to influenza virus, on day 64 PR8 primed WT, T-p110δ^{E1020K} and p110δ^{D910A} mice were re-challenged with Influenza A/HKx31, the heterotypic H3N1 strain of influenza virus. Since neutralising antibodies do not cross-react between PR8 and HKx31, memory CD8$^+$ T cells play a central role in recall responses and protective immunity in this setting. The details of this experimental setup was recommended by Alice Denton (Babraham institute) for an initial experiment. On day post HKx31 infection, there was no difference in total proportions and numbers of viable CD8$^+$ T cells in WT and T-p110δ^{E1020K} mice in the spleen and lung. However, the numbers of CD8$^+$ T cells were reduced in the spleen of p110δ^{D910A} mice with a trend in lungs but no differences in proportions in both organs (**Figure 5.2.7a**). I examined antigen specific CD8$^+$ T response to the immunodominant epitope NP$_{366-374}$ by using MHC class I tetramer in the lungs and spleens of WT, T-p110δ^{E1020K} and p110δ^{D910A} mice. There was no difference in T-p110δ^{E1020K} mice compared to WT mice; however, the numbers of NP$_{366-374}$ specific CD8+ T cells were significnalty reduced in p110δ^{D910A} mice, with no differences in proportions (**Figure 5.2.7b**). There was no difference in body weight between WT and T-p110δ^{E1020K} mice, however p110δ^{D910A} mice lost significantly more body weight than WT mice (**Figure 5.2.7c**). Viral titres in the lungs were measured and no difference between WT and T-p110δ^{E1020K} mice was detected, however p110δ^{D910A} mice had significantly increased viral titres compared to WT mice (**Figure 5.2.7d**).

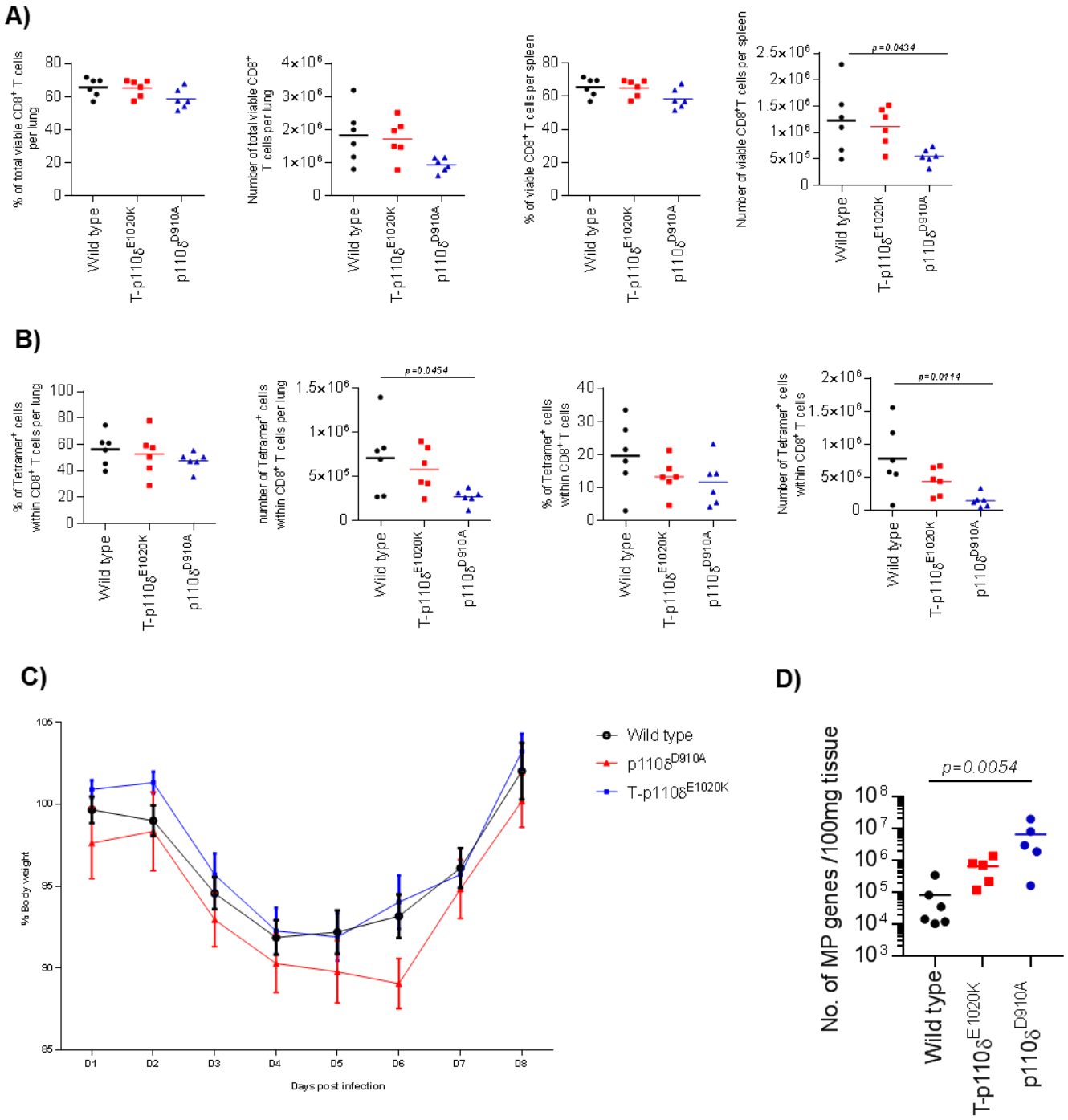

Figure 5.2.7: No difference in recall capacity of antigenic-specific CD8$^+$ T cells in T-p110δ^{E1020K} mice compared to wild type mice following secondary challenge with influenza

Wild type, T-p110δ^{E1020K} and p110δ^{D910A} mice were primed with PR8 via the intraperitoneal route on day 0, followed by challenge with HKx31 on day 64. Mice were culled at day 8 post infection. **(A)** Graphs showing proportions and numbers of viable CD8$^+$ T cells in the lungs and spleens **(B)** Graphs showing the proportions and numbers of of $NP_{366-374}$ specific CD8$^+$ T cells among viable CD8$^+$ T cells in the lungs and spleen. **(C)** Graph representing body weight of WT, T-p110δ^{E1020K} and p110δ^{D910A} mice at different time points post HKx31 challenge , relative to weight at day 0, set as 100%. **(D)** Viral load in the lungs of WT, T-p110δ^{E1020K} and p110δ^{D910A} mice at day 8 post HKx31 challenge. Data in A-D from one independent experiments (n=7-5 per group) *P values* are shown.

5.3 Discussion

As established in chapter 4 that following primary infection with Lm-OVA and influenza, significantly reduced numbers of MPECs in T-p110δ^{E1020K} mice were detected. This led to the prediction that the population of resting memory CD8$^+$ T cells will be reduced in T-p110δ^{E1020K} mice because of downregulation of key markers involved in long term CD8$^+$ T cell survival such as CD127, CD62L and Eomes. As during acute infection, memory CD8$^+$ T cells for maintenance do not rely on antigen but start relying on cytokines such as IL-17 or IL-15 for survival by undergoing homeostatic proliferation via their receptors [388]. However, at day 40 post Lm-OVA infection, the numbers of resting memory CD8$^+$ T cells in T-p110δ^{E1020K} mice were comparable to WT mice. This is in contrast to data shown using mice that express a constitutively active Akt transgene in CD8$^+$T cells. Following acute LCMV infection, these mice undergo a normal CD8$^+$ T cell expansion phase but have impaired survival of MPECs due to sustained Akt phosphorylation causing inactivation of Foxo thereby reducing expression of memory associated genes [121]. In addition, mice with a specific deletion of tuberous sclerosis 1 (Tsc1) in CD8$^+$ T cells, a major regulator of mTORc1 signalling, have an increased SLEC to MPEC ratio at the peak of the primary responses to Lm-OVA, resulting in enhanced contraction and poor generation of memory CD8$^+$ T cells [389]. Inhibition of mTOR signaling by rapamycin also promotes the generation of MPECs and differentiation into memory CD8$^+$ T cells following acute LCMV infection [131]. Foxo1 and Foxo3 have shown contrasting results in maintenance of memory CD8$^+$ T cells to infections. Studies focusing on Foxo3 in CD8$^+$ T cells have shown increase in the maintenance of Lm-OVA CD8$^+$ T cells due to reduced expression of pro-apoptotic molecules BIM and PUMA, which influences their homeostatic proliferation and survival in the long-term [126-128]. Upon Foxo1 deletion following resolution of infection, memory CD8$^+$ T cells decline and lose their characteristic gene expression profile associated with survival and trafficking genes such as Il7ra, Ccr7, Klf2, Sell Tcf7, Eomes, and Bcl2 [125, 381]. Also by the direct or indirect repression of T-bet , IFNγ and granzyme B that are hallmarks of effector T cells , Foxo1 can promote the generation of functional memory CD8$^+$ T cells [123, 124, 348]. In addition, there is also data to suggest that SLECs are also able to persist for some time following primary infections [390]. In T-p110δ^{E1020K} mice, increased PIP_3 production could influence other PH domain containing proteins other than Akt;

therefore, there is a possibility that other Akt independent pathways might be playing a role in sustaining the survival of memory $CD8^+$ T cells in T-p110δ^{E1020K} mice in response to Lm-OVA infection. Similar to primary infections, $CD4^+$ T cells also play an important role in providing help to $CD8^+$ T cells by influencing the generation, survival and recall ability of memory $CD8^+$ T cells [391] .

The composition of resting memory $CD8^+$ T cells post Lm-OVA infection in T-p110δ^{E1020K} mice contained fewer MPECs and T_{CM} populations as characterised by $CD62L^{high}CD44^{high}$ in all the organs analysed. Along with this, there was a significant reduction in the expression of Eomes in Lm-OVA specific $CD8^+$ T cells in T-p110δ^{E1020K} mice. This is consistent with studies looking at deletion of Pten, or expression of constitutively active myristoylated-Akt, within $CD8^+$ T cells where inhibition of development and survival of memory $CD8^+$ T cells are observed [122]. When examining how hyperactive p110δ regulated attributes of functional long-lived memory $CD8^+$ T cells, at day 40 CD8 T cells in T-p110δ^{E1020K} mice display a subtle loss of poly-cytokine producing ability, suggesting that overtime $CD8^+$ T cells with hyperactive p110δ lose their effector abilities.

Following the analysis of the memory $CD8^+$ T cells generated post primary infection; I next examined the ability of these cells to mount a recall response. Upon re-infection with Lm-OVA, $CD8^+$ T cells in T-p110δ^{E1020K} mice were able to mount comparable recall responses to WT mice at day 5 post infection. Even though phenotypically less memory $CD8^+$ T cells were detected, this did not translate into a defective recall response. However, in a subsequent experiment, mice were culled at day 3 post infection, and a reduction in Lm-OVA specific $CD8^+$ T cells was detected in T-p110δ^{E1020K} mice. It is plausible that $CD4^+$ T cells with hyperactive p110δ activity are providing help to $CD8^+$ T cells in T-p110δ^{E1020K} mice to mount effective recall responses at later time points following secondary challenge as the infection progresses. As it is well known that $CD4^+$ T cell help is required for memory cells to mount effective secondary responses [374, 392-394]. The results collectively imply a possible delay in kinetics of antigenic specific memory $CD8^+$ T cells in T-p110δ^{E1020K} in response to secondary challenge, perhaps due to reduced proliferating ability of these cells in T-p110^{E1020K}. A potential experiment could be carried out to track the proliferating ability of memory $CD8^+$ T cells in response to secondary challenge with

Lm-OVA at different time points in T-p110δ^{E1020K} mice. Upon SIINFEKL peptide re-stimulation, Lm-OVA specific CD8^{+} T cells in T-p110δ^{E1020K} acquire the ability to produce increased granzyme B and effector cytokines. Thus, in response to Lm-OVA re-challenge, memory CD8^{+} T cells detected in T-p110δ^{E1020K} mice have a defective expansion at an earlier time point that can be overcome as the infection progresses. All these studies highlight Akt/mTORc/Foxo playing important roles in maintaining and generating memory responses.

Similar to the primary response in T-p110δ^{E1020K} mice shown in chapter 4, it seems that a combination of factors could be influencing the survival and the ability of memory CD8^{+} T cells to mount an effective recall response. The use of OT1 adoptive transfer experiments helps to answer at least one of the confounding factors influencing the CD8^{+} T cell response, the influence of other T cells with hyperactive p110δ activity. In the single OT1 adoptive transfer experiments, the expansion of E1020K OT1 donor cells were reduced compared to WT OT1 donor cells following re-infection at day 5. There were differences in memory cell differentiation before secondary challenge; however, it is uncertain whether the differences in memory cells amongst the E1020K OT1 donor cells caused a reduced secondary expansion. Therefore, a potential caveat of the recall response assessed in the single adoptive transfer experiment might be that the defective recall response of E1020K OT1 donor cells could be attributed to the reduced primary response detected rather than a memory defect. To avoid this, ovalbumin specific memory CD8^{+} T cells can be sorted from WT and E1020K OT1 donor cells and adoptively transferred into naïve recipient mice followed by Lm-OVA infection to access the ability of OT1 memory cells to mount a recall response. Upon SIINFEKL peptide re-stimulation, E1020K OT1 donor cells were able to produce enhanced granzyme B and similar levels of effector cytokines. It is plausible that in T-p110δ^{E1020K} mice, CD4^{+} T cells with hyperactive p110δ activity augments the increase in effector cytokines detected. In the competitive OT1 adoptive transfer experiments, the primary expansion phase and the contraction phase was similar amongst the two groups, suggesting that hyperactive p110δ does not affect survival of memory CD8^{+} T cells in response to Lm-OVA infection when present in a competitive environment. However, following secondary Lm-OVA challenge, E1020K OT1 donor cells expanded to a lesser extent compared to WT OT1 donor cells. This suggests that memory E1020K OT1 donor cells are not able to compete well for the antigen in the presence

of WT OT1 donor cells. The competitive adoptive transfer experiments indicate that there might be differences in the thresholds of E1020K memory $CD8^+$ T cells to expand for activating stimuli in the presence of a competitive environment. It seems that survival signals are provided by WT OT1 cells during the contraction phase but following secondary challenge E1020K OT1 cells are unable to compete for antigen to promote expansion and survival. Previously our group has reported that the expansion of $p110\delta^{D910A}$ OT1 cells in a competitive environment undergo equivalent expansion as WT OT1 cells following and primary and secondary challenge [115]. Enhanced accumulation of $p110\delta^{D910A}$ OT1 cells were observed in the lymph nodes and bone marrow that are associated with long-term memory. Whether the differences between $p110\delta^{D910A}$ and E1020K OT1 cells is due to differences within the memory subsets that allows increase homing to lymph nodes able to mount effective recall responses, will have to be investigated by sorting memory populations and transferring them into naïve recipient mice followed by Lm-OVA infection. In a competitive environment, Eomes deficient $CD8^+$ T cell mice were shown to respond comparably as WT $CD8^+$ T cells following primary acute LCMV infection at day 8, however following re-infection Eomes deficient $CD8^+$ T cells mounted a less robust response [386]. These results suggest that Eomes enables $CD8^+$ T cells to compete for signals and niches that promote memory differentiation. The defect in $CD8^+$ T cell response due to hyperactive p110δ maybe due to reduced expression of memory associated markers, allowing the cells to compete inefficiently in a completive environment.

I also investigated the ability of T-$p110\delta^{E1020K}$ and $p110\delta^{D910A}$ mice to mount recall responses to a heterosubtypic infection with influenza virus. Preliminary data indicated that no difference was detected in T-$p110\delta^{E1020K}$ mice compared to WT mice. However, in $p110\delta^{D910A}$ mice, the numbers of antigenic-specific $CD8^+$ T cells were reduced compared to WT mice. Along with this, viral load was increased with enhanced body weight loss observed at day 6 compared to the WT mice. This suggests that $CD8^+$ T cells in $p110\delta^{D910A}$ have a defect in efficiently clearing the virus owing perhaps to the ineffective $CD8^+$ T cell response. It is plausible that at an earlier time point post secondary infection, a defect could also occur in T-$p110\delta^{E1020K}$ mice similar to that observed following Lm-OVA infection, this will have to be confirmed in future experiments.

Chapter 6

Effect of hyperactive p110δ in the $CD8^+$ T cell response to acute and chronic Lymphocytic choriomeningitis virus

6.1 Introduction

Generating virus specific effector $CD8^+$ T cells is an essential component of antiviral immunity, as these cells are the first line of defence for complete virus clearance for most viral infections. However, certain viral infections exist where the virus is able to escape immune detection and can persist in a chronic state within the host for a longer period. These include viruses such as human immunodeficiency virus (HIV), hepatitis C or B virus and herpes viruses [296]. Failure to control pathogen clearance leads to sustained antigen loads and inflammation that result in $CD8^+$ T cell exhaustion. T cells undergoing persistent chronic infection are characterised by their increased expression of inhibitory markers such as PD-1, Tim3, LAG-3, CTLA4 and others. In addition, exhausted T cells are impaired in their ability to co-produce TNFα, IFNγ and IL-2 [395]. Overall, exhausted T cells lose robust effector functions, express multiple inhibitory receptors and are defined by an altered transcriptional programme [395].

Although recurrent respiratory infections is the most common symptom presented by APDS patients, nearly half of the reported patients also exhibit an inability to control persistent viral infections that include EBV and CMV [138, 141, 151, 155]. EBV specific $CD8^+$ T cells from patients show increase expression of inhibitory receptors such as PD-1 and 2B4, which may prevent their effective cytotoxic function [141, 153, 155]. Furthermore, inhibition of PD-1 has shown to enhance *in vitro* proliferation and effector cytokine production [153]. Therefore, I investigated whether $CD8^+$ T cells in T-p110δ^{E1020K} mice were more likely to undergo T cell exhaustion in response to a persistent infection. To achieve this, I made use of murine lymphocytic choriomeningitis virus (LCMV) as a model antigen. It was selected as it offers the advantage of directly comparing the same virus in an acute and chronic setting. Infection with LCMV Armstrong strain results in an acute infection, which is resolved within 8- 10 days. This strain has been used extensively to investigate effector and memory $CD8^+$ T cell differentiation. In contrast, infection with LCMV Clone 13 results in a systemic, chronic infection that lasts for several weeks and is accompanied by T cell exhaustion. The variances between these two strains are due to two amino acid differences affecting the viral polymerase that gives the virus a replicative advantage and glycoprotein that enables the Clone 13 virus to bind to its cellular receptor with a higher affinity then the Armstrong strain [271, 273].

Dominant epitopes of LCMV recognized by $CD8^+$ T cells are conserved between LCMV Armstrong and Clone 13, allowing for analysis of $CD8^+$ T cells with the same TCR specificity in these two different infection scenarios. MHC class I and class II MHC tetramers were used to quantify $CD8^+$ and $CD4^+$ antigenic specific T cells. For all the experiments described in this chapter, I used the LCMV immunodominant H-$2D^b$ restricted glycoprotein (GP) peptide amino acids 33-41 (GP_{33-41}) epitope to track LCMV specific $CD8^+$ T cells in WT and T-p110δ^{E1020K} mice following infection with LCMV Armstrong and Clone 13 strain. $CD4^+$ T cells are important for supporting $CD8^+$ T cell responses during chronic infection. Importance of $CD4^+$ T cells during chronic infection has been illustrated by mouse models and in human infections. Therefore, iin order to track antigenic-specific $CD4^+$ T cells responses, the I-A^b-restricted $CD4^+$ T cell epitope GP_{61-80} was used. The experiments described in this chapter are all preliminary but do give an indication that $CD8^+$ T cells do undergo T cell exhaustion following chronic infection in T-p110δ^{E1020K} mice. Using this model, information can be collected to understand in depth about the mechanisms underlying T cell exhaustion due to hyperactive p110δ activity.

6.2 Results

6.2.1 Normal expansion of antigenic specific CD8$^+$ T cells in T-p110 p110δ^{E1020K} mice following infection with LCMV Armstrong strain

To first determine the antigenic specific CD8$^+$ T cell response to acute LCMV Armstrong strain, WT and T-p110δ^{E1020K} mice were infected via intraperitoneal route with 2 x 10^5 PFU LCMV Armstrong strain on day 0 and culled at day 8 post infection. Upon infection, there were no differences in total viable CD8$^+$ T cells between WT and T-p110δ^{E1020K} mice in spleen and lymph nodes (**Figure 6.2.1a and b**). MHC class I tetramer staining against the immunodominant epitope GP$_{33-41}$ revealed that the number and proportions of antigenic specific CD8$^+$ T cells were comparable between the two groups (**Figure 6.2.1a and b**). These results are similar to that observed following primary infections with Listeria and influenza as shown in chapter 4. Furthermore, the number and proportions of T-p110δ^{E1020K} MPECs were significantly lower than in WT mice following infection (**Figure 6.2.1c**). The proportions of SLECs were significantly higher than WT mice (**Figure 6.2.1c**). There was no difference in CD44^{high} CD62L^{low} populations among the antigenic specific CD8$^+$ T cells in both groups (**Figure 6.2.1d**). Overall, these results suggest that the phenotype of CD8$^+$ T cells in response to acute infections with different pathogens are similar in T-p110δ^{E1020K} mice.

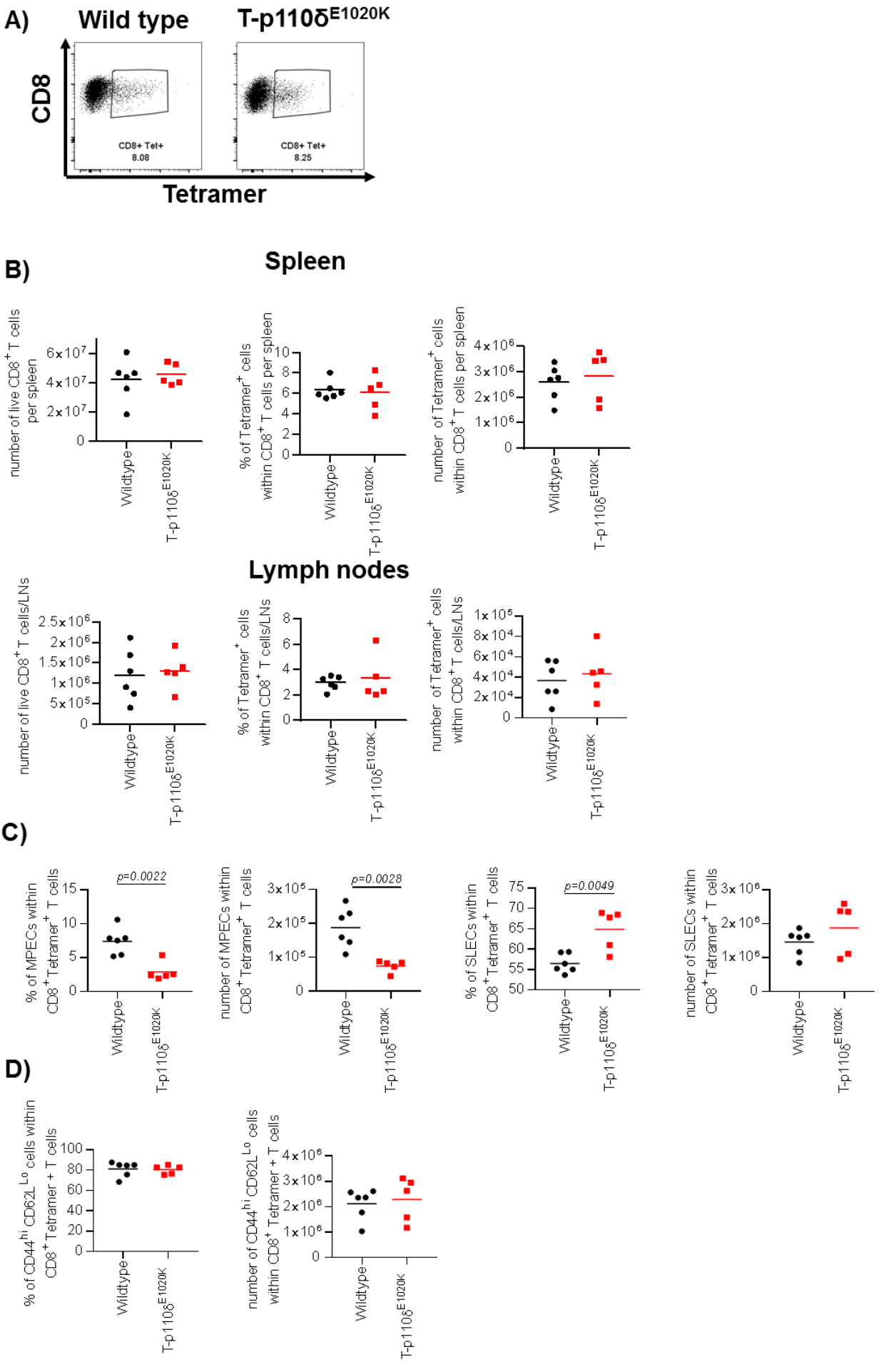
A)
Wild type
T-p110δE1020K
CD8
CD8+ Tet+
8.08
CD8+ Tet+
8.25
Tetramer
B)
Spleen
number of live CD8+ T cells per spleen
% of Tetramer+ cells within CD8+ T cells per spleen
number of Tetramer+ cells within CD8+ T cells per spleen
Lymph nodes
number of live CD8+ T cells/LNs
% of Tetramer+ cells within CD8+ T cells/LNs
number of Tetramer+ cells within CD8+ T cells/LNs
Wildtype
T-p110δE1020K
C)
% of MPECs within CD8+Tetramer+ T cells
p=0.0022
number of MPECs within CD8+Tetramer+ T cells
p=0.0028
% of SLECs within CD8+Tetramer+ T cells
p=0.0049
number of SLECs within CD8+Tetramer+ T cells
D)
% of CD44hi CD62LLo cells within CD8+Tetramer + T cells
number of CD44hi CD62LLo cells within CD8+ Tetramer + T cells

Figure 6.2.1: No difference in antigenic-specific $CD8^+$ T cells at day 8 post infection with LCMV Armstrong

WT and T-p110δ^{E1020K} mice were infected with 2 x 10^5 LCMV Armstrong via intraperitoneal route at day 0 and culled at day 8 post infection. **(A)** Representative flow cytometry plots of GP_{33-41} specific $CD8^+$ T cells in the spleen **(B)** Graphs showing proportions and numbers of total live $CD8^+$ T cells, GP_{33-41} specific $CD8^+$ T cells in the spleen and lymph nodes. **(C)** Numbers and proportions of MPECs and SLECs within GP_{33-41} specific $CD8^+$ T cells in the spleen. **(D)** Numbers and proportions of $CD44^{hi}$ $CD62L^{lo}$ cells within GP_{33-41} specific $CD8^+$ T cells. Data representative of one independent experiment with n=6 per group. *P values* are shown.

6.2.2 Intact $CD8^+$ T cell antiviral function in T-p11δ^{E1020K} following LCMV Armstrong infection

Next, I investigated whether the antiviral and cytotoxic activity was affected in $CD8^+$ T cells in T-p110δ^{E1020K} mice. In order to do this splenocytes were isolated from infected WT and T-p110δ^{E1020K} mice at day 8 post infection; these were then re-stimulated for 5.5 hours in the presence of a LCMV specific peptide against GP_{33}. There were no significant differences in the numbers and proportions of $IFN\gamma^+$, $TNF\alpha^+$ single and co-producers between T-p110δ^{E1020K} and WT mice when gated on $CD44^{high}$ $CD8^+$ T cells (**Figure 6.2.2a - c**). There was, however a trend towards increase expression and proportion of granzyme B in the T-p11δ^{E1020K} mice compared to WT mice (**Figure 6.2.2d**). This set of data, together with those from chapter 4, suggests that $CD8^+$ T cells in T-p110δ^{E1020K} mice have a similar effector phenotype in response to different pathogens.

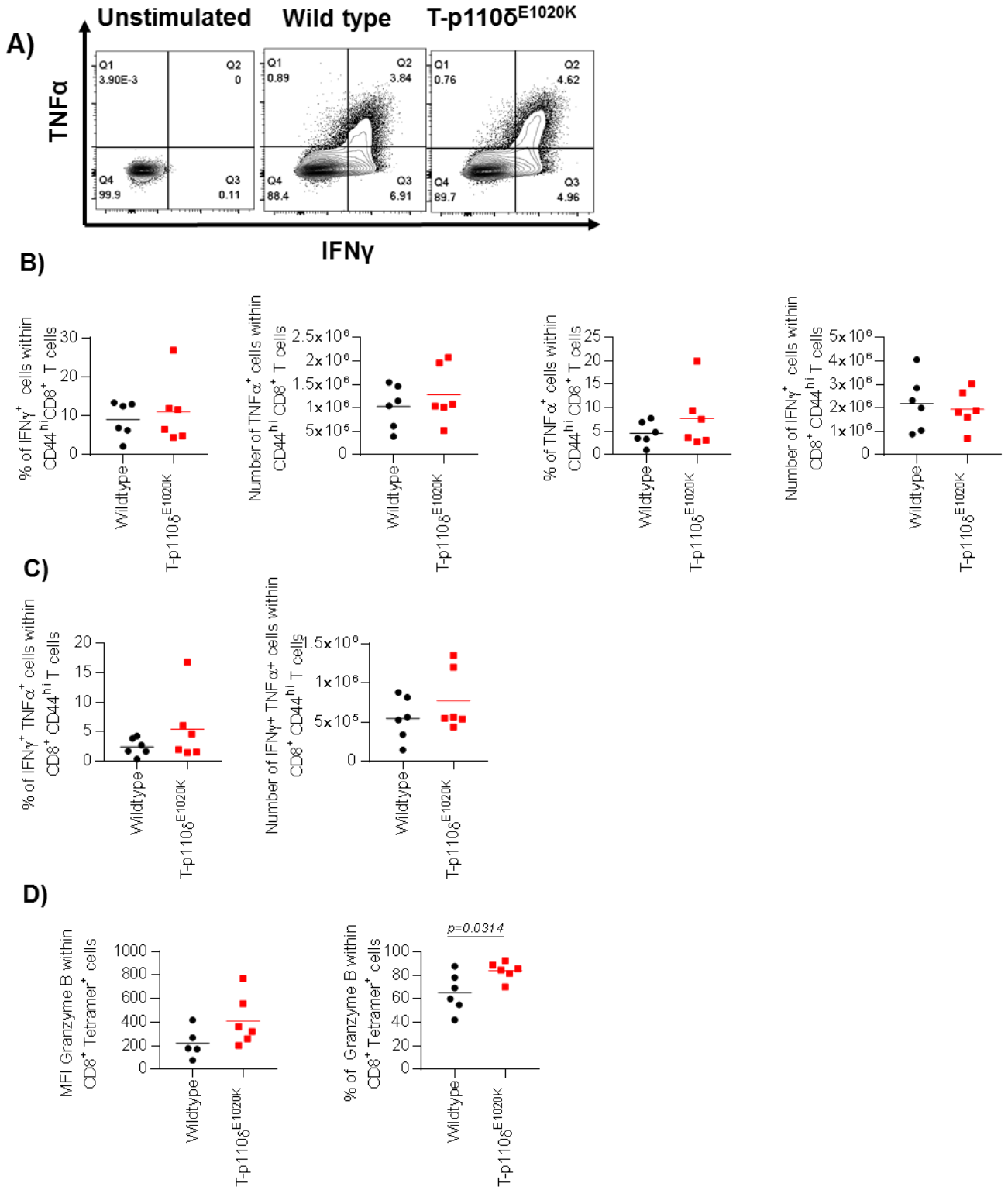

Figure 6.2.2: Comparable anti- viral CD8$^+$ T cell function in T-p110δ^{E1020K} mice at day 8 post acute LCMV infection

WT and T-p110δ^{E1020K} mice were infected with 2 x 10^5 LCMV Armstrong at day 0 and culled at day 8 post infection. Splenocytes from infected mice were re-stimulated *ex vivo* with GP_{33} specific peptide for 5.5 hours in the presence of Brefeldin A. **(A)** Representative flow cytometry plots of IFNγ$^+$ and TNFα$^+$ gated on CD44^{high} CD8$^+$ T cells. **(B)** Graphs showing proportions and numbers of IFNγ$^+$ and TNFα$^+$ cells within CD44^{high} CD8$^+$ T cells. **(C)** Graphs showing proportions and numbers of IFNγ$^+$ TNFα$^+$ co-producing cells within CD44^{high} CD8$^+$ T cells. **(D)** Graphs showing proportions and expression of granzyme B within GP_{33-41} specific CD8$^+$ T cells. Data representative of one independent experiment with n = 6 per group. *P values* are shown.

6.2.3 Reduced memory CD8$^+$ T cells in T-p110δ^{E1020K} at day 35 following LCMV Armstrong infection

APDS patients show reduced numbers of circulating memory CD8$^+$ T cells, therefore I investigated whether the maintenance of resting memory CD8$^+$ T cells differ in T-p110δ^{E1020K} mice in response to infection with LCMV Armstrong. WT and T-p110δ^{E1020K} mice were infected with 2 x 10^5 PFU of LCMV Armstrong strain on Day 0 and culled at day 35 to evaluate the resting memory CD8$^+$ T cells. Upon infection, although total numbers of viable CD8$^+$ T cells were comparable, (**Figure 6.2.3a**) there was a significant reduction in proportions and numbers of LCMV specific CD8$^+$ T cells in T-p110δ^{E1020K} mice compared to WT mice in the spleen and lymph nodes (**Figure 6.2.3 b and c**). To assess functional ability of these memory CD8$^+$ T cells, splenocytes from infected WT and T-p110δ^{E102K} mice were re-stimulated with LCMV specific GP_{33-41} peptide for 5.5 hours to measure cytokine production. Following *ex vivo* re-stimulation, the numbers of CD44^{high} CD8$^+$ T cells were comparable between both groups (**Figure 6.2.3d**). There was a significant reduction in the proportions and numbers of IFNγ$^+$ TNFα$^+$ co-producers within the CD44^{high} CD8$^+$ T cell population in T-p110δ^{E1020K} mice compared to WT mice. In addition, numbers and proportions of polyfunctional cells producing IFNγ$^+$ TNFα$^+$ and IL-2$^+$ was significantly reduced in T-p110δ^{E1020K} mice compared to WT mice (**Figure 6.2.3e and f**). Thus, CD8$^+$ T cells in T-p110δ^{E1020K} mice have reduced memory CD8$^+$ T cells with diminished functional ability at day 35 post acute LCMV infection.

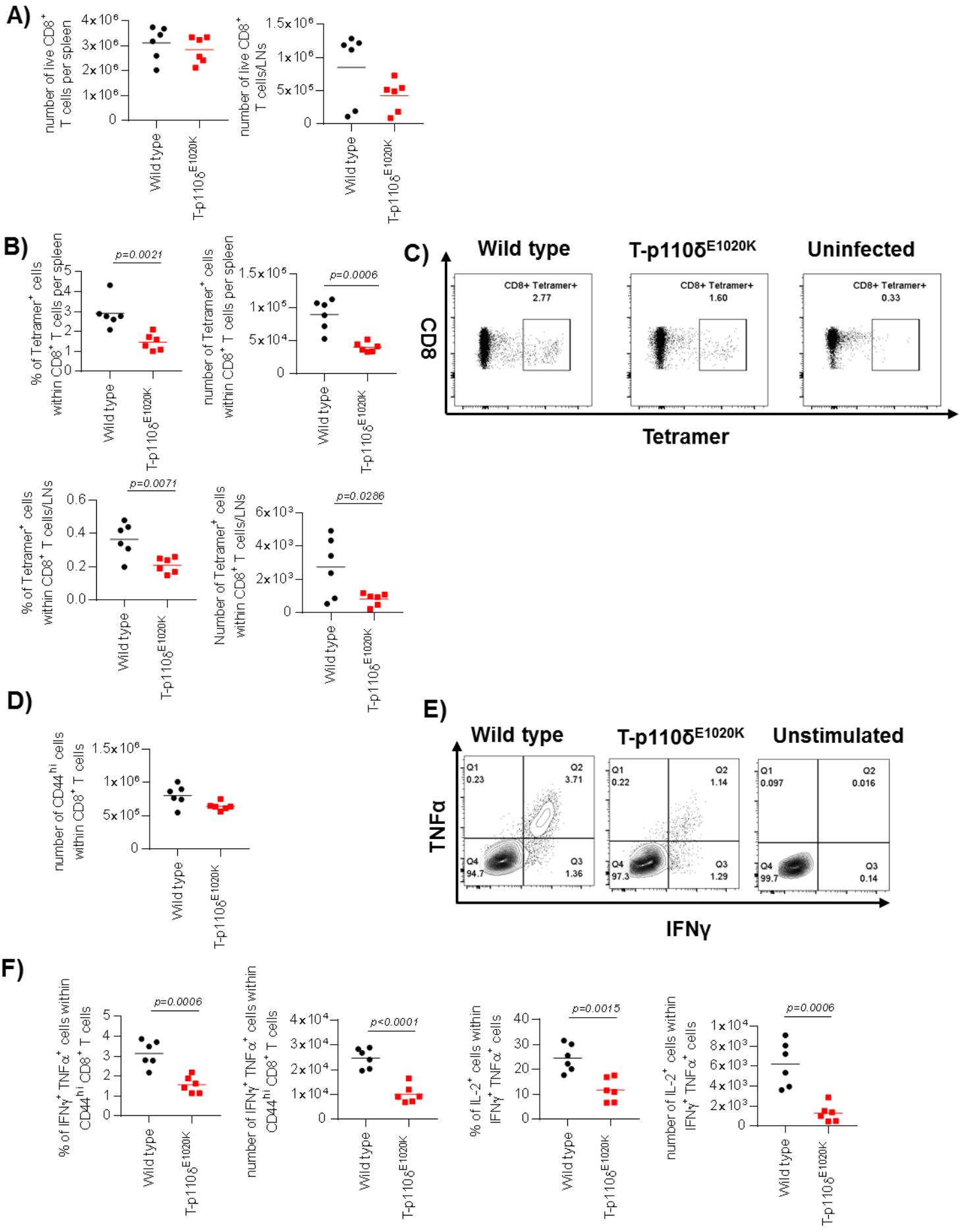
A)
number of live CD8+ T cells per spleen
4x10^6
3x10^6
2x10^6
1x10^6
0
Wild type
T-p110δE1020K
number of live CD8+ T cells/LNs
1.5x10^6
1x10^6
5x10^5
0
Wild type
T-p110δE1020K
B)
% of Tetramer+ cells within CD8+ T cells per spleen
p=0.0021
5
4
3
2
1
0
Wild type
T-p110δE1020K
number of Tetramer+ cells within CD8+ T cells per spleen
p=0.0006
1.5x10^5
1x10^5
5x10^4
0
Wild type
T-p110δE1020K
% of Tetramer+ cells within CD8+ T cells/LNs
p=0.0071
0.6
0.4
0.2
0.0
Wild type
T-p110δE1020K
Number of Tetramer+ cells within CD8+ T cells/LNs
p=0.0286
6x10^3
4x10^3
2x10^3
0
Wild type
T-p110δE1020K
C)
Wild type
T-p110δE1020K
Uninfected
CD8+ Tetramer+ 2.77
CD8+ Tetramer+ 1.60
CD8+ Tetramer+ 0.33
CD8
Tetramer
D)
number of CD44hi cells within CD8+ T cells
1.5x10^6
1x10^6
5x10^5
0
Wild type
T-p110δE1020K
E)
Wild type
T-p110δE1020K
Unstimulated
Q1 0.23
Q2 3.71
Q4 94.7
Q3 1.36
Q1 0.22
Q2 1.14
Q4 97.3
Q3 1.29
Q1 0.097
Q2 0.016
Q4 99.7
Q3 0.14
TNFα
IFNγ
F)
% of IFNγ+ TNFα+ cells within CD44hi CD8+ T cells
p=0.0006
5
4
3
2
1
0
Wild type
T-p110δE1020K
number of IFNγ+ TNFα+ cells within CD44hi CD8+ T cells
p<0.0001
4x10^4
3x10^4
2x10^4
1x10^4
0
Wild type
T-p110δE1020K
% of IL-2+ cells within IFNγ+ TNFα+ cells
p=0.0015
40
30
20
10
0
Wild type
T-p110δE1020K
number of IL-2+ cells within IFNγ+ TNFα+ cells
p=0.0006
1x10^4
8x10^3
6x10^3
4x10^3
2x10^3
0
Wild type
T-p110δE1020K

Figure 6.2.3: Acute viral infection of T-p110δ^{E1020K} mice results in defective resting memory CD8^{+} T cells at day 35 post infection.

WT and T-p110δ^{E1020K} mice were infected with 2 x 10^5 PFU of LCMV Armstrong via the intraperitoneal route on day 0 and culled at day 35. **(A)** Graphs showing the number of viable CD8^{+} T cells in the spleens and lymph nodes. **(B)** Graphs showing the proportions and numbers of GP_{33-41} specific CD8^{+} T cells in the spleens and lymph nodes. **(C)** Representative flow cytometry plots of GP_{33-41} specific CD8^{+} T cells in the spleen. **(D)** Graph showing number of CD44^{high} CD8^{+} T cells in WT and T-p110δ^{E1020K} mice following 5.5 hours *ex vivo* re-stimulation with GP_{33} peptide. **(E)** Representative flow cytometry plots of IFNγ^{+} TNFα^{+} within CD44^{high} CD8 T cells. **(F)** Graphs showing proportions and numbers of IFNγ^{+} TNFα^{+} co-producers and IFNγ^{+} TNFα^{+} IL-2^{+} triple cytokine producers within CD44^{high} CD8^{+}T cells. Data representative of one independent experiment with n=6 per group. *P values* are shown.

6.2.4 Reduced antigenic-specific CD8^{+} T cells following infection with LCMV Clone 13

Initially to evaluate the role of hyperactive p110δ in chronic infection, WT and T-p110δ^{E1020K} mice were infected with LCMV Clone 13 on day 0 and mice were culled on day 32 post infection. Following infection the primary response to LCMV Clone 13 was unaffected in T-p110δ^{E1020K} mice, since similar proportions of GP_{33-41} specific CD8^{+} T cells were detected at day 8 in blood. Interestingly, by day 15 the proportions of GP_{33-41} specific CD8^{+} T cells in T-p110δ^{E1020K} mice were significantly reduced in blood compared to WT mice (**Figure 6.2.4a**) and a significant reduction in proportions and trend in numbers of GP_{33-41} specific CD8^{+} T cells in the spleen and lymph nodes on day 32 (**Figure 6.2.4b**). Surprisingly, in a second experiment where infection was taken out to 62 days, no difference was observed in GP_{33-41} specific CD8^{+} T cells in the spleen between both groups with significant reduction in numbers in the lymph nodes of T-p110δ^{E1020K} mice (**Figure 6.2.4c**). This could potentially mean that as virus starts clearing in the WT mice, the number of LCMV specific CD8^{+} T cells in the WT mice reaches a plateau matching the numbers in T-p110δ^{E1020K} mice at day 62 post infection.

The impact of reduced CD8^{+} T cells in T-p110δ^{E1020K} mice was assessed by measuring body weight loss and viral load. Interestingly, increased body weight loss from day 13

until day 21 (**Figure 6.2.4d**) and a trend for increased viral load at both day 32 and day 62 in the liver in T-p110δ^{E1020K} mice compared to WT mice was detected in T-p110δ^{E1020K} mice (**Figure 6.2.4e**). The reduction in body weight loss correlates with the reduced antigenic-specific CD8^{+} T cells detected in T-p110δ^{E1020K} mice. Due to technical issues, viral load was not measured in the serum of the infected mice. Overall, these preliminary results indicate that CD8^{+} T cells in T-p110δ^{E1020K} mice are not able to expand as well the WT CD8^{+} T cells and are not protected to the extent as WT mice following chronic infection.

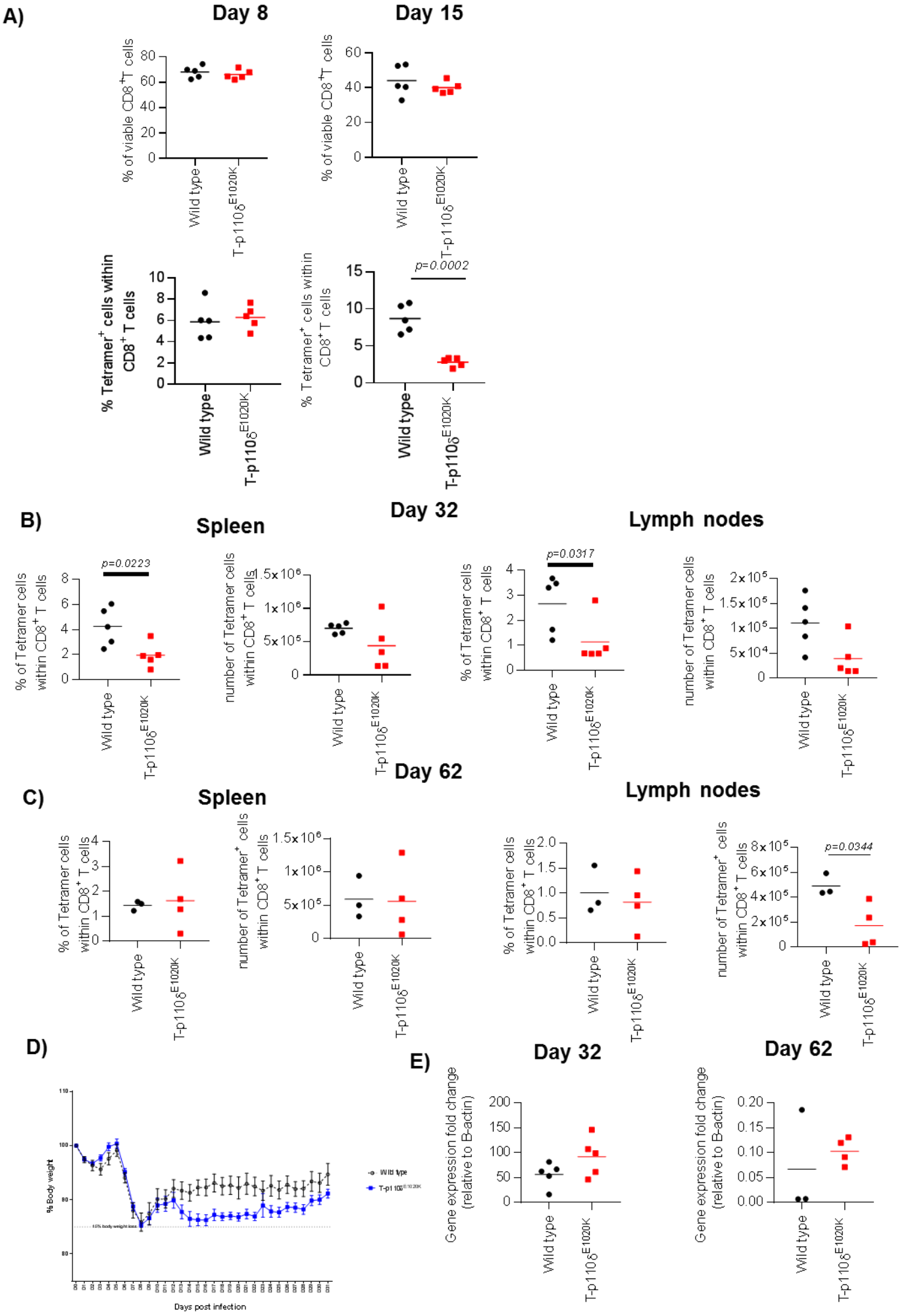
A)
Day 8
Day 15
% of viable CD8+T cells
Wild type
T-p110δE1020K
% Tetramer+ cells within CD8+ T cells
p=0.0002
B)
Spleen
Day 32
Lymph nodes
% of Tetramer cells within CD8+ T cells
number of Tetramer cells within CD8+ T cells
p=0.0223
p=0.0317
C)
Spleen
Day 62
Lymph nodes
number of Tetramer+ cells within CD8+ T cells
p=0.0344
D)
% Body weight
Days post infection
E)
Day 32
Day 62
Gene expression fold change (relative to B-actin)

Figure 6.2.4: CD8 T cells in T-p110δ^{E1020K} have impaired CD8$^+$ T cell response and compromised control of chronic LCMV Clone 13 infection

WT and T-p110δ^{E1020K} mice were infected with 1 x 10^6 PFU of LCMV Clone 13 on day 0. **(A)** Graphs showing proportions of viable CD8 T cells and GP_{33-41} specific CD8 T cells in blood at different time points. **(B)** Graphs showing proportions and numbers of GP_{33-41} specific CD8 T cells at day 32 in the spleen and lymph nodes. **(C)** Graphs showing proportions and numbers of GP_{33-41} specific CD8 T cells at day 62 in the spleen and lymph nodes. **(D)** Graph representing body weight of WT and T-p110δ^{E1020K} mice at different time points post LCMV Clone 13 infection, relative to weight at day 0, set as 100%, data represents combination of 2 experiments with n=8-9 per group **(E)** Viral load in the liver of WT and T-p110δ^{E1020K} mice after day 32 and 62 post LCMV Clone 13 infection. *P values* are shown

6.2.5 Functionality of CD8$^+$ T cells responses is disrupted in T-p110δ^{E1020K} mice following infection with LCMV Clone 13

Next, I investigated whether hyperactive p110δ activity influenced the effector function of CD8$^+$ T cells post LCMV Clone 13 infection by measuring antigen-induced production of cytokines (IFNγ$^+$, TNFα$^+$, and IL-2$^+$) using intracellular staining. At day 62, splenocytes from infected WT and T-p110δ^{E1020K} mice were re-stimulated *ex vivo* with GP_{33-41} peptide for 5.5 hours to measure cytokine production. There was no difference in the numbers of total viable CD8$^+$ T cells and CD44^{high} CD8$^+$ T cells between the two groups (**Figure 6.2.5a**). Compared to WT mice, CD8$^+$ T cells from T-p110δ^{E1020K} mice produced reduced IFNγ$^+$ and TNFα$^+$ at day 62 post infection. In addition, CD8$^+$ T cell in T-p110δ^{E1020K} exhibited reduced polyfunctionality compared to WT CD8$^+$ T cells, with minimal co-production of IFNγ$^+$ TNFα$^+$ and IL-2$^+$ (**Figure 6.2.5b-d**). Similar results were also observed at day 32 post LCMV Clone 13 infection (data shown in appendix). This set of data indicates that chronic infection dampens effector function in CD8$^+$ T cells in T-p110δ^{E1020K} mice.

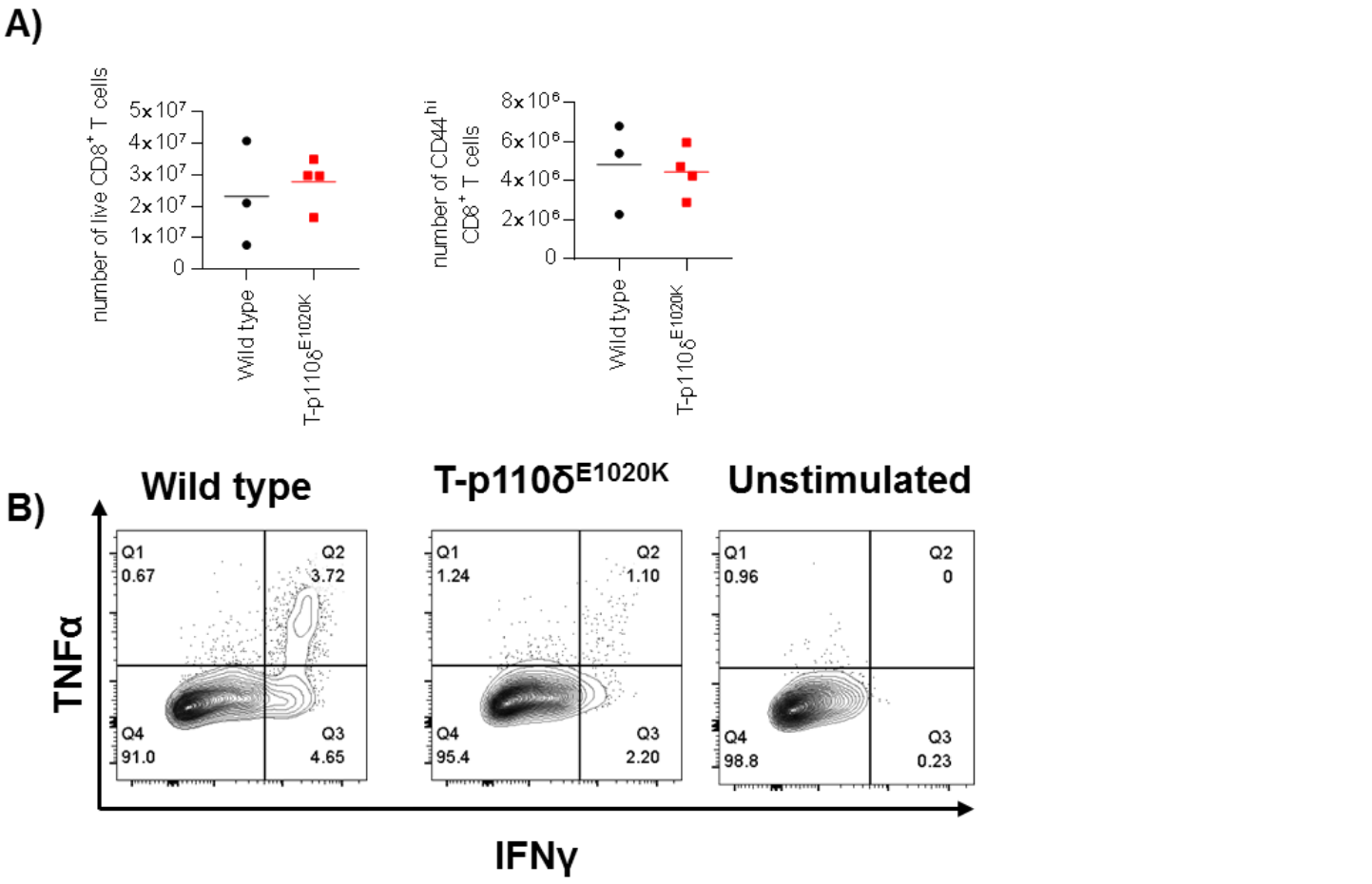
A)
number of live CD8+ T cells
5x10^7
4x10^7
3x10^7
2x10^7
1x10^7
0
Wild type
T-p110δE1020K
number of CD44hi CD8+ T cells
8x10^6
6x10^6
4x10^6
2x10^6
0
Wild type
T-p110δE1020K
B)
Wild type
T-p110δE1020K
Unstimulated
TNFα
IFNγ
Q1 0.67
Q2 3.72
Q4 91.0
Q3 4.65
Q1 1.24
Q2 1.10
Q4 95.4
Q3 2.20
Q1 0.96
Q2 0
Q4 98.8
Q3 0.23
C)
% of IFNγ+ cells within CD44hi CD8+ T cells
p=0.0146
Number of IFNγ+ cells within CD44hi CD8+ T cells
p=0.0371
% of TNFα+ cells within CD44hi CD8+ T cells
Number of TNFα+ cells within CD44hi CD8+ T cells
Wild type
T-p110δE1020K
D)
% of IFNγ+ TNFα+ cells within CD44hi CD8+ T cells
p=0.0108
number of IFNγ+ TNFα+ cells within CD44hi CD8+ T cells
p=0.0261
number of IL-2+ cells within IFNγ+ TNFα+ cells
p=0.0166
Wild type
T-p110δE1020K

Figure 6.2.5: Reduced antiviral function of $CD8^+$ T cells in T-$p110\delta^{E1020K}$ mice following chronic infection

On day 62 post infection, splenocytes from WT and T-$p110\delta^{E1020K}$ mice were re-stimulated *ex vivo* with GP_{33-41} peptide for 5.5 hours in the presence of Brefeldin A. Following stimulation, cells were stained for cell surface CD8, CD44 and intracellular cytokines (IFN-γ, IL-2, and TNFα). **(A)** Graphs showing absolute numbers of $CD8^+$ T cells and $CD44^{high}$ $CD8^+$ T cells. **(B)** Representative flow cytometry plots showing $IFN\gamma^+$ and $TNF\alpha^+$ cells gated on $CD8^+$ $CD44^{high}$ T cells. **(C)** Graphs showing proportions and numbers of $IFN\gamma^+$ and $TNF\alpha^+$ cells within total $CD44^{high}$ $CD8^+$ T cells. **(D)** Graphs showing proportions and numbers of $IFN\gamma^+$ producing LCMV specific $CD8^+$ T cells that also produced $TNF\alpha^+$ and $IL\text{-}2^+$. Data representative of one independent experiment with n= 3-4 per group. *P values* are shown.

6.2.6 Hyperactive p110δ in $CD8^+$ T cells leads to increased expression of inhibitory markers following chronic infection

Chronic infection leads to many phenotypic changes that define exhausted T cells such as the upregulation of inhibitory receptors. Therefore, I decided to look at the expression of inhibitory receptors upon infection with LCMV Clone 13. Following infection at day 62, $CD8^+$ T cells specific GP_{33-41} epitope from T-$p110\delta^{E1020K}$ mice had significantly increased expression of classical exhaustion markers such as PD-1, TIGIT, Tim3 and LAG-3 compared to WT mice (**Figure 6.2.6a-d**). Therefore, as well as reduced cytokine production due to hyperactive p110δ, we observed a corresponding higher expression of multiple inhibitory receptors, a second key feature of exhaustion.

During chronic infection, Eomes expression has been found to correlate with increased expression of T cell exhaustion markers, increased granzyme B and reduced co-production of cytokines [396] . For this reason, the expression of Eomes, T-bet and granzyme B on GP_{33-41} specific $CD8^+$ T cells following LCMV Clone 13 infection was measured. On day 62 post infection, there was no difference in T-bet expression, however Eomes along with granzyme B expression was upregulated in T-$p110\delta^{E1020K}$ mice compared to WT mice (**Figure 6.2.6 e-g**). This set of data suggests

that following chronic infection, $CD8^+$ T cells in T-$p110\delta^{E1020K}$ mice acquire an altered transcriptional programme that is characteristic of T cell exhaustion.

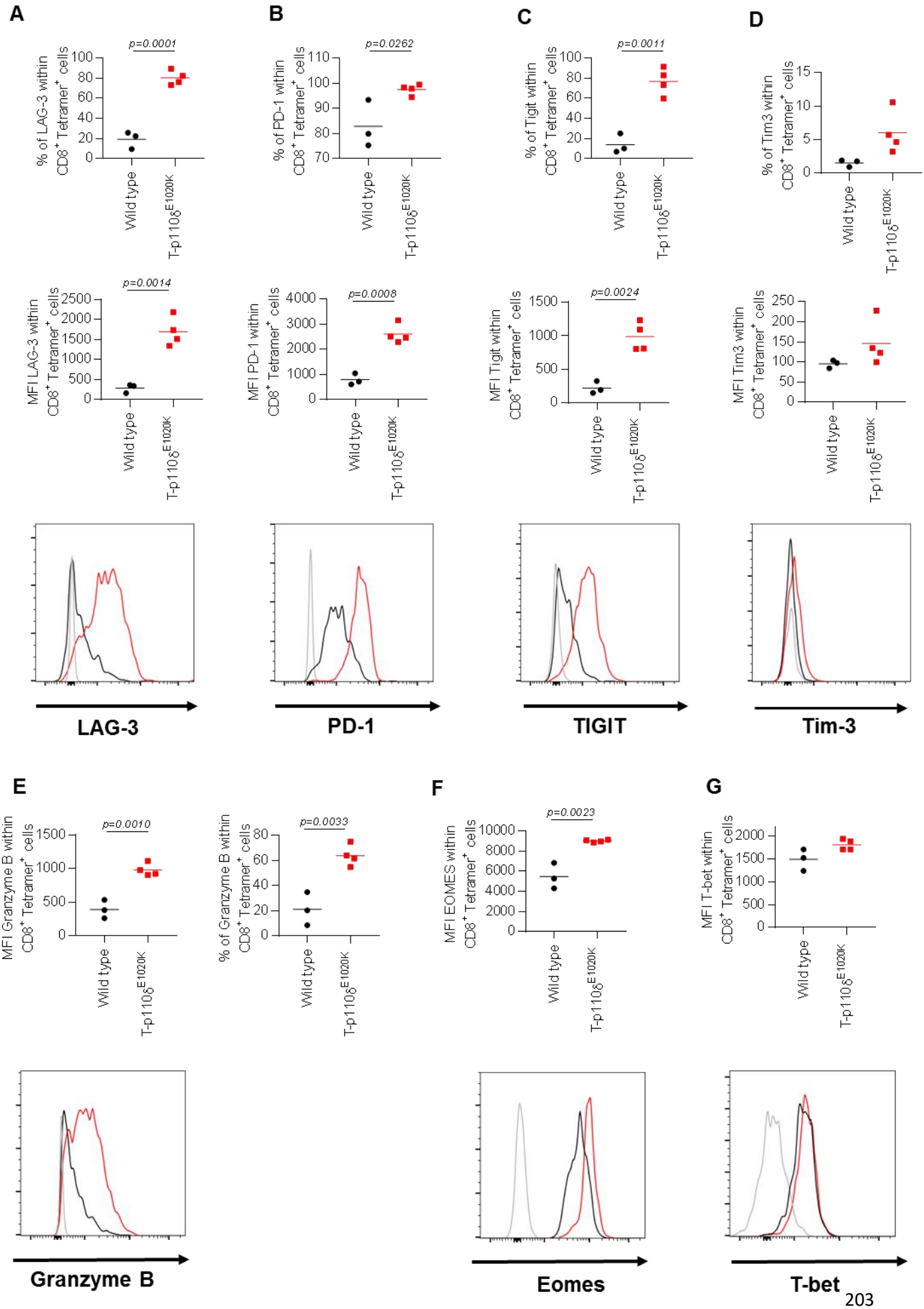
A
B
C
D
p=0.0001
p=0.0262
p=0.0011
% of LAG-3 within CD8+ Tetramer+ cells
% of PD-1 within CD8+ Tetramer+ cells
% of Tigit within CD8+ Tetramer+ cells
% of Tim3 within CD8+ Tetramer+ cells
Wild type
T-p110δE1020K
p=0.0014
p=0.0008
p=0.0024
MFI LAG-3 within CD8+ Tetramer+ cells
MFI PD-1 within CD8+ Tetramer+ cells
MFI Tigit within CD8+ Tetramer+ cells
MFI Tim3 within CD8+ Tetramer+ cells
LAG-3
PD-1
TIGIT
Tim-3
E
F
G
p=0.0010
p=0.0033
p=0.0023
MFI Granzyme B within CD8+ Tetramer+ cells
% of Granzyme B within CD8+ Tetramer+ cells
MFI EOMES within CD8+ Tetramer+ cells
MFI T-bet within CD8+ Tetramer+ cells
Granzyme B
Eomes
T-bet

Figure 6.2.6: CD8$^+$ T cells in T-p110δ^{E1020K} mice express enhanced levels of inhibitory receptors following LCMV Clone 13 infection at day 62.

WT and T-p110δ^{E1020K} mice were infected with 1 x 10^6 PFU of LCMV Clone 13 on day 0 day culled at day 62 post infection. Graphs showing proportions and histograms displaying mean fluorescence intensity (MFI) of **(A)** LAG-3 , **(B)** PD-1, **(C)** TIGIT , **(D)** Tim3 , **(E)** Granzyme B. Graphs and histograms showing MFI of **(F)** Eomes and **(G)** T-bet all pre-gated on GP_{33-41} specific CD8$^+$ T cells . WT is depicted in black and T-p110δ^{E1020K} in red on the histograms. Data representative of one independent experiment with n=3-4 per group. *P values* are shown.

6.2.7 Chronic LCMV infection leads to increased Tfh and Treg cells in T-p110δ^{E1020K} mice

It is reported that mice depleted of CD4$^+$ T cells are unable to clear LCMV virus due to increase CD8$^+$ T cell exhaustion and high viral burden, suggesting that CD4$^+$ T cells play an important role in controlling LCMV Clone 13 infection [397]. Therefore, I next evaluated the role of hyperactive p110δ in the CD4$^+$ T cell response during LCMV Clone 13 infection. In the first experiment, I analysed the expression of antigenic-specific CD4$^+$ T cells in the blood at different time points. Upon infection at day 8, the proportions of viable CD4$^+$ T cells were similar across both groups; however, the proportions of GP_{61-80} specific CD4$^+$ T cells in T-p110δ^{E1020K} mice were reduced compared to WT mice. At day 15, the proportions of viable CD4$^+$ T cells and GP_{61-80} specific CD4$^+$ T cells were comparable across both groups (**Figure 6.2.7a**). At day 32 and 62 post infection, in the spleen the numbers of viable CD4$^+$ T cells in the spleen was similar across both groups. In addition, the proportions and numbers of GP_{61-80} specific T cells were comparable between WT and T-p110δ^{E1020K} mice (**Figure 6.2.7b-c**). This suggests that perhaps initially in the probable acute phase help from CD4$^+$ T cells is limiting for effective CD8$^+$ T cell effector functions in response to chronic infection.

Chronic infections drive the differentiation of virus specific CD4$^+$ T cells from Th1 cells into Tfh cells in order to sustain antiviral antibody production to control persistent virus replication [291]. Tfh cells also produce IL-21, a cytokine important in sustaining CD8$^+$ T cells during chronic infections [398, 399]. At day 32, analysis of Tfh cells by CXCR5 and PD-1 staining showed that total number of Tfh cells and antigenic-specific Tfh

cells in the spleen did not differ between WT and T-p110δ^{E1020K} mice (**Figure 6.2.7e**). However, at day 62 post infection, an increase in total numbers and proportions of Tfh cells amongst CD44^{high} CD4^{+} T cells in T-p110δ^{E1020K} mice was detected. In addition, the numbers of GP_{61-80} specific Tfh cells were increased in T-p110δ^{E1020K} mice, possibly due to an increase in total Tfh cells along with an increase in proportions of Bcl-6^{+} cells within antigenic-specific Tfh cells (**Figure 6.2.7e**). Tregs are also implicated in facilitating disease progression due to inhibition of CD8^{+} T cell response to chronic infection [400]. At day 32 post LCMV infection, no difference in Tregs were detected between WT and T-p110δ^{E1020K} mice, however at day 62 post LCMV Clone 13 infection, the proportion and numbers of total Tregs were higher in T-p110δ^{E1020K} mice compared to WT mice (**Figure 6.2.7f**). This set of data indicates that upon LCMV Clone 13 infection, CD8^{+} T cells in T-p110δ^{E1020K} potentially receive help from an expanded population of Tfh cells as well as inhibitory signals from increased Tregs at later time points in the course of the infection.

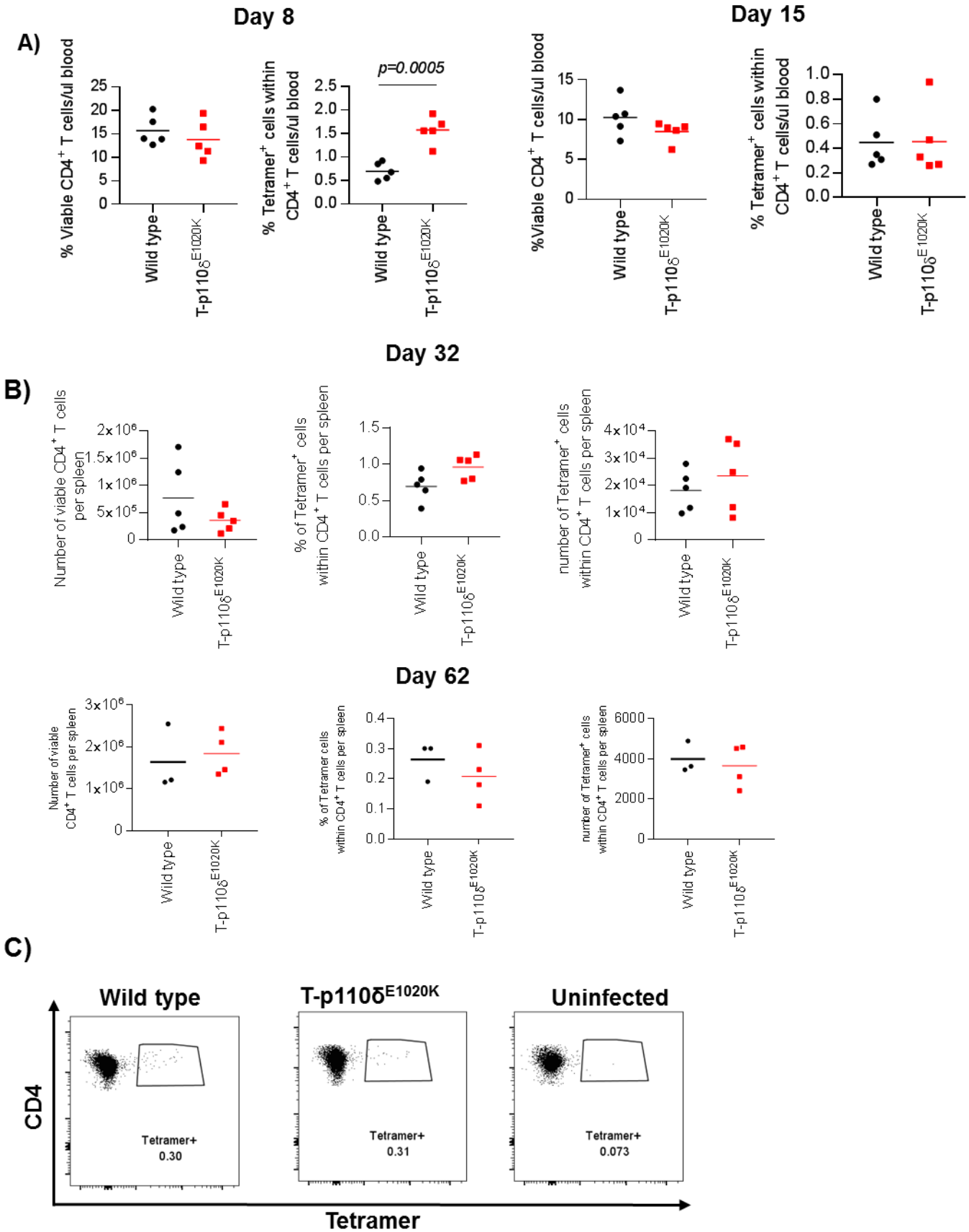
A)
Day 8
% Viable CD4+ T cells/ul blood
% Tetramer+ cells within CD4+ T cells/ul blood
p=0.0005
Day 15
%Viable CD4+ T cells/ul blood
% Tetramer+ cells within CD4+ T cells/ul blood
Wild type
T-p110δE1020K
B)
Day 32
Number of viable CD4+ T cells per spleen
% of Tetramer+ cells within CD4+ T cells per spleen
number of Tetramer+ cells within CD4+ T cells per spleen
Day 62
Number of viable CD4+ T cells per spleen
% of Tetramer cells within CD4+ T cells per spleen
number of Tetramer+ cells within CD4+ T cells per spleen
C)
Wild type
T-p110δE1020K
Uninfected
CD4
Tetramer
Tetramer+
0.30
Tetramer+
0.31
Tetramer+
0.073

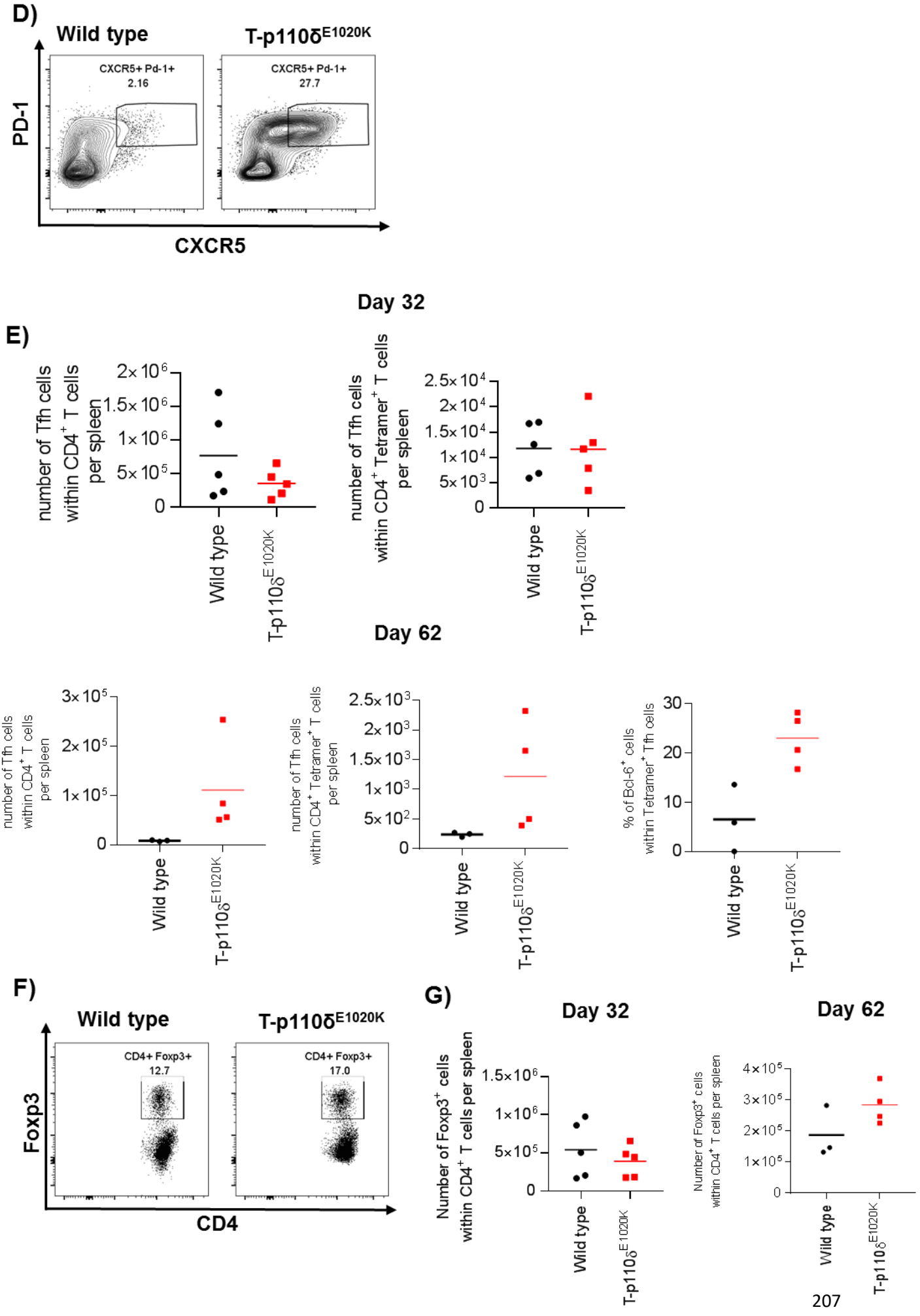
D)
Wild type
T-p110δE1020K
CXCR5+ Pd-1+
2.16
CXCR5+ Pd-1+
27.7
PD-1
CXCR5
Day 32
E)
number of Tfh cells within CD4+ T cells per spleen
2×10^6
1.5×10^6
1×10^6
5×10^5
0
Wild type
T-p110δE1020K
number of Tfh cells within CD4+ Tetramer+ T cells per spleen
2.5×10^4
2×10^4
1.5×10^4
1×10^4
5×10^3
0
Wild type
T-p110δE1020K
Day 62
number of Tfh cells within CD4+ T cells per spleen
3×10^5
2×10^5
1×10^5
0
Wild type
T-p110δE1020K
number of Tfh cells within CD4+ Tetramer+ T cells per spleen
2.5×10^3
2×10^3
1.5×10^3
1×10^3
5×10^2
0
Wild type
T-p110δE1020K
% of Bcl-6+ cells within Tetramer+ Tfh cells
30
20
10
0
Wild type
T-p110δE1020K
F)
Wild type
T-p110δE1020K
CD4+ Foxp3+
12.7
CD4+ Foxp3+
17.0
Foxp3
CD4
G)
Day 32
Number of Foxp3+ cells within CD4+ T cells per spleen
1.5×10^6
1×10^6
5×10^5
0
Wild type
T-p110δE1020K
Day 62
Number of Foxp3+ cells within CD4+ T cells per spleen
4×10^5
3×10^5
2×10^5
1×10^5
0
Wild type
T-p110δE1020K

Figure 6.2.7: Increase T follicular helper (Tfh) and Regulatory T cells (Tregs) in T-p110δ^{E1020K} mice at day 62 post LCMV Clone 13 infection.

WT and T-p110δ^{E1020K} mice were infected with 1 × 10^6 PFU of LCMV Clone 13 on day 0. **(A)** Graphs showing proportions of viable CD4$^+$ T cells and GP_{61-80} specific CD4$^+$ T cells in blood at day 8 and 15 post infection **(B)** Graphs showing numbers of viable CD4 T cells, proportions and number of GP_{61-80} specific CD4$^+$ T cells in spleen at day 32 and day 62 . **(C)** Representative flow cytometry plots showing GP_{61-80} specific CD4$^+$ T cells in spleen at day 62. **(D)** Representative flow cytometry plots showing total Tfh cells gated on CD4$^+$ CD44^{high} T cells at day 62. **(E)** Graphs showing numbers of total Tfh cells and GP_{61-80} specific Tfh cells in the spleen at day 32 and 62**.** Graph showing proportions of Bcl-6$^+$ cells within GP_{61-80} specific Tfh cells in the spleen at day 62. **(F)** Representative flow cytometry plots of Foxp3$^+$ cells within viable CD4$^+$ T cells at day 62. **(G)** Graphs showing numbers of Foxp3$^+$ cells within viable CD4$^+$ T cells at day 32 and 62 in the spleen. Data in A-B Data representative from one independent with experiment (n=5 per mice group). Data showing day 32 results is from one independent experiment (n=5 per mice group) group. Data showing day 62 results if from one independent experiment (n=3-4 mice per group) *P values* are shown .

6.3 Discussion

In response to primary infection with LCMV Armstrong strain, the expansion of $CD8^+$ T cells at day 8 was comparable between WT and T-p110δ^{E1020K} mice. Hyperactive p110δ caused an expansion of SLECs at the apparent expense of MPECs. Following *ex vivo* peptide re-stimulation, there was no difference in effector cytokines but an increase in granzyme B. These results are similar to that observed with primary responses to Lm-OVA and influenza as shown in chapter 4. Interestingly at day 35 post LCMV Armstrong infection, there was a reduction in the numbers and proportions of antigenic specific $CD8^+$ T cells in T-p110δ^{E1020K} mice. This could be due to reduced MPECs detected at day 8 post infection causing defective generation of memory $CD8^+$ T cells. Following *ex vivo* peptide re-stimulation, these antigenic specific $CD8^+$ T cells produced less cytokines, suggesting that memory $CD8^+$ T cells in T-p110δ^{E1020K} mice become functionally less effective following acute LCMV infection, similar to that observed following Lm-OVA infection as shown in Chapter 4. These results suggest that hyperactive p110δ leads to impaired formation of polyfunctional memory $CD8^+$ T cells. The question of whether these resting memory $CD8^+$ T cells in T-p110δ^{E1020K} are defective in their recall response needs to be determined. As I have previously shown, $CD8^+$ T cells in T-p110δ^{E1020K} mice have defective recall responses at day 3 post secondary infection with Lm-OVA but at later time are able to mount similar recall responses to WT mice in response to both Lm-OVA (at day 5) and influenza (at day 8) infections. Whether this is true for this LCMV Armstrong strain is yet be determined through future experiments.

The results observed in response to LCMV Armstrong strain are similar to that shown by Kim and colleagues using transgenic mice that express constitutively active Akt in $CD8^+$ T cells [121]. This study showed that sustained activation of Akt in $CD8^+$ T cells impaired the generation of $CD8^+$ T cell memory, without affecting the primary expansion but with greater effector function (increased IFNγ and granzyme B expression) in response to the LCMV Armstrong strain. They further went on to show that these mice had compromised protective recall responses and viral clearance due to diminished IL-7- and/or IL-15 dependent survival signals that might have contributed to the exaggerated loss of $CD8^+$ T cells with constitutive Akt expression [121]. It is important to note that their use of a $CD8^+$ T cell specific model meant the role of $CD4^+$

T cells with constitutive Akt was not observed; therefore, it will be important to determine whether $CD4^+$ T cells in T-p110δ^{E1020K} mice play any role in the primary response and generation of memory $CD8^+$ T cells to acute LCMV infection. Treatment of mice with rapamycin following LCMV Armstrong infections also resulted in increased quantity and quality of antigenic-specific $CD8^+$ T cells. Following acute infection with LCMV $CD8^+$ T cells with hyperactive p110δ become short lived and adopt phenotypically reduced memory population that translates into reduce memory cells, highlighting again the important role of effector proteins downstream of increased p110δ activity involved in memory $CD8^+$ T cell differentiation.

A chronic infection using LCMV Clone 13 in this chapter has revealed detrimental role for hyperactive p110δ activity in T cells on the anti-viral immune response of $CD8^+$ T cells. Following infection with LCMV Clone 13 , T-p110δ^{E1020K} mice showed greater weight loss compared to WT mice, which is usually ascribed to immune-mediated pathology [401]. Furthermore, there was a trend towards increased viral loads in the livers of T-p110δ^{E1020K} mice compared to WT mice. Future experiments will be required to carefully measure viral titres in a number of various organs such as spleen and kidneys. One possible explanation of the weight loss observed in the T-p110δ^{E1020K} mice is due to the inability to control viral titers sufficiently, resulting in the mice succumbing to infection. Reduced proportions of antigenic-specific $CD8^+$ T cells observed at day 15 and 32 also support this. In order to further confirm this, an experiment measuring viral titers at different time points when the mice appear to be more susceptible to infection according to body weight loss is necessary. The number of antigenic-specific $CD8^+$ T cells in T-p110δ^{E1020K} were reduced at day 32 but not at day 62 post infection compared to WT mice. Clearance of LCMV Clone 13 occurs mostly within 60-90 days post infection, and this depends on the infectious dose used. Therefore, it might be that with the dose used for these experiments, the virus is cleared in WT mice at day 62 or earlier. As substantial antigen was not available for the antigenic specific $CD8^+$ T cells to proliferate in WT mice, the response reached a plateau matching the T-p110δ^{E1020K} response. Additionally exhausted T cells are known to respond poorly to typical homeostatic cytokines required for memory T cell maintenance and rely on available antigen to persist during chronic infection for survival [402].

In response to chronic infection with LCMV Clone 13, $CD8^+$ T cells with hyperactive p110δ acquire phenotypic T cell exhaustion characteristics. At day 62, there was an increase in the expression of inhibitory receptors such as, Tim3, LAG-3, PD-1, and TIGIT on $CD8^+$ T cells in T-$p110\delta^{E1020K}$ mice. Characteristically, the higher the number of inhibitory receptors co-expressed on exhausted $CD8^+$ T cells, the greater the level of exhaustion. It will be interesting to determine whether blockade of multiple inhibitory receptors will reverse the T cell exhaustion phenotype. Combining PD-1 pathway blockade along with other inhibitory receptors have been shown to improve $CD8^+$ T cell response and viral control following chronic LCMV infection [403-405]. Blockade of inhibitory receptors have also been reported for the treatment of melanoma, HIV, hepatitis B and C patients [406-408]. During chronic infection, $CD8^+$ T cells are impaired in their ability to sustain phosphorylation of PI3K, consequently Akt and mTOR that contributes to their functional exhaustion [127, 136]. This in turn leads to increase activity of Foxo1 which was required to sustain PD1 expression and to adopt a terminally exhausted state during chronic infection by increase Eomes expression, however the increase in Foxo1 activity also caused an increased in Bcl2 expression. Therefore suggesting that during chronic infection, $CD8^+$ T cells are able to adapt to persistent infection via a positive feedback pathway involving Foxo1 [136]. Additionally increase PD-1 expression has been shown to enhance levels of phosphatases such as, PTEN, SHP-1 or SHP-2, thereby inhibiting PI3K signalling [409, 410] . Thus, a situation could be arising in the T-$p110\delta^{E1020K}$ mice whereby the induction of exhaustion is a compensatory mechanism to restore $CD8^+$ T cell function when there is detrimental p110δ activity.

At day 62 post LCMV Clone 13 infection, antigenic $CD8^+$ T cells in T-$p110\delta^{E1020K}$ mice express elevated Eomes and granzyme B expression. Chronic infection usually leads to loss of T-bet and conversion of antigenic specific $CD8^+$ T cells into $Eomes^{high}$ expressing cells [396]. Increase levels of inhibitory receptors has been shown to be associated with $Tbet^{dim}$ and $Eomes^{high}$ expression in total $CD8^+$ T cells during chronic HIV infection [411]. McLane et al showed that the subcellular localisation of T-bet and Eomes is different during chronic LCMV infection, T-bet is more cytoplasmic, on the other hand, Eomes is more nuclear and associated with increased PD-1 expression. Inhibiting PD-1 can influence the localisation of T-bet and Eomes, leading to reversal of exhaustion [412]. $Eomes^{high}$ expressing $CD8^+$ T cells display increased expression

of inhibitory receptors, reduced co-production of cytokines along with enhanced granzyme B levels and cytotoxicity, these are referred to as terminally exhausted $CD8^+$ T cells [396]. Therefore, it could be that regardless of the reduced anti-viral activity, $CD8^+$ T cells with hyperactive p110δ might have enhanced killing capability following chronic infection. However recently in a cohort of 39 APDS patients, $CD8^+$ T cells from patients exhibited increased expression of granzyme B and perforin but associated with impaired cytotoxicity [155]. Mice with Foxo3 ablation in T cells, demonstrated reduced apoptosis and increase abundance of polyfunctional $CD8^+$ T cells along with improve viral control is observed in response to chronic LCMV infection [127]. Whereas Foxo1 null $CD8^+$ T cells failed to persist and control chronic LCMV infection [136]. Therefore, highlighting the non-redundant roles played by Foxo1 and Foxo3 in regulating $CD8^+$ T cells responses during chronic infections as well.

$CD4^+$ T cells play an important role for controlling chronic infections as depleting $CD4^+$ T cell leads to increased viral burden, functional $CD8^+$ T cell exhaustion and immune dysregulation [397]. At day 8 post infection with LCMV Clone 13, there was a reduction in the proportions of antigen-specific $CD4^+$ T cells but at later time points, no difference was detected. It is possible that the initial reduction in antigenic-specific $CD4^+$ T cells leads to $CD8^+$ T cell defects as the infection continues due to limited $CD4^+$ T cell help available earlier on in the course of infection. However, at later time points as the differences in antigenic-specific $CD4^+$ T cells are comparable, the help from $CD4^+$ T cells is probably not enhanced and that could be one factor contributing to the defective $CD8^+$ T cell response in T-p110δ^{E1020K} mice.

Tregs play a major role in regulating $CD8^+$ T cell exhaustion as Treg depletion has been shown to rescue $CD8^+$ T cells with increase effector abilities and reduced viral load following chronic infection [400, 413]. There is data to suggest that simultaneously depleting Tregs and blockade of PD1 signaling has a synergistic effect in controlling T cell exhaustion, implying that Tregs can effectively maintain $CD8^+$ T cell exhaustion [400]. An increase in Tregs were observed at day 62 post LCMV Clone 13 infection in T-p110δ^{E1020K} mice that could potentially suppress antigenic-specific $CD8^+$ T cell responses. During chronic infections, loss of typical antiviral Th1 responses occurs and this shifts towards a Tfh phenotype such that both virus specific and unrelated $CD4^+$ T cells display this phenotypic shift [288]. Possible mechanisms

by which Tfh cells can benefit the antigenic-specific $CD8^+$ T cells in T-p110δ^{E1020K} mice could be by supporting the $CD8^+$ T cell response through production of IL-21[399] [414]. IL-21 signaling has been shown to enhance effector responses of $CD8^+$ T cells, avoiding deletion and resolving persistent infection following chronic viral infection [414]. IL-21 is also able to suppress infection induced Tregs therefore indirectly increasing $CD8^+$ T cell function during chronic infection. Additionally, Tfh cells by reducing Th1 driven immunopathology, and by their more established role of providing help for a robust antibody response can also aid the $CD8^+$ T cells response. At day 32 post LCMV Clone 13 infection, no difference in Tfh and Treg cells were observed, therefore it could be that survival signals from Tfh cells are limited leading to reduced antigenic-specific $CD8^+$ T cells in T-p110δ^{E1020K} mice. At day 62 increased Tfh and Treg cells were observed in T-p110δ^{E1020K} mice and no difference in antigenic-specific $CD8^+$ T cells was detected. It could be that increased Tfh cells might lead to increase IL-21 production that could help $CD8^+$ T cell survival via inhibiting Tregs, however the T cell exhaustion phenotype was enhanced compared to WT mice suggesting that Tregs could be influencing the $CD8^+$ T cell response. Whether the Tfh cells generated during LCMV Clone 13 infection function as optimal Tfh cells to be determined, in addition whether the suppression from Tfr cells and Tregs can outplay the effect of Tfh cells will be important to understand the $CD4^+$ T cell role in T-p110δ^{E1020K} during chronic LCMV infection.

The $CD8^+$ T cell response to LCMV Clone 13 can be influenced by a number of different variables such as the strength of antigen stimulation, the duration of infection, help from different $CD4^+$ T cells subtypes, the number of inhibitory receptors expressed. In order to investigate the effect of hyperactive p110δ on intrinsic $CD8^+$ T cell response, a cross can be done with P14 TCR transgenic mice that are specific for the LCMV GP_{33-41} epitope. This would allow avoiding extrinsic factors such as influence of $CD4^+$ T cells. The data presented in this chapter is preliminary; thus, repeats and further work will be necessary to better understand how hyperactive p110δ regulates T cell responses to LCMV Armstrong and Clone 13 infections. However, the results observed following LCMV Clone 13 infection indicate an exhaustive phenotype of $CD8^+$ T cell due to hyperactive p110δ recapitulating the phenotype in APDS patients, therefore this model serves as an ideal way forward to understand the molecular mechanisms underlying T cell exhaustion. In addition, to

test out potential therapeutic opportunities by using checkpoint inhibitors such as blockade of PD-1 /PD-L1 interactions. It seems that a scenario exists where sustained antigenic signalling due to the presence of persistent virus reduced TCR signal transduction rather than enhances it due to hyperactive p110δ.

Chapter 7
Conclusions

The p110δ isoform belonging to class IA PI3K is important in regulating numerous immune cell responses. Studies using genetic mouse models and pharmacological inhibition have aided in our understanding of the role of p110δ in immune cells. Further, the identification of LOF and GOF mutations in the PIK3CD gene highlighted the importance of efficient regulation of PI3K activity, as both inhibition and hyperactivation can result in immunodeficiency [415]. The work described in the preceding result chapters have established a mouse model that recapitulates the features of the T cell phenotype demonstrated by APDS patients and thus serves as a valuable model to understand the mechanisms underlying this disease phenotype.

Using the T-p110δ^{E1020K} mouse model, I performed *in vitro* and *in vivo* phenotyping experiments looking at the effect of the mutation in different T cell subsets. *In vitro* CD4^{+} T cell differentiation experiments have built on previous studies investigating the role of p110δ in regulating CD4^{+} T cell differentiation. Increases in Th1, Th2, Th17 and Tfh responses were observed in T-p110δ^{E1020K} mice compared to WT mice. Consistently with published data, iTreg differentiation was reduced owing to perhaps the role played by mTORc1 and mTORc2 in regulating CD4^{+} T cell differentiation. However, the difference in Foxp3^{+} iTreg induction between T-p110δ^{E1020K} and WT mice was small, bringing the biological relevance of this defect to the overall immune response into question.

Deletion of PTEN targeted to the T cell compartment by using CD4Cre (or LckCre) has been associated in most cases with the development of T cell lymphomas and signs of autoimmunity by around 10-17 weeks of age [75, 351]. In T-p110δ^{E1020K} mice, no signs of autoimmunity as determined by measure ANA levels or lymphoma development was observed up to ages of at least 14 weeks. This could possibly be due to a balance of between increased T helper cytokines and peripheral Tregs (**Chapter 3**). Additionally, T cells from T-p110δ^{E1020K} mice proliferate normally but undergo increased apoptosis compared to WT T cells, this could potentially be an adaptive mechanism to avoid uncontrolled growth in response to p110δ hyperactivation in T-p110δ^{E1020K} mice. Possibly T-p110δ^{E1020K} mice could have increased expression of phosphatases that might negatively regulate the increased PI3K activity as a mechanism to balance the response, this will require further investigation. Detailed analysis of recently generated proteomics data and gene microarray data on T cells from WT, T-p110δ^{E1020K} and p110δ^{D910A} mice will be very

useful in identifying additional pathways or proteins that could explain differences occurring between PTEN deficient T cell mice and T-p110δ^{E1020K} mice.

Data generated using F-p110δ^{E1020K} mice revealed a similar phenotype to PTEN deficient Treg mice with signs of autoimmunity emerging with increased age [105, 106]. However, despite the increased IFNγ producing cells detected among Tregs, these cells were able to suppress conventional T cells effectively (**Chapter 3**). It will be of interest to see whether, with age, T-p110δ^{E1020K} mice show a similar phenotype as F-p110δ^{E1020K} with signs of autoimmunity, as approximately 29% of APDS patients have been reported to display clinical signs of autoimmunity in analysis of a large cohort [151]. Further analysis of Tregs from APDS patients should also provide insight into the driving force behind the development of autoimmunity in these patients.

In response to immunisation with NP-KLH to examine humoral immune responses, help from T cells with hyperactive p110δ was not the limiting factor in causing antibody deficiencies but it was due to an intrinsic defect within B cells with hyperactive p110δ activity, consistent with APDS patients showing reduced CSR. Recently published data from other groups using mouse models expressing the E1020K mutation in immune cells also support this finding (**Chapter 3**) [306, 307]. The defect in B cells is most likely due to loss of Aicda expression that is important for CSR, and recent data generated by our group showed diminished Aicda expression and IgG1 producing cells in an *in vitro* CSR experiment that was reversed following p110δ inhibition (Tamara Verkerk, not published). Additionally B-p110δ^{E1020K} are susceptible to *Streptococcus pneumoniae* infections owing to an innate-like B cell subset influencing the early response to infection [305]. On the other hand, T-p110δ^{E1020K} mice were protected but the underlying mechanism is not clear yet and will be investigated in the future. Therefore, B cells with hyperactive p110δ are regulating aspects of APDS via antibody dependent and independent mechanisms.

Using three different pathogens, I have shown that the primary expansion phase of the CD8^{+} T cell response is normal in T-p110δ^{E1020K} mice, with greater killing abilities in response to Lm-OVA infection. However, single OT1 adoptive transfer experiments revealed an intrinsic defect in the primary expansion of CD8^{+} T cells with hyperactive p110δ in response to primary infection with Lm-OVA and WSN-OVA, thus suggesting the possible effect/help of other T cells harbouring the mutation. Despite the intrinsic

defect, these $CD8^+$ T cells were able to produce increased levels of cytokines and granzyme B at the expense of defective memory formation (**Chapter 4**). This is consistent with the phenotype displayed by APDS patients where $CD8^+$ T cells undergo increased AICD but display characteristics of enhanced effector function indicating that increased p110δ signalling potentially promotes $CD8^+$ T cell terminal effector differentiation and reduced memory cells, which might be one of the factors contributing to the occurrence of persistent infections. It is possible that the low $CD4^+$ T cell counts observed in APDS patients could limit survival signals for $CD8^+$ T cells following TCR stimulation.

In competitive adoptive transfer experiments when E1020K OT1 and WT OT1 cells were co-transferred into the same mouse, no difference in expansion of E1020K OT1 cells was detected following Lm-OVA infection, suggesting that extrinsic signals provided by WT OT1 cells can compensate for the deficient expansion of E1020K OT1 cells observed in the single OT1 adoptive transfer experiments (**Chapter 4).** Similarly, our group has reported equal expansion of $p110\delta^{D910A}$ OT1 and WT OT1 T cells following primary Lm-OVA infection [115]. Possibly in both cases help is provided by the co-transferred WT OT1 $CD8^+$ T cells that are able to promote optimal proliferation, and it seems that such help relies on normal p110δ activity. It will be important to follow this work up with experiments to determine how the WT OT1 cells can restore E1020K OT1 cell expansion in this competitive environment. A possible mechanism could be by survival signals via IL-2 production or CD40L expression on WT OT1 cells, as CD40L-expressing $CD8^+$ T cells resemble functional $CD4^+$ helper T cells [416].

In all primary infection experiments, phenotypically reduced memory $CD8^+$ T cells were detected as demonstrated by reduced MPECs and T_{CM} cells in T-$p110\delta^{E1020K}$ mice. However, no difference in recall response was detected at day 5 following Lm-OVA infection, but a reduction was detected at day 3 post infection in a preliminary experiment (**Chapter 5**). This suggests that perhaps at later time points help from other T cells might rescue the defective $CD8^+$ T cell memory response in T-$p110\delta^{E1020K}$ mice, given the role played by $CD4^+$ T cells in promoting recall responses to acute infections such as via enhanced Th1 responses or increased CD40-CD40L interactions [393, 394, 417]. In single and competitive OT1 adoptive transfer experiments, the recall response detected at day 5 was reduced due to hyperactive p110δ in $CD8^+$ T cells (**Chapter 5**). These results demonstrate that hyperactive p110δ

in $CD8^+$ T cells do lead to a defective recall response to Lm-OVA infection, albeit with increased or similar effector capacities. Reinfection of PR8 primed mice with Hkx31 did not reveal any differences in recall response at day 8 post-secondary infection (**Chapter 5**). Similar to Lm-OVA infections, it could be that differences become apparent at an earlier time point and that help from $CD4^+$ T cells might be confounding the $CD8^+$ T cell response at the later time point. Therefore, it will be important to determine whether a memory defect is observed following a viral infection due to hyperactive p110δ.

Using LCMV clone 13 as a model of exhaustion proved valuable as it demonstrated the T cell exhaustion phenotype similar to that observed in APDS patients. Impaired T cell effector functions in APDS patients have been associated with an inability to control chronic viral infections that include EBV and CMV. Following infection with LCMV clone 13, I detected increased upregulation of characteristic T cell exhaustion markers on hyperactive $CD8^+$ T cells that might limit T cell function, and that was indeed true when assessing cytokine production (**Chapter 6**).

Using T-$p110\delta^{E1020K}$ mice in LCMV clone 13 infection conditions is therefore ideal to understand how hyperactive p110δ leads to T cell exhaustion. Edwards et al recently confirmed this phenotype in APDS patients in a large cohort of 39 patients, they showed increased expression of T cell exhaustion markers associated with reduced IL-2, increased apoptosis and reduced cytotoxicity despite an increase in granzyme B and perforin [155]. As a way forward, future experiments should utilise the LCMV P14 transgenic mice, as these mice encode a TCR that is specific for a peptide (P14) from LCMV presented by the MHC class I molecule. Using these mice will aid in investigating the $CD8^+$ T cell intrinsic response to a chronic infection without the contribution from other T cells. The gene expression profiles of $CD8^+$ T cells with hyperactive p110δ in comparison to WT $CD8^+$ T cells following chronic infection could be determined. This will help in providing insights into the mechanism leading to T cell exhaustion by looking at the differential expression of genes involved in different cellular process, transcription factors, and metabolic processes. In order to further add to our understanding about the role of the p110δ isoform in response to chronic TCR signalling, $p110\delta^{D910A}$ mice should also be included and it will be intriguing to determine whether a reversal of the T-$p110\delta^{E1020K}$ phenotype is observed in $p110\delta^{D910A}$ mice.

Invariant natural killer T (iNKT) cells are an innate-like T cell subset that express an invariant αβ TCR and different NK cells marker. These cells recognise glycolipid antigens presented by CD1d molecule and are activated by the antigen α-galactosylceramide (α-GalCer). Following activation, iNKT cells by secreting numerous cytokines can cause maturation of APCs and provide help to conventional $CD4^+$ and $CD8^+$ T cells. During acute influenza infections, iNKT cells have been shown to reduce the recruitment and immunosuppressive activity of myeloid-derived suppressor cells (MDSCs) leading to increased $CD8^+$ T cell responses (3). Adoptive transfer of iNKT cells have been shown to restore viral specific $CD8^+$ T cells responses alongside reduced viral load with increase survival. iNKT cells by producing IFNγ results in enhancing the cytolytic ability of antigen specific $CD8^+$ T cells in response to influenza (1,2, 4). Different genetic defects that are associated with high susceptibility to EBV have shown to have impaired iNKT cell development and functions. Therefore, in response to acute infections, increased p110δ activity could enhance the functional role of iNKT cells contributing to the clearance of pathogen and enhanced cytolytic ability of antigen specific $CD8^+$ T cells. Conversely, in response to chronic infections, in T-$p110\delta^{E1020K}$ mice the function of iNKT is impaired contributing to reduced $CD8^+$ T cell responses. Future work should include detailed phenotypic and functional analysis of iNKT cells within different organs, in order to fully encompass the role of these cells on conventional T cells with hyperactive p110δ activity in the context of acute and chronic infections.

The effect of checkpoint inhibitors such as PD-1 blocking antibodies could be investigated to determine whether reversal of exhaustion phenotype is observed. Checkpoint blockade targeting inhibitory receptor pathways such as PD-1 have demonstrated to provide some benefit in patients suffering from chronic infection and cancer, however it has been reported to be associated with lack of long-term clinical benefits in patients receiving these treatments [418-422]. In T cells, PD-1 besides suppressing TCR, PI3K and mTOR signalling, also promotes conditions that may enhance the accumulation of suppressive Tregs by dampening glycolysis and promoting fatty acid oxidation (FAO). It is also known that virus driven expansion of Tregs contributes to T cell exhaustion and chronic infection [423, 424]. Increased anabolic metabolism and glycolysis in exhausted T cells due to blockade of PD-1 has been shown to be mTOR dependent [136]. Therefore, rapamycin also serves as a

therapeutic strategy; however, PI3K affects other downstream pathways as well as mTOR. Thus, a global p110δ inhibition might be more beneficial, and whether it should be oral or inhaled should come down to the clinical symptom prolife displayed by the patients. Inhaled therapy might prove to be useful in patients that are primarily affected by severe respiratory infections and might have a better safety profile due to local p110δ inhibition in the airways only. On the other hand, oral inhibitors will be useful in patients with a broader clinical profile that include for example complications of bronchiectasis, bacterial and viral infections, and lymphoma [172]. However, caution will have to be taken with careful dosing so that normal p110δ activity is achieved rather tipping the scale over to reduced p110δ activity that is also associated with immune cell dysfunction [415].

APDS patients display signs of both T cell exhaustion and senescence suggesting that both could contribute to the inability to clear virus. However, patients free from viremia also display increased expression of the T cell senescence marker CD57 [415]. Whether the inability to effectively control herpesvirus leads to T cell senescence in APDS needs to be determined. However, it is important to note that different factors could affect this phenotype such as environmental exposure and age of the patients at the time of diagnosis. With more patients being diagnosed, a correlation between exhaustion/senescence and causal factors could be beneficial to understand additional factors that contribute to this phenotype.

It is plausible that increased Akt activity, due to hyperactive p110δ, drives the differentiation of $CD8^+$ T cells into effector like cells over memory cells. The converse has been shown to be true in $p110\delta^{D910A}$ mice where $CD8^+$ memory T cells are more abundant. These defects could be due to the altered signalling of proteins downstream of increased Akt activity that include mTORc1 and Foxo transcription factors amongst others. In response to acute infections, $CD8^+$ T cells are able to produce normal or higher cytokines and granzyme B depending on the experimental setting but have defects in memory cell differentiation that seems to translate into reduced expansion of $CD8^+$ T cells upon reinfection, albeit with normal or enhanced effector function. In direct contrast, $CD8^+$ T cells with increased p110δ activity undergo T cell exhaustion that might limit clearance of virus following chronic infections, which are more relevant

to APDS patients. These results suggest that depending on the context of infection, hyperactive p110δ in $CD8^+$ T cells have different outcomes.

In conclusion, the data presented in this thesis confirms the previously established role for p110δ dependent signalling in maintaining effective immune cell function and development. In addition, I showed that p110δ hyperactivity could also disrupt the molecular processes required to mount an effective T cell mediated immune response to chronic infection. My data demonstrates the importance of effective regulation of the PI3K signalling pathway in immune cells and contribute to our current understanding of the mechanisms underlying the immunodeficiency observed in APDS patients.

Chapter 8
Appendices

8.1

Chapter 3 (Section 3.2.6)

A)

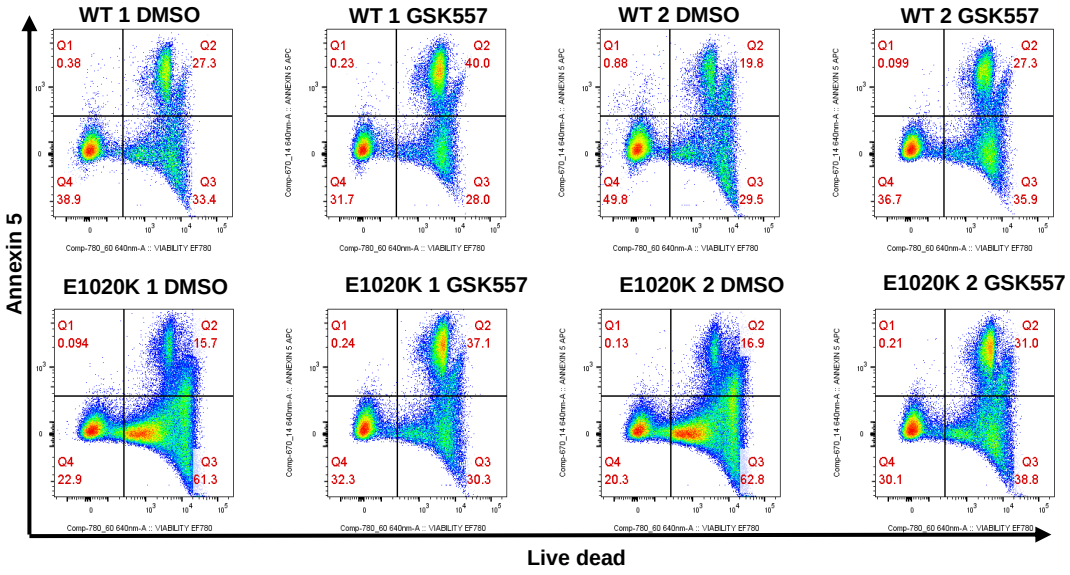

B)

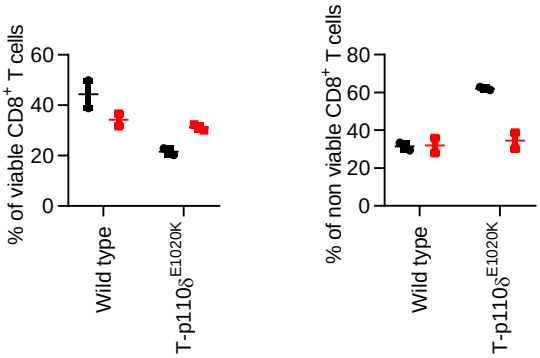

Figure 8.1: Increase cell death in T cells with hyperactive p110δ following peptide stimulation

Naïve ($CD62L^{high}CD44^{low}$) $CD8^+$ T cells were sorted from WT OT1 and E1020K OT1 mice and stimulated SIINFEKL peptide loaded dendritic cells in the presence or absence of 10 nM GSK2269557 for 72 hours. **(A)** Representative flow cytometry plots illustrating non-viable and viable $CD8^+$ T cells. **(B)** Graphs showing proportions of non-viable and viable cells by using Annexin 5 and viability dye in $CD8^+$ T cells. Data representative of one independent experiment with n = 2, each dot represents one mouse.

8.2

Chapter 3 (Section 3.2.9)

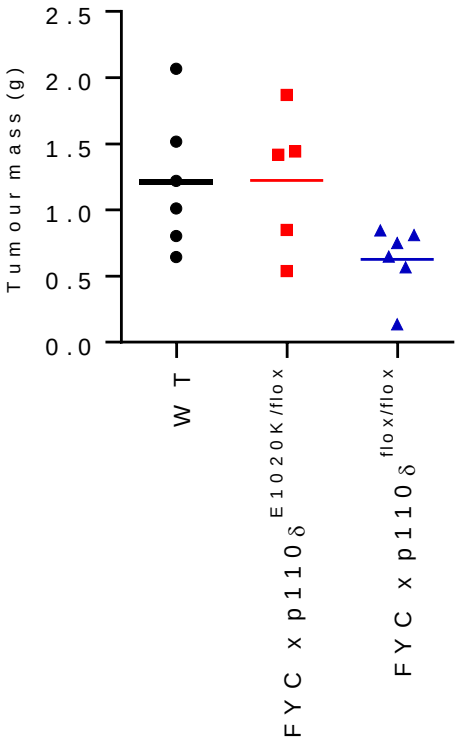

Figure 8.2: Mice were injected with 5 x 10^5 EL4-OVA cells in 100 µl PBS per mouse. Subcutaneously injected in the shaved flank of isoflurane-anaesthetised mice. Mice were culled on Day 17 and tumour weights were recorded. The EL4-OVA cell line also known as EG7-OVA was obtained from Ee Lyn Lim. The EL4 cells were originally derived from a lymphogenous leuokosis after treatment of C57BL/6 mice with 9:10-dimethyl-1:2-benzanthracene. The EL4-OVA cells line was derived by a transfection of EL4 cells with a pAc-neo-OVA plasmid, expressing chicken ovalbumin and the neomycin resistance gene (information obtained from Lyn's thesis). In this experiment, WT, F-p110δ^{E1020K} and FYC x p110δ$^{flox/flox}$ mice (p110δ specifically deleted in Foxp3$^+$ cells) were used.

8.3

Chapter 6 (6.2.5)

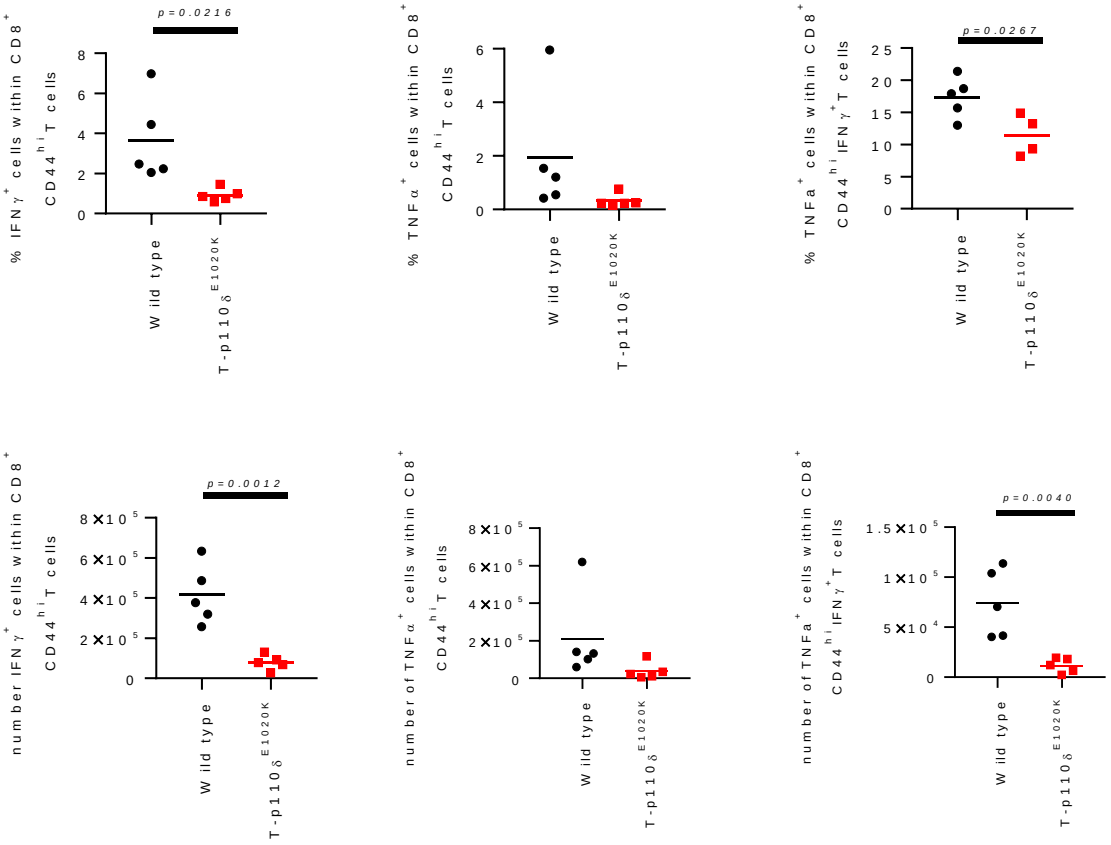

Cytokine data following LCMV clone 13 infection

References

1. Aifantis, I., et al., *Regulation of T-cell progenitor survival and cell-cycle entry by the pre-T-cell receptor.* Immunological Reviews, 2006. **209**(1): p. 159-169.
2. Germain, R.N., *T-cell development and the CD4–CD8 lineage decision.* Nature Reviews Immunology, 2002. **2**: p. 309.
3. Weinreich, M.A. and K.A. Hogquist, *Thymic Emigration: When and How T Cells Leave Home.* The Journal of Immunology, 2008. **181**(4): p. 2265-2270.
4. Soond, D.R., et al., *Does the PI3K pathway promote or antagonize regulatory T cell development and function?* Front Immunol, 2012. **3**: p. 244.
5. Lio, C.-W.J. and C.-S. Hsieh, *A Two-Step Process for Thymic Regulatory T Cell Development.* Immunity, 2008. **28**(1): p. 100-111.
6. Hsieh, C.-S., H.-M. Lee, and C.-W.J. Lio, *Selection of regulatory T cells in the thymus.* Nature Reviews Immunology, 2012. **12**: p. 157.
7. Zhu, J., H. Yamane, and W.E. Paul, *Differentiation of effector CD4 T cell populations (*).* Annu Rev Immunol, 2010. **28**: p. 445-89.
8. Berger, A., *Th1 and Th2 responses: what are they?* BMJ, 2000. **321**(7258): p. 424.
9. Nakayama, T., et al., *Th2 Cells in Health and Disease.* Annu Rev Immunol, 2017. **35**(1): p. 53-84.
10. Zambrano-Zaragoza, J., et al., *Th17 Cells in Autoimmune and Infectious Diseases.* International Journal of Inflammation, 2014. **2014**: p. 12.
11. Luckheeram, R.V., et al., *CD4(+)T cells: differentiation and functions.* Clin Dev Immunol, 2012. **2012**: p. 925135.
12. Liang, S.C., et al., *Interleukin (IL)-22 and IL-17 are coexpressed by Th17 cells and cooperatively enhance expression of antimicrobial peptides.* J Exp Med, 2006. **203**(10): p. 2271-9.
13. Lee, Y.K., et al., *Late developmental plasticity in the T helper 17 lineage.* Immunity, 2009. **30**(1): p. 92-107.
14. Végran, F., L. Apetoh, and F. Ghiringhelli, *Th9 Cells: A Novel CD4 T-cell Subset in the Immune War against Cancer.* Cancer Research, 2015. **75**(3): p. 475-479.
15. Vyas, S.P. and R. Goswami, *A Decade of Th9 Cells: Role of Th9 Cells in Inflammatory Bowel Disease.* Front Immunol, 2018. **9**(1139).
16. Trifari, S., et al., *Identification of a human helper T cell population that has abundant production of interleukin 22 and is distinct from TH-17, TH1 and TH2 cells.* Nat Immunol, 2009. **10**: p. 864.
17. Tamasauskiene, L. and B. Sitkauskiene, *Role of Th22 and IL-22 in pathogenesis of allergic airway diseases: Pro-inflammatory or anti-inflammatory effect?* Pediatrics & Neonatology, 2018. **59**(4): p. 339-344.
18. Sakaguchi, S., *Naturally Arising CD4+ Regulatory T Cells for Immunologic Self-Tolerance and Negative Control of Immune Responses.* Annu Rev Immunol, 2004. **22**(1): p. 531-562.
19. Sakaguchi, S., et al., *Regulatory T cells: how do they suppress immune responses?* International Immunology, 2009. **21**(10): p. 1105-1111.
20. Zhang, N. and M.J. Bevan, *CD8(+) T cells: foot soldiers of the immune system.* Immunity, 2011. **35**(2): p. 161-8.
21. Nolz, J.C., G.R. Starbeck-Miller, and J.T. Harty, *Naive, effector and memory CD8 T-cell trafficking: parallels and distinctions.* Immunotherapy, 2011. **3**(10): p. 1223-1233.
22. Kim, E.H. and M. Suresh, *Role of PI3K/Akt signaling in memory CD8 T cell differentiation.* Front Immunol, 2013. **4**(20).
23. Joshi, N.S., et al., *Inflammation directs memory precursor and short-lived effector CD8(+) T cell fates via the graded expression of T-bet transcription factor.* Immunity, 2007. **27**(2): p. 281-95.
24. Kaech, S.M., et al., *Selective expression of the interleukin 7 receptor identifies effector CD8 T cells that give rise to long-lived memory cells.* Nat Immunol, 2003. **4**: p. 1191.

25. Intlekofer, A.M., et al., *Effector and memory CD8+ T cell fate coupled by T-bet and eomesodermin.* Nat Immunol, 2005. **6**: p. 1236.
26. Sallusto, F., J. Geginat, and A. Lanzavecchia, *Central Memory and Effector Memory T Cell Subsets: Function, Generation, and Maintenance.* Annu Rev Immunol, 2004. **22**(1): p. 745-763.
27. Williams, M.A. and M.J. Bevan, *Effector and Memory CTL Differentiation.* Annu Rev Immunol, 2007. **25**(1): p. 171-192.
28. Vanhaesebroeck, B., et al., *The emerging mechanisms of isoform-specific PI3K signalling.* Nature Reviews Molecular Cell Biology, 2010. **11**: p. 329.
29. Okkenhaug, K., *Signaling by the phosphoinositide 3-kinase family in immune cells.* Annu Rev Immunol, 2013. **31**: p. 675-704.
30. Kihara, A., et al., *Two Distinct Vps34 Phosphatidylinositol 3–Kinase Complexes Function in Autophagy and Carboxypeptidase Y Sorting inSaccharomyces cerevisiae.* The Journal of Cell Biology, 2001. **152**(3): p. 519-530.
31. Maffucci, T. and M. Falasca, *New insight into the intracellular roles of class II phosphoinositide 3-kinases.* Biochem Soc Trans, 2014. **42**(5): p. 1378-82.
32. Parekh, V.V., et al., *Impaired autophagy, defective T cell homeostasis, and a wasting syndrome in mice with a T cell-specific deletion of Vps34.* J Immunol, 2013. **190**(10): p. 5086-101.
33. McLeod, I.X., et al., *The class III kinase Vps34 promotes T lymphocyte survival through regulating IL-7Ralpha surface expression.* J Immunol, 2011. **187**(10): p. 5051-61.
34. Falasca, M. and T. Maffucci, *Role of class II phosphoinositide 3-kinase in cell signalling.* Biochemical Society Transactions, 2007. **35**(2): p. 211-214.
35. Campa, C.C., I. Franco, and E. Hirsch, *PI3K-C2α: One enzyme for two products coupling vesicle trafficking and signal transduction.* FEBS Letters, 2015. **589**(14): p. 1552-1558.
36. Falasca, M., et al., *Class II Phosphoinositide 3-Kinases as Novel Drug Targets.* Journal of Medicinal Chemistry, 2017. **60**(1): p. 47-65.
37. Falasca, M. and T. Maffucci, *Regulation and cellular functions of class II phosphoinositide 3-kinases.* Biochem J, 2012. **443**(3): p. 587-601.
38. Stahelin, R.V., et al., *Structural and membrane binding analysis of the Phox homology domain of phosphoinositide 3-kinase-C2alpha.* J Biol Chem, 2006. **281**(51): p. 39396-406.
39. Hawkins, P.T., et al., *Signalling through Class I PI3Ks in mammalian cells.* Biochemical Society Transactions, 2006. **34**(5): p. 647-662.
40. Engelman, J.A., J. Luo, and L.C. Cantley, *The evolution of phosphatidylinositol 3-kinases as regulators of growth and metabolism.* Nature Reviews Genetics, 2006. **7**: p. 606.
41. Chantry, D., et al., *p110δ, a Novel Phosphatidylinositol 3-Kinase Catalytic Subunit That Associates with p85 and Is Expressed Predominantly in Leukocytes.* Journal of Biological Chemistry, 1997. **272**(31): p. 19236-19241.
42. Koyasu, S., *The role of PI3K in immune cells.* Nat Immunol, 2003. **4**: p. 313.
43. Kok, K., et al., *Regulation of p110δ PI 3-Kinase Gene Expression.* PLoS One, 2009. **4**(4): p. e5145.
44. Zhou, S., et al., *SH2 domains recognize specific phosphopeptide sequences.* Cell, 1993. **72**(5): p. 767-778.
45. Yu, J., et al., *Regulation of the p85/p110 Phosphatidylinositol 3'-Kinase: Stabilization and Inhibition of the p110α Catalytic Subunit by the p85 Regulatory Subunit.* Mol Cell Biol, 1998. **18**(3): p. 1379-1387.
46. Stephens, L.R., et al., *The Gβγ Sensitivity of a PI3K Is Dependent upon a Tightly Associated Adaptor, p101.* Cell, 1997. **89**(1): p. 105-114.
47. Suire, S., et al., *p84, a New Gβγ-Activated Regulatory Subunit of the Type IB Phosphoinositide 3-Kinase p110&#x3b3.* Current Biology, 2005. **15**(6): p. 566-570.
48. Okkenhaug, K. and B. Vanhaesebroeck, *PI3K in lymphocyte development, differentiation and activation.* Nature Reviews Immunology, 2003. **3**: p. 317.
49. Rommel, C., M. Camps, and H. Ji, *PI3Kδ and PI3Kγ: partners in crime in inflammation in rheumatoid arthritis and beyond?* Nature Reviews Immunology, 2007. **7**: p. 191.

50. Guillermet-Guibert, J., et al., *The p110beta isoform of phosphoinositide 3-kinase signals downstream of G protein-coupled receptors and is functionally redundant with p110gamma.* Proc Natl Acad Sci U S A, 2008. **105**(24): p. 8292-7.
51. Saudemont, A., et al., *p110gamma and p110delta isoforms of phosphoinositide 3-kinase differentially regulate natural killer cell migration in health and disease.* Proc Natl Acad Sci U S A, 2009. **106**(14): p. 5795-800.
52. Schmid, M.C., et al., *Receptor tyrosine kinases and TLR/IL1Rs unexpectedly activate myeloid cell PI3kgamma, a single convergent point promoting tumor inflammation and progression.* Cancer Cell, 2011. **19**(6): p. 715-27.
53. Croessmann, S., et al., *PIK3CA C2 Domain Deletions Hyperactivate Phosphoinositide 3-kinase (PI3K), Generate Oncogene Dependence, and Are Exquisitely Sensitive to PI3Kα Inhibitors.* Clinical Cancer Research, 2018. **24**(6): p. 1426-1435.
54. Martin, V., et al., *Deletion of the p110β isoform of phosphoinositide 3-kinase in platelets reveals its central role in Akt activation and thrombus formation in vitro and in vivo.* Blood, 2010. **115**(10): p. 2008-2013.
55. Manning, B.D. and L.C. Cantley, *AKT/PKB signaling: navigating downstream.* Cell, 2007. **129**(7): p. 1261-74.
56. Bhaskar, P.T. and N. Hay, *The two TORCs and Akt.* Dev Cell, 2007. **12**(4): p. 487-502.
57. Novy, P., et al., *Intrinsic IL-21 Signaling Is Critical for CD8 T Cell Survival and Memory Formation in Response to Vaccinia Viral Infection.* The Journal of Immunology, 2011. **186**(5): p. 2729-2738.
58. Okkenhaug, K., et al., *The p110 Isoform of Phosphoinositide 3-Kinase Controls Clonal Expansion and Differentiation of Th Cells.* The Journal of Immunology, 2006. **177**(8): p. 5122-5128.
59. Fruman, D.A., *Phosphoinositide 3-kinase and its targets in B-cell and T-cell signaling.* Curr Opin Immunol, 2004. **16**(3): p. 314-20.
60. Gerriets, V.A. and J.C. Rathmell, *Metabolic pathways in T cell fate and function.* Trends Immunol, 2012. **33**(4): p. 168-73.
61. Finlay, D.K., et al., *PDK1 regulation of mTOR and hypoxia-inducible factor 1 integrate metabolism and migration of CD8+ T cells.* J Exp Med, 2012. **209**(13): p. 2441-53.
62. Salmond, R.J., et al., *MAPK, Phosphatidylinositol 3-Kinase, and Mammalian Target of Rapamycin Pathways Converge at the Level of Ribosomal Protein S6 Phosphorylation to Control Metabolic Signaling in CD8 T Cells.* The Journal of Immunology, 2009. **183**(11): p. 7388-7397.
63. Efeyan, A. and D.M. Sabatini, *mTOR and cancer: many loops in one pathway.* Current opinion in cell biology, 2010. **22**(2): p. 169-176.
64. Hay, N., *Interplay between FOXO, TOR, and Akt.* Biochim Biophys Acta, 2011. **1813**(11): p. 1965-70.
65. Finlay, D.K., *Regulation of glucose metabolism in T cells: new insight into the role of Phosphoinositide 3-kinases.* Front Immunol, 2012. **3**: p. 247.
66. Berg, L.J., et al., *TEC FAMILY KINASES IN T LYMPHOCYTE DEVELOPMENT AND FUNCTION.* Annu Rev Immunol, 2005. **23**(1): p. 549-600.
67. Yang, W.-C., et al., *Tec Kinase Signaling in T Cells Is Regulated by Phosphatidylinositol 3-Kinase and the Tec Pleckstrin Homology Domain.* The Journal of Immunology, 2001. **166**(1): p. 387-395.
68. Zhong, Y., et al., *Targeting Interleukin-2-Inducible T-cell Kinase (ITK) in T-Cell Related Diseases.* Postdoc journal : a journal of postdoctoral research and postdoctoral affairs, 2014. **2**(6): p. 1-11.
69. Dower, N.A., et al., *RasGRP is essential for mouse thymocyte differentiation and TCR signaling.* Nat Immunol, 2000. **1**: p. 317.

70. Roose, J.P., et al., *A Diacylglycerol-Protein Kinase C-RasGRP1 Pathway Directs Ras Activation upon Antigen Receptor Stimulation of T Cells.* Mol Cell Biol, 2005. **25**(11): p. 4426-4441.
71. Buggy, J.J. and L. Elias, *Bruton Tyrosine Kinase (BTK) and Its Role in B-cell Malignancy.* International Reviews of Immunology, 2012. **31**(2): p. 119-132.
72. Gutierrez, A., et al., *High frequency of PTEN, PI3K, and AKT abnormalities in T-cell acute lymphoblastic leukemia.* Blood, 2009. **114**(3): p. 647-650.
73. Stambolic, V., et al., *Negative Regulation of PKB/Akt-Dependent Cell Survival by the Tumor Suppressor PTEN.* Cell, 1998. **95**(1): p. 29-39.
74. Buckler, J.L., et al., *Cutting Edge: T Cell Requirement for CD28 Costimulation Is Due to Negative Regulation of TCR Signals by PTEN.* The Journal of Immunology, 2006. **177**(7): p. 4262-4266.
75. Suzuki, A., et al., *T Cell-Specific Loss of Pten Leads to Defects in Central and Peripheral Tolerance.* Immunity, 2001. **14**(5): p. 523-534.
76. Newton, R.H., et al., *Suppression of T-cell lymphomagenesis in mice requires PTEN phosphatase activity.* Blood, 2015. **125**(5): p. 852-855.
77. Cristofano, A.D., et al., *Impaired Fas Response and Autoimmunity in Pten^{+/−} Mice.* Science, 1999. **285**(5436): p. 2122-2125.
78. Soond, D.R., et al., *Pten loss in CD4 T cells enhances their helper function but does not lead to autoimmunity or lymphoma.* J Immunol, 2012. **188**(12): p. 5935-43.
79. Kerr, W.G., *Inhibitor and activator: dual functions for SHIP in immunity and cancer.* Annals of the New York Academy of Sciences, 2011. **1217**(1): p. 1-17.
80. Tarasenko, T., et al., *T cell-specific deletion of the inositol phosphatase SHIP reveals its role in regulating Th1/Th2 and cytotoxic responses.* Proc Natl Acad Sci U S A, 2007. **104**(27): p. 11382-7.
81. Garçon, F., et al., *CD28 provides T-cell costimulation and enhances PI3K activity at the immune synapse independently of its capacity to interact with the p85/p110 heterodimer.* Blood, 2008. **111**(3): p. 1464-1471.
82. Boomer, J.S. and J.M. Green, *An enigmatic tail of CD28 signaling.* Cold Spring Harb Perspect Biol, 2010. **2**(8): p. a002436.
83. Parry, R.V., et al., *CD28 and Inducible Costimulatory Protein Src Homology 2 Binding Domains Show Distinct Regulation of Phosphatidylinositol 3-Kinase, Bcl-x_L, and IL-2 Expression in Primary Human CD4 T Lymphocytes.* The Journal of Immunology, 2003. **171**(1): p. 166-174.
84. Fos, C., et al., *ICOS Ligation Recruits the p50α PI3K Regulatory Subunit to the Immunological Synapse.* The Journal of Immunology, 2008. **181**(3): p. 1969-1977.
85. Gigoux, M., et al., *Inducible costimulator promotes helper T-cell differentiation through phosphoinositide 3-kinase.* Proc Natl Acad Sci U S A, 2009. **106**(48): p. 20371-6.
86. Acosta, Y.Y., et al., *Suppression of CD4+ T Lymphocyte Activation in Vitro and Experimental Encephalomyelitis in Vivo by the Phosphatidyl Inositol 3-Kinase Inhibitor PIK-75.* International Journal of Immunopathology and Pharmacology, 2014. **27**(1): p. 53-67.
87. Acosta, Y.Y., et al., *Biased binding of class IA phosphatidyl inositol 3-kinase subunits to inducible costimulator (CD278).* Cellular and Molecular Life Sciences, 2011. **68**(18): p. 3065-3079.
88. Ramadani, F., et al., *The PI3K Isoforms p110α and p110δ Are Essential for Pre–B Cell Receptor Signaling and B Cell Development.* Science Signaling, 2010. **3**(134): p. ra60-ra60.
89. Aragoneses-Fenoll, L., et al., *T-Cell-Specific Loss of the PI-3-Kinase p110α Catalytic Subunit Results in Enhanced Cytokine Production and Antitumor Response.* Front Immunol, 2018. **9**(332).
90. Okkenhaug, K., et al., *Impaired B and T Cell Antigen Receptor Signaling in p110δ PI 3-Kinase Mutant Mice.* Science, 2002. **297**(5583): p. 1031-1034.

91. Banham-Hall, E., M.R. Clatworthy, and K. Okkenhaug, *The Therapeutic Potential for PI3K Inhibitors in Autoimmune Rheumatic Diseases.* The Open Rheumatology Journal, 2012. **6**: p. 245-258.
92. Nashed, B.F., et al., *Role of the phosphoinositide 3-kinase p110delta in generation of type 2 cytokine responses and allergic airway inflammation.* Eur J Immunol, 2007. **37**(2): p. 416-24.
93. Shang, S.-Q., et al., *Inhibition of phosphoinositide 3-kinase delta attenuates experimental autoimmune encephalomyelitis in mice.* International Journal of Clinical and Experimental Medicine, 2015. **8**(11): p. 20645-20651.
94. Haylock-Jacobs, S., et al., *PI3Kdelta drives the pathogenesis of experimental autoimmune encephalomyelitis by inhibiting effector T cell apoptosis and promoting Th17 differentiation.* J Autoimmun, 2011. **36**(3-4): p. 278-87.
95. Soond, D.R., et al., *PI3K p110delta regulates T-cell cytokine production during primary and secondary immune responses in mice and humans.* Blood, 2010. **115**(11): p. 2203-13.
96. Delgoffe, G.M., et al., *The mTOR kinase differentially regulates effector and regulatory T cell lineage commitment.* Immunity, 2009. **30**(6): p. 832-44.
97. Delgoffe, G.M., et al., *The kinase mTOR regulates the differentiation of helper T cells through the selective activation of signaling by mTORc1 and mTORc2.* Nat Immunol, 2011. **12**(4): p. 295-303.
98. Kurebayashi, Y., et al., *PI3K-Akt-mTORc1-S6K1/2 axis controls Th17 differentiation by regulating Gfi1 expression and nuclear translocation of RORgamma.* Cell Rep, 2012. **1**(4): p. 360-73.
99. Lee, K., et al., *Mammalian target of rapamycin protein complex 2 regulates differentiation of Th1 and Th2 cell subsets via distinct signaling pathways.* Immunity, 2010. **32**(6): p. 743-53.
100. Patton, D.T., et al., *Cutting Edge: The Phosphoinositide 3-Kinase p110 Is Critical for the Function of CD4+CD25+Foxp3+ Regulatory T Cells.* The Journal of Immunology, 2006. **177**(10): p. 6598-6602.
101. Ouyang, W., et al., *Foxo proteins cooperatively control the differentiation of Foxp3+ regulatory T cells.* Nat Immunol, 2010. **11**: p. 618.
102. Kerdiles, Y.M., et al., *Foxo transcription factors control regulatory T cell development and function.* Immunity, 2010. **33**(6): p. 890-904.
103. Liu, D., et al., *The p110delta isoform of phosphatidylinositol 3-kinase controls susceptibility to Leishmania major by regulating expansion and tissue homing of regulatory T cells.* J Immunol, 2009. **183**(3): p. 1921-33.
104. Ali, K., et al., *Inactivation of PI(3)K p110delta breaks regulatory T-cell-mediated immune tolerance to cancer.* Nature, 2014. **510**(7505): p. 407-411.
105. Shrestha, S., et al., *Treg cells require the phosphatase PTEN to restrain TH1 and TFH cell responses.* Nat Immunol, 2015. **16**(2): p. 178-87.
106. Huynh, A., et al., *Control of PI(3) kinase in Treg cells maintains homeostasis and lineage stability.* Nat Immunol, 2015. **16**(2): p. 188-96.
107. Nurieva, R.I., et al., *Generation of T follicular helper cells is mediated by interleukin-21 but independent of T helper 1, 2, or 17 cell lineages.* Immunity, 2008. **29**(1): p. 138-49.
108. Nurieva, R.I., et al., *Bcl6 Mediates the Development of T Follicular Helper Cells.* Science, 2009. **325**(5943): p. 1001-1005.
109. Yu, D., et al., *The transcriptional repressor Bcl-6 directs T follicular helper cell lineage commitment.* Immunity, 2009. **31**(3): p. 457-68.
110. Rolf, J., et al., *Phosphoinositide 3-kinase activity in T cells regulates the magnitude of the germinal center reaction.* J Immunol, 2010. **185**(7): p. 4042-52.
111. Stone, E.L., et al., *ICOS coreceptor signaling inactivates the transcription factor FOXO1 to promote Tfh cell differentiation.* Immunity, 2015. **42**(2): p. 239-251.
112. Weber, J.P., et al., *ICOS maintains the T follicular helper cell phenotype by down-regulating Kruppel-like factor 2.* J Exp Med, 2015. **212**(2): p. 217-33.

113. Lee, J.Y., et al., *The transcription factor KLF2 restrains CD4(+) T follicular helper cell differentiation.* Immunity, 2015. **42**(2): p. 252-264.
114. Ye, L., et al., *mTOR Promotes Antiviral Humoral Immunity by Differentially Regulating CD4 Helper T Cell and B Cell Responses.* J Virol, 2017. **91**(4).
115. Pearce, V.Q., et al., *PI3Kdelta Regulates the Magnitude of CD8+ T Cell Responses after Challenge with Listeria monocytogenes.* J Immunol, 2015. **195**(7): p. 3206-17.
116. Putz, E.M., et al., *PI3Kdelta is essential for tumor clearance mediated by cytotoxic T lymphocytes.* PLoS One, 2012. **7**(7): p. e40852.
117. Berard, M. and D.F. Tough, *Qualitative differences between naïve and memory T cells.* Immunology, 2002. **106**(2): p. 127-138.
118. Okkenhaug, K., et al., *Impaired B and T cell antigen receptor signaling in p110delta PI 3-kinase mutant mice.* Science's STKE, 2002. **297**(5583): p. 1031.
119. Gracias, D.T., et al., *Phosphatidylinositol 3-Kinase p110delta Isoform Regulates CD8+ T Cell Responses during Acute Viral and Intracellular Bacterial Infections.* J Immunol, 2016. **196**(3): p. 1186-98.
120. Sarkar, S., et al., *Functional and genomic profiling of effector CD8 T cell subsets with distinct memory fates.* J Exp Med, 2008. **205**(3): p. 625-40.
121. Kim, E.H., et al., *Signal integration by Akt regulates CD8 T cell effector and memory differentiation.* J Immunol, 2012. **188**(9): p. 4305-14.
122. Hand, T.W., et al., *Differential effects of STAT5 and PI3K/AKT signaling on effector and memory CD8 T-cell survival.* Proc Natl Acad Sci U S A, 2010. **107**(38): p. 16601-6.
123. Hess Michelini, R., et al., *Differentiation of CD8 memory T cells depends on Foxo1.* J Exp Med, 2013. **210**(6): p. 1189-200.
124. Rao, R.R., et al., *Transcription factor Foxo1 represses T-bet-mediated effector functions and promotes memory CD8(+) T cell differentiation.* Immunity, 2012. **36**(3): p. 374-87.
125. Kim, M.V., et al., *The transcription factor Foxo1 controls central-memory CD8+ T cell responses to infection.* Immunity, 2013. **39**(2): p. 286-97.
126. Tzelepis, F., et al., *Intrinsic role of FoxO3a in the development of CD8+ T cell memory.* J Immunol, 2013. **190**(3): p. 1066-75.
127. Sullivan, J.A., et al., *FOXO3 regulates the CD8 T cell response to a chronic viral infection.* J Virol, 2012. **86**(17): p. 9025-34.
128. Sullivan, J.A., et al., *FOXO3 regulates CD8 T cell memory by T cell-intrinsic mechanisms.* PLoS Pathog, 2012. **8**(2): p. e1002533.
129. Togher, S., et al., *FoxO3 is a negative regulator of primary CD8+ T-cell expansion but not of memory formation.* Immunol Cell Biol, 2015. **93**(2): p. 120-5.
130. Dejean, A.S., et al., *Transcription factor Foxo3 controls the magnitude of T cell immune responses by modulating the function of dendritic cells.* Nat Immunol, 2009. **10**(5): p. 504-13.
131. Araki, K., et al., *mTOR regulates memory CD8 T-cell differentiation.* Nature, 2009. **460**(7251): p. 108-12.
132. Rao, R.R., et al., *The mTOR kinase determines effector versus memory CD8+ T cell fate by regulating the expression of transcription factors T-bet and Eomesodermin.* Immunity, 2010. **32**(1): p. 67-78.
133. Pollizzi, K.N., et al., *mTORc1 and mTORc2 selectively regulate CD8+ T cell differentiation.* J Clin Invest, 2015. **125**(5): p. 2090-2108.
134. Shrestha, S., et al., *Tsc1 promotes the differentiation of memory CD8⁺ T cells via orchestrating the transcriptional and metabolic programs.* Proceedings of the National Academy of Sciences, 2014. **111**(41): p. 14858-14863.
135. Zhang, L., et al., *Mammalian Target of Rapamycin Complex 2 Controls CD8 T Cell Memory Differentiation in a Foxo1-Dependent Manner.* Cell Rep, 2016. **14**(5): p. 1206-1217.

136. Staron, M.M., et al., *The transcription factor FoxO1 sustains expression of the inhibitory receptor PD-1 and survival of antiviral CD8(+) T cells during chronic infection.* Immunity, 2014. **41**(5): p. 802-14.
137. Lucas, C.L., et al., *Heterozygous splice mutation in PIK3R1 causes human immunodeficiency with lymphoproliferation due to dominant activation of PI3K.* J Exp Med, 2014. **211**(13): p. 2537-47.
138. Angulo, I., et al., *Phosphoinositide 3-kinase delta gene mutation predisposes to respiratory infection and airway damage.* Science, 2013. **342**(6160): p. 866-71.
139. Michalovich, D. and S. Nejentsev, *Activated PI3 Kinase Delta Syndrome: From Genetics to Therapy.* Front Immunol, 2018. **9**(369).
140. !!! INVALID CITATION !!!
141. Lucas, C.L., et al., *Dominant-activating germline mutations in the gene encoding the PI(3)K catalytic subunit p110delta result in T cell senescence and human immunodeficiency.* Nat Immunol, 2014. **15**(1): p. 88-97.
142. Jou, S.-T., et al., *Identification of variations in the human phosphoinositide 3-kinase p110δ gene in children with primary B-cell immunodeficiency of unknown aetiology.* International Journal of Immunogenetics, 2006. **33**(5): p. 361-369.
143. Burke, J.E., et al., *Oncogenic mutations mimic and enhance dynamic events in the natural activation of phosphoinositide 3-kinase p110alpha (PIK3CA).* Proc Natl Acad Sci U S A, 2012. **109**(38): p. 15259-64.
144. Wan, G., et al., *The H1047R point mutation in p110 alpha changes the morphology of human colon HCT116 cancer cells.* Cell Death Discovery, 2015. **1**: p. 15044.
145. Crank, M.C., et al., *Mutations in PIK3CD can cause hyper IgM syndrome (HIGM) associated with increased cancer susceptibility.* J Clin Immunol, 2014. **34**(3): p. 272-6.
146. Tsujita, Y., et al., *Phosphatase and tensin homolog (PTEN) mutation can cause activated phosphatidylinositol 3-kinase delta syndrome-like immunodeficiency.* J Allergy Clin Immunol, 2016. **138**(6): p. 1672-1680 e10.
147. Heurtier, L., et al., *Mutations in the adaptor-binding domain and associated linker region of p110δ cause Activated PI3K-δ Syndrome 1 (APDS1).* Haematologica, 2017. **102**(7): p. e278-e281.
148. Luo, Y., et al., *Identification of a novel de novo gain-of-function mutation of PIK3CD in a patient with activated phosphoinositide 3-kinase δ syndrome.* Clinical Immunology, 2018. **197**: p. 60-67.
149. Wentink, M., et al., *Genetic defects in PI3Kδ affect B-cell differentiation and maturation leading to hypogammaglobulineamia and recurrent infections.* Clinical Immunology, 2017. **176**: p. 77-86.
150. Dulau Florea, A.E., et al., *Abnormal B-cell maturation in the bone marrow of patients with germline mutations in PIK3CD.* J Allergy Clin Immunol, 2017. **139**(3): p. 1032-1035 e6.
151. Coulter, T.I., et al., *Clinical spectrum and features of activated phosphoinositide 3-kinase delta syndrome: A large patient cohort study.* J Allergy Clin Immunol, 2017. **139**(2): p. 597-606 e4.
152. Kracker, S., et al., *Occurrence of B-cell lymphomas in patients with activated phosphoinositide 3-kinase delta syndrome.* J Allergy Clin Immunol, 2014. **134**(1): p. 233-6.
153. Wentink, M.W.J., et al., *Exhaustion of the CD8(+) T Cell Compartment in Patients with Mutations in Phosphoinositide 3-Kinase Delta.* Front Immunol, 2018. **9**: p. 446.
154. Cannons, J.L., et al., *Genetic Defects in Phosphoinositide 3-Kinase delta Influence CD8(+) T Cell Survival, Differentiation, and Function.* Front Immunol, 2018. **9**: p. 1758.
155. Edwards, E.S.J., et al., *Activating PIK3CD mutations impair human cytotoxic lymphocyte differentiation and function and EBV immunity.* J Allergy Clin Immunol, 2018.
156. Hauck, F., et al., *Variant PIK3R1 Hypermorphic Mutation and Clinical Phenotypes in a Family with Short Statures, Mild Immunodeficiency and Lymphoma.* Klin Padiatr, 2017. **229**(03): p. 113-117.

157. Deau, M.-C., et al., *A human immunodeficiency caused by mutations in the PIK3R1 gene.* J Clin Invest, 2014. **124**(9): p. 3923-3928.
158. Martinez-Saavedra, M.T., et al., *Gain-of-function mutation in PIK3R1 in a patient with a narrow clinical phenotype of respiratory infections.* Clin Immunol, 2016. **173**: p. 117-120.
159. Kuhlen, M., et al., *De novo PIK3R1 gain-of-function with recurrent sinopulmonary infections, long-lasting chronic CMV-lymphadenitis and microcephaly.* Clin Immunol, 2016. **162**: p. 27-30.
160. Petrovski, S., et al., *Dominant Splice Site Mutations in PIK3R1 Cause Hyper IgM Syndrome, Lymphadenopathy and Short Stature.* J Clin Immunol, 2016. **36**(5): p. 462-71.
161. Dornan, G.L., et al., *Conformational disruption of PI3Kδ regulation by immunodeficiency mutations in PIK3CD and PIK3R1.* Proceedings of the National Academy of Sciences, 2017. **114**(8): p. 1982-1987.
162. Dyment, David A., et al., *Mutations in PIK3R1 Cause SHORT Syndrome.* The American Journal of Human Genetics, 2013. **93**(1): p. 158-166.
163. Bárcena, C., et al., *Exome sequencing identifies a novel mutation in PIK3R1 as the cause of SHORT syndrome.* BMC Medical Genetics, 2014. **15**(1): p. 51.
164. Boisson, B., P. Quartier, and J.-L. Casanova, *Immunological loss-of-function due to genetic gain-of-function in humans: autosomal dominance of the third kind.* Current Opinion in Immunology, 2015. **32**: p. 90-105.
165. Driessen, G.J., et al., *Increased PI3K/Akt activity and deregulated humoral immune response in human PTEN deficiency.* Journal of Allergy and Clinical Immunology, 2016. **138**(6): p. 1744-1747.e5.
166. Browning, M.J., et al., *Cowden's syndrome with immunodeficiency.* Journal of Medical Genetics, 2015. **52**(12): p. 856-859.
167. Schubert, D., et al., *Autosomal dominant immune dysregulation syndrome in humans with CTLA4 mutations.* Nat Med, 2014. **20**(12): p. 1410-6.
168. Rudd, C.E. and H. Schneider, *Unifying concepts in CD28, ICOS and CTLA4 co-receptor signalling.* Nat Rev Immunol, 2003. **3**(7): p. 544-56.
169. S Lear, A.C., *Respiratory infection and primary immune deficiency – what does the general physician need to know?* J R Coll Physicians Edinb, 2014. **44**: p. 149-55.
170. Furman, R.R., et al., *Idelalisib and Rituximab in Relapsed Chronic Lymphocytic Leukemia.* New England Journal of Medicine, 2014. **370**(11): p. 997-1007.
171. Gopal, A.K., et al., *PI3Kdelta inhibition by idelalisib in patients with relapsed indolent lymphoma.* N Engl J Med, 2014. **370**(11): p. 1008-18.
172. Rao, V.K., et al., *Effective 'Activated PI3Kδ Syndrome'-targeted therapy with the PI3Kδ inhibitor leniolisib.* Blood, 2017.
173. Radoshevich, L. and P. Cossart, *Listeria monocytogenes: towards a complete picture of its physiology and pathogenesis.* Nature Reviews Microbiology, 2017. **16**: p. 32.
174. Cossart, P. and A. Helenius, *Endocytosis of viruses and bacteria.* Cold Spring Harbor perspectives in biology, 2014. **6**.
175. Bonazzi, M., M. Lecuit, and P. Cossart, *Listeria monocytogenes internalin and E-cadherin: from bench to bedside.* Cold Spring Harbor perspectives in biology, 2009. **1**: p. a003087.
176. Lecuit, M., et al., *A single amino acid in E-cadherin responsible for host specificity towards the human pathogen Listeria monocytogenes.* The EMBO Journal, 1999. **18**: p. 3956-3963.
177. Lecuit, M., et al., *A Transgenic Model for Listeriosis: Role of Internalin in Crossing the Intestinal Barrier.* Science, 2001. **292**(5522): p. 1722-1725.
178. Bou Ghanem, E.N., et al., *InlA Promotes Dissemination of Listeria monocytogenes to the Mesenteric Lymph Nodes during Food Borne Infection of Mice.* PLoS Pathog, 2012. **8**(11): p. e1003015-e1003015.
179. Pitts, M.G. and S.E.F. D'Orazio, *A Comparison of Oral and Intravenous Mouse Models of Listeriosis.* Pathogens, 2018. **7**(1): p. 13-13.

180. Shen, Y., et al., *InIB-dependent internalization of Listeria is mediated by the Met receptor tyrosine kinase.* Cell, 2000. **103**: p. 501-10.
181. Gaillard, J.L., F. Jaubert, and P. Berche, *The inlAB locus mediates the entry of Listeria monocytogenes into hepatocytes in vivo.* The Journal of experimental medicine, 1996. **183**: p. 359-69.
182. Smith, G.A., et al., *The two distinct phospholipases C of Listeria monocytogenes have overlapping roles in escape from a vacuole and cell-to-cell spread.* Infect Immun, 1995. **63**(11): p. 4231-7.
183. Xayarath, B., F. Alonzo, and N.E. Freitag, *Identification of a peptide-pheromone that enhances Listeria monocytogenes escape from host cell vacuoles.* PLoS Pathog, 2015. **11**(3): p. e1004707-e1004707.
184. Birmingham, C.L., et al., *Listeriolysin O allows Listeria monocytogenes replication in macrophage vacuoles.* Nature, 2008. **451**: p. 350-354.
185. Hamon, M., H. Bierne, and P. Cossart, *Listeria monocytogenes: a multifaceted model.* Nature Reviews Microbiology, 2006. **4**: p. 423-434.
186. Khan, S.H. and V.P. Badovinac, *Listeria monocytogenes: a model pathogen to study antigen-specific memory CD8 T cell responses.* Seminars in immunopathology, 2015. **37**: p. 301-10.
187. Zenewicz, L.A. and H. Shen, *Innate and adaptive immune responses to Listeria monocytogenes: a short overview.* Microbes and Infection, 2007. **9**: p. 1208-1215.
188. Ozören, N., et al., *Distinct roles of TLR2 and the adaptor ASC in IL-1beta/IL-18 secretion in response to Listeria monocytogenes.* Journal of immunology (Baltimore, Md. : 1950), 2006. **176**(7): p. 4337-42.
189. Torres, D., et al., *Toll-like receptor 2 is required for optimal control of Listeria monocytogenes infection.* Infect Immun, 2004. **72**(4): p. 2131-9.
190. Seki, E., et al., *Critical roles of myeloid differentiation factor 88-dependent proinflammatory cytokine release in early phase clearance of Listeria monocytogenes in mice.* Journal of immunology (Baltimore, Md. : 1950), 2002. **169**: p. 3863-8.
191. Edelson, B.T. and E.R. Unanue, *MyD88-dependent but Toll-like receptor 2-independent innate immunity to Listeria: no role for either in macrophage listericidal activity.* Journal of immunology (Baltimore, Md. : 1950), 2002. **169**(7): p. 3869-75.
192. Schuppler, M. and M.J. Loessner, *The Opportunistic Pathogen Listeria monocytogenes: Pathogenicity and Interaction with the Mucosal Immune System.* International journal of inflammation, 2010. **2010**: p. 704321.
193. Barreau, F., et al., *CARD15/NOD2 Is Required for Peyer's Patches Homeostasis in Mice.* PLoS ONE, 2007. **2**: p. e523.
194. Rogers, H.W. and E.R. Unanue, *Neutrophils are involved in acute, nonspecific resistance to Listeria monocytogenes in mice.* Infection and immunity, 1993. **61**: p. 5090-6.
195. Witter, A.R., B.M. Okunnu, and R.E. Berg, *The Essential Role of Neutrophils during Infection with the Intracellular Bacterial Pathogen Listeria monocytogenes.* Journal of immunology (Baltimore, Md. : 1950), 2016. **197**: p. 1557-65.
196. Conlan, J.W. and R.J. North, *Neutrophils are essential for early anti-Listeria defense in the liver, but not in the spleen or peritoneal cavity, as revealed by a granulocyte-depleting monoclonal antibody.* J Exp Med, 1994. **179**(1): p. 259-68.
197. Carr, K.D., et al., *Specific depletion reveals a novel role for neutrophil-mediated protection in the liver during Listeria monocytogenes infection.* European Journal of Immunology, 2011. **41**(9): p. 2666-2676.
198. Segal, A.W., *HOW NEUTROPHILS KILL MICROBES.* Annual Review of Immunology, 2005. **23**: p. 197-223.
199. Gregory, S.H., L.K. Barczynski, and E.J. Wing, *Effector function of hepatocytes and Kupffer cells in the resolution of systemic bacterial infections.* Journal of Leukocyte Biology, 1992. **51**: p. 421-424.

200. Tripp, C.S., S.F. Wolf, and E.R. Unanue, *Interleukin 12 and tumor necrosis factor alpha are costimulators of interferon gamma production by natural killer cells in severe combined immunodeficiency mice with listeriosis, and interleukin 10 is a physiologic antagonist.* Proceedings of the National Academy of Sciences of the United States of America, 1993. **90**: p. 3725-9.
201. Shaughnessy, L.M. and J.A. Swanson, *The role of the activated macrophage in clearing Listeria monocytogenes infection.* Frontiers in bioscience : a journal and virtual library, 2007. **12**: p. 2683-92.
202. Stavru, F., C. Archambaud, and P. Cossart, *Cell biology and immunology of Listeria monocytogenes infections: novel insights.* Immunological Reviews, 2011. **240**: p. 160-184.
203. Skoberne, M., et al., *Dynamic antigen presentation patterns of Listeria monocytogenes-derived CD8 T cell epitopes in vivo.* Journal of immunology (Baltimore, Md. : 1950), 2001. **167**: p. 2209-18.
204. Jung, S., et al., *In vivo depletion of CD11c+ dendritic cells abrogates priming of CD8+ T cells by exogenous cell-associated antigens.* Immunity, 2002. **17**: p. 211-20.
205. Reinicke, A.T., et al., *Dendritic Cell Cross-Priming Is Essential for Immune Responses to Listeria monocytogenes.* PLoS ONE, 2009. **4**: p. e7210.
206. Janda, J., et al., *Cross-presentation of Listeria-derived CD8 T cell epitopes requires unstable bacterial translation products.* Journal of immunology (Baltimore, Md. : 1950), 2004. **173**: p. 5644-51.
207. Tvinnereim, A.R., S.E. Hamilton, and J.T. Harty, *CD8(+)-T-cell response to secreted and nonsecreted antigens delivered by recombinant Listeria monocytogenes during secondary infection.* Infection and immunity, 2002. **70**: p. 153-62.
208. Badovinac, V.P., B.B. Porter, and J.T. Harty, *Programmed contraction of CD8+ T cells after infection.* Nature Immunology, 2002. **3**: p. 619-626.
209. Pepper, M., et al., *Different routes of bacterial infection induce long-lived TH1 memory cells and short-lived TH17 cells.* Nature immunology, 2010. **11**: p. 83-9.
210. Emmerling, P., H. Finger, and J. Bockemühl, *Listeria monocytogenes infection in nude mice.* Infect Immun, 1975. **12**(2): p. 437-9.
211. Newborg, M.F. and R.J. North, *On the mechanism of T cell-independent anti-Listeria resistance in nude mice.* Journal of immunology (Baltimore, Md. : 1950), 1980. **124**(2): p. 571-6.
212. Carrero, J.A., B. Calderon, and E.R. Unanue, *Lymphocytes are detrimental during the early innate immune response against Listeria monocytogenes.* J Exp Med, 2006. **203**(4): p. 933-40.
213. O'Connell, R.M., et al., *Type I interferon production enhances susceptibility to Listeria monocytogenes infection.* J Exp Med, 2004. **200**(4): p. 437-45.
214. Carrero, J.A., B. Calderon, and E.R. Unanue, *Type I Interferon Sensitizes Lymphocytes to Apoptosis and Reduces Resistance to Listeria Infection.* J Exp Med, 2004. **200**(4): p. 535-540.
215. Carrero, J.A., B. Calderon, and E.R. Unanue, *Listeriolysin O from Listeria monocytogenes is a lymphocyte apoptogenic molecule.* J Immunol, 2004. **172**(8): p. 4866-4874.
216. Kursar, M., et al., *Organ-specific CD4+ T cell response during Listeria monocytogenes infection.* Journal of immunology (Baltimore, Md. : 1950), 2002. **168**: p. 6382-7.
217. Shen, H., et al., *A specific role for B cells in the generation of CD8 T cell memory by recombinant Listeria monocytogenes.* Journal of immunology (Baltimore, Md. : 1950), 2003. **170**: p. 1443-51.
218. Zhai, S.L., et al., *Influenza D Virus in Animal Species in Guangdong Province, Southern China.* Emerg Infect Dis, 2017. **23**(8): p. 1392-1396.
219. Bouvier, N.M. and P. Palese, *The biology of influenza viruses.* Vaccine, 2008. **26**: p. D49-D53.
220. Chen, X., et al., *Host Immune Response to Influenza A Virus Infection.* Front Immunol, 2018. **9**(320).
221. Ibricevic, A., et al., *Influenza Virus Receptor Specificity and Cell Tropism in Mouse and Human Airway Epithelial Cells.* Journal of Virology, 2006. **80**: p. 7469-7480.

222. Bouvier, N.M. and A.C. Lowen, *Animal Models for Influenza Virus Pathogenesis and Transmission.* Viruses, 2010. **2**(8): p. 1530-1563.
223. Gerber, P., C.G. Loosli, and D. Hambre, *Antigenic variants of influenza A virus, PR8 strain. I. Their development during serial passage in the lungs of partially immune mice.* J Exp Med, 1955. **101**(6): p. 627-38.
224. Askovich, P.S., et al., *Differential host response, rather than early viral replication efficiency, correlates with pathogenicity caused by influenza viruses.* PloS one, 2013. **8**: p. e74863.
225. Laidlaw, B.J., et al., *Cooperativity Between CD8+ T Cells, Non-Neutralizing Antibodies, and Alveolar Macrophages Is Important for Heterosubtypic Influenza Virus Immunity.* PLoS Pathogens, 2013. **9**: p. e1003207.
226. Quan, F.S., et al., *A bivalent influenza VLP vaccine confers complete inhibition of virus replication in lungs.* Vaccine, 2008. **26**(26): p. 3352-3361.
227. Blazejewska, P., et al., *Pathogenicity of different PR8 influenza A virus variants in mice is determined by both viral and host factors.* Virology, 2011. **412**(1): p. 36-45.
228. Ward, A.C., *Changes in the neuraminidase of neurovirulent influenza virus strains.* Virus Genes, 1995. **10**(3): p. 253-260.
229. Goto, H. and Y. Kawaoka, *A novel mechanism for the acquisition of virulence by a human influenza A virus.* Proc Natl Acad Sci U S A, 1998. **95**(17): p. 10224-8.
230. Mueller, S., et al., *Live attenuated influenza virus vaccines by computer-aided rational design.* Nature biotechnology, 2010. **28**: p. 723-6.
231. Medina, R.A. and A. García-Sastre, *Influenza A viruses: new research developments.* Nature Reviews Microbiology, 2011. **9**: p. 590-603.
232. Rutigliano, J.A., et al., *Highly Pathological Influenza A Virus Infection Is Associated with Augmented Expression of PD-1 by Functionally Compromised Virus-Specific CD8+ T Cells.* Journal of Virology, 2014. **88**: p. 1636-1651.
233. Manicassamy, B., et al., *Analysis of in vivo dynamics of influenza virus infection in mice using a GFP reporter virus.* Proceedings of the National Academy of Sciences, 2010. **107**: p. 11531-11536.
234. Pulendran, B. and M.S. Maddur, *Innate immune sensing and response to influenza.* Current topics in microbiology and immunology, 2015. **386**: p. 23-71.
235. Vareille, M., et al., *The airway epithelium: soldier in the fight against respiratory viruses.* Clinical microbiology reviews, 2011. **24**: p. 210-29.
236. Ho, A.W.S., et al., *Lung CD103+ Dendritic Cells Efficiently Transport Influenza Virus to the Lymph Node and Load Viral Antigen onto MHC Class I for Presentation to CD8 T Cells.* The Journal of Immunology, 2011. **187**: p. 6011-6021.
237. Kim, T.S. and T.J. Braciale, *Respiratory dendritic cell subsets differ in their capacity to support the induction of virus-specific cytotoxic CD8+ T cell responses.* PLoS One, 2009. **4**(1): p. e4204-e4204.
238. McGill, J., N. Van Rooijen, and K.L. Legge, *Protective influenza-specific CD8 T cell responses require interactions with dendritic cells in the lungs.* The Journal of experimental medicine, 2008. **205**: p. 1635-46.
239. Pichlmair, A., et al., *RIG-I-Mediated Antiviral Responses to Single-Stranded RNA Bearing 5'-Phosphates.* Science, 2006. **314**: p. 997-1001.
240. Yoneyama, M., et al., *Viral RNA detection by RIG-I-like receptors.* Current Opinion in Immunology, 2015. **32**: p. 48-53.
241. Schulz, O., et al., *Toll-like receptor 3 promotes cross-priming to virus-infected cells.* Nature, 2005. **433**: p. 887-892.
242. Lund, J.M., et al., *Recognition of single-stranded RNA viruses by Toll-like receptor 7.* Proceedings of the National Academy of Sciences, 2004. **101**: p. 5598-5603.
243. McAuley, J.L., et al., *Activation of the NLRP3 Inflammasome by IAV Virulence Protein PB1-F2 Contributes to Severe Pathophysiology and Disease.* PLoS Pathogens, 2013. **9**: p. e1003392.

244. Pothlichet, J., et al., *Type I IFN Triggers RIG-I/TLR3/NLRP3-dependent Inflammasome Activation in Influenza A Virus Infected Cells.* PLoS Pathog, 2013. **9**(4): p. e1003256-e1003256.
245. Mordstein, M., et al., *Interferon-λ Contributes to Innate Immunity of Mice against Influenza A Virus but Not against Hepatotropic Viruses.* PLoS Pathogens, 2008. **4**: p. e1000151.
246. Schneider, W.M., M.D. Chevillotte, and C.M. Rice, *Interferon-stimulated genes: a complex web of host defenses.* Annual review of immunology, 2014. **32**: p. 513-45.
247. Staeheli, P., et al., *Mx protein: constitutive expression in 3T3 cells transformed with cloned Mx cDNA confers selective resistance to influenza virus.* Cell, 1986. **44**: p. 147-58.
248. Kreijtz, J.H.C.M., R.A.M. Fouchier, and G.F. Rimmelzwaan, *Immune responses to influenza virus infection.* Virus Research, 2011. **162**: p. 19-30.
249. Soghoian, D.Z. and H. Streeck, *Cytolytic CD4(+) T cells in viral immunity.* Expert review of vaccines, 2010. **9**: p. 1453-63.
250. Marshall, N.B., et al., *NKG2C/E Marks the Unique Cytotoxic CD4 T Cell Subset, ThCTL, Generated by Influenza Infection.* Journal of immunology (Baltimore, Md. : 1950), 2017. **198**(3): p. 1142-1155.
251. Brown, D.M., et al., *Multifunctional CD4 cells expressing gamma interferon and perforin mediate protection against lethal influenza virus infection.* J Virol, 2012. **86**(12): p. 6792-803.
252. Hua, L., et al., *Cytokine-Dependent Induction of CD4+ T cells with Cytotoxic Potential during Influenza Virus Infection.* J Virol, 2013. **87**(21): p. 11884-11893.
253. Mozdzanowska, K., et al., *Treatment of Influenza Virus-Infected SCID Mice with Nonneutralizing Antibodies Specific for the Transmembrane Proteins Matrix 2 and Neuraminidase Reduces the Pulmonary Virus Titer but Fails to Clear the Infection.* Virology, 1999. **254**: p. 138-146.
254. Carragher, D.M., et al., *A novel role for non-neutralizing antibodies against nucleoprotein in facilitating resistance to influenza virus.* Journal of immunology (Baltimore, Md. : 1950), 2008. **181**: p. 4168-76.
255. Sridhar, S., *Heterosubtypic T-Cell Immunity to Influenza in Humans: Challenges for Universal T-Cell Influenza Vaccines.* Frontiers in immunology, 2016. **7**: p. 195.
256. Jayasekera, J.P., E.A. Moseman, and M.C. Carroll, *Natural Antibody and Complement Mediate Neutralization of Influenza Virus in the Absence of Prior Immunity.* J Virol, 2007. **81**(7): p. 3487-3494.
257. ZWEERINK, H.J., et al., *Cytotoxic T cells kill influenza virus infected cells but do not distinguish between serologically distinct type A viruses.* Nature, 1977. **267**: p. 354-356.
258. Braciale, T.J., *Immunologic recognition of influenza virus-infected cells. II. Expression of influenza A matrix protein on the infected cell surface and its role in recognition by cross-reactive cytotoxic T cells.* The Journal of experimental medicine, 1977. **146**: p. 673-89.
259. Sevilla, N., et al., *Immunosuppression and resultant viral persistence by specific viral targeting of dendritic cells.* The Journal of experimental medicine, 2000. **192**: p. 1249-1260.
260. Borrow, P. and M.B.A. Oldstone, *Mechanism of lymphocytic choriomeningitis virus entry into cells.* Virology, 1994. **198**: p. 1-9.
261. Cao, W., et al., *Identification of α-dystroglycan as a receptor for lymphocytic choriomeningitis virus and Lassa fever virus.* Science, 1998. **282**: p. 2079-2081.
262. Riviere, Y., et al., *NOTES The S RNA Segment of Lymphocytic Choriomeningitis Virus Codes for the Nucleoprotein and Glycoproteins 1 and 2t.* JOURNAL OF VIROLOGY, 1985. **53**: p. 966-968.
263. Cornu, T.I., J.C. De, and L. Torre, *RING Finger Z Protein of Lymphocytic Choriomeningitis Virus (LCMV) Inhibits Transcription and RNA Replication of an LCMV S-Segment Minigenome.* J Virol, 2001. **75**(19): p. 9415-9426.
264. Cornu, T.I., H. Feldmann, and J. Carlos De La Torre, *Cells Expressing the RING Finger Z Protein Are Resistant to Arenavirus Infection.* JOURNAL OF VIROLOGY, 2004. **78**: p. 2979-2983.
265. Fehling, S.K., F. Lennartz, and T. Strecker, *Multifunctional nature of the arenavirus RING finger protein Z*, 2012, Multidisciplinary Digital Publishing Institute (MDPI). p. 2973-3011.

266. Dutko, F.J. and M.B.A. Oldstone, *Genomic and Biological Variation among Commonly Used Lymphocytic Choriomeningitis Virus Strains*, 1983. p. 1689-1698.
267. Zhou, X., et al., *Role of lymphocytic choriomeningitis virus (LCMV) in understanding viral immunology: Past, present and future.* Viruses, 2012. **4**: p. 2650-2669.
268. Armstrong, C. and R.D. Lillie, *Experimental Lymphocytic Choriomeningitis of Monkeys and Mice Produced by a Virus Encountered in Studies of the 1933 St. Louis Encephalitis Epidemic.* Public Health Reports (1896-1970), 1934. **49**(35): p. 1019-1019.
269. Matloubian, M., et al., *Molecular determinants of macrophage tropism and viral persistence: importance of single amino acid changes in the polymerase and glycoprotein of lymphocytic choriomeningitis virus.* Journal of virology, 1993. **67**: p. 7340-9.
270. Salvato, M., et al., *Molecular basis of viral persistence: a single amino acid change in the glycoprotein of lymphocytic choriomeningitis virus is associated with suppression of the antiviral cytotoxic T-lymphocyte response and establishment of persistence.* Journal of virology, 1991. **65**: p. 1863-9.
271. Smelt, S.C., et al., *Differences in affinity of binding of lymphocytic choriomeningitis virus strains to the cellular receptor alpha-dystroglycan correlate with viral tropism and disease kinetics.* J Virol, 2001. **75**(1): p. 448-57.
272. Ahmed, R., et al., *Genetic analysis of in vivo-selected viral variants causing chronic infection: importance of mutation in the L RNA segment of lymphocytic choriomeningitis virus.* J Virol, 1988. **62**(9): p. 3301-8.
273. Bergthaler, A., et al., *Viral replicative capacity is the primary determinant of lymphocytic choriomeningitis virus persistence and immunosuppression.* Proc Natl Acad Sci U S A, 2010. **107**(50): p. 21641-6.
274. Kunz, S., et al., *Molecular analysis of the interaction of LCMV with its cellular receptor-dystroglycan.* The Journal of Cell Biology, 2001. **155**(2): p. 301-310.
275. Loo, Y.-M. and M. Gale, *Immune Signaling by RIG-I-like Receptors.* Immunity, 2011. **34**: p. 680-692.
276. Kawai, T. and S. Akira, *Toll-like Receptors and Their Crosstalk with Other Innate Receptors in Infection and Immunity.* Immunity, 2011. **34**: p. 637-650.
277. Jung, A., et al., *Lymphocytoid choriomeningitis virus activates plasmacytoid dendritic cells and induces a cytotoxic T-cell response via MyD88.* Journal of virology, 2008. **82**: p. 196-206.
278. Clingan, J.M., et al., *Differential roles for RIG-I-like receptors and nucleic acid-sensing TLR pathways in controlling a chronic viral infection.* Journal of immunology (Baltimore, Md. : 1950), 2012. **188**: p. 4432-40.
279. Belz, G.T., et al., *CD8alpha+ dendritic cells selectively present MHC class I-restricted noncytolytic viral and intracellular bacterial antigens in vivo.* Journal of immunology (Baltimore, Md. : 1950), 2005. **175**: p. 196-200.
280. Dalod, M., et al., *Dendritic Cell Responses to Early Murine Cytomegalovirus Infection.* The Journal of Experimental Medicine, 2003. **197**: p. 885-898.
281. Kägi, D., et al., *Cytotoxicity mediated by T cells and natural killer cells is greatly impaired in perforin-deficient mice.* Nature, 1994. **369**: p. 31-37.
282. Nansen, A., et al., *Compromised virus control and augmented perforin-mediated immunopathology in IFN-gamma-deficient mice infected with lymphocytic choriomeningitis virus.* Journal of immunology (Baltimore, Md. : 1950), 1999. **163**(11): p. 6114-22.
283. Ciurea, A., et al., *Impairment of CD4(+) T cell responses during chronic virus infection prevents neutralizing antibody responses against virus escape mutants.* J Exp Med, 2001. **193**(3): p. 297-305.
284. Fuller, M.J., et al., *Maintenance, Loss, and Resurgence of T Cell Responses During Acute, Protracted, and Chronic Viral Infections.* The Journal of Immunology, 2004. **172**(7): p. 4204-4214.

285. Ahmed, R., et al., *Selection of genetic variants of lymphocytic choriomeningitis virus in spleens of persistently infected mice. Role in suppression of cytotoxic T lymphocyte response and viral persistence.* The Journal of experimental medicine, 1984. **160**: p. 521-40.
286. Norris, B.A., et al., *Chronic but Not Acute Virus Infection Induces Sustained Expansion of Myeloid Suppressor Cell Numbers that Inhibit Viral-Specific T Cell Immunity.* Immunity, 2013. **38**(2): p. 309-321.
287. Wherry, E.J., *T cell exhaustion.* Nature Immunology, 2011. **12**: p. 492-499.
288. Vella, L.A., R.S. Herati, and E.J. Wherry, *CD4+T Cell Differentiation in Chronic Viral Infections: The Tfh Perspective*, 2017. p. 1072-1087.
289. Matloubian, M., R.J. Concepcion, and R. Ahmed, *CD4+ T cells are required to sustain CD8+ cytotoxic T-cell responses during chronic viral infection.* Journal of virology, 1994. **68**: p. 8056-63.
290. Brooks, D.G., et al., *Intrinsic functional dysregulation of CD4 T cells occurs rapidly following persistent viral infection.* Journal of virology, 2005. **79**: p. 10514-27.
291. Fahey, L.M., et al., *Viral persistence redirects CD4 T cell differentiation toward T follicular helper cells.* J Exp Med, 2011. **208**(5): p. 987-99.
292. Zajac, A.J., et al., *Viral Immune Evasion Due to Persistence of Activated T Cells Without Effector Function.* The Journal of Experimental Medicine, 1998. **188**: p. 2205-2213.
293. Kaufmann, D.E., et al., *Upregulation of CTLA-4 by HIV-specific CD4+ T cells correlates with disease progression and defines a reversible immune dysfunction.* Nat Immunol, 2007. **8**(11): p. 1246-1254.
294. Jiang, Y., Y. Li, and B. Zhu, *T-cell exhaustion in the tumor microenvironment.* Cell death & disease, 2015. **6**(6): p. e1792-e1792.
295. Wherry, E.J., et al., *Viral persistence alters CD8 T-cell immunodominance and tissue distribution and results in distinct stages of functional impairment.* Journal of virology, 2003. **77**: p. 4911-27.
296. Yi, J.S., M.A. Cox, and A.J. Zajac, *T-cell exhaustion: characteristics, causes and conversion.* Immunology, 2010. **129**(4): p. 474-81.
297. Odorizzi, P.M. and E.J. Wherry, *Inhibitory receptors on lymphocytes: insights from infections.* Journal of immunology (Baltimore, Md. : 1950), 2012. **188**(7): p. 2957-65.
298. Butte, M.J., et al., *Programmed Death-1 Ligand 1 Interacts Specifically with the B7-1 Costimulatory Molecule to Inhibit T Cell Responses.* Immunity, 2007. **27**(1): p. 111-122.
299. Quigley, M., et al., *Transcriptional analysis of HIV-specific CD8+ T cells shows that PD-1 inhibits T cell function by upregulating BATF.* Nat Med, 2010. **16**(10): p. 1147-1151.
300. Brooks, D.G., et al., *Interleukin-10 determines viral clearance or persistence in vivo.* Nature Medicine, 2006. **12**: p. 1301-1309.
301. Ejrnaes, M., et al., *Resolution of a chronic viral infection after interleukin-10 receptor blockade.* The Journal of Experimental Medicine, 2006. **203**: p. 2461-2472.
302. Ng, C.T. and M.B.A. Oldstone, *Infected CD8α- dendritic cells are the predominant source of IL-10 during establishment of persistent viral infection.* Proceedings of the National Academy of Sciences of the United States of America, 2012. **109**: p. 14116-21.
303. Said, E.A., et al., *Programmed death-1–induced interleukin-10 production by monocytes impairs CD4+ T cell activation during HIV infection.* Nature Medicine, 2010. **16**: p. 452-459.
304. Tinoco, R., et al., *Cell-Intrinsic Transforming Growth Factor-β Signaling Mediates Virus-Specific CD8+ T Cell Deletion and Viral Persistence In Vivo.* Immunity, 2009. **31**: p. 145-157.
305. Stark, A.K., et al., *PI3Kdelta hyper-activation promotes development of B cells that exacerbate Streptococcus pneumoniae infection in an antibody-independent manner.* Nat Commun, 2018. **9**(1): p. 3174.
306. Wray-Dutra, M.N., et al., *Activated PIK3CD drives innate B cell expansion yet limits B cell–intrinsic immune responses.* J Exp Med, 2018.

307. Preite, S., et al., *Hyperactivated PI3Kdelta promotes self and commensal reactivity at the expense of optimal humoral immunity.* Nat Immunol, 2018. **19**(9): p. 986-1000.
308. Hobeika, E., et al., *Testing gene function early in the B cell lineage in mb1-cre mice.* Proceedings of the National Academy of Sciences, 2006. **103**(37): p. 13789-13794.
309. Lee, P.P., et al., *A Critical Role for Dnmt1 and DNA Methylation in T Cell Development, Function, and Survival.* Immunity, 2001. **15**(5): p. 763-774.
310. Hogquist, K.A., et al., *T cell receptor antagonist peptides induce positive selection.* Cell, 1994. **76**(1): p. 17-27.
311. Rubtsov, Y.P., et al., *Regulatory T Cell-Derived Interleukin-10 Limits Inflammation at Environmental Interfaces.* Immunity, 2008. **28**(4): p. 546-558.
312. Pope, C., et al., *Organ-Specific Regulation of the CD8 T Cell Response to Listeria monocytogenes Infection.* The Journal of Immunology, 2001. **166**(5): p. 3402-3409.
313. Brundage, R.A., et al., *Expression and phosphorylation of the Listeria monocytogenes ActA protein in mammalian cells.* Proceedings of the National Academy of Sciences, 1993. **90**(24): p. 11890-11894.
314. Clark, J., et al., *Quantification of PtdInsP(3) molecular species in cells and tissues by mass spectrometry.* Nature methods, 2011. **8**(3): p. 267-272.
315. Cahn, A., et al., *Safety, pharmacokinetics and dose-response characteristics of GSK2269557, an inhaled PI3Kdelta inhibitor under development for the treatment of COPD.* Pulm Pharmacol Ther, 2017. **46**: p. 69-77.
316. Irizarry, R.A., et al., *Exploration, normalization, and summaries of high density oligonucleotide array probe level data.* Biostatistics, 2003. **4**(2): p. 249-264.
317. Gentleman, R.C., et al., *Bioconductor: open software development for computational biology and bioinformatics.* Genome Biology, 2004. **5**(10): p. R80-R80.
318. Gautier, L., et al., *affy—analysis of Affymetrix GeneChip data at the probe level.* Bioinformatics, 2004. **20**(3): p. 307-315.
319. Gu, Z., R. Eils, and M. Schlesner, *Complex heatmaps reveal patterns and correlations in multidimensional genomic data.* Bioinformatics, 2016. **32**(18): p. 2847-2849.
320. Wiśniewski, J.R., et al., *A "Proteomic Ruler" for Protein Copy Number and Concentration Estimation without Spike-in Standards.* Molecular & Cellular Proteomics : MCP, 2014. **13**(12): p. 3497-3506.
321. Down, K., et al., *Optimization of Novel Indazoles as Highly Potent and Selective Inhibitors of Phosphoinositide 3-Kinase δ for the Treatment of Respiratory Disease.* Journal of Medicinal Chemistry, 2015. **58**(18): p. 7381-7399.
322. Stokoe, D., et al., *Dual Role of Phosphatidylinositol-3,4,5-trisphosphate in the Activation of Protein Kinase B.* Science, 1997. **277**(5325): p. 567-570.
323. Alessi, D.R., et al., *Characterization of a 3-phosphoinositide-dependent protein kinase which phosphorylates and activates protein kinase Bα.* Current Biology, 1997. **7**(4): p. 261-269.
324. Jacinto, E., et al., *SIN1/MIP1 Maintains rictor-mTOR Complex Integrity and Regulates Akt Phosphorylation and Substrate Specificity.* Cell, 2006. **127**(1): p. 125-137.
325. Sarbassov, D.D., et al., *Prolonged Rapamycin Treatment Inhibits mTORc2 Assembly and Akt/PKB.* Molecular Cell, 2006. **22**(2): p. 159-168.
326. Sansom, D.M., *CD28, CTLA-4 and their ligands: who does what and to whom?* Immunology, 2000. **101**(2): p. 169-177.
327. Walker, L.S.K., *Treg and CTLA-4: Two intertwining pathways to immune tolerance.* J Autoimmun, 2013. **45**: p. 49-57.
328. Sojka, D.K., A. Hughson, and D.J. Fowell, *CTLA-4 is required by CD4+CD25+ Treg to control CD4+ T-cell lymphopenia-induced proliferation.* European Journal of Immunology, 2009. **39**(6): p. 1544-1551.

329. Waterhouse, P., et al., *Lymphoproliferative Disorders with Early Lethality in Mice Deficient in Ctla-4.* Science, 1995. **270**(5238): p. 985-988.
330. Patton, D.T., et al., *The PI3K p110delta regulates expression of CD38 on regulatory T cells.* PLoS One, 2011. **6**(3): p. e17359.
331. Dong, C. and R.A. Flavell, *Cell fate decision: T-helper 1 and 2 subsets in immune responses.* Arthritis Research & Therapy, 2000. **2**(3): p. 179.
332. Han, J.M., S.J. Patterson, and M.K. Levings, *The Role of the PI3K Signaling Pathway in CD4(+) T Cell Differentiation and Function.* Front Immunol, 2012. **3**: p. 245.
333. Nagata, S. and P. Golstein, *The Fas death factor.* Science, 1995. **267**(5203): p. 1449-1456.
334. Krammer, P.H., *CD95's deadly mission in the immune system.* Nature, 2000. **407**: p. 789.
335. Vogelzang, A., et al., *A fundamental role for interleukin-21 in the generation of T follicular helper cells.* Immunity, 2008. **29**(1): p. 127-37.
336. Johnston, R.J., et al., *Bcl6 and Blimp-1 are reciprocal and antagonistic regulators of T follicular helper cell differentiation.* Science, 2009. **325**(5943): p. 1006-10.
337. Chung, Y., et al., *Follicular regulatory T cells expressing Foxp3 and Bcl-6 suppress germinal center reactions.* Nat Med, 2011. **17**(8): p. 983-8.
338. Linterman, M.A., et al., *Foxp3+ follicular regulatory T cells control the germinal center response.* Nat Med, 2011. **17**(8): p. 975-82.
339. Ronchetti, S., et al., *Glucocorticoid-Induced Tumour Necrosis Factor Receptor-Related Protein: A Key Marker of Functional Regulatory T Cells.* Journal of Immunology Research, 2015. **2015**: p. 171520.
340. Deaglio, S., et al., *Adenosine generation catalyzed by CD39 and CD73 expressed on regulatory T cells mediates immune suppression.* J Exp Med, 2007. **204**(6): p. 1257-1265.
341. Borsellino, G., et al., *Expression of ectonucleotidase CD39 by Foxp3⁺ Treg cells: hydrolysis of extracellular ATP and immune suppression.* Blood, 2007. **110**(4): p. 1225-1232.
342. Schenk, U., et al., *ATP Inhibits the Generation and Function of Regulatory T Cells Through the Activation of Purinergic P2X Receptors.* Science Signaling, 2011. **4**(162): p. ra12-ra12.
343. Elkord, E. and B.K. Al-Ramadi, *Helios expression in FoxP3+ T regulatory cells.* Expert Opinion on Biological Therapy, 2012. **12**(11): p. 1423-1425.
344. Kornete, M., E. Sgouroudis, and C.A. Piccirillo, *ICOS-Dependent Homeostasis and Function of Foxp3⁺ Regulatory T Cells in Islets of Nonobese Diabetic Mice.* The Journal of Immunology, 2012. **188**(3): p. 1064-1074.
345. Chen, Y., et al., *Murine regulatory T cells contain hyper-proliferative and death-prone subsets with differential ICOS expression.* Journal of immunology (Baltimore, Md. : 1950), 2012. **188**(4): p. 1698-1707.
346. Kitz, A., et al., *AKT isoforms modulate Th1-like Treg generation and function in human autoimmune disease.* EMBO Rep, 2016. **17**(8): p. 1169-83.
347. Kerdiles, Y.M., et al., *Foxo1 links homing and survival of naive T cells by regulating L-selectin, CCR7 and interleukin 7 receptor.* Nat Immunol, 2009. **10**(2): p. 176-84.
348. Ouyang, W., et al., *An essential role of the Forkhead-box transcription factor Foxo1 in control of T cell homeostasis and tolerance.* Immunity, 2009. **30**(3): p. 358-71.
349. Sinclair, L.V., et al., *Phosphatidylinositol-3-OH kinase and nutrient-sensing mTOR pathways control T lymphocyte trafficking.* Nat Immunol, 2008. **9**(5): p. 513-21.
350. Hagenbeek, T.J. and H. Spits, *T-cell lymphomas in T-cell-specific Pten-deficient mice originate in the thymus.* Leukemia, 2008. **22**(3): p. 608-19.
351. Liu, X., et al., *Distinct roles for PTEN in prevention of T cell lymphoma and autoimmunity in mice.* J Clin Invest, 2010. **120**(7): p. 2497-507.
352. Edwards, E.S.J., et al., *Activating PIK3CD mutations impair human cytotoxic lymphocyte differentiation and function and EBV immunity.* Journal of Allergy and Clinical Immunology.

353. Luo, Y., et al., *Identification of a novel de novo gain-of-function mutation of PIK3CD in a patient with activated phosphoinositide 3-kinase delta syndrome.* Clin Immunol, 2018.
354. Haxhinasto, S., D. Mathis, and C. Benoist, *The AKT-mTOR axis regulates de novo differentiation of CD4+Foxp3+ cells.* J Exp Med, 2008. **205**(3): p. 565-74.
355. Harada, Y., et al., *Transcription factors Foxo3a and Foxo1 couple the E3 ligase Cbl-b to the induction of Foxp3 expression in induced regulatory T cells.* J Exp Med, 2010. **207**(7): p. 1381-91.
356. Battaglia, M., A. Stabilini, and M.G. Roncarolo, *Rapamycin selectively expands CD4+CD25+FoxP3+ regulatory T cells.* Blood, 2005. **105**(12): p. 4743-8.
357. Dang, E.V., et al., *Control of T(H)17/T(reg) balance by hypoxia-inducible factor 1.* Cell, 2011. **146**(5): p. 772-84.
358. Guicciardi, M.E. and G.J. Gores, *Life and death by death receptors.* The FASEB Journal, 2009. **23**(6): p. 1625-1637.
359. Lu, B., et al., *Phosphatidylinositol 3-Kinase/Akt Positively Regulates Fas (CD95)-Mediated Apoptosis in Epidermal Cl41 Cells.* The Journal of Immunology, 2006. **176**(11): p. 6785-6793.
360. Larsen, S.E., et al., *Sensitivity to Restimulation-Induced Cell Death Is Linked to Glycolytic Metabolism in Human T Cells.* The Journal of Immunology, 2017. **198**(1): p. 147-155.
361. Barbera Betancourt, A., et al., *Inhibition of Phosphoinositide 3-Kinase p110delta Does Not Affect T Cell Driven Development of Type 1 Diabetes Despite Significant Effects on Cytokine Production.* PLoS One, 2016. **11**(1): p. e0146516.
362. Suarez-Fueyo, A., et al., *Enhanced phosphoinositide 3-kinase delta activity is a frequent event in systemic lupus erythematosus that confers resistance to activation-induced T cell death.* J Immunol, 2011. **187**(5): p. 2376-85.
363. Dengler, H.S., et al., *Distinct functions for the transcription factor Foxo1 at various stages of B cell differentiation.* Nat Immunol, 2008. **9**: p. 1388.
364. Kaech, S.M., et al., *Selective expression of the interleukin 7 receptor identifies effector CD8 T cells that give rise to long-lived memory cells.* Nat Immunol, 2003. **4**(12): p. 1191-8.
365. Voehringer, D., et al., *Viral Infections Induce Abundant Numbers of Senescent CD8 T Cells.* The Journal of Immunology, 2001. **167**(9): p. 4838-4843.
366. Joshi, N.S., et al., *Increased numbers of preexisting memory CD8 T cells and decreased T-bet expression can restrain terminal differentiation of secondary effector and memory CD8 T cells.* J Immunol, 2011. **187**(8): p. 4068-76.
367. Sallusto, F., et al., *Two subsets of memory T lymphocytes with distinct homing potentials and effector functions.* Nature, 1999. **401**: p. 708.
368. Masopust, D., et al., *Preferential Localization of Effector Memory Cells in Nonlymphoid Tissue.* Science, 2001. **291**(5512): p. 2413-2417.
369. Jameson, S.C. and D. Masopust, *Diversity in T cell memory: an embarrassment of riches.* Immunity, 2009. **31**(6): p. 859-71.
370. Voehringer, D., M. Koschella, and H. Pircher, *Lack of proliferative capacity of human effector and memory T cells expressing killer cell lectinlike receptor G1 (KLRG1).* Blood, 2002. **100**(10): p. 3698-702.
371. Müllbacher, A., et al., *Granzymes are the essential downstream effector molecules for the control of primary virus infections by cytolytic leukocytes.* Proceedings of the National Academy of Sciences, 1999. **96**(24): p. 13950-13955.
372. Riberdy, J.M., et al., *Diminished Primary and Secondary Influenza Virus-Specific CD8⁺ T-Cell Responses in CD4-Depleted Ig^{−/−} Mice.* J Virol, 2000. **74**(20): p. 9762-9765.
373. Betts, R.J., et al., *Influenza A virus infection results in a robust, antigen-responsive, and widely disseminated Foxp3+ regulatory T cell response.* J Virol, 2012. **86**(5): p. 2817-25.
374. Marzo, A.L., et al., *Fully Functional Memory CD8 T Cells in the Absence of CD4 T Cells.* The Journal of Immunology, 2004. **173**(2): p. 969-975.

375. Leon, B., et al., *FoxP3+ regulatory T cells promote influenza-specific Tfh responses by controlling IL-2 availability.* Nat Commun, 2014. **5**: p. 3495.
376. Zeng, R., et al., *The molecular basis of IL-21–mediated proliferation.* Blood, 2007. **109**(10): p. 4135-4142.
377. Tian, Y. and A.J. Zajac, *IL-21 and T Cell Differentiation: Consider the Context.* Trends Immunol, 2016. **37**(8): p. 557-568.
378. Kim, J.M., J.P. Rasmussen, and A.Y. Rudensky, *Regulatory T cells prevent catastrophic autoimmunity throughout the lifespan of mice.* Nat Immunol, 2006. **8**: p. 191.
379. Cheng, L.E., et al., *Enhanced signaling through the IL-2 receptor in CD8+ T cells regulated by antigen recognition results in preferential proliferation and expansion of responding CD8+ T cells rather than promotion of cell death.* Proc Natl Acad Sci U S A, 2002. **99**(5): p. 3001-6.
380. Tay, N.Q., et al., *CD40L Expression Allows CD8+ T Cells to Promote Their Own Expansion and Differentiation through Dendritic Cells.* Front Immunol, 2017. **8**(1484).
381. Utzschneider, D.T., et al., *Active Maintenance of T Cell Memory in Acute and Chronic Viral Infection Depends on Continuous Expression of FOXO1.* Cell Rep, 2018. **22**(13): p. 3454-3467.
382. Sullivan, B.M., et al., *Antigen-driven effector CD8 T cell function regulated by T-bet.* Proc Natl Acad Sci U S A, 2003. **100**(26): p. 15818-23.
383. Ertelt, J.M., et al., *Foxp3+ regulatory T cells impede the priming of protective CD8+ T cells.* J Immunol, 2011. **187**(5): p. 2569-77.
384. Rowe, J.H., J.M. Ertelt, and S.S. Way, *Foxp3(+) regulatory T cells, immune stimulation and host defence against infection.* Immunology, 2012. **136**(1): p. 1-10.
385. Kaech, S.M. and E.J. Wherry, *Heterogeneity and cell-fate decisions in effector and memory CD8+ T cell differentiation during viral infection.* Immunity, 2007. **27**(3): p. 393-405.
386. Banerjee, A., et al., *Cutting edge: The transcription factor eomesodermin enables CD8+ T cells to compete for the memory cell niche.* J Immunol, 2010. **185**(9): p. 4988-92.
387. Cui, W. and S.M. Kaech, *Generation of effector CD8+ T cells and their conversion to memory T cells.* Immunological Reviews, 2010. **236**(1): p. 151-166.
388. Boettler, T., et al., *Expression of the interleukin-7 receptor alpha chain (CD127) on virus-specific CD8+ T cells identifies functionally and phenotypically defined memory T cells during acute resolving hepatitis B virus infection.* J Virol, 2006. **80**(7): p. 3532-40.
389. Krishna, S., et al., *Role of tumor suppressor TSC1 in regulating antigen-specific primary and memory CD8 T cell responses to bacterial infection.* Infect Immun, 2014. **82**(7): p. 3045-57.
390. Olson, J.A., et al., *Effector-like CD8(+) T cells in the memory population mediate potent protective immunity.* Immunity, 2013. **38**(6): p. 1250-60.
391. Smith, C.M., et al., *Cognate CD4(+) T cell licensing of dendritic cells in CD8(+) T cell immunity.* Nat Immunol, 2004. **5**(11): p. 1143-8.
392. Bevan, M.J., *Helping the CD8+ T-cell response.* Nature Reviews Immunology, 2004. **4**: p. 595.
393. Janssen, E.M., et al., *CD4+ T cells are required for secondary expansion and memory in CD8+ T lymphocytes.* Nature, 2003. **421**: p. 852.
394. Sun, J.C. and M.J. Bevan, *Defective CD8 T cell memory following acute infection without CD4 T cell help.* Science, 2003. **300**(5617): p. 339-42.
395. Wherry, E.J. and M. Kurachi, *Molecular and cellular insights into T cell exhaustion.* Nat Rev Immunol, 2015. **15**(8): p. 486-99.
396. Paley, M.A., et al., *Progenitor and terminal subsets of CD8+ T cells cooperate to contain chronic viral infection.* Science, 2012. **338**(6111): p. 1220-5.
397. Aubert, R.D., et al., *Antigen-specific CD4 T-cell help rescues exhausted CD8 T cells during chronic viral infection.* Proc Natl Acad Sci U S A, 2011. **108**(52): p. 21182-21187.
398. Elsaesser, H., K. Sauer, and D.G. Brooks, *IL-21 is required to control chronic viral infection.* Science (New York, N.Y.), 2009. **324**: p. 1569-72.
399. Yi, J.S., M. Du, and A.J. Zajac, *A vital role for interleukin-21 in the control of a chronic viral infection.* Science, 2009. **324**(5934): p. 1572-6.

400. Penaloza-MacMaster, P., et al., *Interplay between regulatory T cells and PD-1 in modulating T cell exhaustion and viral control during chronic LCMV infection.* J Exp Med, 2014. **211**(9): p. 1905-18.
401. Crotty, S., et al., *Hypogammaglobulinemia and exacerbated CD8 T-cell–mediated immunopathology in SAP-deficient mice with chronic LCMV infection mimics human XLP disease.* Blood, 2006. **108**(9): p. 3085-3093.
402. Shin, H. and E.J. Wherry, *CD8 T cell dysfunction during chronic viral infection.* Current Opinion in Immunology, 2007. **19**(4): p. 408-415.
403. Blackburn, S.D., et al., *Coregulation of CD8+ T cell exhaustion by multiple inhibitory receptors during chronic viral infection.* Nat Immunol, 2009. **10**(1): p. 29-37.
404. Jin, H.T., et al., *Cooperation of Tim-3 and PD-1 in CD8 T-cell exhaustion during chronic viral infection.* Proc Natl Acad Sci U S A, 2010. **107**(33): p. 14733-8.
405. Lee, J., et al., *Reinvigorating Exhausted T Cells by Blockade of the PD-1 Pathway.* For Immunopathol Dis Therap, 2015. **6**(1-2): p. 7-17.
406. Sharma, A., et al., *Ipilimumab Administration in Patients With Advanced Melanoma and Hepatitis B and C.* Journal of Clinical Oncology, 2013. **31**(21): p. e370-e372.
407. Lipson, E.J., et al., *Durable cancer regression off-treatment and effective reinduction therapy with an anti-PD-1 antibody.* Clin Cancer Res, 2013. **19**(2): p. 462-8.
408. Davar, D., et al., *PD-1 Blockade in Advanced Melanoma in Patients with Hepatitis C and/or HIV.* Case Rep Oncol Med, 2015. **2015**: p. 737389.
409. Patsoukis, N., et al., *PD-1 increases PTEN phosphatase activity while decreasing PTEN protein stability by inhibiting casein kinase 2.* Mol Cell Biol, 2013. **33**(16): p. 3091-8.
410. Yokosuka, T., et al., *Programmed cell death 1 forms negative costimulatory microclusters that directly inhibit T cell receptor signaling by recruiting phosphatase SHP2.* J Exp Med, 2012. **209**(6): p. 1201-17.
411. Buggert, M., et al., *T-bet and Eomes are differentially linked to the exhausted phenotype of CD8+ T cells in HIV infection.* PLoS Pathog, 2014. **10**(7): p. e1004251.
412. McLane, L.M., et al., *Modulation of the subcellular localization of T-bet and Eomes alters CD8 exhaustion during chronic LCMV infection.* The Journal of Immunology, 2017. **198**(1 Supplement): p. 121.7-121.7.
413. Dietze, K.K., et al., *Transient depletion of regulatory T cells in transgenic mice reactivates virus-specific CD8(+) T cells and reduces chronic retroviral set points.* Proc Natl Acad Sci U S A, 2011. **108**(6): p. 2420-2425.
414. Elsaesser, H., K. Sauer, and D.G. Brooks, *IL-21 Is Required to Control Chronic Viral Infection.* Science (New York, N.Y.), 2009. **324**(5934): p. 1569-1572.
415. Lucas, C.L., et al., *PI3Kdelta and primary immunodeficiencies.* Nat Rev Immunol, 2016. **16**(11): p. 702-714.
416. Frentsch, M., et al., *CD40L expression permits CD8(+) T cells to execute immunologic helper functions.* Blood, 2013. **122**(3): p. 405-412.
417. Shedlock, D.J. and H. Shen, *Requirement for CD4 T Cell Help in Generating Functional CD8 T Cell Memory.* Science, 2003. **300**(5617): p. 337-339.
418. Velu, V., et al., *Enhancing SIV-Specific Immunity In Vivo by PD-1 Blockade.* Nature, 2009. **458**(7235): p. 206-210.
419. Barber, D.L., et al., *Restoring function in exhausted CD8 T cells during chronic viral infection.* Nature, 2005. **439**: p. 682.
420. Blackburn, S.D., et al., *Coregulation of CD8+ T cell exhaustion by multiple inhibitory receptors during chronic viral infection.* Nature immunology, 2009. **10**: p. 29-37.
421. Topalian, S.L., et al., *Safety, Activity, and Immune Correlates of Anti–PD-1 Antibody in Cancer.* N Engl J Med, 2012. **366**(26): p. 2443-2454.
422. Pauken, K.E. and E.J. Wherry, *Overcoming T cell exhaustion in infection and cancer.* Trends Immunol, 2015. **36**(4): p. 265-276.

423. Buck, M.D., et al., *Metabolic Instruction of Immunity.* Cell, 2017. **169**(4): p. 570-586.
424. Schmitz, I., et al., *IL-21 Restricts Virus-driven Treg Cell Expansion in Chronic LCMV Infection.* PLoS Pathog, 2013. **9**(5): p. e1003362.